AGARD-AG-300-VOL.4

AGARD-AG-300-VOL.4

AGARD

ADVISORY GROUP FOR AEROSPACE RESEARCH & DEVELOPMENT

7 RUE ANCELLE 92200 NEUILLY SUR SEINE FRANCE

AGARDograph No.300

AGARD Flight Test Techniques Series Volume 4 on Determination of Antennae Patterns and Radar Reflection Characteristics of Aircraft

by

H.Bothe and D.Macdonald

Edited by

A.Pool

NORTH ATLANTIC TREATY ORGANIZATION

DISTRIBUTION AND AVAILABILITY
ON BACK COVER

NORTH ATLANTIC TREATY ORGANIZATION

ADVISORY GROUP FOR AEROSPACE RESEARCH AND DEVELOPMENT

(ORGANISATION DU TRAITE DE L'ATLANTIQUE NORD)

AGARDograph No.300 Vol.4

DETERMINATION OF ANTENNAE PATTERNS AND RADAR REFLECTION CHARACTERISTICS OF AIRCRAFT

by

H.Bothe and D.Macdonald

A Volume of the

AGARD FLIGHT TEST TECHNIQUES SERIES

Edited by

A.Pool

This AGARDograph has been sponsored by the Flight Mechanics Panel of AGARD.

THE MISSION OF AGARD

The mission of AGARD is to bring together the leading personalities of the NATO nations in the fields of science and technology relating to aerospace for the following purposes:

- Exchanging of scientific and technical information;
- Continuously stimulating advances in the aerospace sciences relevant to strengthening the common defence posture;
- Improving the co-operation among member nations in aerospace research and development;
- Providing scientific and technical advice and assistance to the Military Committee in the field of aerospace research and development (with particular regard to its military application);
- Rendering scientific and technical assistance, as requested, to other NATO bodies and to member nations in connection with research and development problems in the aerospace field;
- Providing assistance to member nations for the purpose of increasing their scientific and technical potential;
- Recommending effective ways for the member nations to use their research and development capabilities for the common benefit of the NATO community.

The highest authority within AGARD is the National Delegates Board consisting of officially appointed senior representatives from each member nation. The mission of AGARD is carried out through the Panels which are composed of experts appointed by the National Delegates, the Consultant and Exchange Programme and the Aerospace Applications Studies Programme. The results of AGARD work are reported to the member nations and the NATO Authorities through the AGARD series of publications of which this is one.

Participation in AGARD activities is by invitation only and is normally limited to citizens of the NATO nations.

Published May 1986

ISBN 92-835-1530-7

Printed by Specialised Printing Services Limited
40 Chigwell Lane, Loughton, Essex IG10 3TZ

PREFACE

Since its founding in 1952, the Advisory Group for Aerospace Research and Development has published, through the Flight Mechanics Panel, a number of standard texts in the field of flight testing. The original Flight Test Manual was published in the years 1954 to 1956. The Manual was divided into four volumes: I. Performance, II. Stability and Control, III. Instrumentation Catalog, and IV. Instrumentation Systems.

As a result of developments in the field of flight test instrumentation, the Flight Test Instrumentation Group of the Flight Mechanics Panel was established in 1968 to update Volumes III and IV of the Flight Test Manual by the publication of the Flight Test Instrumentation Series, AGARDograph 160. In its published volumes AGARDograph 160 has covered recent developments in flight test instrumentation.

In 1978, the Flight Mechanics Panel decided that further specialist monographs should be published covering aspects of Volume I and II of the original Flight Test Manual, including the flight testing of aircraft systems. In March 1981, the Flight Test Techniques Group was established to carry out this task. The monographs of this Series (with the exception of AG 237 which was separately numbered) are being published as individually numbered volumes of AGARDograph 300. At the end of each volume of AGARDograph 300 two general Annexes are printed; Annex 1 provides a list of the volumes published in the Flight Test Instrumentation Series and in the Flight Test Techniques Series. Annex 2 contains a list of handbooks that are available on a variety of flight test subjects, not necessarily related to the contents of the volume concerned.

Special thanks and appreciation are extended to Mr F.N.Stoliker (US), who chaired the Group for two years from its inception in 1981, established the ground rules for the operation of the Group and marked the outlines for future publications.

In the preparation of the present volume the members of the Flight Test Techniques Group listed below have taken an active part. AGARD has been most fortunate in finding these competent people willing to contribute their knowledge and time in the preparation of this volume.

Adolph, C.E.	AFFTC/US.
Bogue, R.K.	NASA/US.
Borek, R.W.	NASA/US.
Bothe, H.	DFVLR/GE.
Bull, E.J.	A & AEE/UK.
Carabelli, R.	SAI/IT.
Galan, R.C.	CEV/FR.
Lapchine, N.	CEV/FR.
Moreau, J.	CEV/FR.
Norris, E.J.	A & AEE/UK.
Phillips, A.D.	AFFTC/US.
Pool, A. (editor)	NLR/NE.
Sanderson, K.C.	NASA/US.

J.T.M. van DOORN, NLR/NE.
Member, Flight Mechanics Panel
Chairman, Flight Test
Techniques Group.

ACKNOWLEDGEMENT

The authors acknowledge the invaluable assistance provided by many colleagues in the compilation of this paper. In particular thanks are due to Mr S.C.Woolcook, Manager of the UK Radio Modelling Facility, Dr D.L.Mensa of the Pacific Missile Test Center, PMTC, California, Mr L.R.Hughes of Teledyne Micronetics, Messrs C.A.Lupica and J.Micheals of RADC, Griffiss AFB, Mr C.Barnes of RATSCAT, Mr D.DeCarlo of the US Naval Air Test Center, Patuxent River, Messrs F.N.Stoliker and R.Mahlum of the USAF Flight Test Center and Mr R.W.Borek of the AMES-DRYDEN Flight Research Facility, Edwards AFB, M.P.Gaudon et al of CELAR, France, M.Renaudie of C.E.V., Bretigny, France, and M.N.Lapchine of C.E.V. Istres, France. In addition a lecture given by Mr W.F.Bahret in AGARD Lecture Series 59, October 1973 and a technical note by Mr D.Cooper when with NASA at Edwards AFB, have provided useful material for Chapter 2.2.

CONTENTS

	Page
PREFACE	iii
SYMBOLS AND ABBREVIATIONS	vi
SUMMARY	1
GENERAL INTRODUCTION	1
PART 1 DETERMINATION OF ANTENNA PATTERNS	2
1.1 DEFINITIONS	2
1.1.1 Introduction	2
1.1.2 Antenna Radiation Pattern (ARP)	2
1.1.3 Polarisation	2
1.1.4 Aspect Angle	2
1.1.5 Coordinate Systems	3
1.2 AIRCRAFT ANTENNAS	7
1.2.1 Aircraft Radio Aids	7
1.2.2 Types of Antennas	9
1.2.3 Antenna Positioning	12
1.2.4 Configuration of Aircraft	13
1.3 THE DETERMINATION OF THE ARP BY MATHEMATICAL MODELLING	14
1.3.1 Advantages and Disadvantages	14
1.3.2 Integral Equation Method	14
1.3.3 Geometrical Diffraction Method	15
1.4 THE DETERMINATION OF ARP OF FULL-SIZE AIRCRAFT IN FLIGHT	17
1.4.1 Advantages and Disadvantages	17
1.4.2 The Air-Ground Propagation Channel	17
1.4.3 Aspect Angle Determination and Flight Profiles	20
1.4.3.1 Aspect Angle Determination	20
1.4.3.2 Flight Trajectories for Dynamic ARP Measurements	23
1.4.4 System Considerations	29
1.4.4.1 Airborne Systems	29
1.4.4.2 Ground Systems	30
1.4.5 Pattern Calibration	34
1.4.5.1 Flyby Procedure	34
1.4.5.2 Calculation of the Effect of Ground Reflections	38
1.5 THE STATIC DETERMINATION OF ARP OF FULL-SIZE AIRCRAFT ON THE GROUND	45
1.5.1 Advantages and Disadvantages	45
1.5.2 System Consideration	45
1.6 THE DETERMINATION OF ARP BY SUB-SCALE MODEL MEASUREMENTS	49
1.6.1 Advantages and Disadvantages	49
1.6.2 Model Laws	49
1.6.3 Far Field Measurements	50
1.6.4 Anechoic Chamber Measurements	51
1.6.5 Comparison of Measurements on Full-Size Aircraft and Sub-Scale Models	54
PART 2 DETERMINATION OF RADAR REFLECTION CHARACTERISTICS	57
2.1 DEFINITIONS	57
2.1.1 Radar Cross Section (RCS) or Radar Echoing Area (REA)	57
2.1.2 Angular Noise or Glint	57
2.1.3 Polarisation	59
2.1.4 Near Zone, Fresnel Zone and Fraunhofer Zones	61
2.2 THE PARAMETRIC DEPENDENCE OF σ IN THE RADAR EQUATION	61
2.2.1 Derivation of the Radar Equation	61
2.2.2 The Effect of Radar Frequency	64
2.2.3 The Effects of Radar Polarisation	64
2.2.4 The Effects of Target Aspect Angle	66
2.2.5 Transmitter Waveform and Receiver Processing	66
2.2.6 The Effect of Target Range	67
2.2.7 The Effect of Partial Illumination	67
2.2.8 The Effect of Pulse Length	67

CONTENTS

	Page
2.3 THE DETERMINATION OF RCS OF REAL AIRCRAFT IN FLIGHT	67
2.3.1 Purpose: Advantages and Disadvantages	67
2.3.2 System Considerations	68
2.3.3 Existing Measurement Facilities	74
2.3.3.1 The US Naval Research Laboratory (NLR) Dynamic Measurement Facility	74
2.3.3.2 Edwards AFB, California, USA	75
2.3.3.3 Griffiss AFB, New York State, USA	76
2.3.3.4 CEV Bretigny, France	78
2.4 THE DETERMINATION OF RCS OF REAL AIRCRAFT, STATISTICALLY, ON THE GROUND	79
2.4.1 Purpose: Advantages and Disadvantages	79
2.4.2 System Considerations	80
2.4.3 Examples of Established Measurement Facilities	82
2.4.3.1 Holloman AFB, New Mexico, USA	82
2.4.3.2 Teledyne Micronetics, RCS Measurement Facility, San Diego, USA	82
2.4.3.3 ONERA, Chalais Meudon, France	82
2.4.3.4 CELAR, Bruz (Rennes), France	82
2.4.3.5 DFVLR, Oberpfaffenhofen, Germany	83
2.5 THE DETERMINATION OF RCS AND GLINT BY SUB-SCALE METHODS	85
2.5.1 General	85
2.5.2 The Principle of Scaled Modelling	85
2.5.3 Some Implementations of Scaled Modelling	85
2.5.3.1 Optical Simulation	85
2.5.3.2 Ultrasonic Simulation	85
2.5.3.3 Radio Modelling — Thorn-EMI, UK	87
2.5.3.4 Radio Modelling — Teledyne Micronetics, USA	89
2.5.3.5 Radio Modelling — Pacific Missile Test Centre, Pt Mugu, USA	90
2.6 CONCLUDING COMMENTS	90
REFERENCES	93
APPENDICES	95
1.A DERIVATION OF RADIO WAVE PROPAGATION PARAMETERS	95
1.B DERIVATION OF THE TRANSFORMATION EQUATIONS FOR THE ASPECT ANGLE	98
2.A RADIO MODELLING IN THE UK	101
2.A1 Description of Facility	101
2.A2 Typical Measurements and Studies	111
2.A3 Validity of Data Produced in Relation to Full Scale Dynamic Measurements	112
2.A4 Data Reduction	119
2.A5 Continuing Developments	120

SYMBOLS AND ABBREVIATIONS

Part 1

a	radius of earth 6365 km (3437 NM)
A	effective area of antenna
A_T	longitudinal amplitude taper
A_R	effective area of receiving antenna
c	velocity of light
d	horizontal distance aircraft-ground station
d_1	horizontal distance point of reflection to ground antenna
d_2	horizontal distance point of reflection to airborne antenna
D	distance between a vehicle and a ground station
D	divergence factor
E	electric field intensity
$\vec{E}_o$	field strength of direct wave
$\vec{E}_R$	resultant field strength vector
f	frequency
G_M	multipath gain
G_R	gain of receiving antenna
G_S	gain of standard gain antenna compared to an isotropic radiator
G_T	gain of transmitting antenna
h	antenna height
h_1	height of ground antenna
h_2	height of airborne antenna
h_R	height of reflection area
h_{1c}	height of ground antenna, corrected for elevated reflection area
h_{2c}	height of airborne antenna, corrected for elevated reflection area
k	refraction correction factor (k = 4/3)
l	distance of antenna from the radio horizon
L	general losses (e.g. cable)
M	rotation matrix
n	index of reflection
P_A	measured power input of aircraft antenna
P_R	received power
P_S	measured power input of a standard gain antenna
P_T	transmitted power
P_{EA}	power received from an aircraft antenna
P_{ES}	power received from a standard gain antenna
ΔP	difference of power
r	distance
$\vec{R}$	reflection coefficient
$\vec{R}_H$	reflection coefficient of horizontal polarisation
$\vec{R}_V$	reflection coefficient of vertical polarisation
S_r	power density
X	coordinates of a cartesian system
Y	coordinates of a cartesian system
Z	coordinates of a cartesian system
α	slope of reflection area
β_A	position dependent angle (see Fig 1.26)
β_E	position dependent angle (see Fig 1.27)
ε_o	permittivity of free space
ε_r	relative permittivity
θ	phase lag of electromagnetic wave, angular path length difference
θ	vehicle pitch (nose up is positive)
θ_D	depression angle
θ_E	earth curvature
λ	wavelength
λ	rotational angle around the X-axis
μ	permeability
μ	rotational angle around the Y-axis
ν	rotational angle around the Z-axis
ρ	azimuth angle of ground tracking system
ρ_E	elevation angle of ground tracking system
σ	conductivity
ϕ	vehicle roll (right wing down is positive)
Φ	phase of reflection coefficient
Φ_A	horizontal aspect angle
Φ_E	vertical aspect angle

Ψ	vehicle heading relative to true North (right turn is positive)
ψ	angle of incidence

Part 2

AGC	Automatic Gain Control
A_r	receiver antenna capture area
B_n	noise bandwidth
CW	continuous wave
dB	decibel ($10 \log_{10} P_1/P_2$)
D	maximum linear dimension
E	electric field
E^s	scattered electric field
E^i or e^i	incident electric field
F_n	noise figure
G_r	gain of receiver antenna
G_t	gain of transmitter antenna
H	horizontal
HCN	hydrogen cyanide
K	Boltzmann's constant (1.38×10^{-23} watts/hertz/kelvin)
LL	transmit and receive LEFT HAND CIRCULAR POLARISATION
P	power
P_t	power transmitted
P_r	power received
P	scaling factor
Q	magnification factor
R	range
R_t	range of radar to target
RME	Radio Modelling Equipment
RPV	Remotely Piloted Vehicle
RR	transmit and receive RIGHT HAND CIRCULAR POLARISATION
RL	transmit right hand and receive LEFT HAND CIRCULAR POLARISATION
S_{min}	minimum detectable signal
S/N	signal to noise ratio
$S/N_{(min)}$	minimum value for detection
T	temperature in kelvin
THz	10^{12} Hertz
V	vertical
v	voltage
VDU	Voltage Display Unit
λ	wavelength
σ	Radar Cross Section (RCS)

DETERMINATION OF ANTENNA PATTERNS AND RADAR REFLECTION CHARACTERISTICS OF AIRCRAFT

by

Helmut Bothe
DFVLR/FF-FL
PO BOX 3267
3300 Braunschweig
Germany

and

Donald Macdonald
Royal Signals and Radar Establishment *
Malvern
Worcestershire
Great Britain

SUMMARY

This AGARDograph is divided into two parts: Determination of Antenna Patterns of Aircraft, by H. Bothe, and Determination of Radar Reflection Characteristics of Aircraft, by D. Macdonald.

Part 1 describes the different types of aircraft antennas, their radiation characteristics and their preferred siting on the airframe. Great emphasis is placed on the various methods for determining aircraft antenna radiation patterns (ARP) and advantages, disadvantages and limitations of each method are indicated. Mathematical modelling, model measurements and in-flight measurements in conjunction with the applied flight test technique are included. Examples of practical results are given.

Part 2 describes methods of determing aircraft radar characteristics, indicating advantages, disadvantages and limitations of each method. Relevant fundamentals of radar theory are included only as necessary to appreciation of the real meaning of radar cross section (RCS) and angular glint. The measuring methods included are dynamic full-scale, static full-scale, sub-scale optical, ultrasonic and radio modelling. References are made to RCS measuring facilities in the USA and Europe and the UK Radio Modelling Facility is used extensively to exemplify the sub-scale technique.

GENERAL INTRODUCTION

Although the two authors have had regular contacts during the time this AGARDograph was written, each author only bears responsibility for his own part. Mr Macdonald has, in addition, assisted Dr. Bothe by correcting the English language of the first part.

The reason for combining the two subjects in one AGARDograph is, that many of the techniques used for the one subject are similar to those used for the other subject. In practice, however, this similarity does not go very far and the research and the execution of tests for the two subjects is very often done by different institutes. For that reason the two subjects are treated separately.

Although the primary object of the AGARDograph is to acquaint flight test engineers with the principles of the flight test techniques for the subjects, the authors were asked to include brief discussions of other test methods that are available. Flight testing is very expensive and the flight test engineers should be aware of those other methods which, though they cannot replace flight testing completely, may significantly reduce the flight time required. It will be found that both authors discuss the possibilities of full-scale ground testing and of reduced-scale model testing. In Part 1 an additional chapter is devoted to mathematical modelling techniques which has no counterpart in Part 2. Although mathematical modelling is used in the design stage of the aircraft for predicting both antenna patterns and radar cross sections, the author of Part 2 is of the opinion that it is not sufficiently advanced to be used in the process of the actual determination of the radar cross section. The complex nature of the radar scattering from aircraft engines and their intakes and from radar installations have so far proved to be intractable to realistic mathematical modelling. Of course, mathematical modelling for antenna pattern determination must also be supplemented by ground test results and be checked by actual flight testing.

* Now with Thorn-EMI Electronics Ltd

PART 1

DETERMINATION OF ANTENNA PATTERNS

by
Helmut Bothe

1.1 DEFINITIONS

1.1.1 Introduction

Antenna patterns are determined in order to obtain information on the spatial energy distribution of the signals transmitted from radio-frequency antennas and on the sensitivity of receiving antennas for signals coming from different directions. For the determination of these spatial distributions a number of methods are used:

- Mathematical modelling
- Dynamic measurements on real aircraft in flight
- Static measurements on full-size models or aircraft on the ground
- Measurements on sub-scale models.

These methods are described separately in Chapters 1.3 to 1.6.

Definitions of the most important notions that are used in this part are given in the remainder of this chapter. Chapter 1.2 decribes the most important characteristics of the antennas used on aircraft.

1.1.2 Antenna Radiation Pattern (ARP)

An important property of a radio frequency link is the electro-magnetic field intensity at every point in space for a given output power of the antenna. As the propagation of radio frequency waves in free space is well known, the spatial distribution of the field intensity needs only be measured at one spatial sphere around the antenna. The information is usually given as distributions along the circumference of flat sections through this sphere: each of these is called an Antenna Radiation Pattern (ARP). Several ARPs are usually required to describe the complete spatial antenna pattern of an antenna.

In many applications only the relative energy distribution is of interest. The radiation energy is then normalized by dividing it by its maximum in the main radiation direction and a relative ARP is derived.

1.1.3 Polarisation

The orientation of the electric field vector in the direction of maximum radiation is defined as the polarisation of the antenna. As an example a vertical dipole or stub will radiate vertical polarisation while a horizontal dipole will generate horizontal polarisation. If several antenna elements with different orientations radiate simultaneously, generally with different amplitudes and phases, the result is an elliptically polarised wave. A circularly polarised wave - a special case of elliptical polarisation - is radiated if two perpendicular linearly polarised fields have a 90° phase difference. Then the electric field vector rotates right-handed or left-handed, depending on the sign of the 90° phase difference. If an antenna is designed to radiate with a certain polarisation and additionally radiates in an undesired orientation, this unwanted component is called cross polarisation. Hence the cross polarisation of vertical is horizontal polarisation and the cross polarisation of circular polarisation is a counter-rotating circularly polarised field. Two counter-rotating fields of different amplitudes sum to an elliptically polarised field.

If the radiating and the receiving antennas of a radio link both have the same polarisation, then the polarisation is said to be matched. A polarisation loss of energy transmission occurs if the antennas have unmatched polarisation.

In air to ground radio links polarisation is usually unmatched because attitude, height and distance of the aircraft with respect to the ground station vary, which results in changes of relative polarisation orientation. Since the polarisation of the airborne antenna radiation is variable with respect to the earth axes, it is nominally assigned the polarisation of the ground receiver antenna.

1.1.4 Aspect Angle

The radiation direction of an aircraft antenna with respect to a receiving station (on the ground or in a second aircraft) is defined by the aspect angle. This is the angle between the roll axis and the line of sight (Fig 1.1). In order to cover the whole sphere, the aspect angle is resolved into two parts. The depression angle is measured in the yaw plane between the roll axis and the projection of the line of sight perpendicular to the yaw plane. In polar ARP plots one of these angles is usually taken as the independent variable, while radiated power is the dependent variable. For static measurements of models or full sized aircraft, the aspect angle is readily obtained from the angle readouts of the pedestal. As will be shown later in-flight measurements are more complex because the aspect angle depends on the relative locations of the ground station and the aircraft, as well as on the attitude of the aircraft.

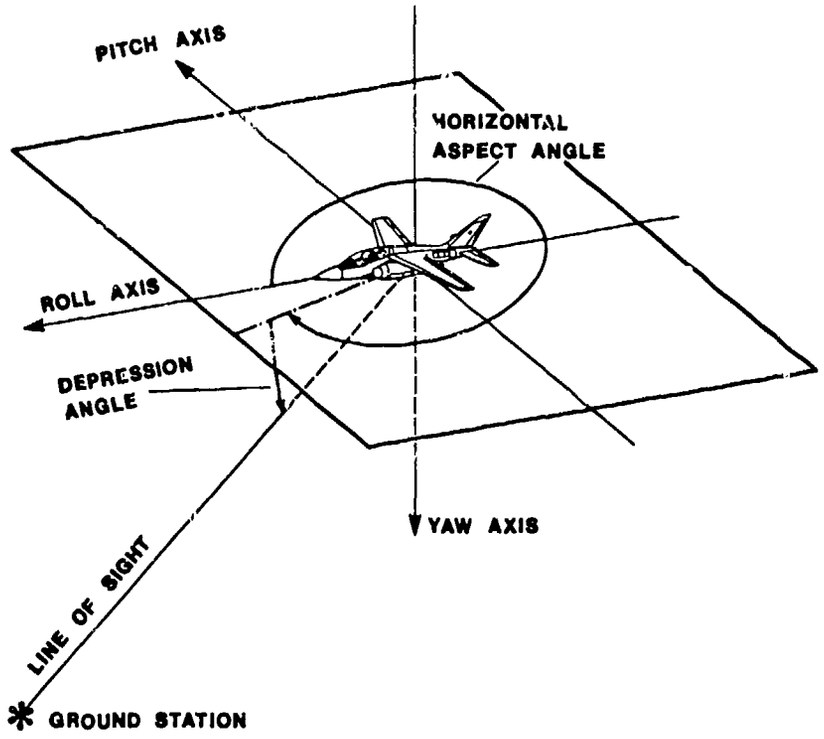

Fig 1.1 Aspect angle and vehicle coordinate system

1.1.5 Coordinate Systems

Spherical coordinates for general use in antenna pattern measurements are defined by IEEE standards published in Ref 1 and shown in Fig 1.2.

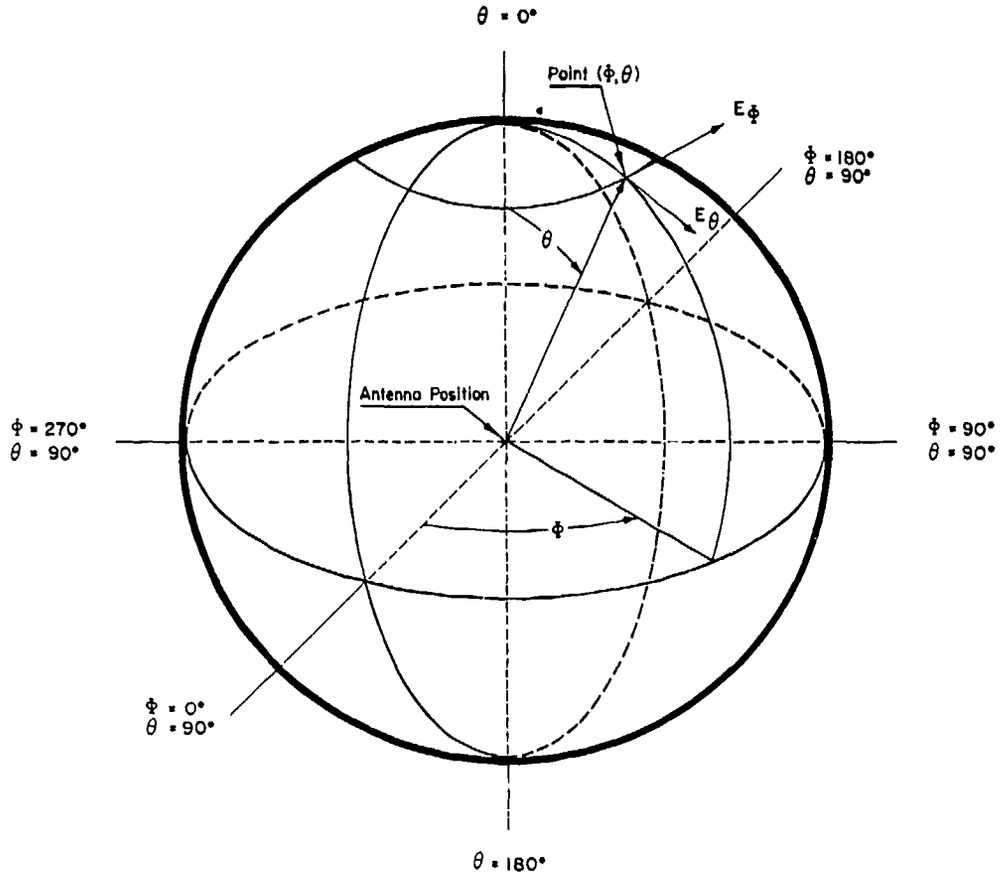

Fig 1.2 IEEE standard antenna coordinate system

In addition the IRIG has published recommendations on how the orientation of an antenna-bearing vehicle should be described in the IEEE standardized system (Ref 2). Fig 1.3 illustrates how the orientation of the vehicle, which is described by its pitch, roll and yaw axes (see Fig 1.1), lies along the Z-axis of the system illustrated in Fig 1.2. The complete roll plane is covered by the angle ϕ and together with the angle θ gives coverage over the entire sphere.

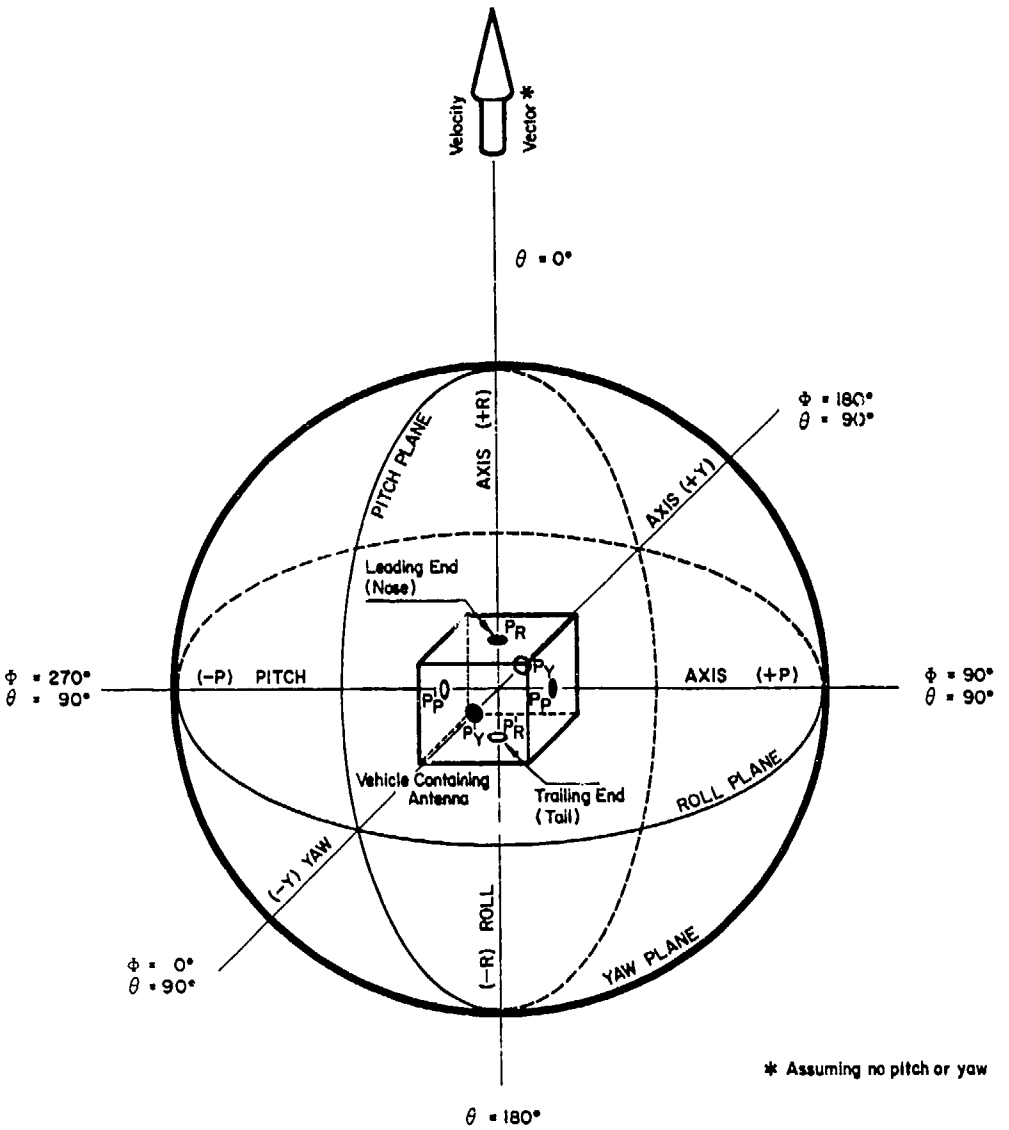

Fig 1.3 Coordinate system of Inter-Range Instrumentation Group (IRIG)

In dynamic aircraft ARP measurements it is common practice to denote the horizontal aspect angle by ϕ, and to measure ϕ from the nose of the aircraft (positive roll axis) so that the right wing coincides with $\phi = 90°$. This requires a 180° rotation of the IEEE coordinate system of Fig 1.2 around the connecting line between $\phi = 0°$, $\theta = 90°$ and $\phi = 180°$, $\theta = 90°$. So the positive yaw axis is at $\theta = 0°$. This arrangement illustrated in Fig 1.4 will be used throughout this book.

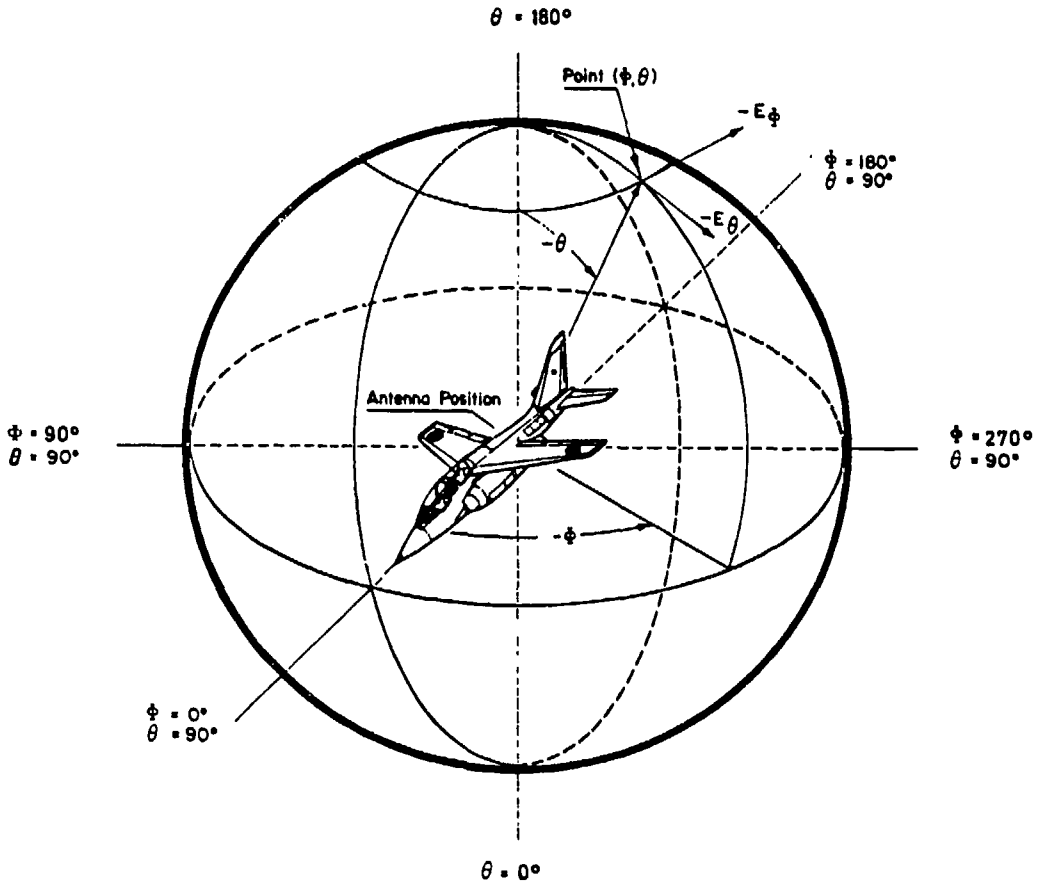

Fig 1.4 Orientation of aircraft to IEEE standard coordinate system in dynamic ARP measurements

The depression angle defined in Fig 1.1 will be denoted θ_D. The relations between θ_D and the angle θ of the IEEE-system are

θ	0°	90°	180°
θ_D	+90°	0°	-90°

In order to achieve easy comparisions between dynamic and static measurements, the same coordinate system and notations will also be used for static measurements of models or full sized aircraft.

Aircraft antenna patterns are often presented in polar diagrams. Horizontal patterns are conveniently recorded by a continuous variation of the horizontal aspect angles while the depression angle θ_D is stepped as a parameter. This leads to a movement of models under test on a cone, and the recorded patterns are conic section patterns. Due to the limited manoeuvrability of a full-sized aircraft in flight, conic section patterns cannot be measured during a complete continuous flight pattern. Nevertheless this type of mapping is frequently applied to model measurements.

The usual polar patterns for in-flight measurements are great circle patterns, which are recorded as the aircraft moves in a complete horizontal circle. If the circle is flown with different angles of roll, radiation patterns in the corresponding inclined planes through the aircraft roll axis are obtained. This means that the depression angle also changes and true parametric plots are thus not achieved.

A "matrix" plot in the form of a spherical surface projection provides radiation intensity at increments of Φ and θ or θ_D over the entire sphere (see Fig 1.5). Radiation intensity appears as a plotted number in each element of the matrix or as contour lines of equal radiation intensity. The first representation allows only a rough angular resolution. The second one suffers from poor resolution of radiation intensity.

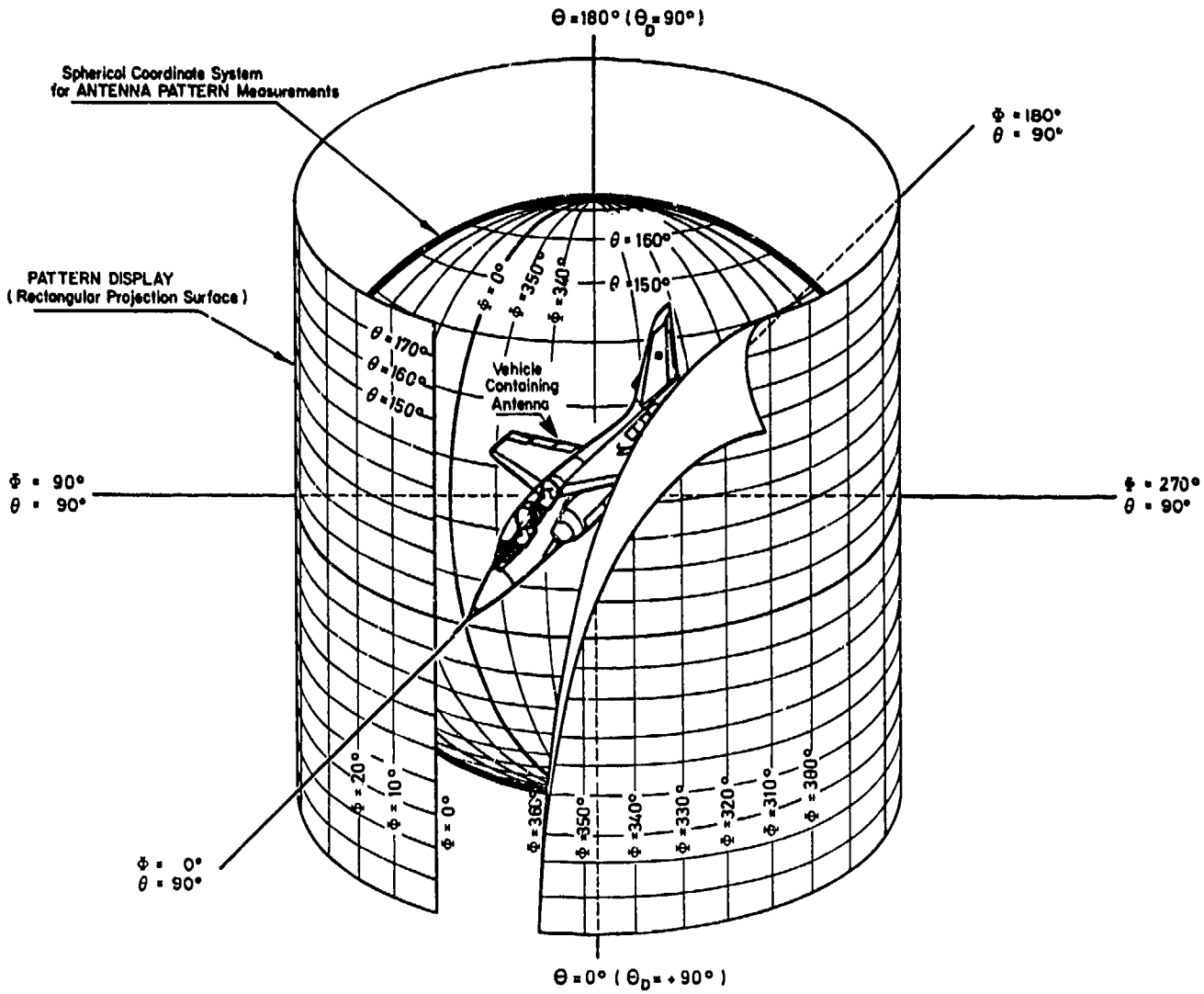

Fig 1.5 Vehicle and antenna coordinate system with projection for matrix representation

1.2 AIRCRAFT ANTENNAS

1.2.1 Aircraft Radio Aids

Aircraft radio aids can be divided into 3 groups: Communication, radio navigation and identification. With one exception -the weather radar- all radio services can be associated with one of these 3 categories.

The aircraft communication services are listed in Tab 1.1.

Tab 1.1 Aircraft communication services

LA = Large Aircraft, SA = Small Aircraft, H = Helicopter

Function	Frequency range	Transmit T Receive R	Transmitter Power	Number of Antennas	Polarisation	Antenna Position(see Fig 1.16 to 1.18)	Antenna Type
Voice Communication HF	3-25 MHz	T R	120 W	1-2	hor.	LA LA 1 to 4 LA 3/4 LA/SA 3	short stubs at wing tips long wire tail cap notch
Voice Communication VHF/FM	30-76 MHz	T R	10 W	1	vert.	LA 1 to 3 SA 2 H 2, 6	stub stub stub
VHF	118-136 MHz	T R	25 W	2-3	vert.	LA 1,2,(6),7,8 SA 2,(6),7,8 SA 5 H 1,2,6,7	stub stub slot stub
Voice Communication UHF	224-400 MHz	T R	50 W	2-3	vert.	LA 1,2,(6),7,8 SA 2,(6),7,8 SA 5 H 1,(2),7	stub stub slot stub
Data Communication (Telemetry)	225- 260 MHz 1435-1535 MHz 2200-2300 MHz 2400-2500 MHz	T R	100 W	1-2	vert./ hor.	LA 1,2,4,6,7,8 (1),4,(7),(8) SA 2,4,6,7,8 2,4,(6),7,8 5 H 1,(2),(6),7	stub 1/2 deer horn (Fig 1.10) stub 1/2 deer horn slot stub

The VHF communication band is used for preference in civil aviation whereas the UHF band is reserved for military applications. Both services are limited to line-of-sight links. For long range communication only the HF-band is applicable.

Tab 1.2 Aeronautical radio navigation services

LA = Large Aircraft, SA = Small Aircraft, H = Helicopter

Function	Frequency range	Transmit T Receive R	Transmitter Power	Number of Antennas	Polarisation	Antenna Positions(see Fig 1.16 to 1.18)	Antenna Type
Long Range Direction Finding(Loran)	1750-1950 kHz	R	-	1	vert.	LA 7	small loop short monopole
Direction Finding (ADF)	190-1750 kHz	R	-	1-2 loop	vert.	LA 1,2,7 SA 2,7 H 2,6,7	small loop short monopole
VOR (Bearing)	108-118 MHz	R	-	1-2	hor.	LA 1,4,(8) LA 5 SA 2,4,(8) SA 5	deer horn 2 half loops deer horn 2 half loops
ILS (Marker)	75 MHz	R	-	1-2	hor.	LA,SA,H6,7	1/2 deer horn
ILS(Localizer)	108-112 MHz	R	-	uses VOR-Antennas	hor.	same as VOR	same as VOR
ILS (Glide Path)	329-335 MHz	R	-	1-2	hor.	LA,H9 LA,SA,H same as VOR	half loop same as VOR
DME/TACAN (Distance/ Bearing)	962-1214 MHz	T R	1kWpeak	1-2	vert.	LA 1,2,4,6,7,8 SA 2,4,6,7,8 SA 5 H 1,(6),7	stub stub slot stub
GPS (NAVSTAR)	1575 MHz	R	-	1	circ.	LA 1,2 SA 2 H (1),2	spiral/ microstrip patch
Radio Altimeter	4.2-4.4 GHz	T R	1W	1-2 T 1-2 R	hor.	LA,SA 7,8 H 6,7	horn horn
Doppler Navigator	8.8 GHz	T R	1W	1-2	hor.	LA,SA 7,8 H 6,7	slot slot
MLS (Replacing ILS in Future)	5-5.25 GHz	R	-	2-4	vert.	LA 9 LA 1,4,8 SA 4,8 H 1,7	horn stub stub stub

The aeronautical radio navigation services listed in Tab 1.2 are used worldwide in civil and military aviation although VOR/ILS is primarily designed for civil applications and TACAN for military purposes.

The services for identification of civil and military aircraft are presented in Tab 1.3.

Tab 1.3 Aeronautical identification services

Function	Frequency range	Transmit T Receive R	Transmitter Power	Number of Antennas	Polarisation	Antenna Positions(see Fig 1.16 to 1.18)	Antenna Type
Secondary Radar Transponder	1030/1090 MHz	T R	1KWpeak	1-2	vert.	LA (6),7,8 SA (6),7,8 H 7	stub stub stub
IFF (military)	1030/1090 MHz	T R	1KWpeak	1-2	vert.	LA 1,2,(6),7,8 SA 2,(6),7,8 H (2),7	stub stub stub

1.2.2 Types of Antennas

Antennas can be classified into single radiating elements, arrays of such elements and reflector or lens type antennas, which can use single radiating elements or arrays as excitation sources. With a few exceptions aircraft antennas require wide angular coverage, which can be achieved only by single radiating elements, and these are generally used.

The basic elements used for aircraft antennas are the dipole, the loop and the slot. Most other types of aircraft antennas for wide angular coverage are derived from these basic elements.

The dipole and its radiation patterns in 3 orthogonal planes are illustrated in Fig 1.6. Omnidirectional coverage is achieved only in the y-z plane. In the two other planes the beam width depends on the ratio between the length of the antenna and the wave length: If the length of the dipole is short compared to the wavelength the beam width is 90°, a half-wavelength dipole has a beam width of 78° and a full-wavelength dipole a width of 47°. Still longer dipoles will produce additional side lobes, which are not acceptable in most aircraft applications.

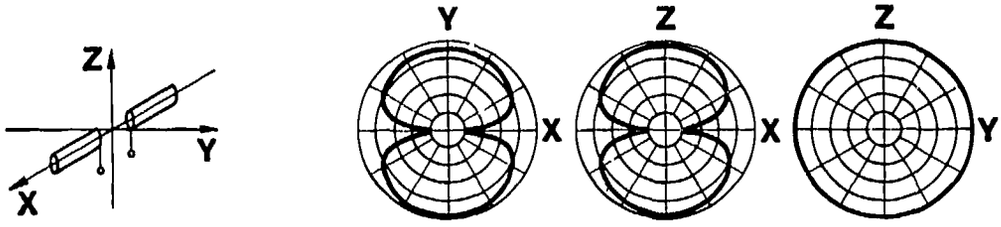

Fig 1.6 The dipole and its radiation patterns

The patterns of a small loop antenna, with a circumference which is much smaller than the wavelength, are the dual of the short dipole and are shown in Fig 1.7. The pattern is omnidirectional in the plane of the loop, and if the circumference is enlarged to a full wavelength, the pattern becomes omnidirectional in the y-z plane (see Fig 1.6) (i.e. perpendicular to the plane of the loop).

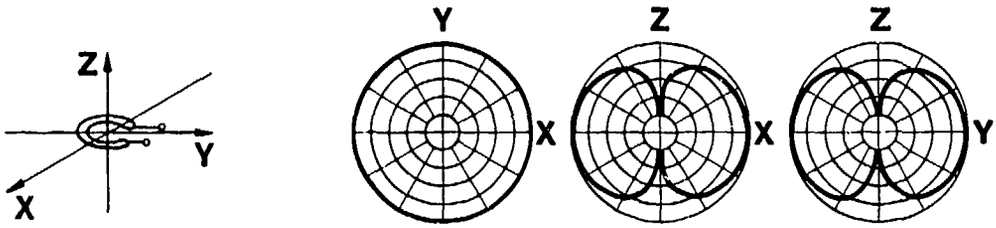

Fig 1.7 The small loop and its radiation patterns

Fig 1.8 represents an antenna which consists of a linear slot in an infinite flat metallic sheet. If the slot is cut in a sheet of finite dimensions, the x-y plane pattern will change drastically, because the fields on the two sides of the plane are equal in magnitude but opposite in phase. Hence there is a null in all directions in the plane of the sheet, and therefore in the x direction of the x-y plane pattern of Fig 1.8.

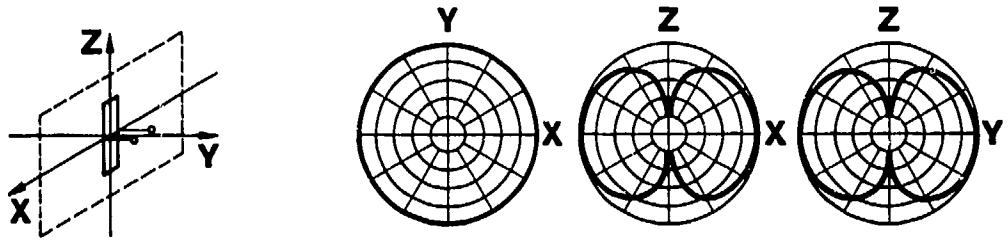

Fig 1.8 The linear slot and its radiation patterns

The aircraft antenna most frequently used is the stub illustrated in Fig 1.9, which is a monopole fed against a ground plane (the airframe). With an infinite flat ground plane the radiation pattern is identical with half the pattern of a dipole. A finite ground plane causes spillage of radiation into the hemisphere behind the plane.

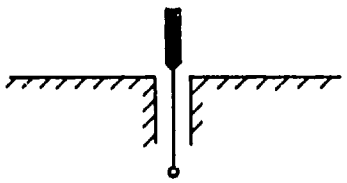

Fig 1.9 Stub antenna

Another antenna derived from the dipole is the deer-horn antenna (Fig 1.10). Its radiation pattern is very dependent on the slope of the bent-back arms. The main difference in the radiation characteristic is in the plane of the elements, where the dipole nulls are filled in by radiation from the bent portion of the conductors. This antenna is sometimes used in an asymmetrical configuration similar to the stub antenna mentioned above. Short asymmetrical deer-horn antennas are often tuned to a particular frequency by a capacitor at the open end of the conductor.

Fig 1.10 Deer-horn antenna

A half-loop antenna operating against an infinite ground plane (Fig 1.11), produces patterns nearly identical, in half-space, to the patterns of Fig 1.7. If the ground plane is of finite dimensions energy is spilled into the hemisphere behind the plane.

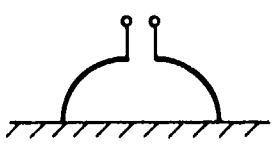

Fig 1.11 Half-loop antenna

Most linear slot antennas used on aircraft are operated with a backing resonant cavity (see Fig 1.12), which limits radiation to one hemisphere and eliminates radiation inside the airframe.

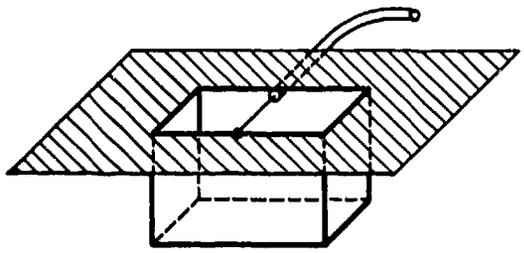

Fig 1.12 Cavity backed slot antenna

The annular slot antenna of Fig 1.13 can be regarded as a top loaded stub antenna retracted into a circular cavity. Its radiation pattern is the same as that of a short half dipole or stub.

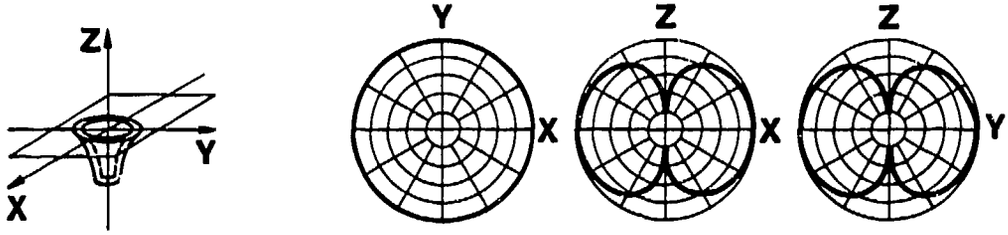

Fig 1.13 Annular slot antenna

In aeronautical microwave applications, especially if larger bandwidths have to be covered, spiral antennas over absorbing sheets, or cavity backed spirals are useful. Fig 1.14 illustrates the mechanical configuration and radiation patterns of a spiral antenna.

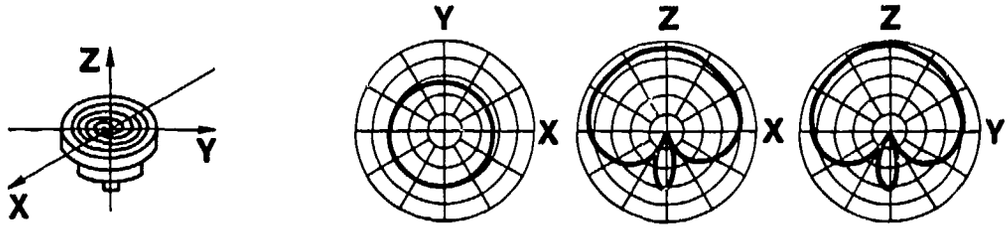

Fig 1.14 Cavity backed spiral antenna

If higher directivity is desired, horn antennas may be used, the basic radiation characteristic of which is shown in Fig 1.15.

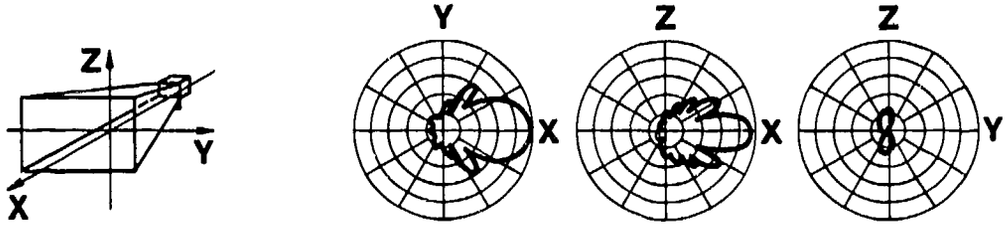

Fig 1.15 Horn antenna

For microwave applications microwave-patch antennas are coming into general use. They consist of a thin dielectric layer on one side plated with specially shaped conducting areas. The other side must be attached to a conducting surface. For aeronautical applications the thin, flat shape is a great advantage. The principle is that discontinuities in the conducting areas (curves, bends, T junctions, changes in conductor width) will radiate electromagnetic energy, especially if the dimensions of the discontinuities are of the order of the wave length. By choosing different shapes for the discontinuities, several types of antennas can be made, especially medium-gain antennas (gain up to 10 dB).

The last columns of Tables 1.1, 1.2 and 1.3 indicate which types of antennas are most commonly used for the services listed there.

1.2.3 Antenna Positioning

The radiation patterns of the different types of antennas discussed in the previous section are degraded to some extent if the antennas are mounted on an aircraft, since energy is reflected or diffracted by the wings, fuselage and tail fin and, to a lesser degree, by smaller assemblies such as the undercarriage, flaps and other antennas. In addition, the performance of antennas on military aircraft suffers when supplementary tanks, ECM-pods, weapons and other stores are mounted below the fuselage or wings.

It is always a problem of optimization to find an antenna position where the deterioration of the antenna's principal radiation pattern is minimized, at least in that section of the sphere where the probability of receiving is high. Moreover those sections of the sphere in which long distance links must be made are most critical. Hence positioning of aircraft antennas requires much experience and investigation when a new aircraft type is developed. Nevertheless, there are certain areas on the aircraft structure where, in general, antennas for the different radio aids give the best results.

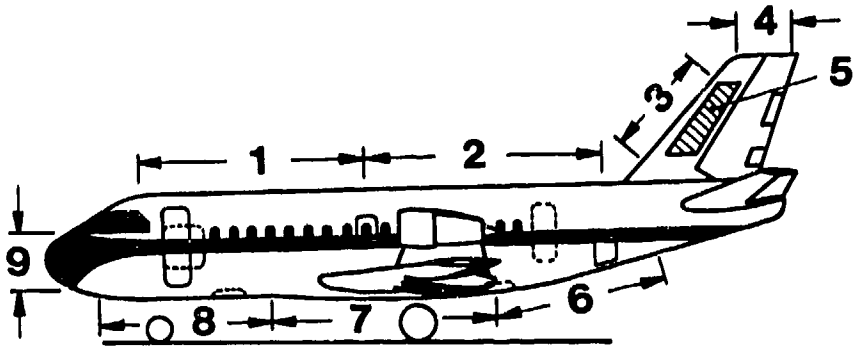

Fig 1.16 Antenna positioning areas (large aircraft)

The surface of a large aircraft can be divided into 9 different areas for antenna positioning, as shown in Fig 1.16. On a small aircraft (Fig 1.17), area 1 is not usable because it is occupied by the cockpit and area 9 is normally not available because of other utilizations e.g. by the engine, or by weapons if military aircraft are considered. The usable surface of a helicopter (Fig 1.18) is even smaller. Antennas positioned in areas 1 and 2 suffer from reflections from the rotor. Areas 5 and 6 are shadowed by the fuselage in the forward direction, which limits the frequency range of antennas in this areas to VHF (UHF), and area 7 is the only one with no severe restrictions.

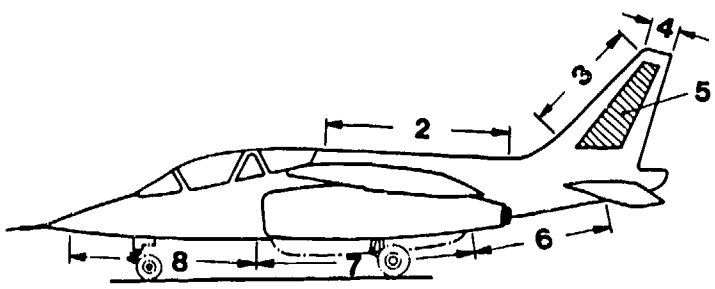

Fig 1.17 Antenna positioning areas (small aircraft)

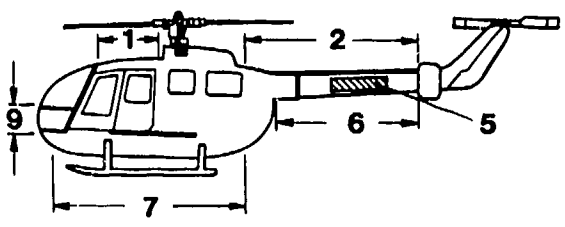

Fig 1.18 Antenna positioning areas (helicopter)

Tables 1.1,1.2 and 1.3 list the different aeronautical radio aids and the viable antenna positioning of the prefered types of antennas. Positions are given for large aircraft (LA), small aircraft (SA) and helicopters (H).

1.2.4 Configuration of Aircraft

Every deformation of the outer contour of an aircraft influences to a certain degree the radiation patterns of the antennas, which form part of the radiating structure. This includes all sections, which can be "seen" from the location of the antenna. For this reason aircraft ARP are first measured in a "clean" configuration and then in one or more altered configurations, where for example landing flaps and/or the undercarriage are in the landing position. The antennas of radio aids which are not used during the approach and landing phase of course need not be measured in the landing configuration.

In addition military aircraft, especially fighters, usually carry weapons and fuel tanks as outer stores, which leads to many different configurations to be considered for ARP measurements. In order to keep down the number of patterns to be measured, a careful study of the interactive effects should be made before planning the test program. Here earlier model measurements can save many flight test hours during dynamic measurements.

Frequently even control surface deflections can influence the ARP of antennas mounted only a few wavelengths away. As an example Fig 1.19 illustrates the radiation pattern of a VHF navigation antenna for VOR and ILS reception. This antenna, a deer-horn type (Fig 1.10), is mounted in position area 5 of a small aircraft (see Fig 1.17). A scaled model measurement of this antenna indicated by the dotted line in Fig 1.19 shows excellent symmetry of the ARP (Ref 13). The dynamic in-flight measurement (solid line) illustrates certain ARP asymmetries in the area of $\Phi \approx 40°$ and $\Phi \approx 220°$ (Ref 14). The reason is, that this pattern is measured during a skidded turn of the aircraft, where the control surface of the vertical stabilizer has a large deflection and affects the radiation characteristics of the nearby antenna.

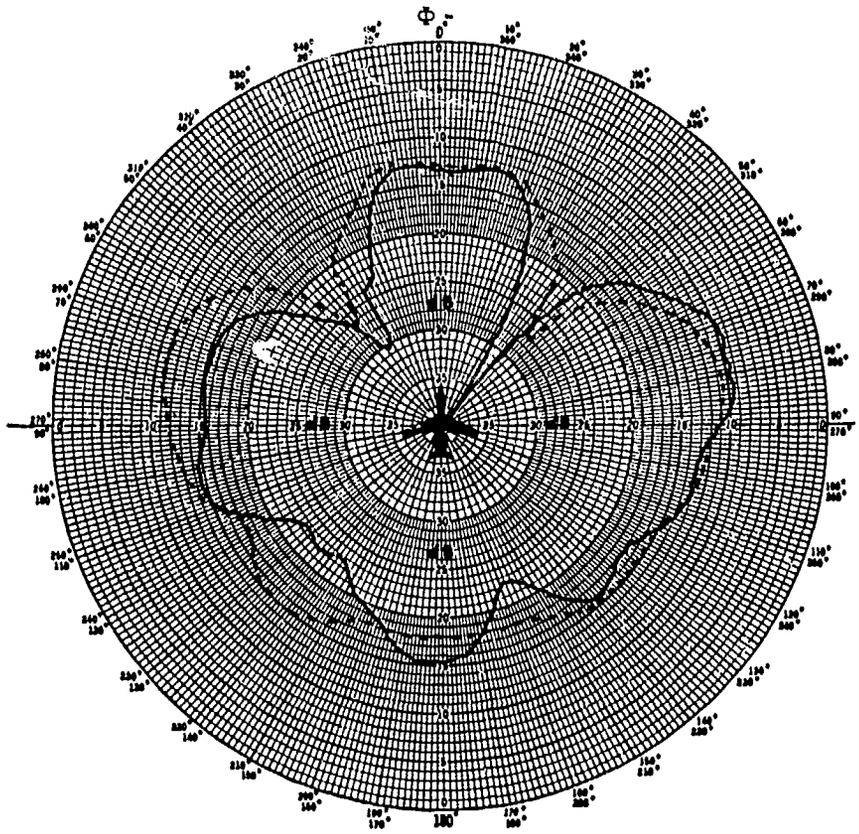

Fig 1.19 Radiation pattern of a VHF-navigation antenna at 114 MHz ..... scaled model measurement ——— dynamic (in-flight) measurement

1.3 THE DETERMINATION OF THE ARP BY MATHEMATICAL MODELLING

1.3.1 Advantages and Disadvantages

Modern high-speed computers with large storage capacity have made possible the theoretical calculation of the ARP of antennas mounted on complex structures such as aircraft or helicopters.

The main advantage of this mathematical method is that, once the shape of the vehicle has been rerepresented in the computer, the influence of different positions of the individual antennas can be easily evaluated. If the position of an antenna has been selected on the basis of a computer evaluation, the number of measurements can be cut down to a minimum.

Disadvantages are that the shape of the vehicle can only be modelled approximately and that surface parameters such as conductivity and susceptibility are only roughly known. Therefore, the calculated results may contain errors and can only be considered as approximated patterns which usually have to be supplemented by full-scale measurements, either statically on ground ranges or by in-flight measurements.

Two different theoretical ARP-computation methods have been developed: the integral equation method and the geometrical theory of diffraction method. Which method must be used will depend on the size of the vehicle compared to the wavelength of the antenna under consideration.

1.3.2 Integral Equation Method

The integral equation method is based on the determination of the surface currents, from which all necessary electromagnetic parameters can be calculated. The vector wave equations are transformed, by means of the second Greens theorem, into two independent equations, the Electric Field Integral Equation and the Magnetic Field Integral Equation. Ref 15 shows that the surface current density depends on the electric field and the magnetic field of the incoming wave from the feed point. Integration must be carried out over the surface of the ideally conducting body of the vehicle under test. The application of the Electric or Magnetic Field Integral Equation depends on the shape of the model surface.

The solution of the integral equations must be obtained by numerical methods (Ref 16). For practical applications, especially for complex structures such as aircraft or helicopters, wire grid modelling allows further simplification of the integral equations. The surface of the device under test is then approximated by a wire grid, as shown in Fig 1.20. Experience has shown that about 100 segments per square of the wavelength are necessary to achieve comparable results between measured and calculated patterns. After the determination of the wire currents, Kirchhoff's laws are applied to the wire junctions.

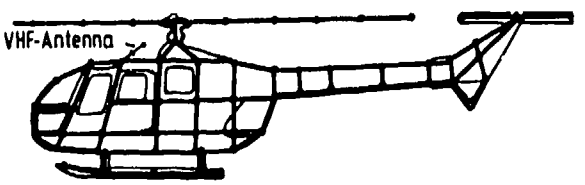

Fig 1.20 Wire-grid model of the helicopter BO 105

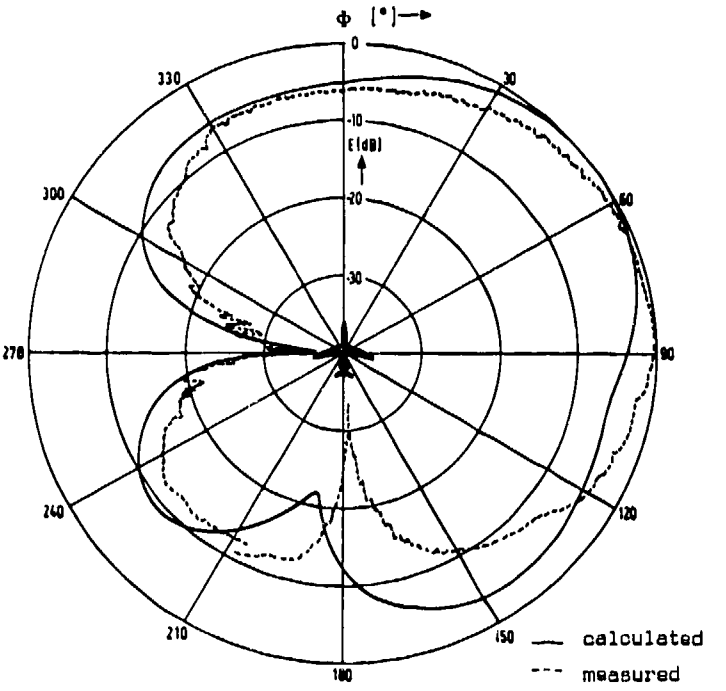

Fig 1.21 Calculated and measured radiation pattern of a VHF antenna of the helicopter BO 105 (Fig 1.20) Frequency 117.6 MHz

At the Institute for Radio Frequency Technology of DFVLR, Germany, the radiation pattern of a VHF antenna mounted on top of a BO 105 helicopter (see Fig 1.21) has been calculated by this method and was compared to the radiation pattern measured in flight (Ref 17). It was necessary to model in great detail only the upper part of the helicopter, including the rotor shaft.

1.3.3 Geometrical Diffraction Method

In the case where the aircraft is large compared to the wavelength, the subject is not totally excited and only currents of certain surface elements contribute to the total field at the point of observation. In this case the geometrical theory of diffraction can be applied with success. The complicated shape of the aircraft is divided into a number of canonic forms, for which diffraction coefficients are known.

All possible rays significantly contributing to the field must be considered and summed at the observation point, and multiple reflections and diffractions must be taken into account. As an example some important rays contributing to the radiation pattern of an antenna on the upper side of the fuselage of an aircraft are illustrated in Fig 1.22.

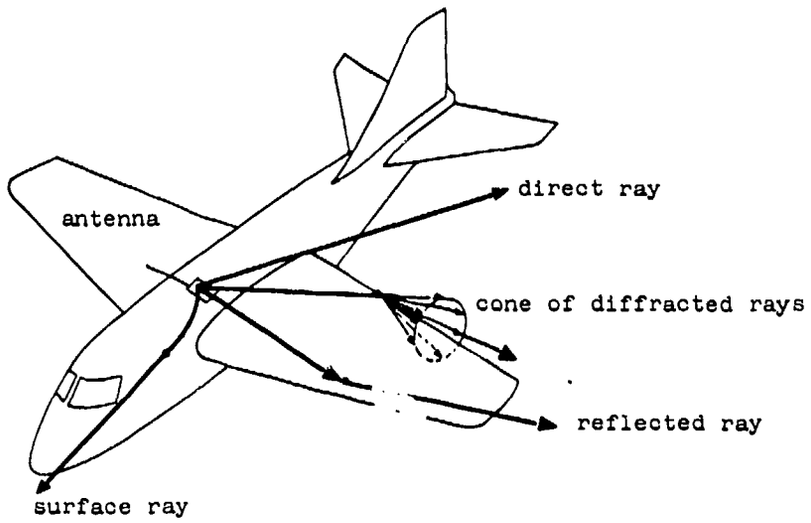

Fig 1.22 Examples of different rays on aircraft surface and edges

After all possible ray paths have been determined, the total field can be computed if the individual reflection-, diffraction- and launch coefficients, the attenuation constant and the divergence coefficient can be obtained. The canonic forms applied to aircraft antenna radiation pattern calculations are the diffraction on curved edges, corners, stubs, half planes and on smoothly curved surfaces. A detailed treatment of this method with a presentation of the individual equations is outside the scope of this volume, the reader is referred to Ref 8, a presentation of the principle of the geometrical theory of diffraction, and to Ref 9, which treats the field computation by the geometrical theory of diffraction.

A few results of a comparison between calculated patterns and patterns obtained from sub-scale model measurements are reported in Ref 10. As an example Fig 1.23 illustrates the differences between the calculated and the measured radiation pattern of a VHF antenna, determined in the roll plane of a HFB 320 aircraft.

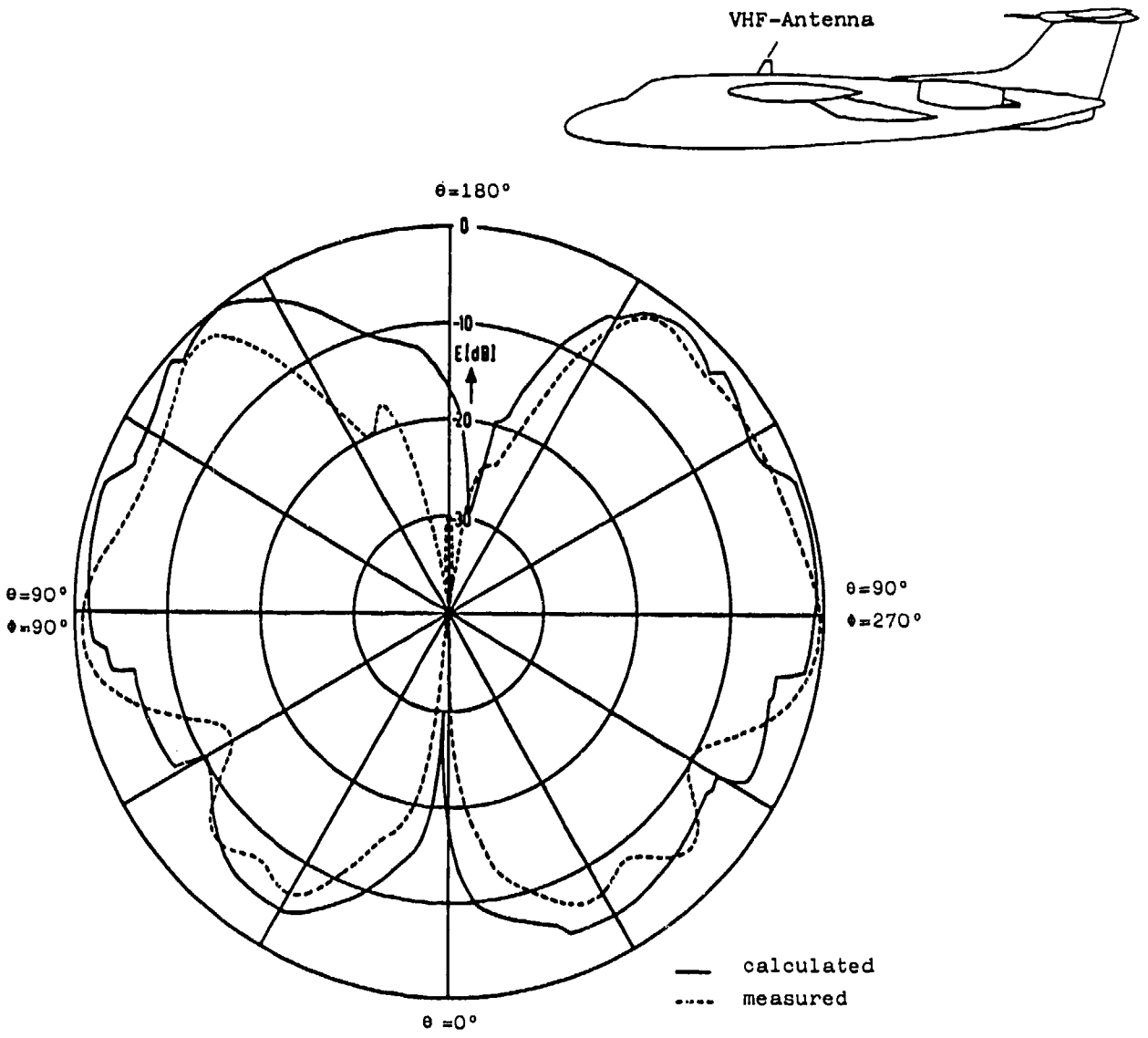

Fig 1.23 Calculated and measured radiation pattern of a VHF antenna in the roll plane of a HFB 320 aircraft

1.4 THE DETERMINATION OF ARP OF FULL-SIZE AIRCRAFT IN FLIGHT

1.4.1 Advantages and Disadvantages

During in-flight measurements of ARP the aircraft antenna under test is part of an air-to-ground radio link. The aircraft flies selected manoeuvres in front of the ground antenna, whereby the following parameters are recorded:

- if the transmitter is on board the aircraft, the transmitted power, if the receiver is on board, the received power
- the (transmitted or received) power at the ground station
- the position of the aircraft relative to the ground station
- the attitude angles of the aircraft.

The gain of the aircraft antenna must then be calculated from the range equation Eq (1.9). The flight trajectory for these tests must be chosen carefully to ensure that the other parameters in the equation remain as well as possible constant and can be calculated with the maximum accuracy. The optimum trajectories are discussed in Section 1.4.3.2.

The advantage of this method is that the antenna gain is measured under actual conditions, without any errors due to modelling imperfections. The effect of moving parts, such as propellers, helicopter rotors and stabilizing rotors is fully taken into account. Measurements of this kind are necessary for the certification of new aircraft types, even if model calculations and model measurements have been carried out.

The main disadvantage of this method is the high cost of the flying hours that are required. For that reason the flight tests usually are the final stage of a long process of modelling. Additional problems of the in-flight measurements are:

- the flight characteristics of the aircraft limit the choise of aspect angles at which measurements can be made
- the effect of ground reflections my vary considerably during the flight tests and it is difficult to eliminate these effects.

The effects of these disadvantages can be reduced by careful planning of the trajectories flown during the tests, as is described below.

1.4.2 The Air-Ground Propagation Channel

In a free space radio-frequency link with an isotropic radiator as a transmitting antenna which has no preferred direction of radiation, the power density S_r at the receiver at a distance r is

$$S_r = \frac{P_T}{4\pi r^2} \tag{1.1}$$

where P_T is the transmitted power and $4\pi r^2$ is the total surface of the sphere on which the power density S_r is measured. If the transmitting antenna radiates in a preferred direction, the ratio of the maximum power density to that of an isotropic radiator with the same total output power is called the gain G_T of the transmitting antenna, and S_r becomes

$$S_r = \frac{P_T \cdot G_T}{4\pi r^2} \tag{1.2}$$

If the receiving antenna has an area A_R, the received power P_R can be expressed as

$$P_R = S_r \cdot A_R \tag{1.3}$$

The following relation between effective area A, gain G and wavelength λ applies to all antennas:

$$\frac{A}{G} = \frac{\lambda^2}{4\pi} \tag{1.4}$$

Equations (1.2) and (1.3) can be combined as

$$\frac{P_R}{A_R} = \frac{P_T G_T}{4\pi r^2} \tag{1.5}$$

and, introducing Eq (1.4) with the gain of the receiving antenna G_R

$$\frac{P_R}{G_R} = \frac{P_T \cdot G_T}{4\pi r^2} \cdot \frac{\lambda^2}{4\pi} \tag{1.6}$$

As $\lambda = c/f$ where c = velocity of light and f = frequency, Eq (1.6) can be written as

$$\frac{P_R}{P_T} = \frac{G_R\, G_T}{(4\pi r)^2} \quad \frac{c^2}{f^2} \tag{1.7}$$

Eq (1.7) can be rewritten as a "gain-loss" equation and can be completed by including a ground reflection multipath gain G_M and general losses L, e.g. cable losses.

$$P_T \cdot G_R \cdot G_T \cdot G_M = P_R \cdot f^2 \cdot r^2 \cdot \left(\frac{4\pi}{c}\right)^2 \cdot L \tag{1.8}$$

In logarithmic units of measure this becomes

$$P_T + G_T + G_R + G_M = P_R + L + 20 \log r + 20 \log f + 2.54 \text{ dB} \tag{1.9}$$

It is

P_T = output power of transmitter in dBW (dB above 1 W)

G_T = gain of transmitting antenna in dB

G_R = gain of receiving antenna in dB

G_M = gain of reflecting ground in dB

P_R = input power of receiver in dBm (dB above 1 milli Watt)

L = line losses (between power measuring terminals and antennas) in dB

r = distance between transmitting and receiving antenna in km (if the distance is measured in NM, the last term (2.54 dB) must be replaced by 7.8 dB)

f = transmitting frequency in MHz

The basic transmission loss designated by the right-hand side of Eq (1.9), depends very much on the geometrical relationships between the transmitting and receiving antennas and the earth below, as discussed in more detail in section 1.4.5.2. According to Ref 11 the airspace above the earth may be separated into three different regions: the line-of-sight, the diffraction and the scatter region. Due to its stable, predictable propagation condition only the line-of-sight region, which offers a direct path between the two antennas, is suitable for in-flight antenna measurements. The separating line which limits the line-of-sight region can easily be derived from Fig 1.24:

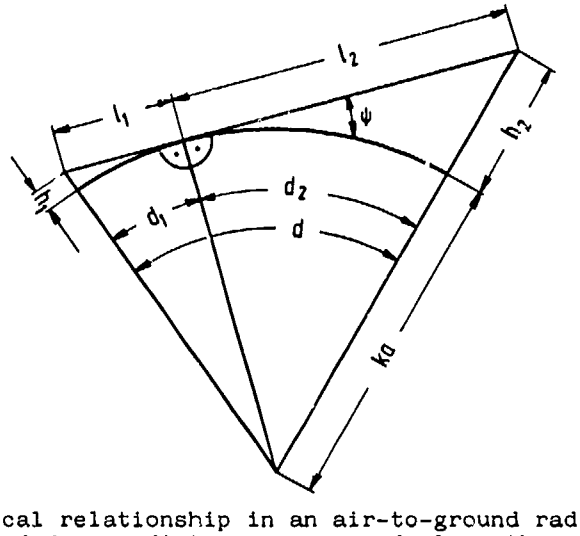

Fig 1.24 Geometrical relationship in an air-to-ground radio link
(d, d_1 and d_2 are distances measured along the surface of the earth)

$$r = l_1 + l_2 = \sqrt{(ka+h_1)^2 - (ka)^2} + \sqrt{(ka+h_2)^2 - (ka)^2} \qquad (1.10)$$

l_1 and l_2 are the distances from the antennas to the radio horizon, h_1 and h_2 are the antenna heights, a is the radius of earth (a = 6365 km), and k = 4/3, a factor which corrects for refraction, assuming that rays are straight lines but that the earth has a radius 4/3 times as large as its actual value. To evaluate Eq (1.10) accurately requires a high computational accuracy. For practical applications where l_1 and l_2 are computed by a pocket calculator the problem can be reformulated using the trianlge sine rule in order to eliminate squares and roots. It is

$$l_1 = (ka + h_1) \sin \cos^{-1}\left(ka/(ka + h_1)\right)$$
$$l_2 = (ka + h_2) \sin \cos^{-1}\left(ka/(ka + h_2)\right)$$

Fig 1.25 shows the limits of the line-of-sight region for different antenna heights h_1 and h_2.

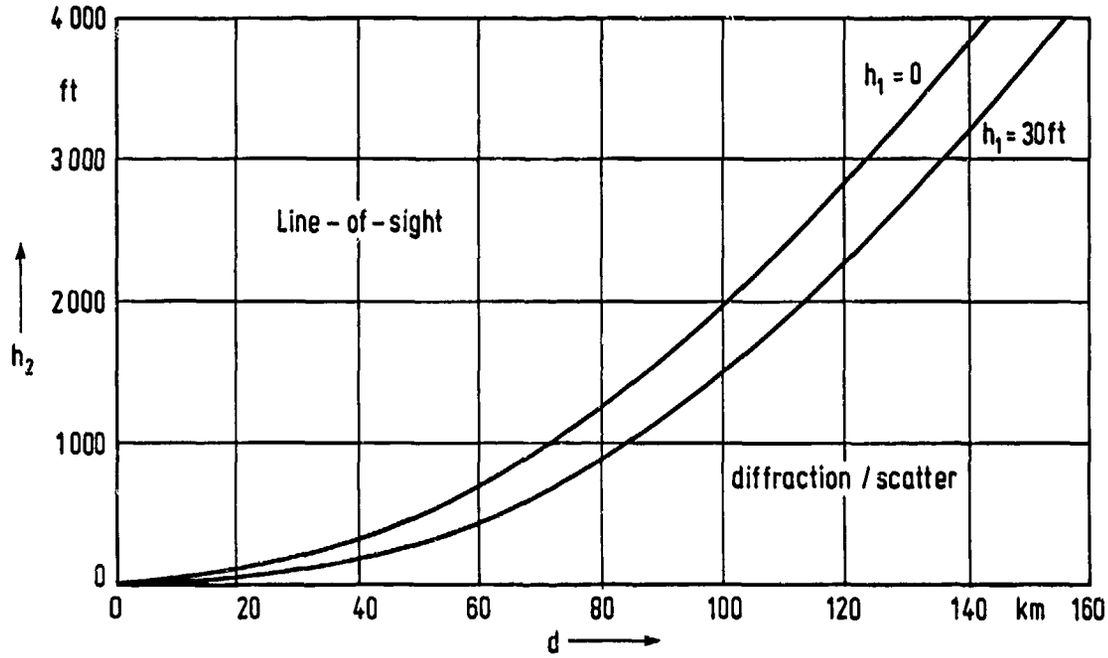

Fig 1.25 Different regions of radio wave propagation

As mentioned above, the ARP (i.e. the variation of the gain of the antenna under test) is determined from the output signal of the receiver in the radio link set up for the test. Because the dynamic range of the received signal is large, the receiver must have a logarithmic characteristic, or an automatic gain control circuit.

As a consequence of the reciprocity theorem of antennas the transmitting and receiving patterns of an antenna are the same. It, therefore, makes no difference whether the antenna under test is the transmitting or receiving antenna in the radio link set up for pattern measurements. Up to frequencies of several GHz the transmitter is usually smaller and weighs less than the receiver. Therefore it is convenient to mount the transmitter in the aircraft. At much higher frequencies the transmitting equipment becomes heavy and voluminous. Then the receiver is usually mounted in the aircraft, and either on-board pattern recording is used, or a telemetry system must transmit the measured signal to a ground processor.

The transmission equation (Eq 1.8) contains two parameters which usually alter the recorded antenna gain signal and therefore have to be compensated by computation.

1. The variation of the received signal due to a change of the distance r of the aircraft to the ground station has to be compensated by multiplying the losses by r^2.

2. The ground reflection multipath gain G_M has to be considered.

This term is investigated in more detail in section 1.4.5. If possible, distance, flight level and receiving antenna height should be chosen such that G_M remains nearly constant during the test flight pattern.

1.4.3 Aspect Angle Determination and Flight Profiles

1.4.3.1 Aspect Angle Determination

As mentioned in section 1.1.3 the radiation direction of an aircraft antenna with respect to a receiving station is defined by the aspect angle illustrated in Fig 1.1. To determine the aspect angle during tests, the following parameters have to be considered:

Location of the ground station
Location of the aircraft
Attitude (pitch, roll and heading) of the aircraft
Earth curvature

In a plane system where the earth curvature is neglected, the aircraft and ground antennas are at almost the same elevation and the pitch and roll angles of the aircraft are small, the determination of the horizontal aspect angle is very simple. As shown in Fig 1.26, the horizontal aspect angle Φ_A becomes

$$\Phi_A = 180° - \beta_A - \Psi \qquad (1.11)$$

if Ψ is the heading angle of the aircraft under test and β_A = 360° - the azimuth angle of the aircraft as seen from the ground system. If the aircraft is tracked from the ground station, β_A can be measured directly. If no such tracking equipment is available at the ground station, β_A must be calculated from the outputs of radio-navigation or inertial systems on board the aircraft (see e.g. Ref 12).

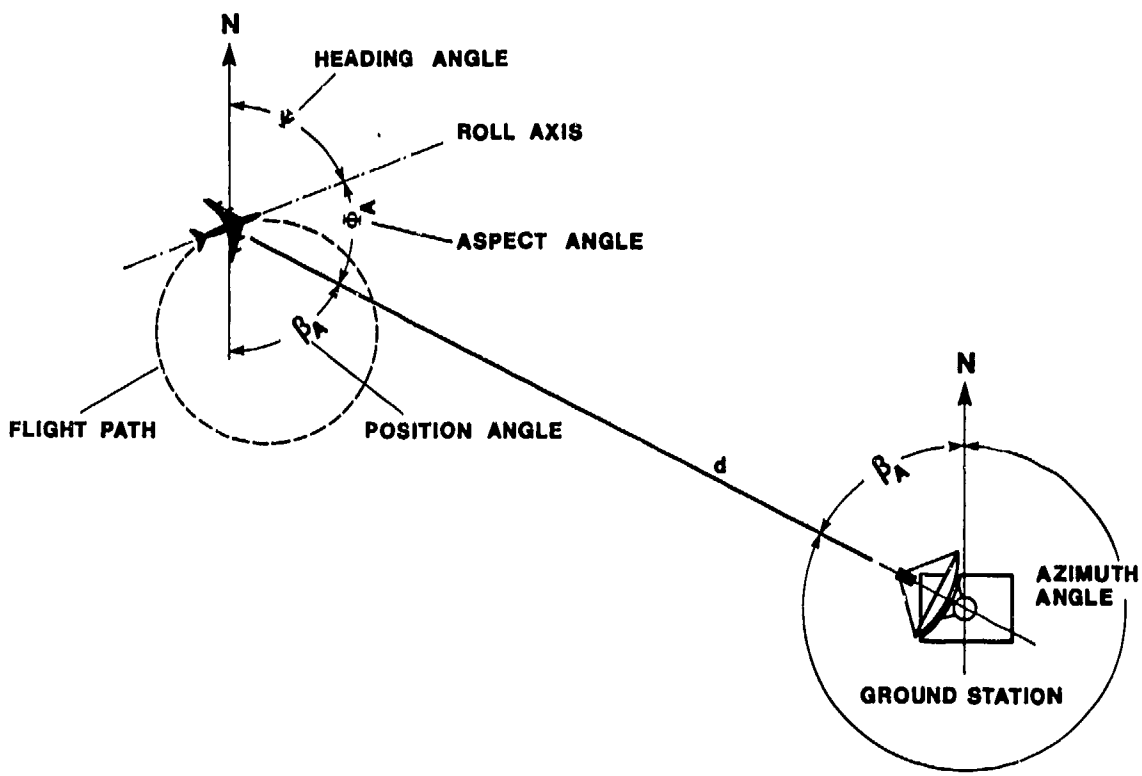

Fig 1.26 Determination of the horizontal aspect angle

The determination of the vertical aspect angle Φ_E is very simple if the test flight is conducted in a vertical plane which also intersects the ground station (Fig 1.27). The vertical aspect angle Φ_E then becomes

$$\Phi_E = \beta_E + \theta \tag{1.12}$$

where θ is the pitch angle of the aircraft. The position-dependent angle β_E equals the elevation tracking angle of the ground system ρ_E. Again β_E can also be computed from available on-board information, derived from radio or inertial navigation equipment and altitude measurements (see Ref 12).

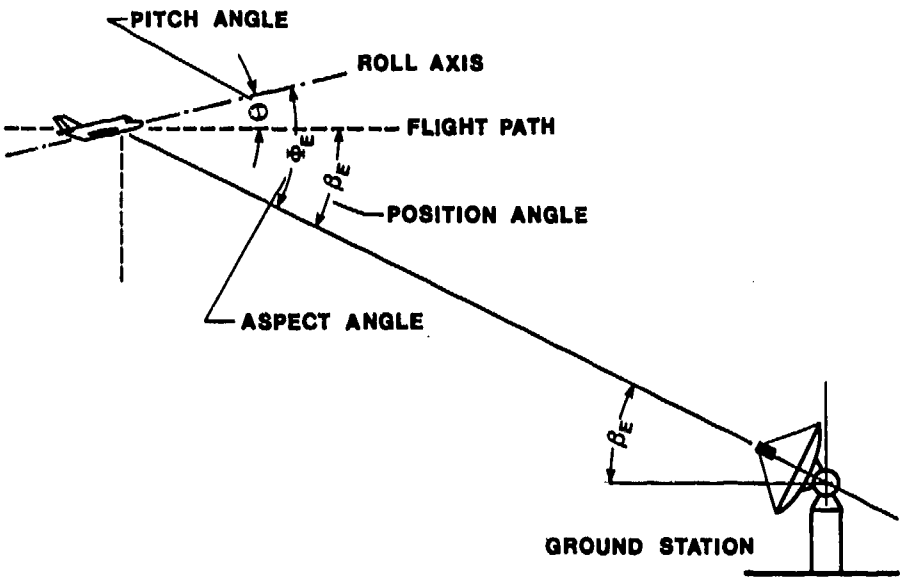

Fig 1.27 Determination of the vertical aspect angle

If the above-mentioned restrictions apply, Eqs (1.11) and (1.12) are useful for the determination of the horizontal and vertical aspect angle. However in many of the flight profiles discussed in the next section the horizontal and vertical position angle vary simultaneously. Also many flight profiles require changes of the angle of roll which influence the horizontal aspect angle.

A universal equation, which takes account of all parameters necessary to compute the two components of the aspect angle Φ_A and Φ_E in the general case, is derived in Appendix 1.B In many applications the simplified equations, Eqs (1.14) or (1.21) and Eq (1.15), are used for on-line data processing and quicklook possibilities or to save computing time.

The angle of the earth curvature θ_E for a horizontal distance d between the aircraft and the ground station is given by

$$\theta_E = \tan^{-1}\left(\frac{d}{a}\right) \tag{1.13}$$

The earth radius averages 6365 km, so θ_E stays below 0,9° if the distance d is limited to 100 km. Therefore the earth curvature has to be considered only if measurements require high angular accuracy. If θ_E is neglected, then the error in Φ_E is of the order of θ_E. In the component Φ_A the effect usually is smaller, except when the angle of roll of the aircraft ϕ exceeds 15° and simultaneously Φ_A approaches 45°, 135°, 225° or 315°.

If the earth curvature is neglected, the conditional equations for Φ_A and Φ_E as given in Appendix B, Eq (1.B11) and Eq (1.B12) reduce to

$$\Phi_A = \tan^{-1}\left(\frac{A_y}{A_x}\right) \tag{1.14}$$

$$\Phi_E = \tan^{-1}\left(\frac{-A_z}{\sqrt{A_x^2 + A_y^2}}\right) \tag{1.15}$$

where

$$A_x = -\cos\beta_E \cos(\Psi-\rho)\cos\theta - \sin\beta_E\sin\theta \tag{1.16}$$

$$A_Y = \cos\beta_E (\sin(\Psi-\rho)\cos\phi - \cos(\Psi-\rho)\sin\theta\sin\phi) + \sin\beta_E\cos\theta\sin\phi \tag{1.17}$$

$$A_Z = -\cos\beta_E (\cos(\Psi-\rho)\cos\theta\cos\phi + \sin(\Psi-\rho)\sin\phi) + \sin\beta_E\cos\theta\cos\phi \tag{1.18}$$

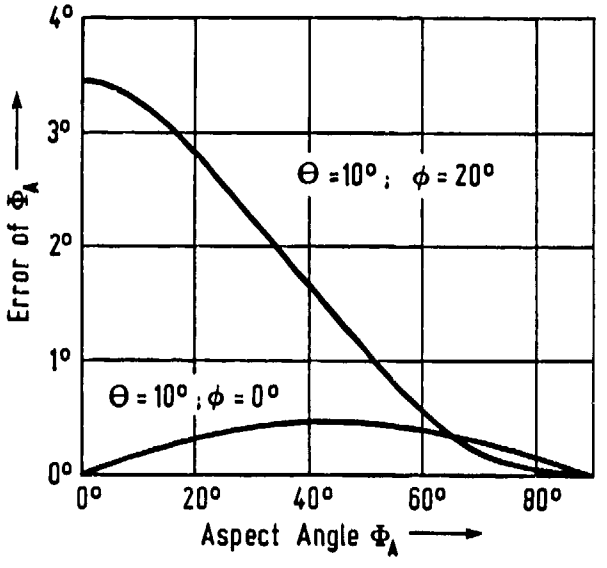

Fig 1.28 Error in the horizontal aspect angle Φ_A if it is not corrected for pitch angle θ (ϕ = angle of roll)

Further simplification is possible if the pitch angle remains small during the test flights. Fig 1.28 illustrates the error of horizontal aspect angle Φ_A, if a pitch angle of 10° is neglected in the computation of Φ_A. The error increases with the angle of roll ϕ. If test flights are performed at low altitudes or large distances from the ground station, so that the vertical position angle β_E also does not exceed 10°, Eq (1.16) and Eq (1.17) can be further reduced to

$$A_x = -\cos(\Psi-\rho) \tag{1.19}$$

$$A_y = \sin(\Psi-\rho)\cos\phi \tag{1.20}$$

and the horizontal aspect angle Φ_A becomes after Eq (1.14)

$$\Phi_A = \tan^{-1}\left(\frac{\tan(\Psi-\rho)}{\cos\phi}\right) \tag{1.21}$$

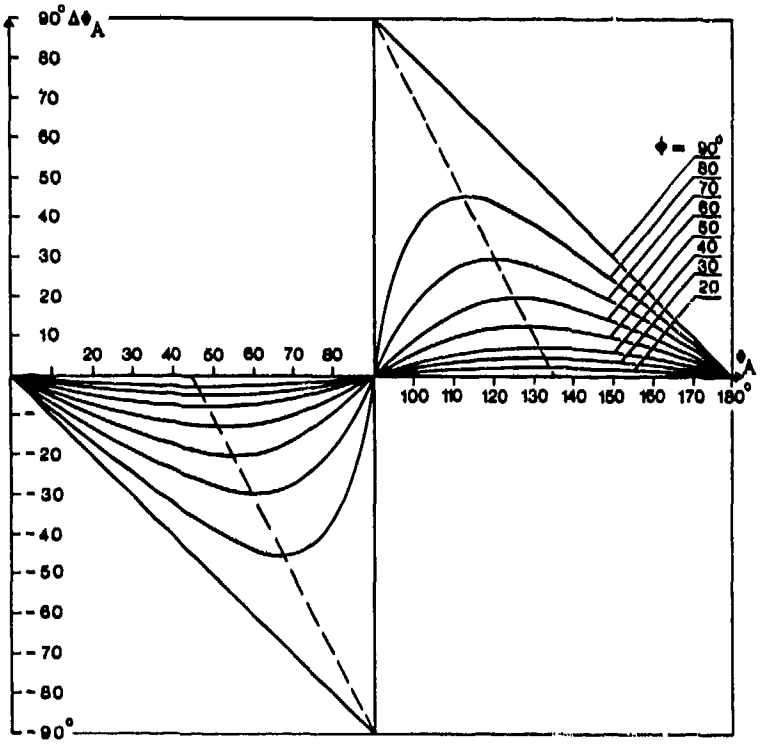

Fig 1.29 Error $\Delta\phi_A$ of horizontal aspect angle ϕ_A if it is not corrected for roll angles ϕ

As Fig 1.29 illustrates, a correction of the horizontal aspect angle ϕ_A as a consequence of roll angle variations is not always necessary. If the roll angle can be limited to a maximum of 20°, the maximum error does not exceed 3.2°.

1.4.3.2 Flight Trajectories for Dynamic ARP Measurements

When measuring an ARP it is not usually necessary to cover the whole sphere above and below the antenna under test. The aspect angle zone of interest depends very much on the manoeuverability of the aircraft and on the kind of radio aid under consideration. Once the angular range to be covered by the measurements is defined, the flight profiles can be selected. Continuous flight trajectories which allow complete continuous radiation pattern recordings are very efficient with respect to flying time and data processing. Such profiles also provide excellent quick-look opportunities if the received power is recorded as a function of the variable angle, e.g. heading. Unfortunately, certain angular areas of the sphere can not be covered by continuous flight trajectories, and measuring requirements may call for additional discontinuous flight trajectories.

The flight test trajectories for ARP can be divided into two main categories, straight trajectories, usually with constant attitude and height, and curved trajectories which always require attitude variations and sometimes also height variations.

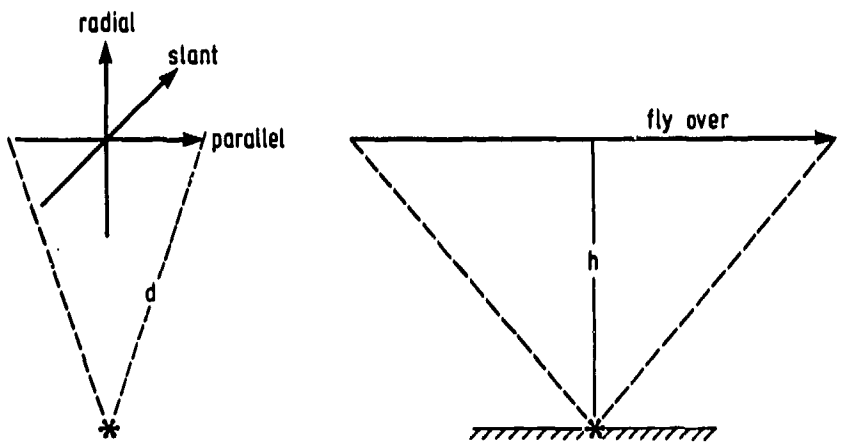

Fig 1.30 Straight flight test trajectories for ARP measurement
d = distance; h = height

The straight trajectories illustrated in Fig 1.30 are very simple to fly, because attitude and height remain constant during the profile, preferably controlled by an autopilot. No complex attitude measuring system and data recording or transmitting system are necessary on board the aircraft. On the other hand one parallel flight provides only part of the data required for a complete 360° polar antenna trajectories plot. It must be supplemented by additional slant and radial flights, and the total flight time is very high. If, in addition, a large range of depression angles must be covered, the same profiles must be flown at different heights, which further increases flight time.

While radial, slant and parallel flights are suitable for horizontal antenna pattern measurements, the fly-over trajectory is better suited to vertical antenna patterns, at least for those below the fuselage of the aircraft. A problem with this profile is that the distance between the ground station and the antenna under test varies greatly, so that the measurements suffer from ground reflections as the height can be optimized only for certain sections of the trajectory.

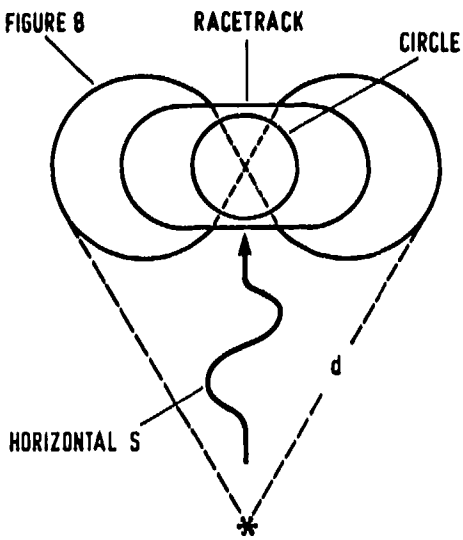

Fig 1.31 Curved flight test trajectories for ARP measurement, fixed height, d = distance

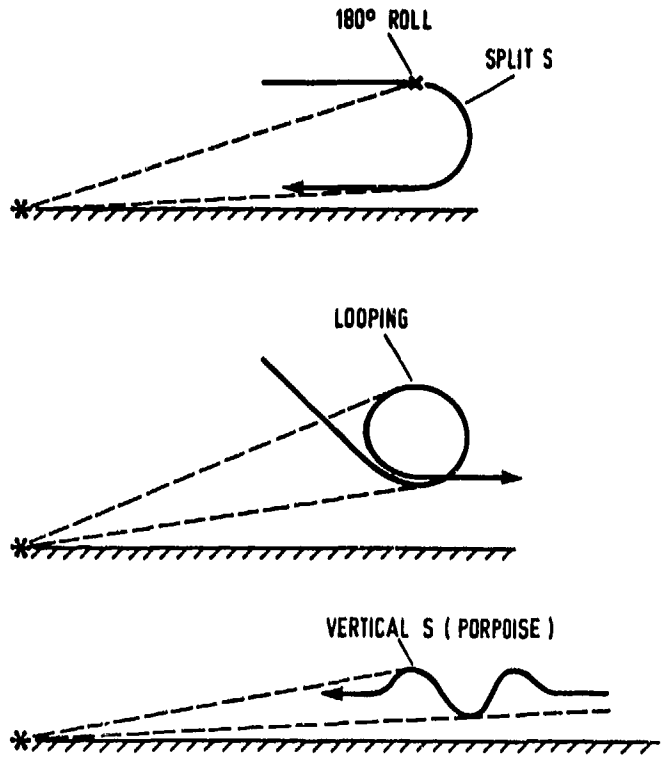

Fig. 1.32 Curved flight test trajectories for ARP measurement, variable height

The curved flight test trajectories for ARP measurement, usually flown at a fixed height, are shown in Fig 1.31. The variable attitude and heading of the aircraft flying these trajectories, usually derived from an AHRS (attitude and heading reference system) or an IRS (inertial reference system), must be recorded or transmitted.

The circle or orbit trajectory is very easy to fly, the aircraft circles in a skidding turn or at a constant bank angle, each turn covering a complete 360° great circle antenna radiation trajectories. Therefore this trajectories is one of the most efficient profiles for ARP measurements as far as flight time is concerned. In a flight at great distance and at low altitude the coverage of the depression angle in the nose and tail area of the aircraft is poor. The coverage of the depression angle can be improved by flying the aircraft at higher altitudes. The disadvantage of this flight test trajectory is, that the drift of the AHRS or inertial system will increase when the aircraft is continously turning in the same direction. Therefore, alternating left and right hand turns are recommended in order to compensate the drift forces.

This requirement is also met by the figure of eight trajectory of Fig 1.31, which allows the aircraft to fly left and right hand turns during the same manoeuver. In the dashed section of this figure no measurements are recommended because the roll rate of the aircraft is very high. To complete a 360° antenna pattern, the manoeuver has to be repeated under conditions where the figure of eight is turned 90° with respect to the ground station.

The racetrack trajectory, very much alike the circle pattern, allows a gyro realignment during the straight course runs connecting the semicircles. The discontinuities at the 0° and 180° azimuth points, where the aircraft has to change from banked to level flight, comprise a disadvantage of this profile because of the great roll rate of the aircraft during the transition period.

If only the nose and tail horizontal patterns of an aircraft antenna need to be measured, the horizontal S flight trajectory illustrated in Fig 1.31 is convenient. Platform drift is minimized by the alternate turns, but the angular range of measurement is limited to, at most, $\pm$ 40° in the horizontal plane.

The candidate curved flight trajectories for ARP measurements in the vertical plane are shown in Fig 1.32. For a split S trajectory the aircraft starts from straight horizontal flight, then performs a 180° roll and finally reverses its flight direction diving to a lower flight level. This manoeuvre gives a nearly 180° coverage of the nose tail elevation cut but can be performed only by highly agile aircraft. The fast rate of change of the pitch angle will make it necessary to use a high sampling rate.

The looping trajectory, where the aircraft performs a 360° vertical turn, extends the coverage to a complete 360° vertical radiation pattern. The same constraints mentioned in conjunction with the split S trajectory apply. Due to the short duration of these fast manoeuvers the drift of the attitude measuring gyros will be negligible.

The vertical S or porpoise trajectory, during which the aircraft alternately dives and climbes, gives a limited coverage of the depression angle in the nose and tail area. If the distance is large it can even provide data on small negative depression angles. Again pitch rate has to be examined carefully, but gyro drift will be negligible.

In many cases a combination of the previously mentioned trajectories is used to achieve a rational and economic flight test programme. Three such combination patterns are dicussed below.

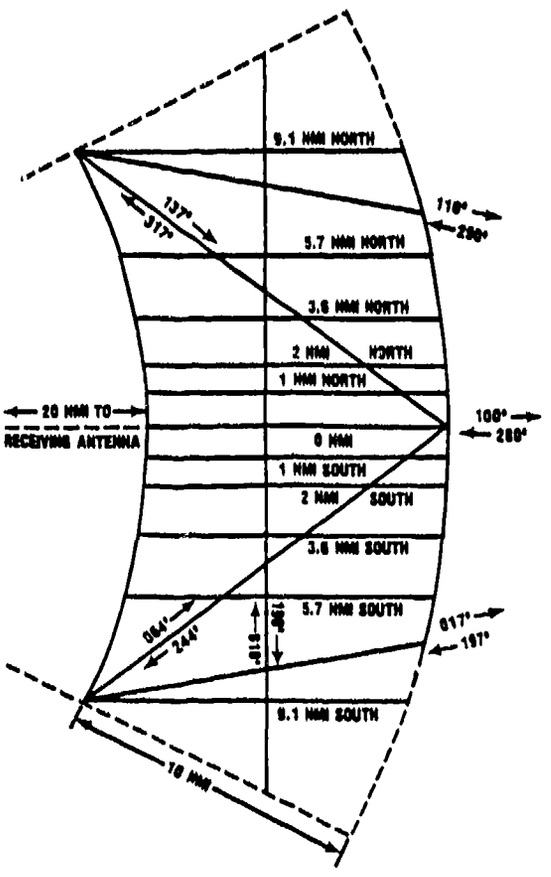

Fig 1.33 Radial run flight profile for antenna measurements at NATC, USA

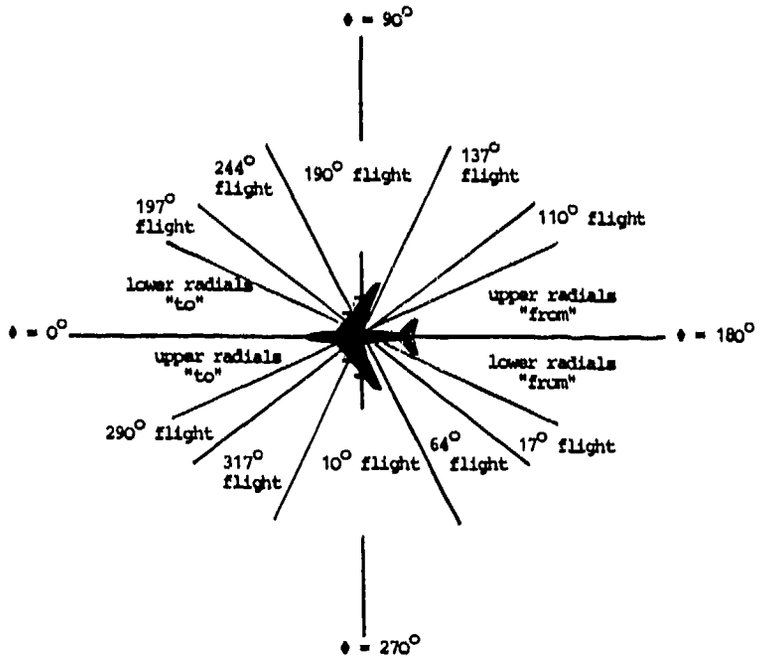

Fig 1.34 Horizontal aspect angle coverage area of radial run flight profile (Fig 1.33)

A typical combination is the radial run flight profile which is used on several US test ranges and is illustrated in Fig 1.33. This profile, composed of several straight trajectories, covers a complete 360° horizontal aspect angle range as shown in Fig 1.34. The flight area where antenna test data is recorded must be chosen carefully so that the multipath conditions for the radio link are acceptable. Moreover, the aircraft must be vectored - usually by a ground radar - to the desired positions and headings. Even a small error in the predetermined flight trajectories can lead to missing sections in the 360° ARP.

The major disadvantage of this combination trajectory is the flight time required to cover the complete 360° aspect angle, which requires at least 32 runs (see Fig 1.33). It is only worth-while if a number of antennas radiating at different frequencies are tested simultaneously. No special test equipment such as an AHRS or an inertial system is necessary on board the aircraft, which makes this profile particularly useful for small aircraft.

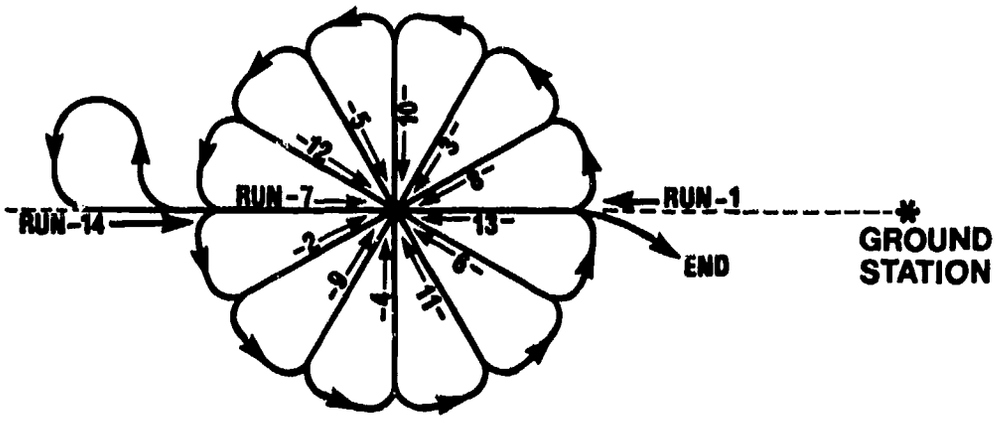

Fig 1.35 Cloverleaf flight pattern for ARP Measurement

Another combination of straight flights is the cloverleaf flight trajectories(Fig 1.35) used in the past by several US test ranges without the aid of an automated measurement system. Range and altitude are chosen so that the depression angle of interest is covered and that the multipath conditions are optimal for the radio link. Each time the aircraft passes the point of measurement (the centre of the pattern) one point of the radiation pattern is recorded. This procedure provides only a rough graphic representation of the antenna pattern with e.g. 24 plotted points, and this is only acceptable at lower (VHF) frequencies. At higher frequencies many more straight runs are necessary in order to cover the fine structure of a pattern, which makes this method impractical above the VHF frequency range. These measurements do not require additional on-board equipment and can be performed without radar support if landmarks or radio navigation are used. The flight time for a 24 point cloverleaf is very high, of the order of several hours. If the area of data collection is enlarged and the headings are properly selected, a nearly complete 360° pattern can be recorded. But then radar support and data processing are necessary. Tab 1.4 shows selected headings and angular coverage of measurements, when a ratio of 1:3 is assumed between the radius of the area where data is collected and the distance from the central point of this area to the receiving station.

Table 1.4 Angular coverage of modified cloverleaf pattern

selected heading	90°	53°	28°	14°	7°	3°	0°
angular coverage	71,5° 108,5°	40,5° 71,5°	21° 40,5°	10,3° 20,8°	5,3° 10,5°	2,3° 4,5°	 0°

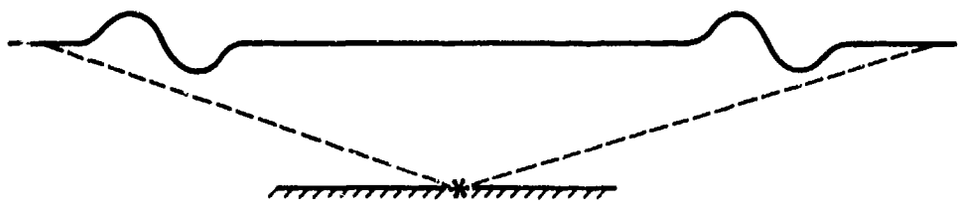

Fig 1.36 Flight trajectory for vertical ARP

A flight pattern frequently used by DFVLR in Germany is illustrated in Fig 1.36 and consists of the straight flyover flight (Fig 1.30) combined with two porpoise patterns (Fig 1.32). This method ensures an uninterrupted measurement of a vertical radiation pattern below the aircraft usually starting at a depression angle θ_D of -10°. When using this trajectory, probable ground reflection problems must be carefully considered as several points of wave cancellation may be met during a test flight. At frequencies of about 1 GHz and higher a highly directive ground antenna can reduce this problem considerably. An alternative, also helpful at low frequencies, is to make use of the ground as a reflector for the receiving antenna. In order to obtain well-defined conditions, the surroundings of the ground antenna are covered with a metallic mesh to a distance of several wavelenghts. This antenna arrangement has only one lobe, (see Fig 1.37), which covers the whole test flight, but corrections must be applied for the variations of gain within that lobe. The large distance variations during the test flight require additional corrections.

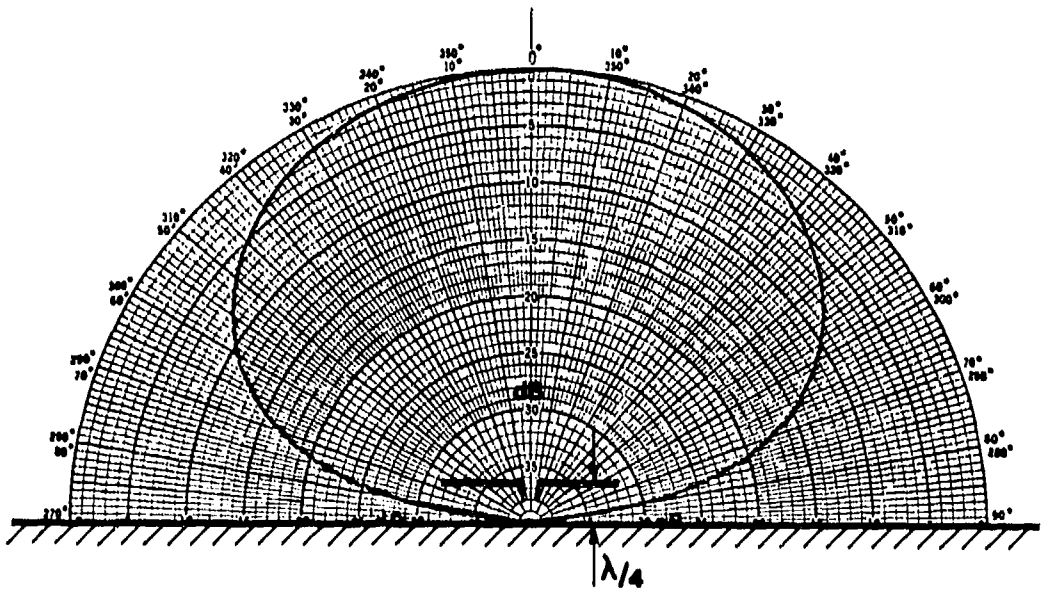

Fig 1.37 Radiation pattern of receiving antenna, distance of reflecting Ground d = λ/4

Several of the above-mentioned flight profiles can add up to a complete 360° coverage of the horizontal aspect angle during one test flight. To cover a larger range of the vertical aspect angle is much more difficult. In order to improve the planning of flight tests for vertical pattern recordings, vertical coverage charts can be used (Ref 13). They are given in Fig 1.38 for ground ranges of up to 40 NM. The correct values for sample point A in Fig 1.38 are

Ground Range	8.65 NM
Slant Range	10 NM
Elevation Angle	30°
Earth curvature θ_E	0.14°
Altitude	30.43 FT
Depression Angle θ_D	30.14°

If any two of the first five variables are given, the others can be found by using the chart. Given the depression angle and any one of the first four variables, the others can be estimated. For ground ranges greater than 40 NM (vertical coverage chart of Fig 1.39), the slant range is within 0.6 NM of the ground range.

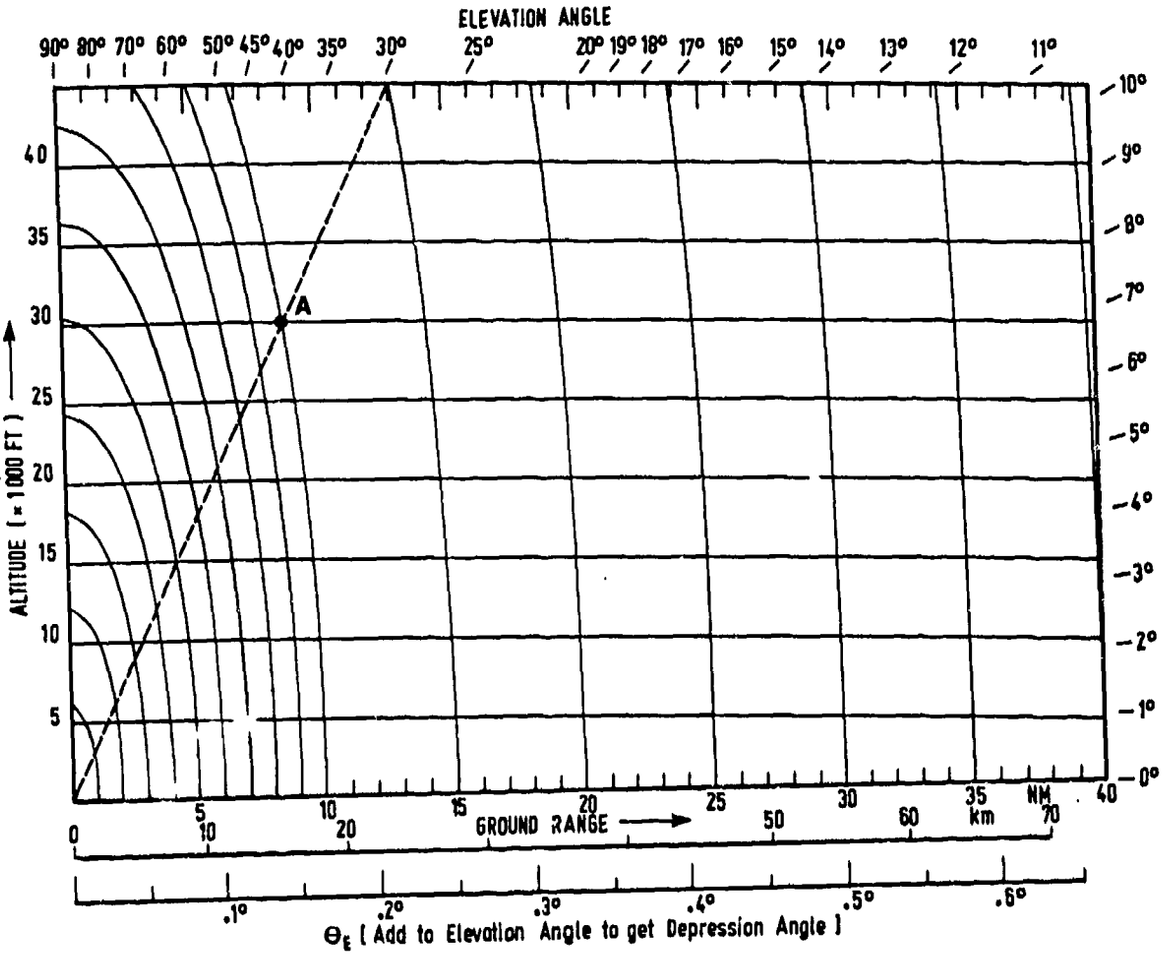

Fig 1.38 Vertical coverage chart (ground range up to 40 NM)

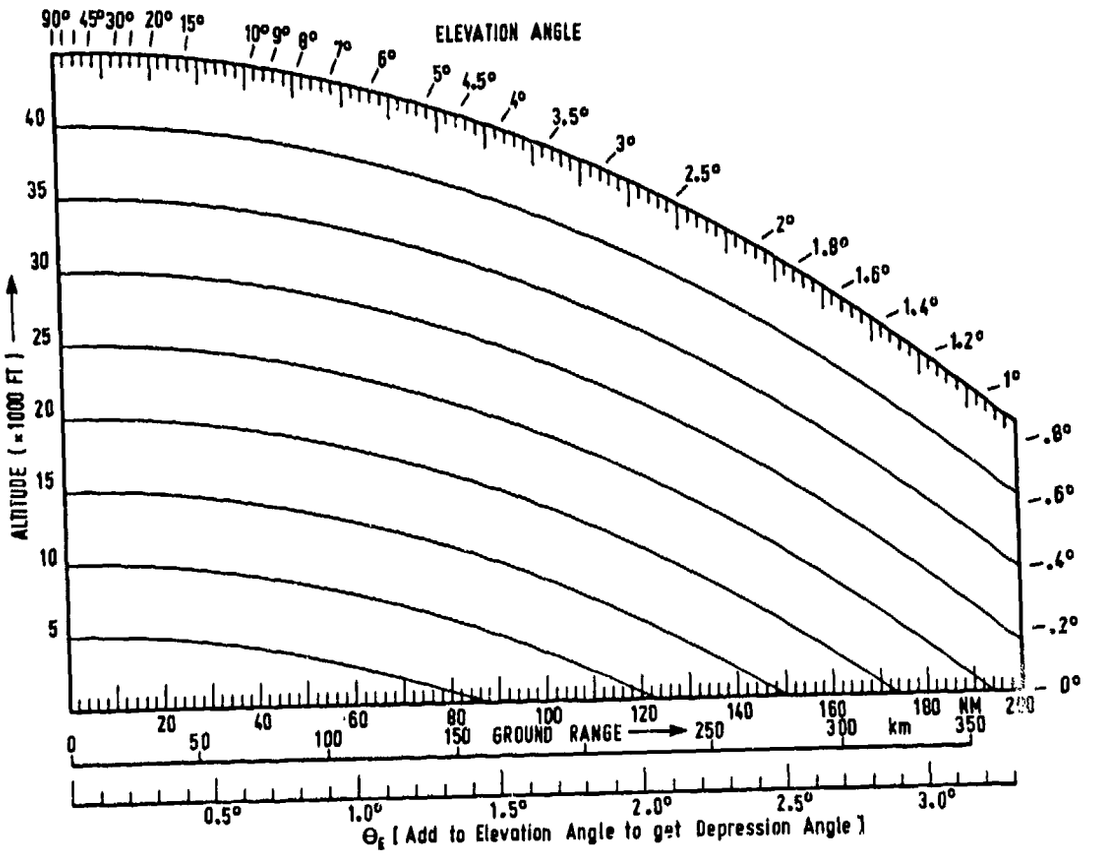

Fig 1.39 Vertical coverage chart (ground range up to 200 NM)

1.4.4 System Considerations

The system configuration for in-flight antenna measurements depends very much on the frequency range the system has to cover and on the size of the vehicles under test, which range from small drones to wide-body aircraft.

An important question is whether the test system should work as an air-to-ground radio link or vice versa. In other words, should the antenna under test act as a transmitting or receiving antenna. If measurement frequencies exceed several GHz, the transmitters become large and heavy, and power consumption increases. In this situation a ground radiating concept has important advantages. In small aircraft, such as fighters, it is often necessary to take out the operational equipment to provide space for the test transmitter. This has, however, the advantage that the existing cabling can often be used for the test installation.

Usually the distance between the airborne and the ground station will be between 20 and 40 km, in order to limit the required transmitter power, the required dynamic range of the receiver, and to reduce the effect of field intensity variations with distance. The total power budget of the antenna measuring link is calculated using Eq (1.9.) Usually the received power should be about 40 dB above the noise level of the receiver system, in order to ensure that a 40 dB dynamic range can be attained in the pattern recordings.

1.4.4.1 Airborne Systems

Depending on whether receiving or transmitting the airborne system of an in-flight antenna measuring device has to contain the necessary HF transmitters or receivers which cover the frequency range under test.

On-board test transmitters are either single-frequency units, which can often replace the original equipment, or wide-band devices, consisting of a frequency synthesizer, a frequency multiplier and power amplifiers, the latter usually one for each octave of the frequency range. As mentioned in Section 1.4.4 a transmitting power of about 1 to 10 watts is required, which for frequencies of up to a few GHz can be provided by semiconductor circuits. At higher frequencies travelling-wave tube amplifiers are used. The stability of the transmitter amplitude must be controlled or monitored carefully to avoid fluctuations corrupting the measured ARP.

On-board test receivers usually have a wide frequency range,with switchable crystal-controlled oscillators converting the incoming signal to the frequency range of the first intermediate-frequency (IF) amplifier. In order to make the receiver suitable for all frequencies that must be received, the second oscillator which converts the first intermediate frequency to the second IF is often a programmable frequency synthesizer. A logarithmic amplifier covering an adequate dynamic range of 60 to 80 dB is usually employed as the second intermediate-frequency amplifier. The accuracy of its logarithmic characteristic should be within $\pm$.5 to 1 dB deviation for the full dynamic range.

As shown in section 1.4.3, several parameters must be measured on board the test aircraft to determine the aspect angle. These are attitude parameters and altitude, with the addition of parameters from navigational aids if the position-dependent part of the aspect angle is not measured by ground-based equipment.

For the on-board acquisition of aircraft position data two approaches are possible: the use of the operational navigation equipment already available in the aircraft or the use of a special flight test package. In the first approach only the data recorder or the telemetry transmitter with their signal conditioning are added to what is already available in the aircraft, but connections must be made to the operational navigation equipment of the aircraft. If safety reasons make that unacceptable, a completely independent sensor package must be installed. If the data recorder or telemetry transmitter is included in that package, the additional cabling in the aircraft will be reduced to a minimum.

Usually ARP measurements require on-board and ground data. If data are recorded on board, only post flight processing and evaluation of the ARP is possible. If real time monitoring is desirable, a telemetry data link has to be installed. This considerably speeds up and improves the handling of the test flights.

A typical example of an ARP measurement system which derives on-board data from the avionic systems of the aircraft is illustrated in Fig 1.40. This system, used at the Naval Air Test Center, Patuxent River, Ma, USA, employs telemetry for data transmission and radar tracking for space position data acquisition.

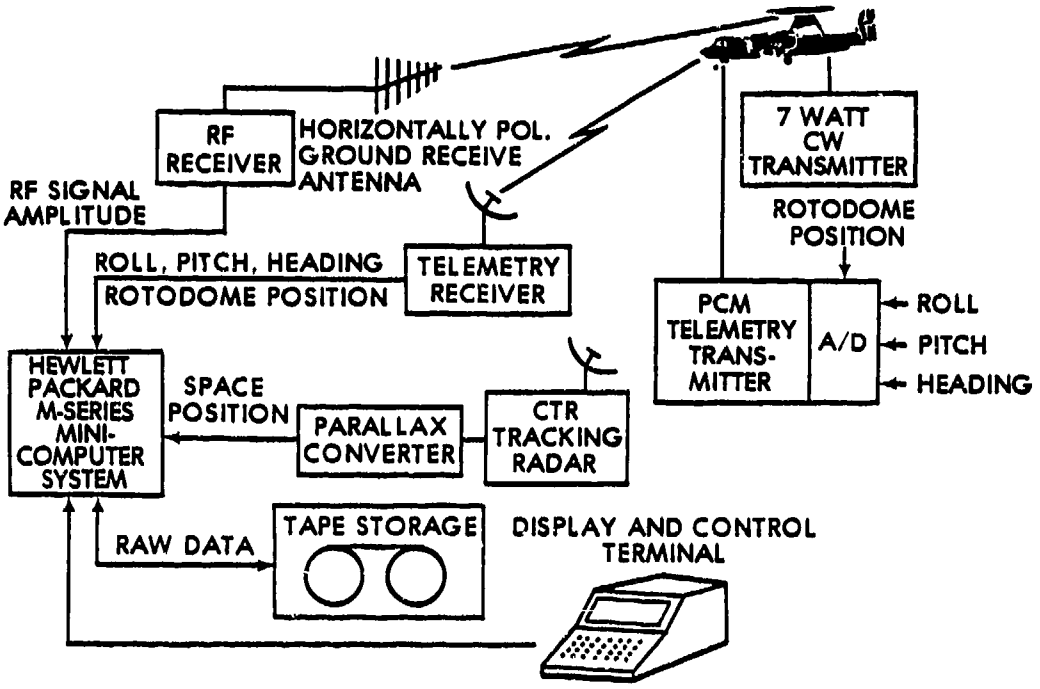

Fig 1.40 Inflight antenna measurement range of NATC

A system of the NLR, Netherlands (Ref 14) makes use of separate on-board and ground data recording with synchronization accomplished by a radio link between the airborne and ground data acquisition units. The data processing scheme of this system is shown in Fig 1.41.

A third example, of DFVLR Germany, is described in Ref 15. It consist of one complete black box which contains all data acquisition units, including radio navigation systems (VOR/DME) for space position data acquisition (see Fig 1.42).

A typical airborne receiver for ARP measurements, developed by DFVLR Germany for flight tests, is shown in Fig 1.43. Depending on the oscillator frequencies, four different test frequencies in the range 0.6 to 20 GHz can be selected. The receiver is of modular construction and can be configured in almost any shape, to adapt it to different conditions of use. The front end of the receiver is preferably mounted close to the antenna terminal, remote from the basic chassis, to minimize cable losses at very high frequencies (Ref 16).

1.4.4.2 Ground Systems

As mentioned above, ground systems for ARP measurement receive or transmitt the signals of the radio-frequency test link. The necessary ground antennas for transmission or reception must be selected carefully, and their bandwidth must be matched to the frequency range of the measurements. Even if log-periodic devices with a wide frequency range of e.g. 1:10 are provided, the total frequency range usually requires more than one antenna.

To reduce ground reflection disturbances, the siting of the ground antennas must be done with great care. The necessary conditions, especially the adjustment of the antenna height above the ground, are outlined in more detail in section 1.4.5.

At frequencies above 1 GHz an adequate effective area of the antenna is achieved only by high gain antennas like horns or parabolic dishes. The half-power beam width of these antennas is so small, that they must be made to track the vehicle under test. In many systems this is done by slaving the pedestal of the measuring antennas to a tracking radar or to a telemetry tracking system used for data transmission.

At high frequencies receiver preamplifiers or transmitter power amplifiers should be as close as possible to the feed systems of the antennas to avoid sensitivity reduction or power loss in cables.

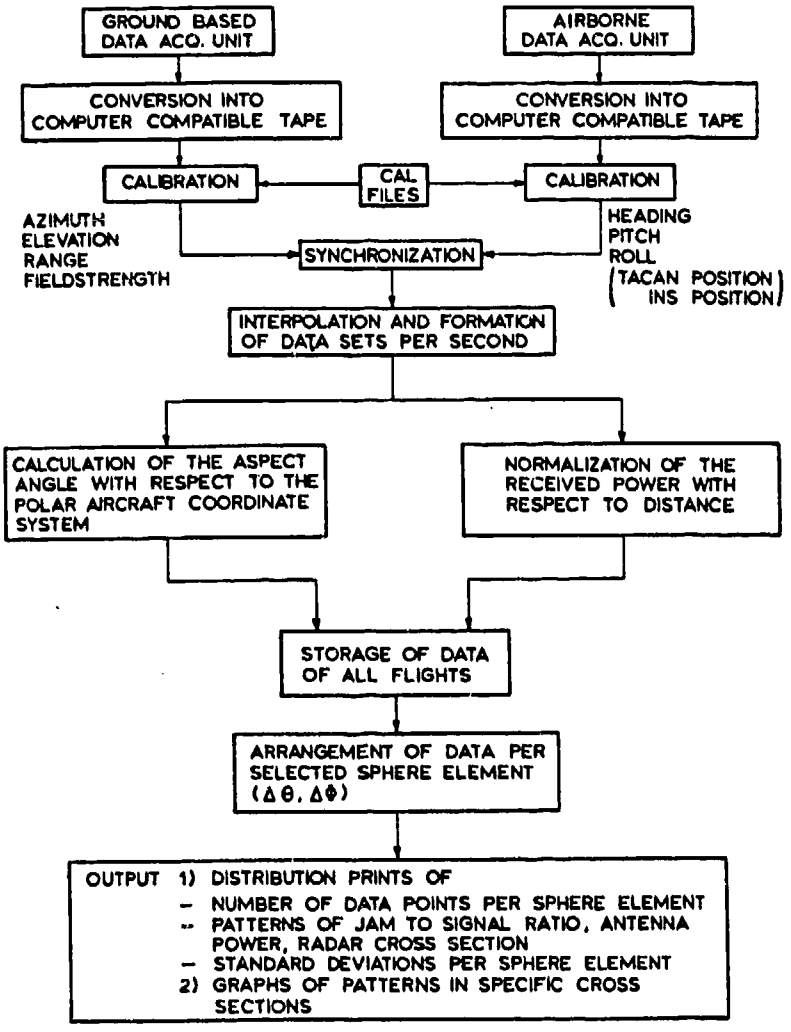

Fig 1.41 Data processing scheme of NLR system

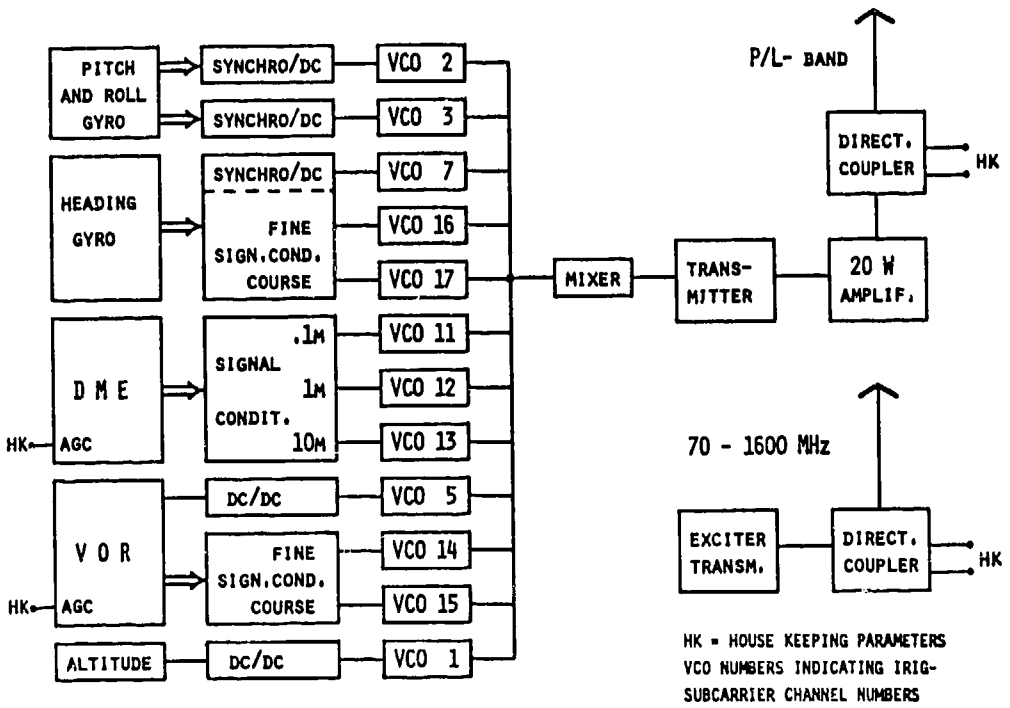

Fig 1.42 Airborne system for antenna pattern measurements (DFVLR)

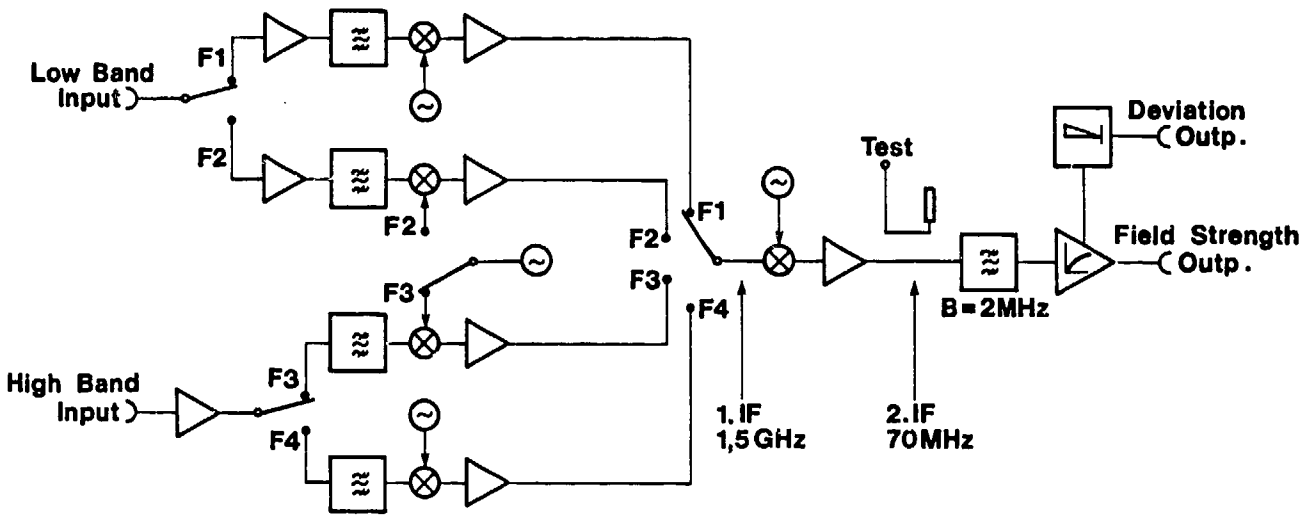

Fig 1.43 Airborne receiver for ARP measurements

A typical configuration of a ground antenna system for ARP measurement is shown in Fig 1.44. Four parabolic dishes, each covering part of the frequency range, are combined with a log-periodic crossed dipole antenna for VHF measurements. The antenna pedestal also carries the RF equipment.

Fig 1.44 Antennas of precision antenna measurement system (PAMS) of USAF/Rome Air Development Center

Fig 1.45 shows a different concept. Here a section of a parabolic dish is mechanically connected to a telemetry tracking antenna. The surface of the dish is designed to operate at up to 20 GHz. Matching to different frequency ranges is accomplished by exchanging the antenna feeds, which illuminate a smaller section of the dish if the frequency is increased. Again a rack on the pedestal holds all RF equipment.

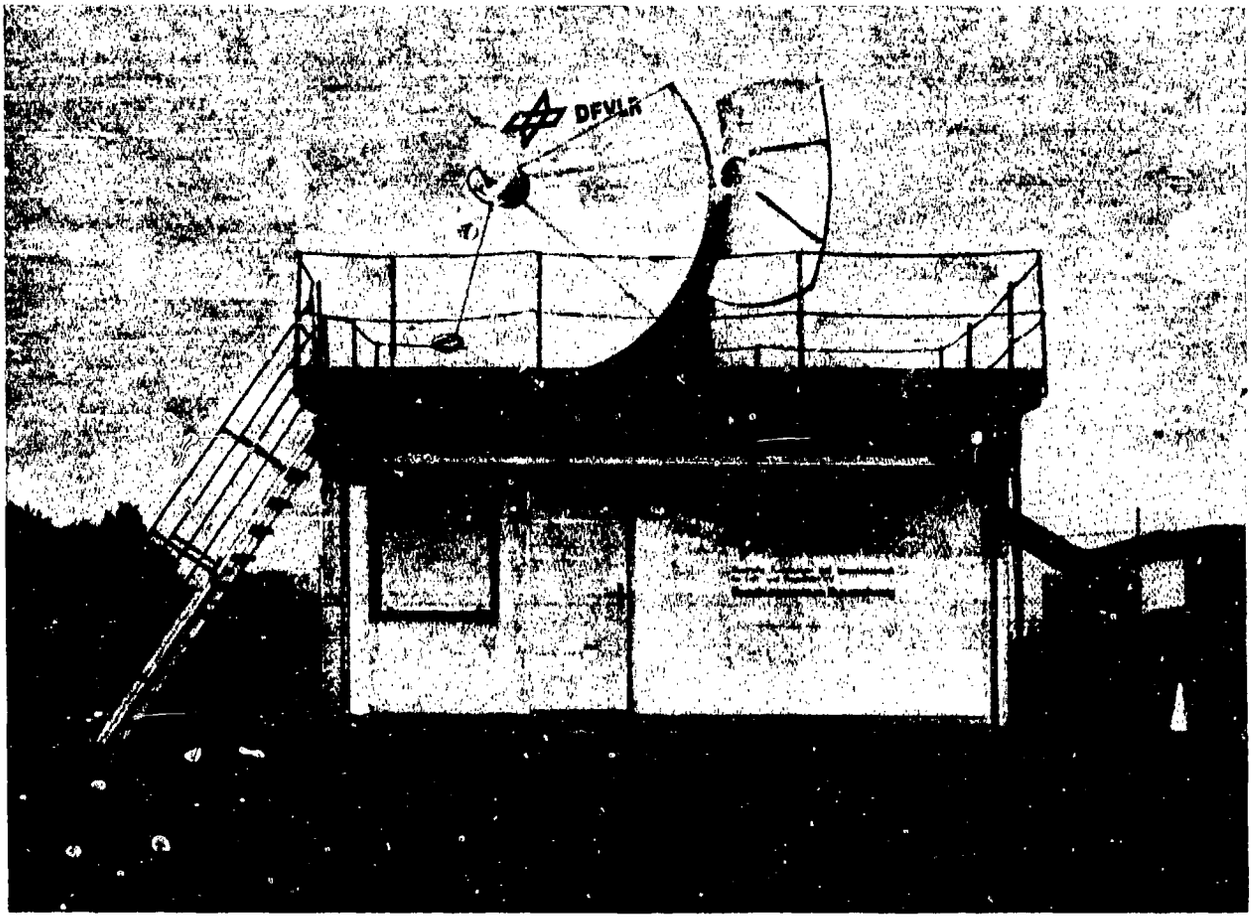

Fig 1.45 RF-reception antennas for ARP measurements at DFVLR

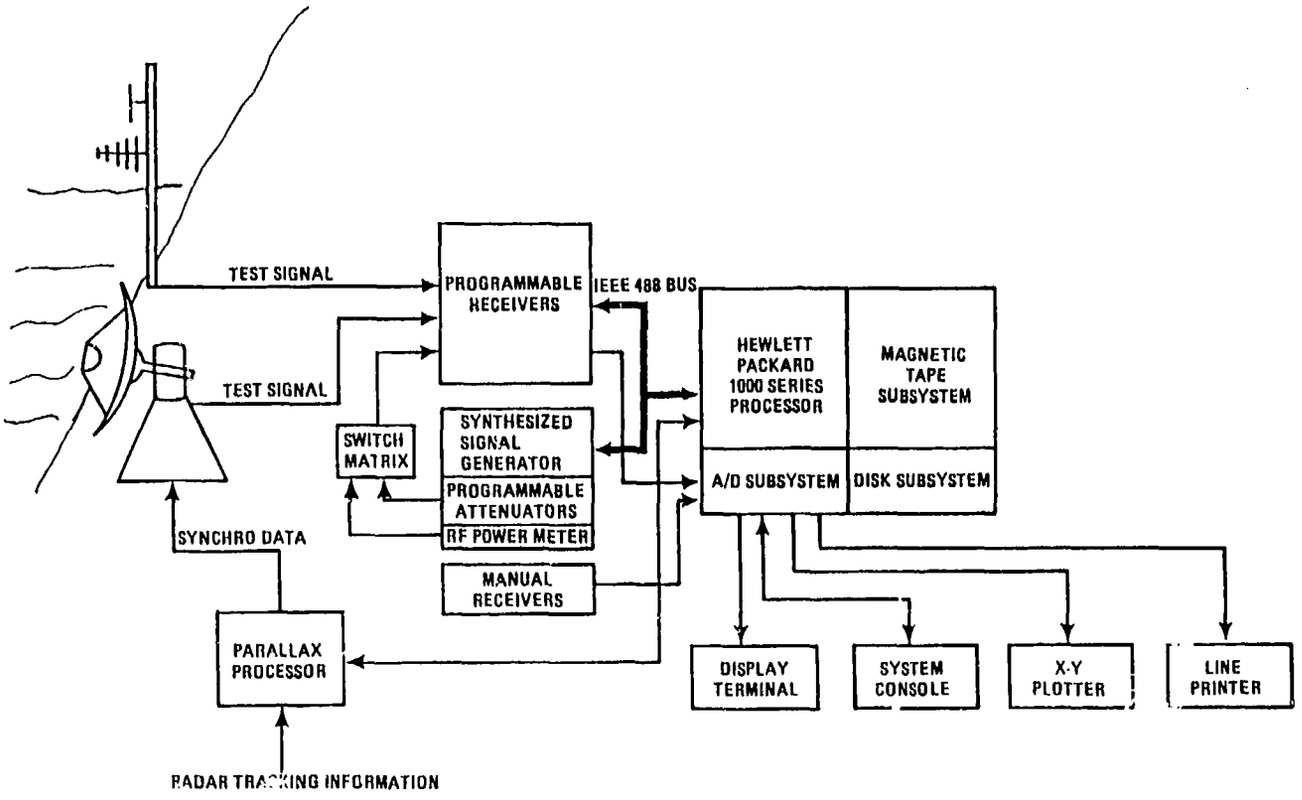

Fig 1.46 In-flight antenna measurements system equipment of NATC

Two data processing systems, one with on-board data recording and synchronization of ground data (Fig 1.41) and one with telemetry transmission (Fig 1.40) have been mentioned already. The Naval Air Test Center ground system of Fig 1.40 is shown in more detail in Fig 1.46. The frequency management of the receiving system is automated to a high degree. A third system with on-line data processing and quick look presentation of results used by DFVLR Germany, is illustrated in Fig 1.47. The FM-subcarrier system has now been replaced by a PCM system.

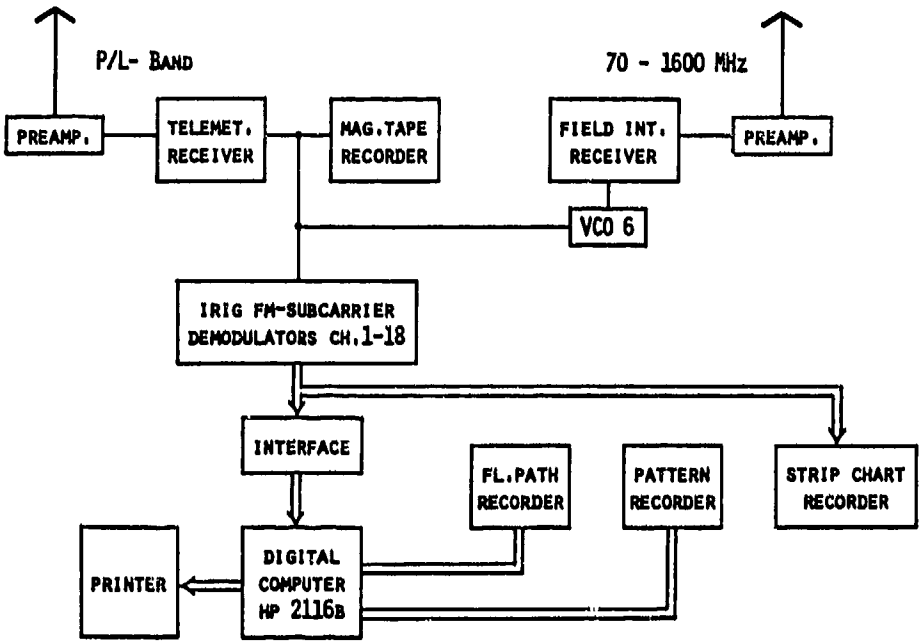

Fig 1.47 Receiving and data processing station for antenna measurements of DFVLR

1.4.5 Pattern Calibration

1.4.5.1 Flyby Procedure

The methods described in Section 1.4.4 provide relative radiation patterns but do not give quantitive information on the efficiency of the on-board system, i.e. on the ratio between the power actually received and the power that would be received from an isotropic radiator excited by the same power and frequency and measured at the same distance as the antenna under test. The actual power measured at the receiving antenna depends not only on this efficiency, but also on the reflected power that varies with the shape and nature of the terrain between the transmitter and the receiver. Usually, this efficiency is calculated for the geometric relationship between transmitter and antenna of the actual flight test by calculating the power that is reflected by the ground in that case. This reflected power can then be subtracted from the received power to obtain the power that would be obtained in an environment without reflections. This calculation is described in Section 1.4.5.2.

DFVLR (German Aerospace Research Establishment) has recently developed a method for measuring this efficiency using the flyby procedure described in this section. This method is based on a comparison between the signals at the ground receiver received from the aircraft and from a standard gain antenna placed on a tower near the aircraft trajectory. The ratio between the signals from this antenna and from a fictitious isotropic antenna is known. The radiation pattern of the isotropic antenna is a circle which DFVLR calles the "isotropic circle". The isotropic circle is usually plotted together with the measured pattern in order to indicate the gain of the antenna under test in each section of the polar plot (see e.g. Fig 1.53). To compare the aircraft under test with a standard gain antenna the flyby procedure shown in Fig 1.48 is conducted. For calibration purposes the aircraft flies past the ground measuring station at a short distance (about 250 m) and at a low height (between 16 and 20 m). Just before this flyby, a tower with a standard gain antenna is erected in the test area. Thus the radiation of the aircraft antenna can be compared to the radiation of the standard gain antenna if both antennas radiated from nearly the same position. The input power to both antennas must be measured. For flight security, the standard gain antenna tower must be removed before the aircraft flights.

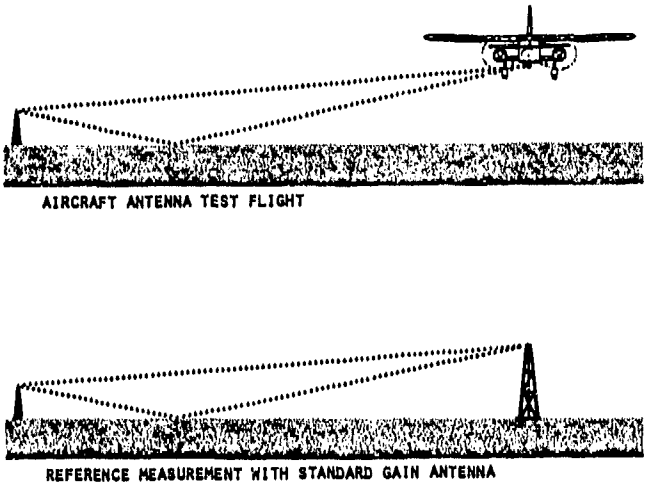

Fig 1.48 Flyby procedure for comparison with standard gain antenna

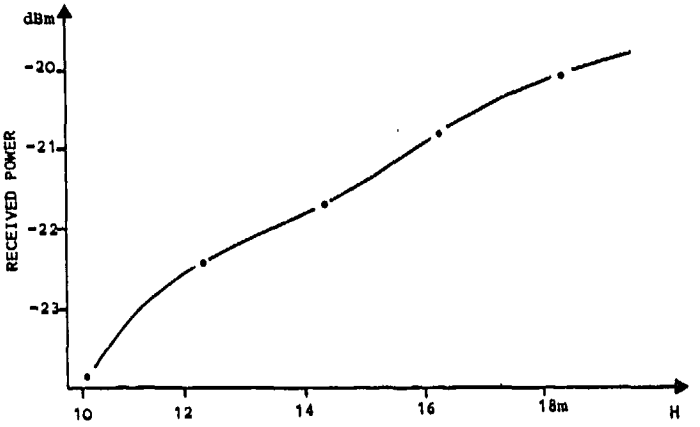

Fig 1.49 Received power as a function of height H of standard gain antenna (f = 335,5 MHz)

Again care must be taken to achieve stable propagation conditions. This means that the antenna heights must be chosen carefully to avoid large power reductions at the receiver due to ground reflections. Propagation conditions have to be nearly the same during the tower and the aircraft derived measurements. Investigations have shown that the aircraft antenna and the standard gain antenna have to radiate from the inside of a fictitious cube which measures about 5 m from edge to edge. Within this cube, spatial differences between the antennas of the comparative measurements can be interpolated linearly (Ref 17). Fig 1.49 shows an example of the relative received power from the standard gain antenna as a function of height. It shows that the heights of aircraft and standard gain antennas must be known within a tolerance of 40 cm if the error is not to exceed 0.2 dB. For the aircraft this high precision can only be achieved by accurate position measurements with kine-theodolites or laser trackers, and it is convenient to measure the position of the standard gain antenna in the same manner. Fig 1.50 shows a photograph of an aircraft under test taken by a kine-theodolite with azimuth and elevation angle information, which has to be corrected for the displacement of the aircraft's reference point from the cross-hairs. A measurement installation at Braunschweig Airport (Fig 1.51) shows two theodolites installed for position measurements.

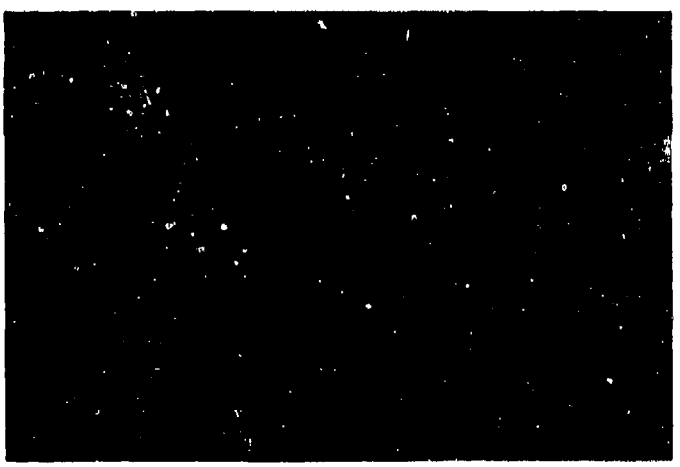

Fig 1.50 Evaluation of theodolite measurement

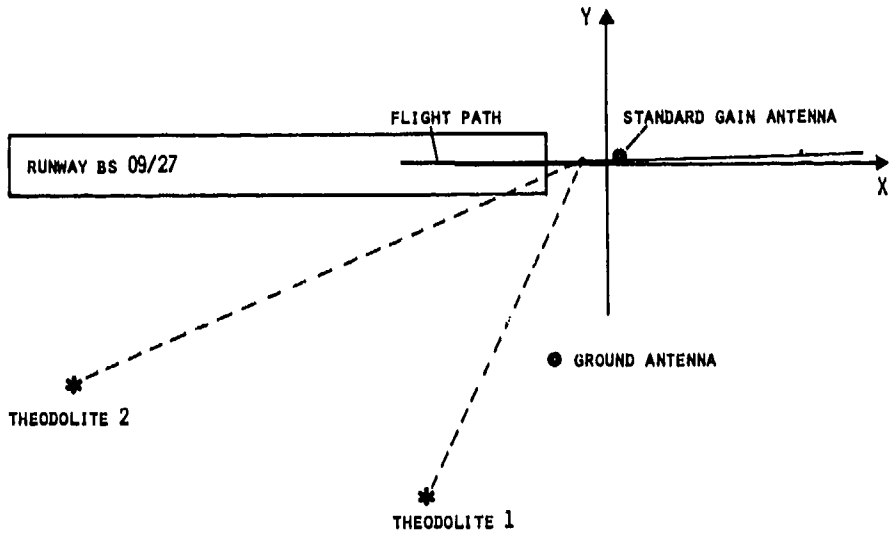

Fig 1.51 Measurement installation at Braunschweig Airport

The flight path with respect to the position of the standard gain antenna of a test is illustrated in Fig 1.52. These curves are used to interpolate the received power of the standard gain antenna to the actual flight path level. The height of the standard gain antenna is varied in steps of 2m to match the flight path in x-direction as closely as possible. Deviations in y-direction are much less sensitive with respect to an alteration of received power.

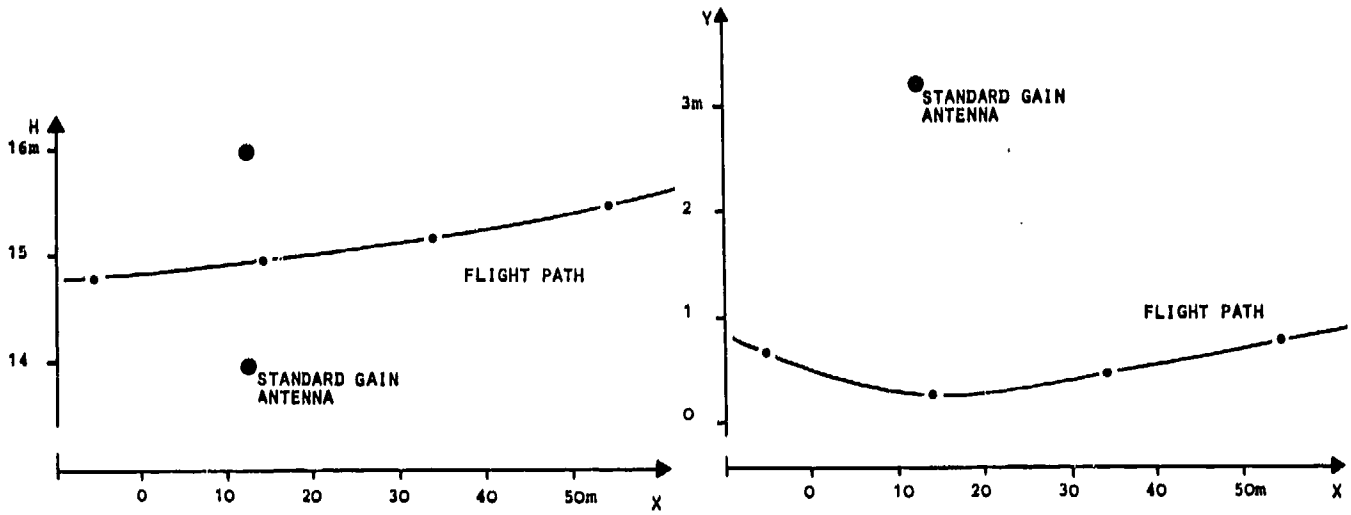

Fig 1.52 Flight path with respect to standard gain antenna

As an example, Fig 1.53 shows the radiation pattern and isotropic circle of a glide slope antenna measured for an HFB320 aircraft. The difference ΔP between the isotropic circle and the radiation pattern has been determined at an angle of 290° and is 13.5 dB. ΔP is calculated from

$$\Delta P = (P_{ES} - P_{EA}) - G_S - (P_S - P_A) \qquad (1.22)$$

where P_{ES} and P_{EA} are the powers received from the standard gain antenna and the aircraft antenna. P_S and P_A are the measured power inputs of both antennas and G_S is the gain of the standard gain antenna compared to an isotropic radiator.

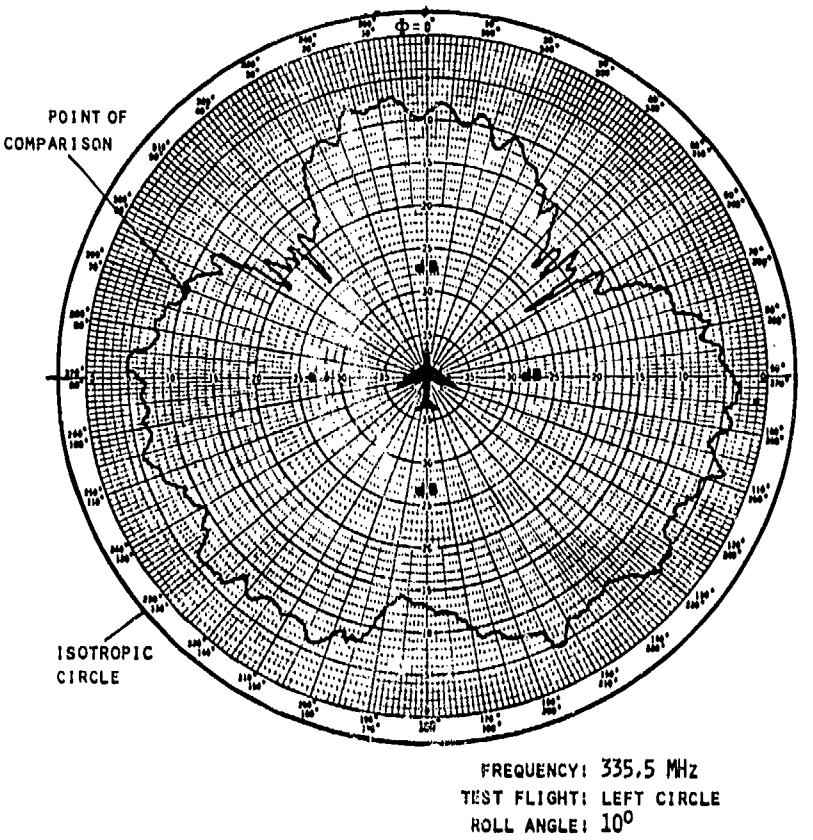

Fig 1.53 Glide slope antenna radiation pattern with isotropic circle

For vertical pattern measurements the substitution method is impractical, since the standard gain antenna cannot be placed several hundred meters above the receiving antenna. Here the difference between the radiation pattern and the isotropic radius is calculated by comparing the theoretical free-space propagation power to the measured received power at the flyover point. This method is applicable due to the stable and predictable propagation conditions during the flyover procedure. Fig 1.54 shows the vertical pattern and isotropic circle of an HFB320 marker antenna. A difference of 10.2 dB has been determined between the measured received power of the aircraft antenna and the calculated received power of an isotropic radiator, excited with the same power.

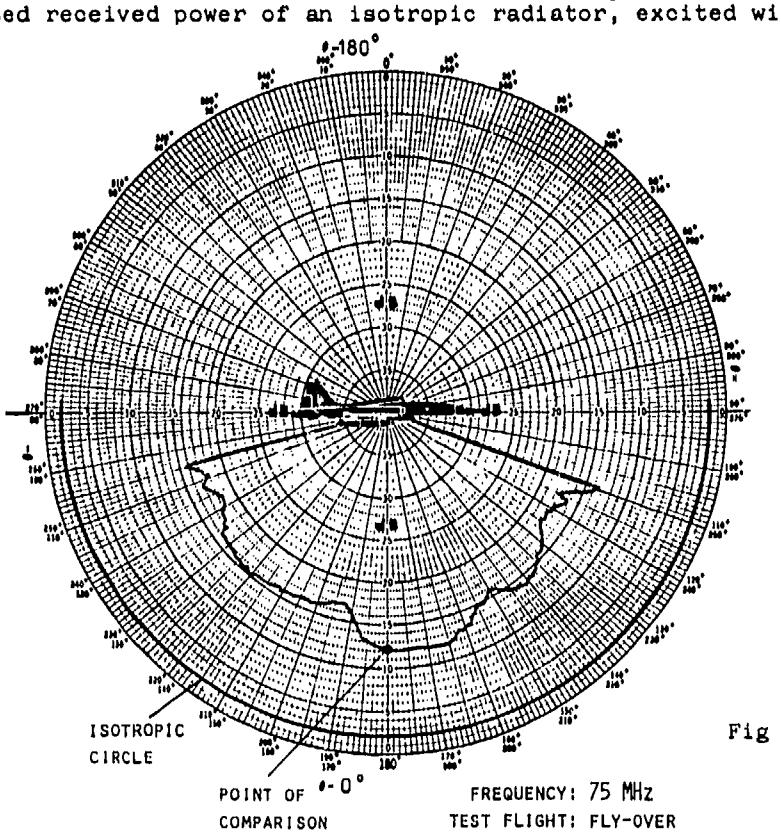

Fig 1.54 Marker antenna radiation pattern with isotropic circle

Considering the accuracy of measuring relative patterns, the radiation intensity is normalized to its maximum value. To record one pattern will take only a short period of time, hence the gain stability of the field intensity measuring device including exciter transmitter is not critical.The main source of inaccuracy caused is due to the nonlinear amplitude response of the receiver and amounts to $\pm$ 1.5 dB error over a full range of 70 dB.

In addition, the calibration error has to be estimated. For horizontal patterns it comprises the following peak error contributions:

Measurement of aircraft antenna excitation power	$\pm$ 0.2 dB;
Measurement of standard gain antenna excitation power	$\pm$ 0.2 dB;
Gain uncertainty of standard gain antenna	$\pm$ 0.5 dB;
Comparision of field intensity	$\pm$ 0.1 dB;

which sums to a maximum peak error of $\pm$ 1 dB.

In the calibration of vertical patterns the following errors can occur:

Measurement of aircraft antenna exciting power	$\pm$ 0.2 dB;
Measurement of received power on ground by a dipole with ground reflector	$\pm$ 1.5 dB;
Error due to deviations from flight path	$\pm$ 0.3 dB;

Summarizing, the standard deviation of error in calibrating aircraft antenna radiation patterns by this flyby procedure is about 1.6 dB for horizontal, and 2.2 dB for vertical patterns.

1.4.5.2 Calculation of the Effect of Ground Reflections

The flyby procedure, which uses a substitution method well known in antenna test range measurements, requires very accurate flight path measurements with time-consuming and expensive analysis.

A more convenient method used at several test ranges in the USA, which offers only slightly reduced accuracy, will now be discussed.

To determine the isotropic circle with respect to an antenna pattern measured dynamically during a test flight, the missing parameters in the range equation of electromagnetic radiation propagation Eq (1.4) can be estimated from theoretical considerations. The gain G_T of the transmitting aircraft antenna over an isotropic radiator can be calculated by rewriting Eq (1.9).

$$G_T = P_R + L + 20 \log r + 20 \log f + 2{,}54 \text{ dB} - P_T - G_R - G_M \qquad (1.23)$$

During a pattern measurement the variables in Eq (1.23) are the received power P_R, the distance r, and the gain of the reflecting ground G_M which depends on r. All other parameters can remain constant.

P_R is normally measured by a calibrated receiver and r is determined by radar or from radio navigation information. The gain or loss due to ground reflections - which can rarely be avoided except when narrow-beam receiving antennas are used at very hight frequencies - can be estimated from a theoretical analysis. The following analysis of ground reflection gain in air to ground radio links is based on a book by Reed and Russel (Ref 18). The calculations are limited to two-path propagation in order to simplify the computation. Reflections from sources other than ground can be avoided by careful installation of the ground receiving antenna.

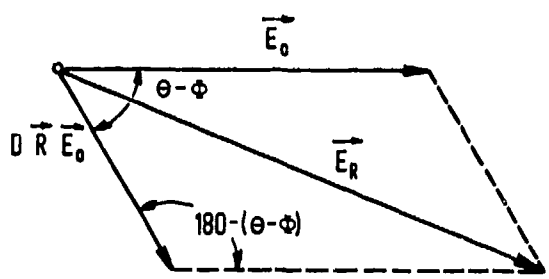

Fig 1.55 Vectorial summing of a direct wave $\vec{E}_0$ and reflected wave $\vec{DRE}_0$

At the receiving antenna the direct wave $\dot{E}_o$ and the ground reflected wave $\dot{D}\dot{R}\dot{E}_o$ are adding vectorially as shown in Fig 1.55 to a resultant vector $\dot{E}_R$. D is the divergence factor and $\dot{R}$ the reflection coefficient. The phase shift of the reflected signal depends on the phase of the reflection coefficient ϕ and the phase lag θ due to the difference in path length of the direct and reflected wave. The total phase lag of the reflected signal is $(\theta - \phi)$. Applying the cosine law to Fig 1.55, the amplitude of the reflected signal becomes

$$E_R^2 = E_o^2 + (DRE_o)^2 - 2\,DRE_o^2 \cos\,(180° - (\theta - \phi)) \tag{1.24}$$

and since $\cos\,(180° - (\theta - \phi) = -\cos\,(\theta - \phi)$

$$E_R = E_o \sqrt{1 + (DR)^2 + 2\,DR \cos\,(\theta - \phi)} \tag{1.25}$$

The gain factor of the reflecting ground G_M then becomes

$$G_M = \frac{E_R}{E_o} = \sqrt{1 + (DR)^2 + 2\,DR \cos\,(\theta - \phi)} \tag{1.26}$$

The gain due to multipath propagation in dB is

$$G_{MdB} = 10 \log \left(1 + (DR)^2 + 2\,DR \cos\,(\theta - \phi)\right) \tag{1.27}$$

The divergence factor D is the ratio of the spread of a beam reflected off a plane surface to the spread of a beam reflected off a spherical surface, which increases with the curvature of the surface and decreases when the angle of incidence increases. The divergence equation based on the geometrical relations shown in Fig 1.24, as quoted from appendix 1.A Eq (1.A7), is

$$D = \left(1 + \frac{2d_1}{d\left(\frac{ka\,h_2}{(d-d_1)^2} - \frac{1}{2}\right)}\right)^{-\frac{1}{2}} \tag{1.28}$$

The reflection coefficient $\dot{R}$, which is the ratio of the reflected ray and the incident ray, depends on the polarization of the incident wave. According to Ref 18 the equation for vertical polarisation is

$$\dot{R}_V = \frac{n^2 \sin\psi - \sqrt{n^2 - \cos^2\psi}}{n^2 \sin\psi + \sqrt{n^2 - \cos^2\psi}} = R_V\, e^{\,j\phi_V} \tag{1.29}$$

and for horizontal polarisation

$$\dot{R}_H = \frac{\sin\psi - \sqrt{n^2 - \cos^2\psi}}{\sin\psi + \sqrt{n^2 - \cos^2\psi}} = R_H\, e^{\,j\phi_H} \tag{1.30}$$

where n is the index of reflection and ψ is the angle of incidence. The index of reflection is given by

$$n^2 = \frac{\epsilon_{r2} - \frac{j\sigma_2}{\omega\epsilon_o}}{\epsilon_{r1}} \tag{1.31}$$

where ϵ_o is the permittivity of free space, ϵ_{r1} is the relative permittivity of air, ϵ_{r2} is the relative permittivity of the reflecting surface, σ_2 is the conductivity of the reflecting surface and ω the angular frequency.

With $\epsilon_o = 1/36\pi 10^9$ farad per meter, $\omega = 2\pi f$ Hz and $\epsilon_{r1} = 1$, Eq (1.31) reduces to

$$n^2 = \epsilon_{r2} - \frac{j\ 18 \cdot 10^9 \sigma_2}{f} \tag{1.32}$$

Some typical values ϵ_{r2} and σ_2 given by Ref 11 and applicable in the UHF range are listed:

Ground reflection constants

material	ϵ_{r2}	σ_2 $(\frac{1}{\text{Ohm}}\ \frac{\text{m}}{\text{m}^2})$
sea water	80	3 - 5
fresh water	80	10^{-2} - 10^{-3}
wet earth	5-30	10^{-1} - 10^{-3}
dry earth	2-5	10^{-4} - 10^{-5}

The angle of incidence ψ of the reflected ray can be calculated from

$$\psi = \tan^{-1}\left(\frac{h_1}{d_1} - \frac{d_1}{2ka}\right) = \tan^{-1}\left(\frac{h_2}{d_2} - \frac{d_2}{2ka}\right) \tag{1.33}$$

which is derived in appendix 1.A, Eqs (1.A8) and (1.A9).

As the last remaining item for the calculation of the gain G_M the phase shift caused by the path length difference θ between the direct and reflected ray has to be known. In appendix 1.A Eq (1.A15) θ is shown to be

$$\theta = 720\ \frac{f}{c}\left(h_1 - \frac{d_1^2}{2ka}\right)^2\ \frac{d-d_1}{d.d_1} \tag{1.34}$$

where c is the velocity of light.

Equations (1.28), (1.31), (1.33) and (1.34) all contain the parameter d_1, which is the distance of the point of reflection to the ground antenna (see Fig 1.24) and is normally unknown. The following cubic equation for d_1 is derived in Appendix 1.A, Eq (1.A17)

$$h_2 = \left(h_1 - \frac{d_1^2}{2ka}\right)\ \frac{d-d_1}{d_1} + \frac{(d-d_1)^2}{2ka} \tag{1.35}$$

d_1 can be calculated using an iterative computer program where d_1 is varied in increments until h_2 equals the desired altitude of the aircraft under test. Ref 19 includes a computer program for the determination of d_1 using the HP 97 calculator.

Values of d_1 are shown in Fig 1.56 and 1.57 as a function of the distance of the aircraft from the receiving antenna and antenna height. These curves facilitate the solution of Eq (1.35), if they are used for the first estimate of d_1. The distance d_1 of the reflection point from the receiving antenna is an important parameter in radiation pattern flight testing. To obtain stable multipath conditions the reflection point should as far as possible be located in a flat area without obstacles. By properly adjusting the heights of transmitting and receiving antenna the reflection point can be moved to an uncritical area.

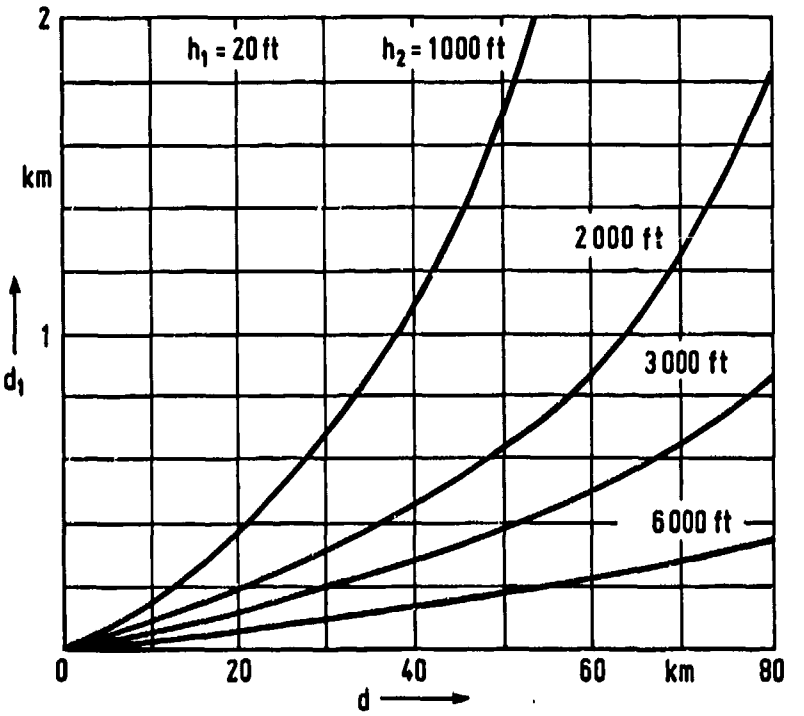

Fig 1.56 Distance of reflection point d_1 from receiving antenna

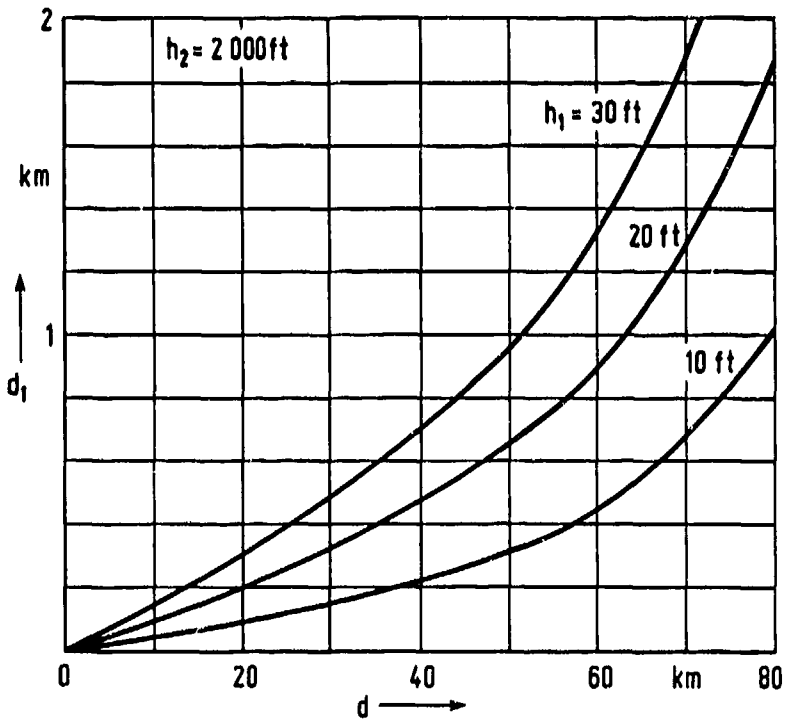

Fig 1.57 Distance of reflection point d_1 from receiving antenna

Now all parameters for calculating the gain G_M due to multipath propagation from Eq (1.27) are defined. A computer program for the determination of G_M using the HP 97 calculator is given in Ref 19. Using this program a few examples of the behaviour of G_M as a function of altitude and have been plotted for different kinds of earth and water surface.

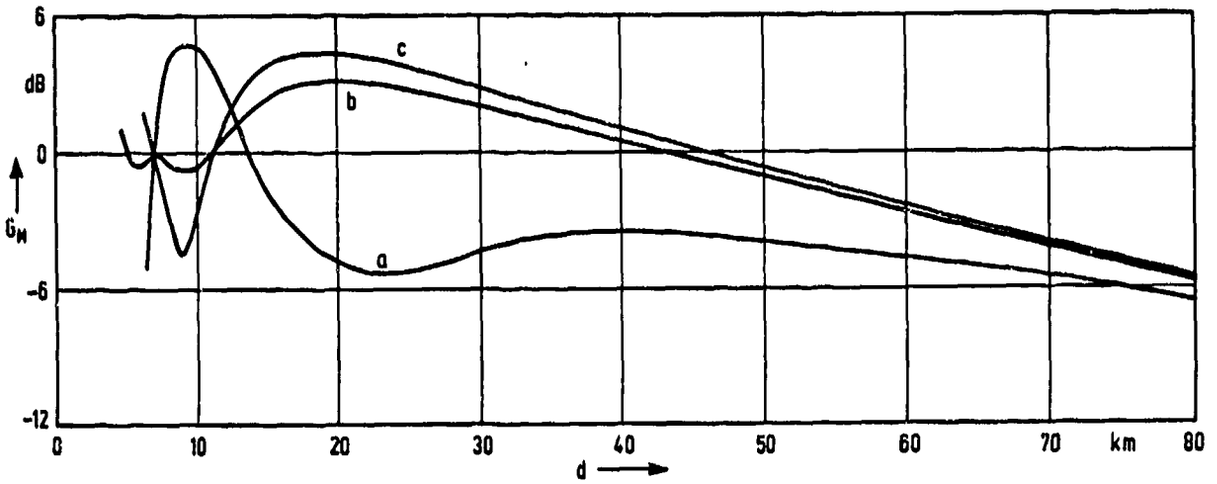

Fig 1.58 Gain G_M of reflecting ground, h_1 = 20 feet, h_2 = 6000 feet, vertical polarisation

f = 120 MHz a sea water (ε = 80, σ = 4 1/Ohm m)

b earth (wet) (ε = 15, $\sigma = 15^{-2}$ 1/Ohm m)

c earth (dry) (ε = 3, $\sigma = 15^{-4}$ 1/Ohm m)

Fig 1.58 illustrates the gain G_M for an air to ground radio link with a 120 MHz carrier frequency. There is only a small difference between wet and dry earth but a significant change if the waves are reflected by sea water due to its high conductivity. Fig 1.58 also shows that, because of the lobe structure of the G_M curve, flight paths at a distance below 15 km, should be avoided for the chosen antenna heights used in Fig 1.58. The reason is that the steep slopes in the G_M-curve cannot be predicted with sufficient accuracy.

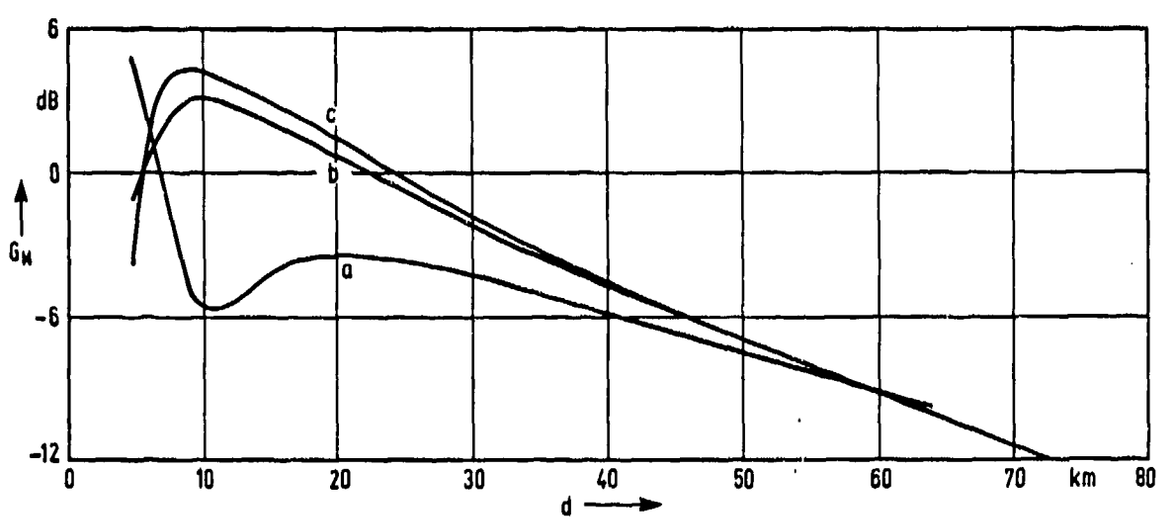

Fig 1.59 Gain G_M of reflecting ground, h_1 = 20 feet, h_2 = 3000 feet, vertical polarisation

f = 120 MHz a sea water (ε = 80, σ = 4 1/Ohm m)

b earth (wet) (ε = 15, $\sigma = 10^{-2}$ 1/Ohm m)

c earth (dry) (ε = 3, $\sigma = 10^{-4}$ 1/Ohm m)

Fig 1.59 illustrates the same situation but for a lower altitude h_2 of the aircraft. Now the usable range goes down to 8 km if the reflecting medium is earth. But at longer distances, e.g. more than 25 km, G_M rapidly drops below 0 dB which is a disadvantage for the power budget of the experimental arrangement.

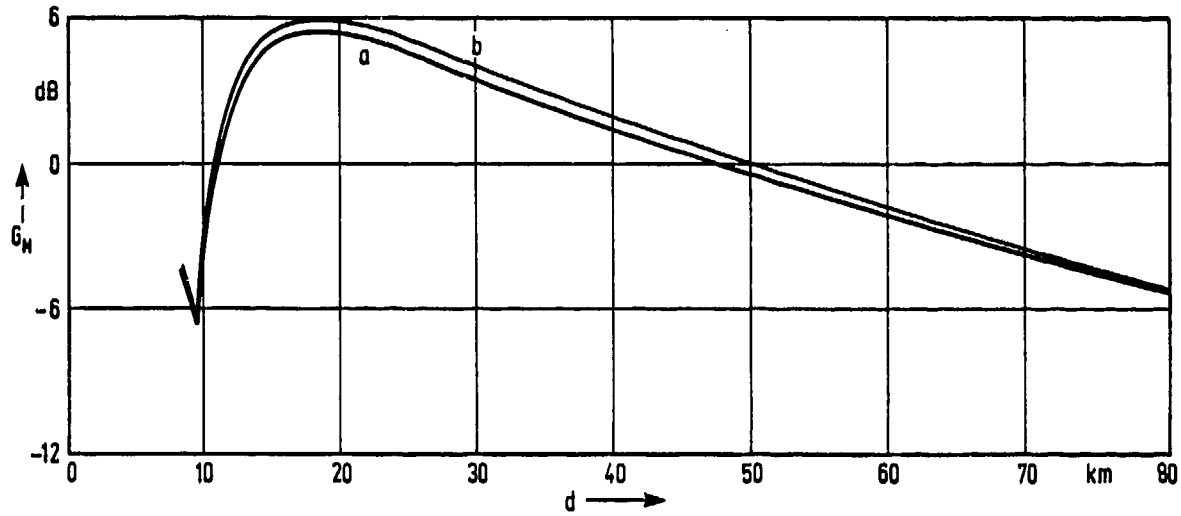

Fig 1.60 Gain of reflecting ground, h_1 = 20 feet, h_2 = 6000 feet, horizontal polarisation

f = 120 MHz a sea water (ε = 80, σ = 4 1/Ohm m)

b earth (dry) (ε = 3, $\sigma = 15^{-4}$ 1/Ohm m)

Fig 1.60 is comparable with Fig 1.58, except that the polarization of the transmitted waves is horizontal. The curves corresponding to the different ground reflectors are closer together, otherwise the same comments apply.

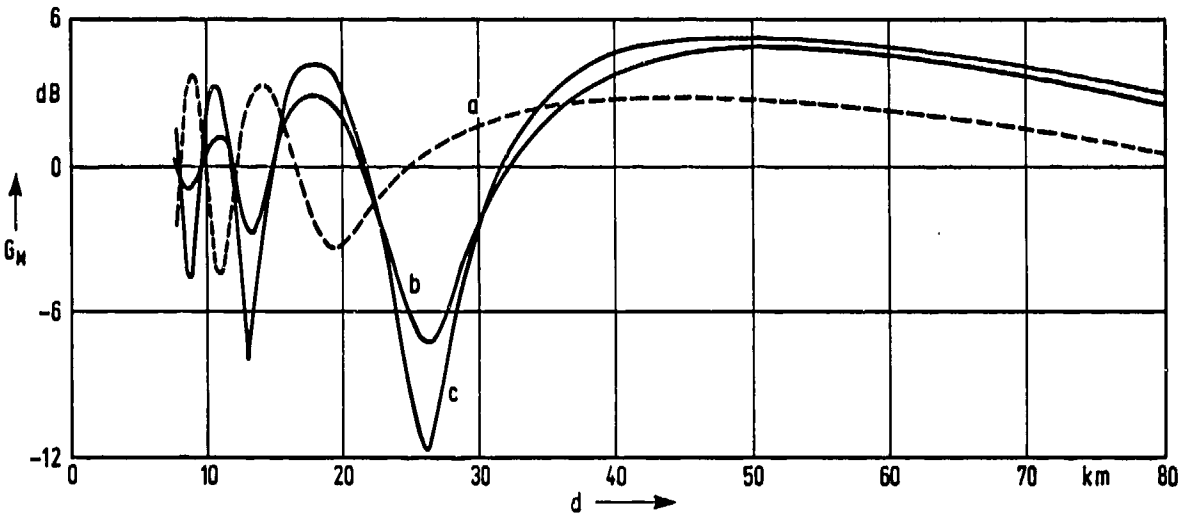

Fig 1.61 Gain of reflecting ground, h_1 = 20 feet, h_2 = 3000 feet, vertical polarisation

f = 360 MHz a sea water (ε = 80, σ = 4 1/Ohm m)

b earth (wet) (ε = 15, $\sigma = 10^{-2}$ 1/Ohm m)

c earth (dry) (ε = 3, $\sigma = 10^{-4}$ 1/Ohm m)

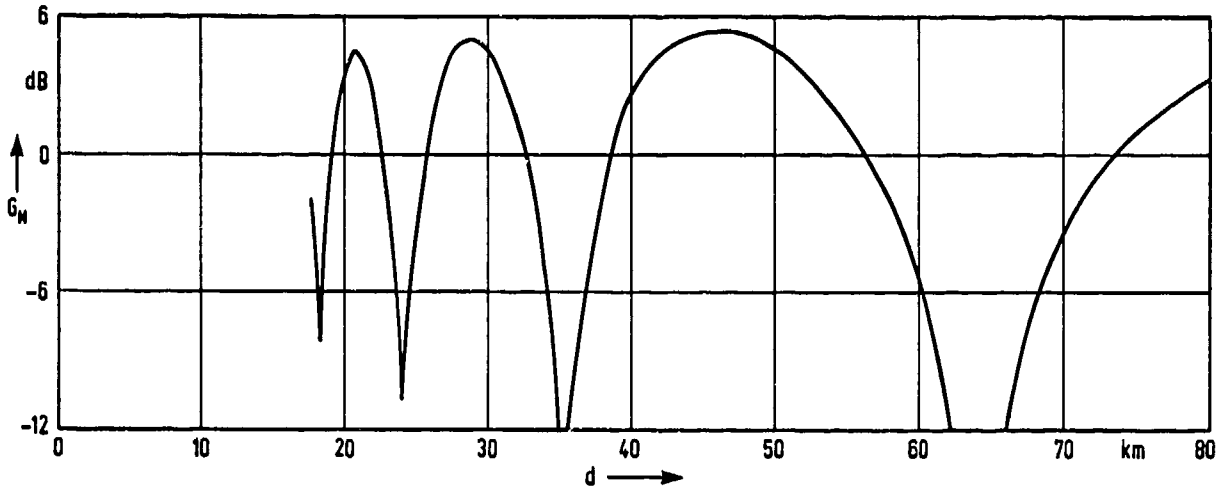

Fig 1.62 Gain of reflecting ground, h_1 = 20 feet, h_2 = 6000 feet, vertical polarisation

f = 1000 MHz dry earth (ϵ= 3, σ= 10^{-4} 1/Ohm m)

For the same physical parameters as in Fig 1.58 the frequency is increased to 360 MHz in Fig 1.61. Due to the decrease in wavelength lobing is increased and the distance of the first gain minimum is farther from the ground antenna so that under these conditions flight paths at distances below 30 km are not advisable. If the frequency is increased once more tc 1000 MHz, the gain curve of Fig 1.62 results. It is obvious that test flights for antenna pattern measurements are now only possible within certain distance windows: after Fig 1.62 for instance between 25 and 32 km or better between 40 and 55 km.

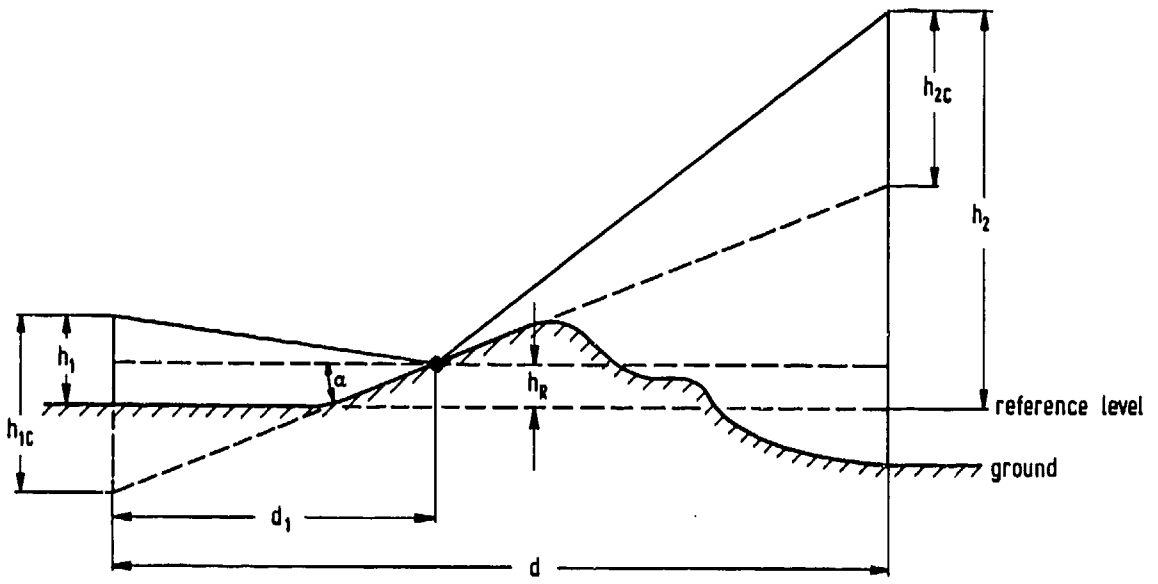

Fig 1.63 Height correction for elevated and inclined reflection area

There is a further problem to consider. If the reflection area is not horizontal, or if its height is significantly different from the heights h_1 and h_2 of the receiving and transmitting antennas, h_1 and h_2 must be corrected. Fig 1.63 illustrates a high and inclined reflection area. If the height of the reflection area is h_R and its slope is α, the corrected altitude h_{1C} and h_{2C} are given by

$$h_{1C} = (h_1 - h_R) + d_1 \tan\alpha \qquad (1.36)$$

and

$$h_{2C} = (h_2 - h_R) - (d-d_1) \tan\alpha \qquad (1.37)$$

If $\alpha=0$ the correction becomes independent of d_1. Otherwise a first approximation for d_1 is determined from Fig 1.56 or Fig 1.57. After that d_1 is corrected subsequently using Equations (1.36) and (1.37). New runs for d_1 with the corrected heights will lead to more accurate heights h_{1C} and h_{2C} until improvements are negligible. This usually occurs after three iterations.

1.5 THE STATIC DETERMINATION OF ARP OF FULL SIZE AIRCRAFT ON THE GROUND

1.5.1 Advantages and Disadvantages

Military aircraft often fly in several configurations with different weapon systems, ECM-pods or fuel tanks at different store points below the wings or fuselage. The effect of the different configurations on antenna radiation patterns must be investigated. If all these patterns were measured in flight, it would require a large number of expensive flying hours. To avoid this, static ARP tests can be executed on full-scale airframes, mockups or airframe sections mounted atop heavy 3-axis positioners on outdoor antenna test ranges.

The advantages of this method are:

Measurements are made on real-size aircraft, no constraints due to model laws have to be considered and no up-translation of frequency is necessary, all measurements are made at the correct frequencies.

The "test aircraft" need not be fully equipped, especially inside the airframe. In many cases a mock-up is adequate and modifications in the configuration can be realized by provisional arrangements, in which only the radio frequency aspects need be taken into account. This, in conjunction with the saving of many flying hours, speeds up the measurements and increases the economy of ARP recording.

Since the aircraft can be inverted, antenna-to-antenna isolation measurements of two or more antennas, mounted on the same airframe, can be made without the influence of ground-coupling during measurements on antennas below the fuselage and wings.

The following disadvantages have to be considered:

Due to the large weight of the airframes under test, the pedestals have to be rugged enough to carry sometimes up to 25 tons.

The large dimensions of the device under test require a large quiet zone for the illuminating field, which leads to high towers and - in conjunction with the far-field condition requirements - to very large test areas.

If reflections of the illuminating RF-signals by ground and other obstacles are present, additional measures must be taken to attain the desired accuracy of the measurements.

1.5.2 System Considerations

The design of antenna test ranges is extensively discussed in Ref 1. For full scale aircraft measurements the effects of transverse and longitudinal amplitude taper at the antenna under test are especially important, because all parts of the airframe which influence the radiation patterns must be illuminated uniformly.

The transverse amplitude taper is affected by the beamwidth of the illuminating antenna. But a low directivity of this antenna, which is usually necessary for a uniform transverse amplitude taper of the incident field, causes reflections from the ground and from obstacles, which again deteriorate the transverse amplitude taper. In addition, care must be taken to illuminate the device under test symmetrically by proper adjustment of the illuminating antenna.

The longitudinal amplitude taper is caused by the attenuation of the radiated field at different distances r of the points under consideration within the space filled up by the device under test. From Eq (1.9) we learn that the field is attenuating by 20 log r. Hence the longitudinal amplitude taper A_T is given by

$$A_T = 20 \log r_2 - 20 \log r_1 = 20 \log (r_2/r_1) \qquad (1.38)$$

r_2 and r_1 being the longest and shortest distances from the device under test to the illuminator. According to Ref 1 the amplitude taper A_T should not exceed 1 dB, i.e. r_2/r_1 should be less than 1.12. A device under test with an extension of 15 m hence requires a source antenna distance of 140 m.

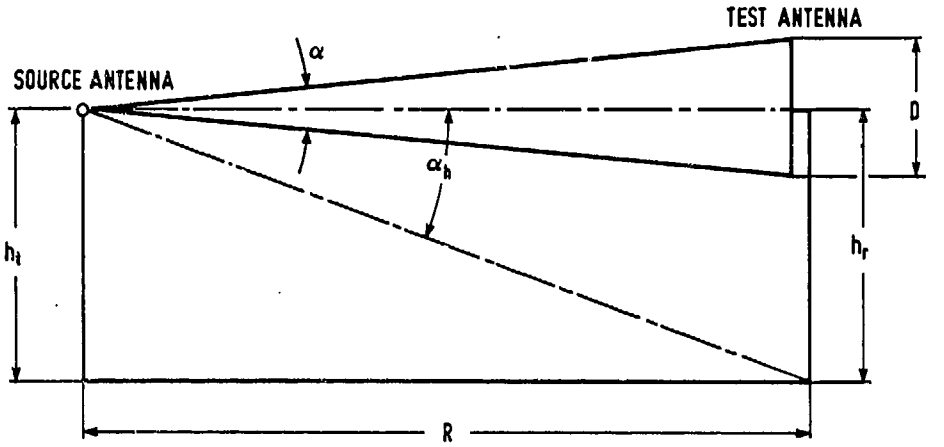

Fig 1.64 Elevated range geometrie

The elevated range geometry shown in Fig 1.64 is designed over a flat surface. In order to fade out ground reflections, the source antenna should be of high directivity and the first null of its pattern should be at the base of the test antenna tower. Under this condition the ground surface in front of the antenna under test does not intercept energy from the main lobe. The height of the test antenna h_r should be four times the diameter D of the device under test (the aircraft) or more. The source antenna height h_t should be approximately equal to h_r.

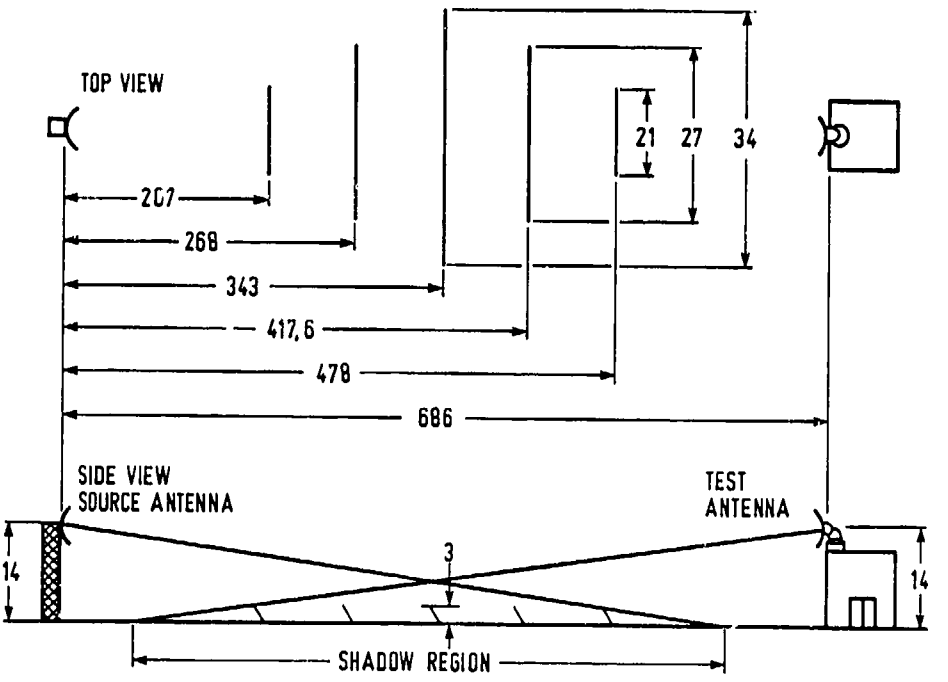

Fig 1.65 Elevated range with diffraction fences
(all measurements in m)

If the achievable height of the supporting test tower is too small, elevated ranges are sometimes improved by diffraction fences as illustrated in Fig 1.65. In the shadow region ground reflected rays are deflected by the fences towards the source antenna. The positions and orientation of the fences are usually determined experimentally. To suppress multiple reflections the fences are tilted.

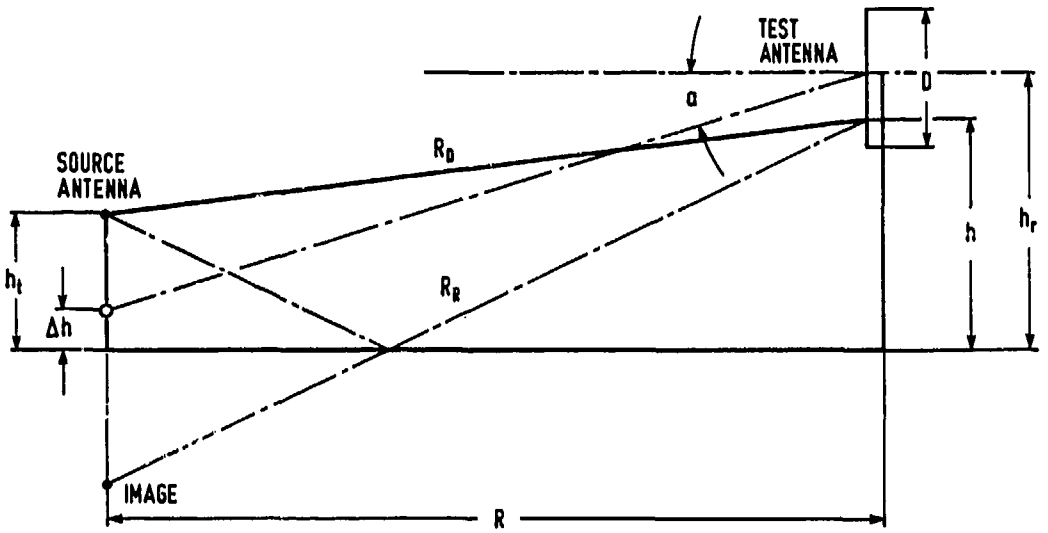

Fig 1.66 Ground reflection range geometry

Another method for reducing the ground reflection problems is to utilize the ground-reflection range illustrated in Fig 1.66. Here use is made of the interference caused by the antenna at height h_t and its image in the ground at $-h_t$. The height of the source antenna h_t is adjusted such that the direct wave from the source to the test antenna is in phase with the reflected wave (from the image) at the centre of the test antenna. By this means the power density at the test antenna is enhanced by 6 dB for a groundreflection coefficient of -1. Since the reflection coefficient of the ground is usually not equal to -1, the virtual center of radiation is displaced by h towards the source antenna and the height of the test antenna has to be increased from h to h_r. The surface of the range must be smooth, so that the energy is specularly reflected. Heavy rainfall may alter the reflection coefficient and due to this the virtual centre of radiation.

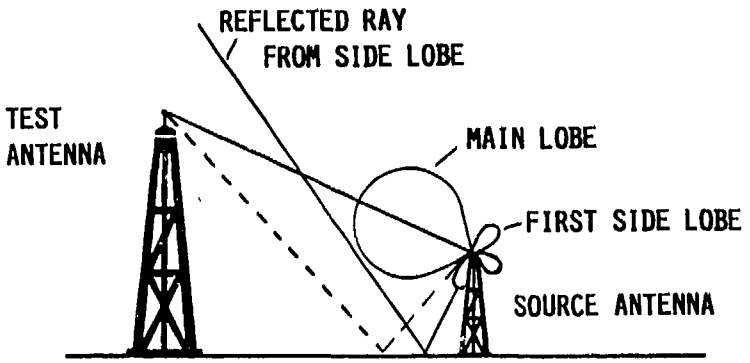

Fig 1.67 Slant range geometry

The slant range geometry shown in Fig 1.67 is designed with the source antenna near the ground. Its free-space radiation pattern points towards the centre of the device under test while its first null is aligned towards the specular ground reflection point. Thus the indirect signal is minimized. Because the tower must be relatively high, the weight of the device under test is limited, but the required test area is much smaller than for elevated ranges.

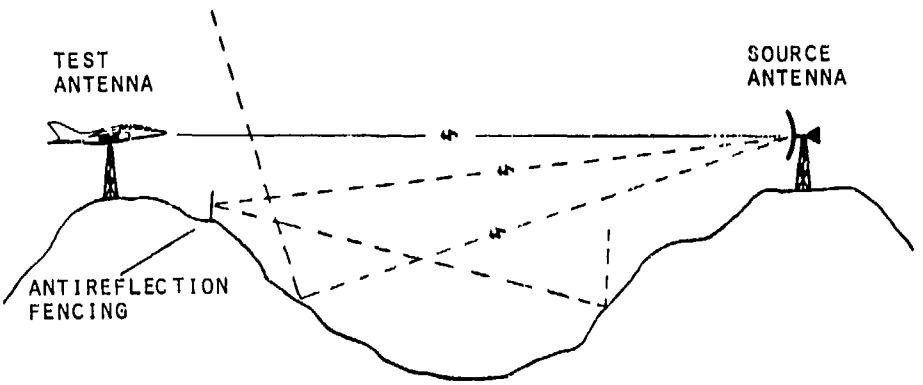

Fig 1.68 Mountainous site range gemoetry

Sometimes ranges for the measurement of ARP of real-size aircraft are installed on mountainous sites (see Fig 1.68). Ground reflections from the valley are absorbed or reflected away by the slope of the mountain which carries the test antenna. Usually additional anti-reflection fencing will improve the performance of the range. A good example of this type of test facility are the RADC ranges of USAF at Newport (NY), where distances of 2000 m to 2300 m across a 140 m deep valley are utilized. Fig 1.69 shows a full-size aircraft in a weaponry/stores configuration mounted atop a 3-axis positioner which can carry up to 25 tons.

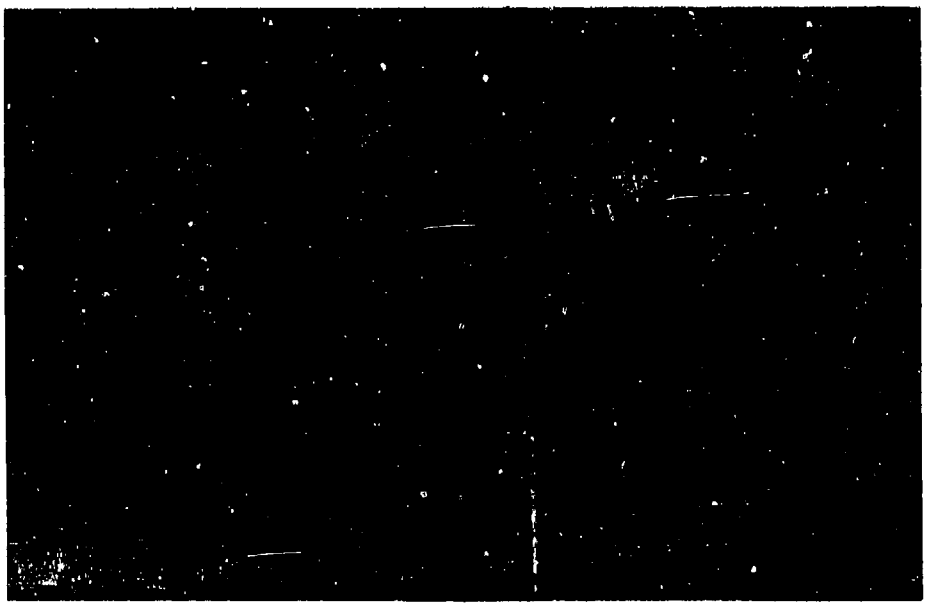

Fig 1.69 ARP measurement of real aircraft at RADC

Measurements over flat country are performed at the RATSCAT facilities, Holloman Air Force Base, New Mexico (Fig 1.70). In order to minimize interference by reflected signals, the test antennas are excited by pulsed signals. The receivers are synchronized with the pulsed sources to permit range gated operation, which suppresses all unwanted signals with a time delay longer than the pulse width of the transmitter. Care must be taken that the pulse width is long enough to prevent a suppression of signals reflected from all possible sections of the device under test, the airframe with the installed antenna. Thus the minimum pulse width is given by the maximum distance of any section of the airframe from the installed antenna. If e.g. this maximum distance is 10 m, the pulse width must be more than 33 ns. Usually reflections from the ground can not be suppressed, because the difference in the path length is much below 10 m.

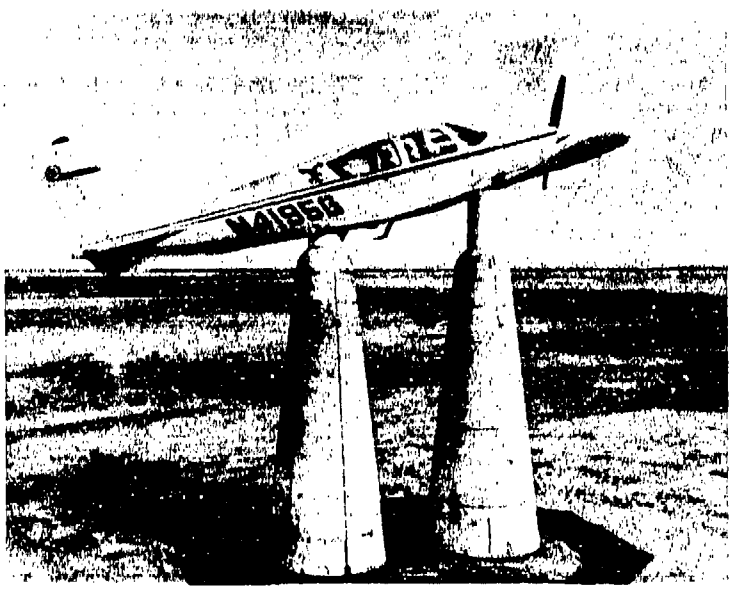

Fig 1.70 Aeroplane under test on turntable of the RATSCAT facilities

1.6 THE DETERMINATION OF ARP BY SUB-SCALE MODEL MEASUREMENTS

1.6.1 Advantages and Disadvantages

In sub-scale modeling for the determination of an ARP by static measurements the device to be tested is scaled down in size to a ratio between 1:5 and 1:50, depending on the size of the original aircraft and the available measurement facilities. Modeling is usually done in two steps. First the antenna itself is scaled down, its radiation characteristics are measured and compared with the characteristics of the original full sized antenna. If for this purpose counterpoises - e.g. a ground plane - are used the same scale factor has to be used. Thereafter the antenna model is integrated into the aircraft model and the ARPs are measured.

Sub-scale modeling has a number of advantages:
The main advantage is the complete free mobility of the model in space, which allows a coverage of the whole sphere, so that true conic section or great circle patterns can be recorded.

Due to the small scale, measurements are frequently made indoors so that the effects of weather are eliminated.

Once a model has been manufactured, it can be used repeatedly for all kinds of antenna and radar cross section measurements, even if later additional antennas or structural modifications of the carrier are planned.

The small dimensions also allow reflecting walls or other obstacles to be screened by absorbing materials to create a clean electromagnetic environment for the measurements.

Model measurements do not require expensive flying hours of an aircraft and can be handled by one or two persons.

The disadvantages of sub-scale model measurements are:

A high precision model must be manufactured. Especially for high-frequency measurements the simulation of the cabin roof and windows is difficult.

The model laws (see next section) can not be performed completely.

Sub scaling of the antenna elements requires much experience about where a certain degree of definition can be neglected and where not.

Extensive comparative measurements have shown, that there are usually differences between statically and dynamically recorded ARPs. Therefore static measurements are usually supplemented by dynamic measurements.

1.6.2 Model Laws

If measurements on sub-scale models are made, the modelling laws must be observed. The important parameters are the frequency f, the permittivity ϵ, the permeability μ and the conductivity σ. If the factor of reduction is denoted by n ($n > 1$), the parameters of the original by the index 1 and those of the model by the index 2, the model laws can be expressed by the following two equations (Ref 20).

$$\epsilon_1 \mu_1 f_1^2 = \frac{\epsilon_2 \mu_2 f_2^2}{n^2} \qquad (1.39)$$

$$\sigma_1 \mu_1 f_1 = \frac{\sigma_2 \mu_2 f_2}{n^2} \qquad (1.40)$$

As antenna measurements are usually conducted in free space, ϵ_1 equals ϵ_2 and μ_1 equals μ_2, so Eqs (1.39) and (1.40) are simplified to

$$f_1 = \frac{f_2}{n} \qquad (1.41)$$

$$\sigma_1 = \frac{\sigma_2}{n} \qquad (1.42)$$

Eq (1.42) creates a problem. The surface of the original aircraft will usually be metal ($\sigma_1 = 35 \frac{1}{\text{Ohm}} \frac{\text{m}}{\text{mm}^2}$) and the best surface conductor of the model could be silver ($\sigma_2 = 62 \frac{1}{\text{Ohm}} \frac{\text{m}}{\text{mm}^2}$) which results in a maximum factor of reduction n of 1.8 only.

Therefore the law expressed by Eq (1.42) will usually be violated as the reduction factor n is normally chosen between 5 and 50, depending on model size and available measurement facilities.

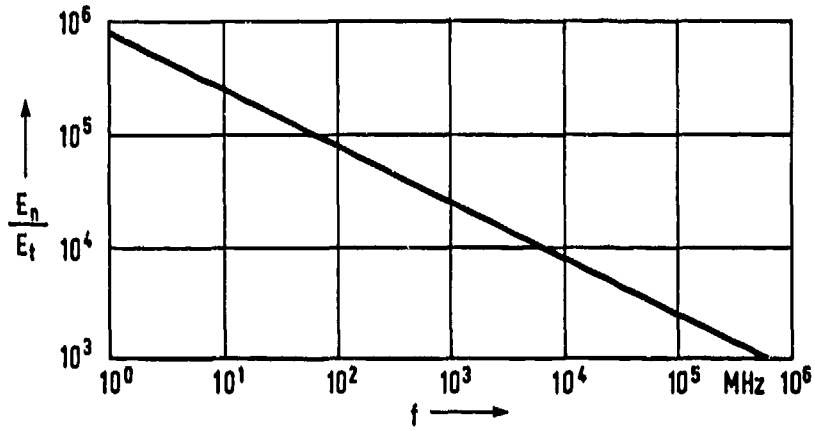

Fig 1.71 Ratio of normal and tangential electric field component on aluminum surface with respect to frequency

The finite conductivities of the full-size aircraft and model surface causes a tangential component E_t of the electric field intensity. As Fig 1.71 illustrates, the ratio of the normal component E_n to the component E_t for aluminum surfaces stays well above 10^3 for frequencies up to 100 GHz. For practical applications this small deviation of the electric field vector from the normal direction is negligible and the violation of the conductivity condition of the model laws is unimportant.

1.6.3 Far Field Measurements

Far field model measurement ranges are usually constructed as elevated ranges (see section 1.5.2) and the design criteria mentioned there are applicable. Due to the small model dimensions and weight, which reduce the load on the pedestal, the distance between the model under test and the source antenna can be varied. The distance can, therefore, be optimized for far field conditions, power budget and ground reflections. Fig 1.72 shows a typical configuration for a far field test range with selectable parabolic source antennas and a model tower supported by a ground rail system.

Fig 1.72 Test range for free field model measurements (DFVLR)

1.6.4 Anechoic Chamber Measurements

Outdoor far field measurements generally suffer from stray signals, depend on weather conditions and require large test areas. These disadvantages can be avoided by indoor anechoic chamber measurements. The side walls, floor and ceiling of a rectangular chamber are covered with absorbing material to simulate the properties of free space. There are still specular reflections from the walls, but they are attenuated to the order of -30 to -50 dB in a section called the quiet zone of the chamber where the device under test is located.

Sometimes the room has a long end portion shaped as a pyramidal horn to minimize direct reflection from walls, floor and ceiling, especially at low frequencies. In its low-frequency range this tapered chamber has a field distribution like that of a pyramidal horn, which differs from a spherical wave. Therefore it cannot be used for gain measurements based directly upon the free space propagation law.

In order to satisfy the far field conditions, chambers range in size up to 15x5 m in cross section and 50 m in length. The test frequencies can then range from 30 MHz to 100 GHz, depending on the properties of the absorbing material.

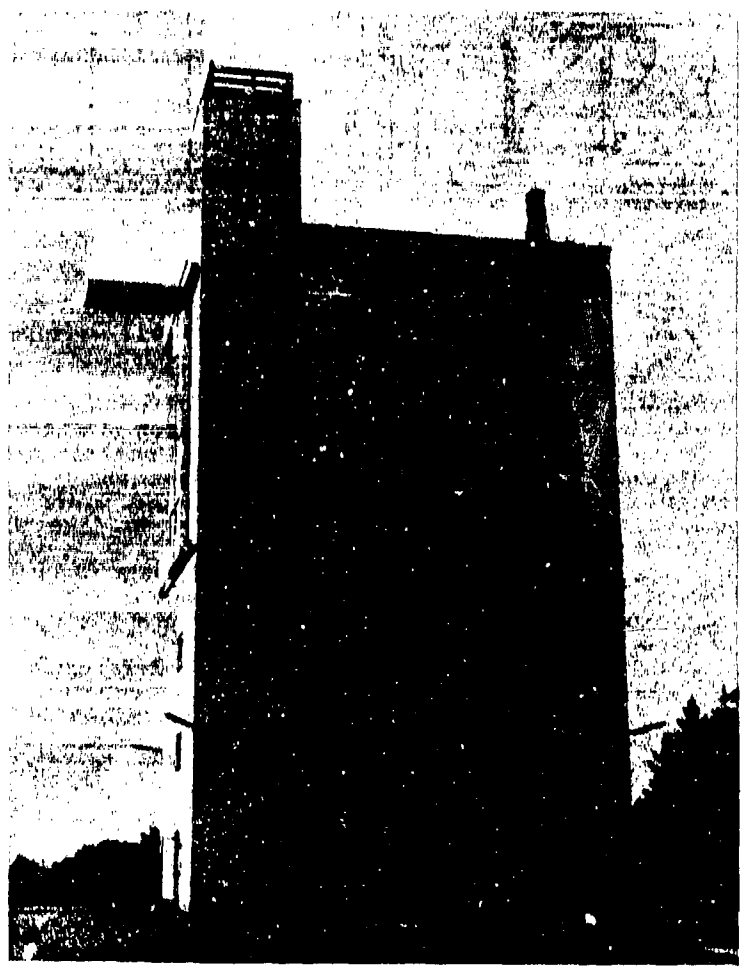

Fig 1.73 Test facility for aerospace antennas, anechoic chamber one side open (MBB Germany)

If one side of the anechoic chamber is open, the large measuring distance of a free field range is combined with the advantanges of an indoor anechoic chamber. Fig 1.73 shows an elevated test range with an anechoic chamber, the open side is weather protected by a thin dielectric awning (Ref 21).

The size of an anechoic chamber can be reduced considerably if the compact-range technique is adopted. This technique makes use of the fact that the wavefront emerging from a parabolic reflector is approximately plane if the feed is positioned at the focal point of the reflector. By this method the distance between the antenna under test and the illuminating antenna is substantially reduced.

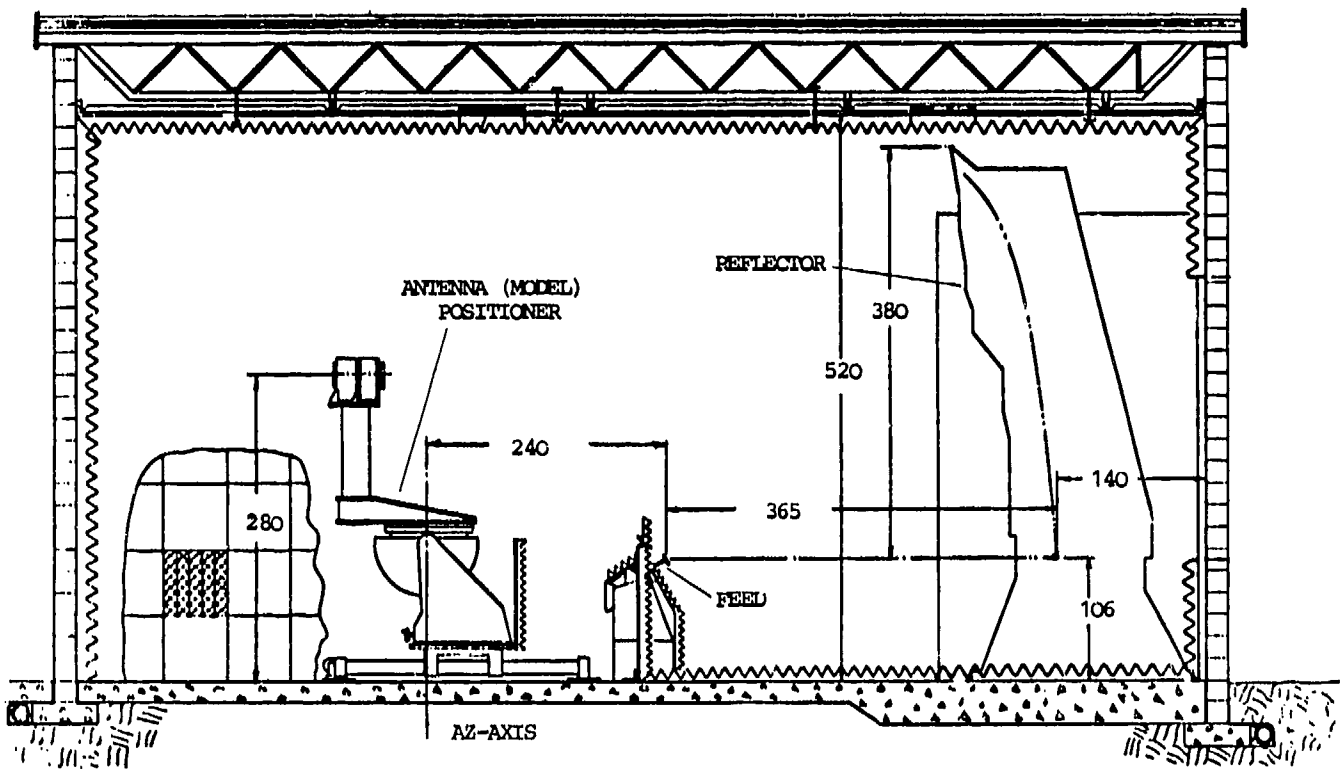

Fig 1.74 Compact range chamber at AERITALIA, Caselle (all measurements in cm)

Fig 1.74 illustrates a compact range chamber with an offset reflector designed for a frequency range of 4-18 GHz. The feed is interchangable for different frequency bands and polarisation is remotely controlled. Feed and model positioners are screened by absorbers to avoid additional reflections. The edge of the parabolic offset reflector (see Fig 1.75) is designed to reduce diffraction effects in order to produce a quiet zone for the measurements. The length of this zone is 120 cm, the diameter depends on the tolerable amplitude taper and ripple. For a diameter of 120 cm amplitude taper stays below 0,5 dB and ripple below 0,30 dB. If 1 dB for amplitude taper and ripple can be tolerated, the diameter of the quiet zone increases to 180 cm. More details are given in Ref 22. The major limitations of a compact range facility are the narrow frequency range and limitatons on the size of the quiet zone.

The development of powerful computers has recently made possible the application of near-field measurements to far-field radiation pattern determination. In this technique the amplitude and phase of the signal from a radiating antenne are measured in its near field. Measured data are stored in a digital computer and the far field is computed by a transformation algorithm. The advantage of this method is that only a small anechoic chamber with moderate sreening is required, even for a high directivity antenna. Once the near field has been determined, arbitrary cuts through the radiation characteristics can be produced by the computer without additional measurements.

For aircraft model radiation pattern determination, near-field scanning methods such as plan cartesian, cylindrical and spherical scanning are available. Only the last can be used for sampling the energy spread over the whole sphere. Fig 1.76 illustrates a sample arrangement, the model is supported by an azimuth over elevation positioner and the probe is adjustable in polarisation.

There have been few applications of this test technique to ARP-modeling of aircraft up to now and no data is available at this time. More detailed descriptions of near field facilities are given in Refs 23 and 24. A comprehensive report of the theoretical background is published in Ref 25.

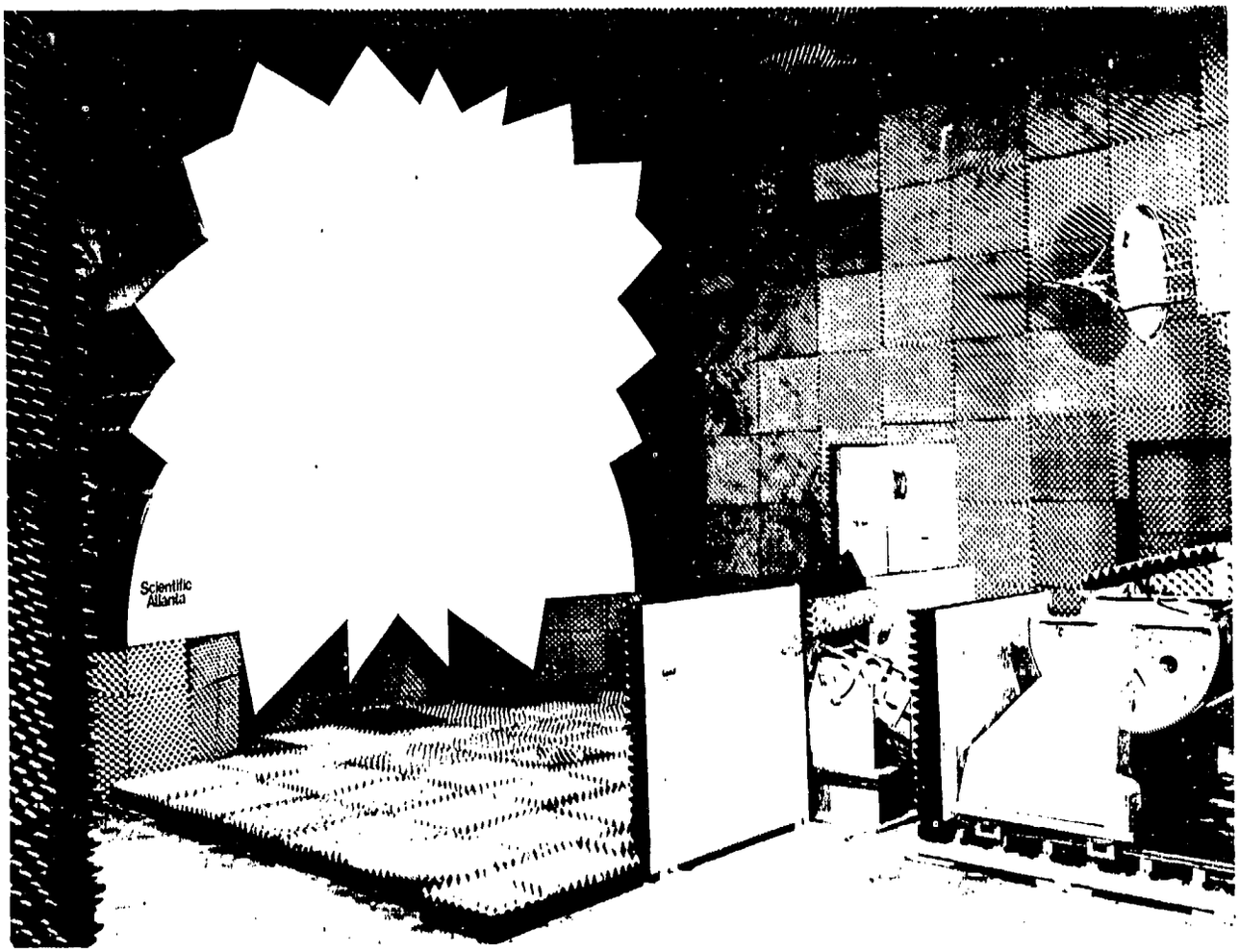

Fig 1.75 Parabolic reflector for illuminating compact anechoic chamber facilities

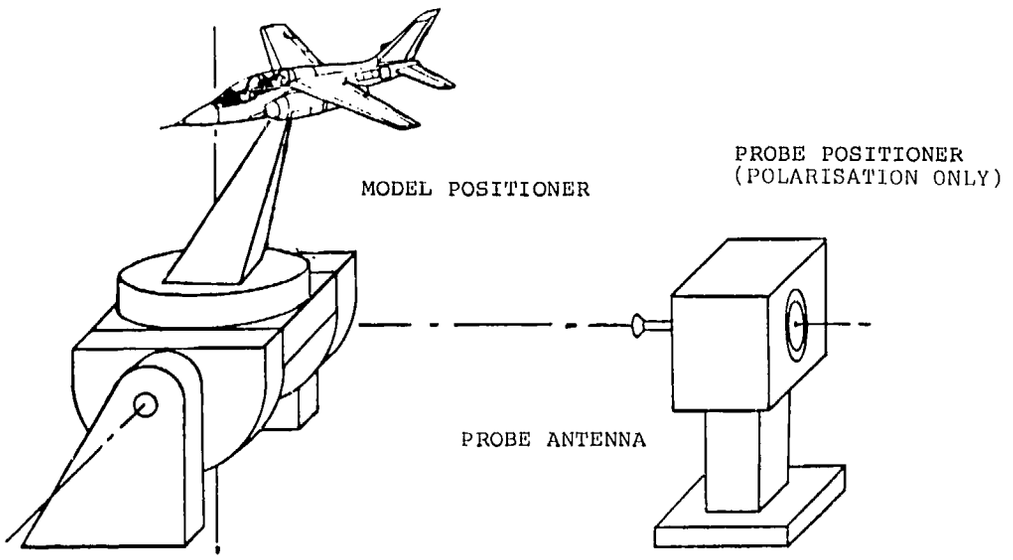

Fig 1.76 Spherical near-field antenna measurement arrangement

1.6.5 Comparison of Measurements on Full-Size Aircraft and Sub-Scale Models

In the DFVLR extensive comparisions between antenna pattern measurements on full-size aircraft and sub-scale models have been made (Refs 3 and 4). For the model measurements the far-field method discussed in section 1.6.3 has been used (see also Fig 1.72). The different types of aircraft investigated have been small single- and twin-engine aircraft of the high- and low-wing type. The results have shown, that about 50% of the measurements differ by less than 2.5 dB and the remainder by less than 5 dB. If larger differences are observed, these are usually caused by different experimental conditions or differences in aircraft configurations (see section 1.2.4). A few examples for the single-engine, low-wing aircraft Piaggio P 149 D are given in Figs 1.77 to 1.80.

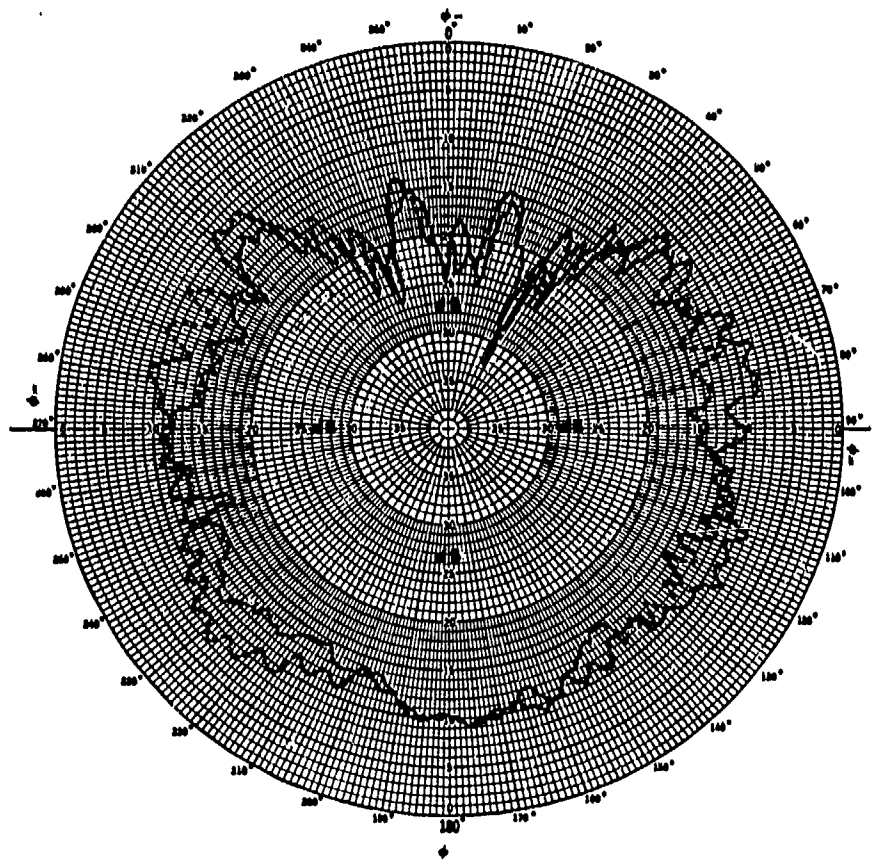

Fig 1.77 Radiation pattern of a DME antenna
Aircraft: Piaggio P 149 D, antenna (stub) below fuselage,
frequency 1011 MHz, test flight: circle, skidded turn
dotted line: sub-scale model measurement

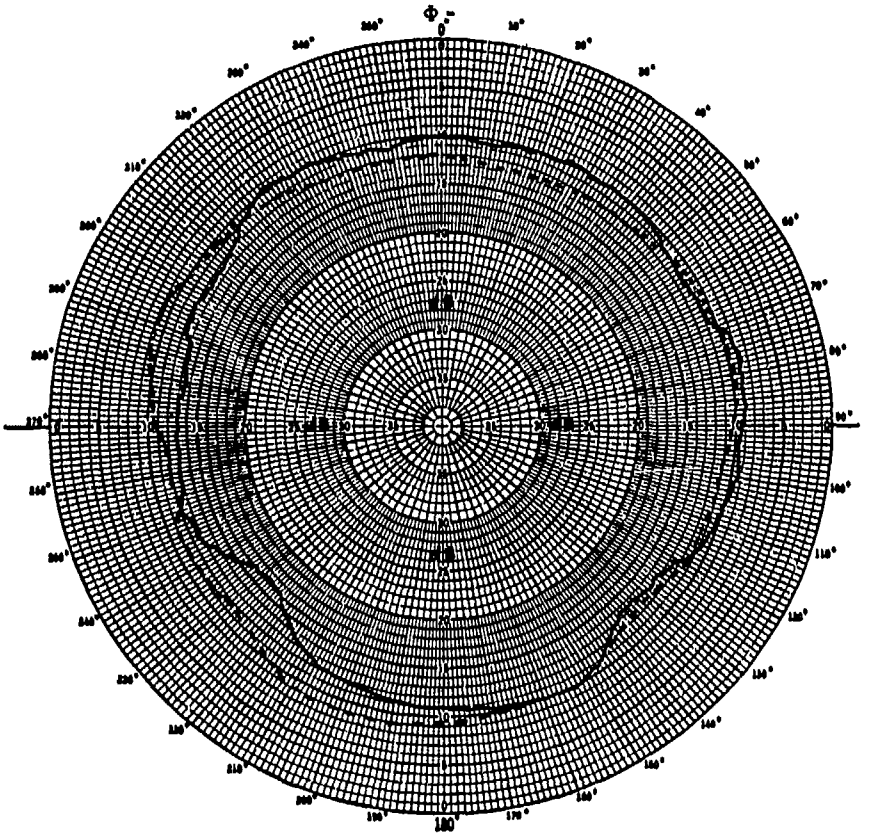

Fig 1.78 Radiation pattern of a communication antenna
Aircraft: Piaggio P 149 D, antenna (stub) below fuselage,
frequency 117.6 MHz, test flight: circle, skidded turn
dotted line: sub-scale model measurement

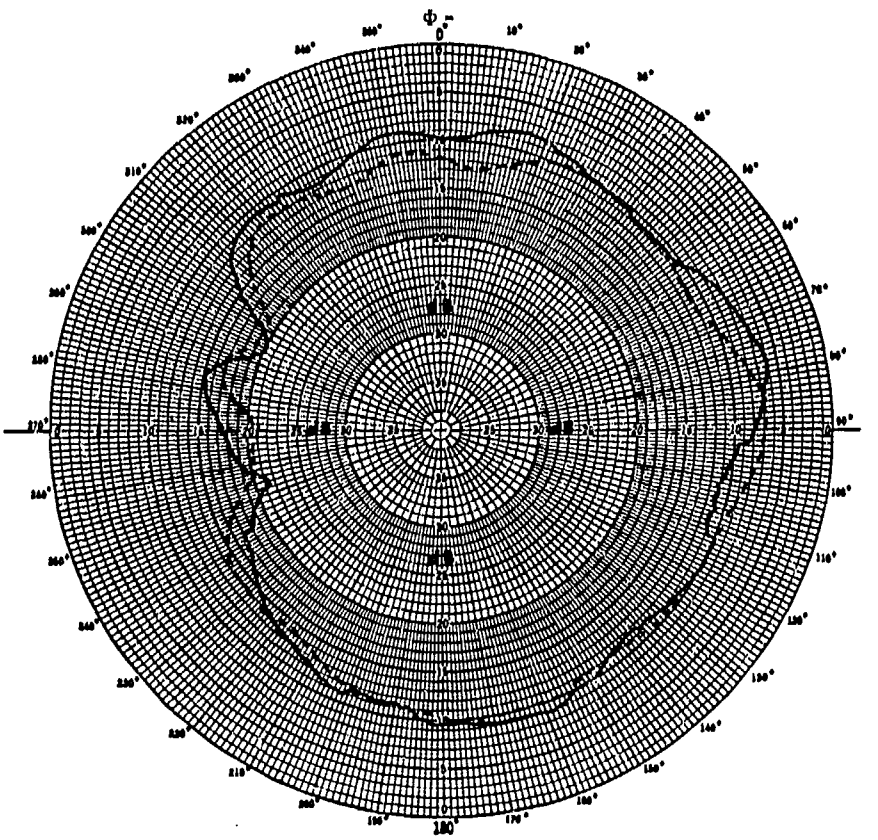

Fig 1.79 Radiation pattern of a communication antenna
Aircraft: Piaggio P 149 D, antenna (stub) below fuselage,
Frequency 117.6 MHz, test flight: circle, angle of roll 30°
dotted line: sub-scale model measurement

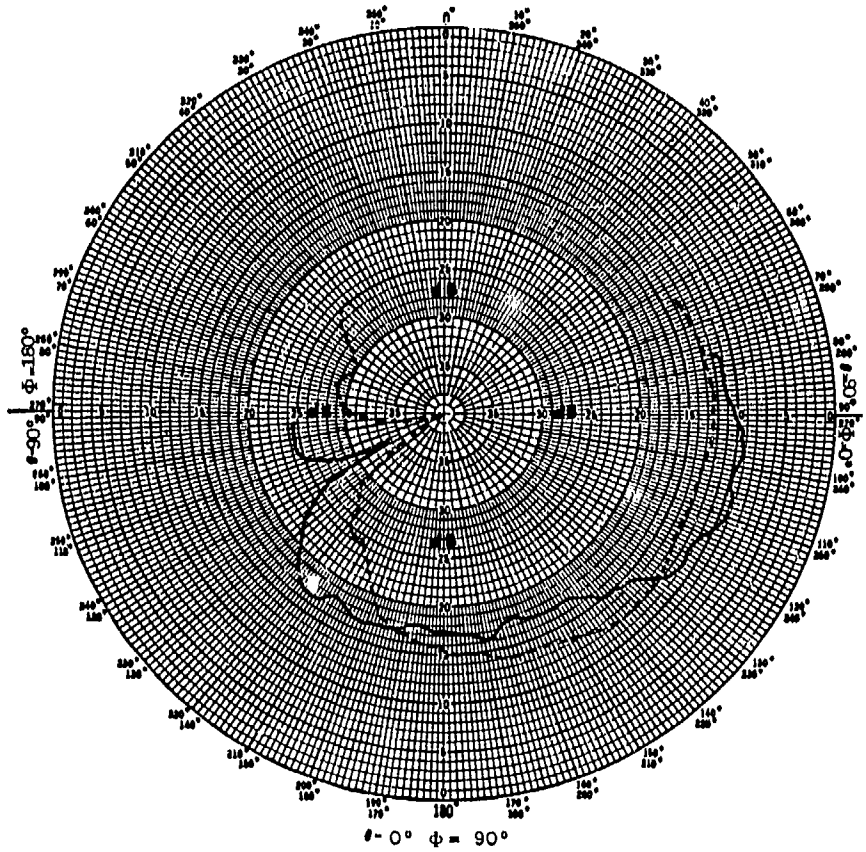

Fig 1.80 Radiation pattern of a glide-slope antenna
Aircraft: Piaggio P 149 D, antenna (folded dipole) integrated into the landing-headlight slot on the left-wing nose, frequency 335,5 MHz, test flight: fly over
dotted line: sub-scale model measurement

PART 2

DETERMINATION OF RADAR REFLECTION CHARACTERISTICS

by
Donald Macdonald

2.1 DEFINITIONS

2.1.1 Radar Cross Section (RCS) or Radar Echoing Area (REA)

In its simplest terms, RCS is defined as a hypothetical area intercepting that amount of power, which when scattered equally in all directions, produces an echo at the radar equal to that from the target. It is given the symbol σ and is most often quoted in square metres.

By definition,

$$\sigma = 4\pi R_r^2 \times \frac{\text{power density at receiver}}{\text{Incident power density at the target}}$$

The radar cross section of a target is a quantitative measure of the ratio of power density in the vector signal scattered in the direction of the receiver to the power density of the radar wave incident upon the target. A complex target comprises a multiplicity of individual scatterers which, when illuminated by a radar transmission become echo sources which combine with constructive and destructive interference, in numbers which depend on the geometry of the engagement. The vectorial nature of the scattering interaction requires specification of the transmitter polarisation and receiver polarisation with reference to target orientation in three dimensions. Radar operating frequency is an additional parameter which must be specified before a single number suffices to define the far field radar cross section for a given target. Thus a single-number specification holds only for the particular target, polarisation combination, aspect and frequency for which it was established. The statistics pertinent to σ as a function of time in a dynamic radar situation are NON-ERGODIC (non-time stationary) and hence their simulation by (say) coloured noise implies an over simplification.

Typically, the value of σ at 5 GHz, and with linear polarisation, has a dynamic range of 60 dB during a 360° azimuthal change of aspect against an aircraft target (Fig 2.1).

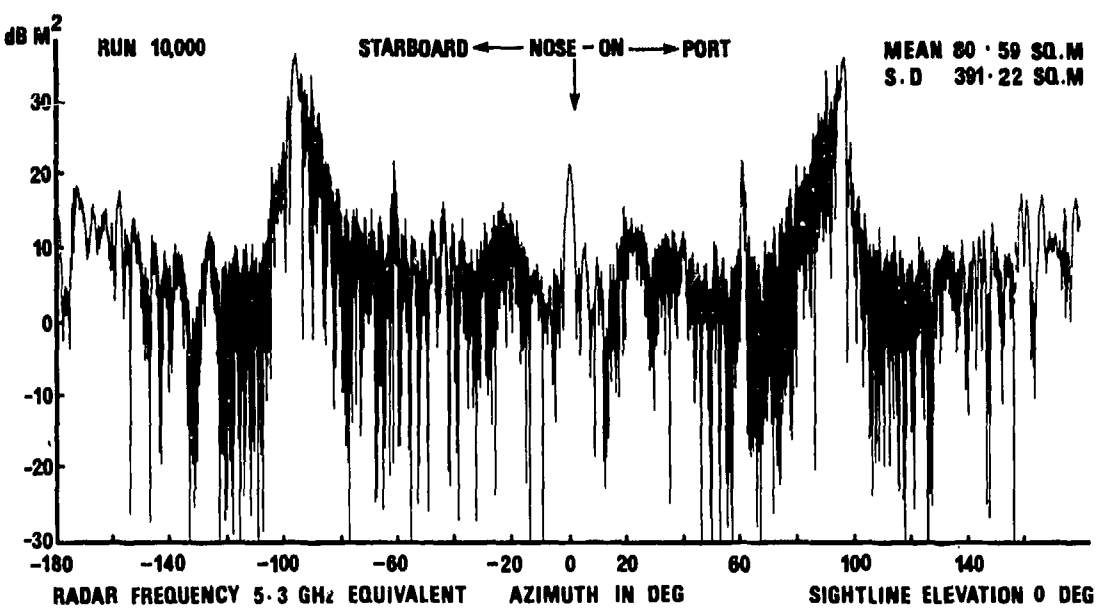

Fig 2.1 Typical wing plane plot of RCS in dBm^2 of single engine jet fighter aircraft

2.1.2 Angular Noise or Glint

Tracking and direction finding radars usually attempt to determine the direction of target centre by schemes which result essentially in finding the normal to the received wavefront. Such a front from a single source would be spherical and all normals to it would pass through the single source target. However, real aircraft targets comprise many echo sources and the resulting interference of their respective re-radiations produces distortions of the wavefront presented to the radar. These perturbations provide the radar with many possible pointing directions even as the target aspect changes

fractions of a degree. Fig 2.2a shows the perturbations due to just two echo sources and the consequent possible pointing errors. Most of the power in these time varying data is contained within the lower few Hz of the power spectrum and to these low-frequency components the radar is particularly able to react. Fig 2.2b. Lower, though still significant power at somewhat higher frequencies results in received signals sometimes indicating the direction of the target centre to be many target widths displaced from the true position. Most operational radars are unable to follow fast glint fluctuations and so do not yield gross errors. The result is that the position of target radar centre is mostly determined as a point moving about the airframe and tending to dwell on the currently dominant source, or to jump between two or three most dominant sources.

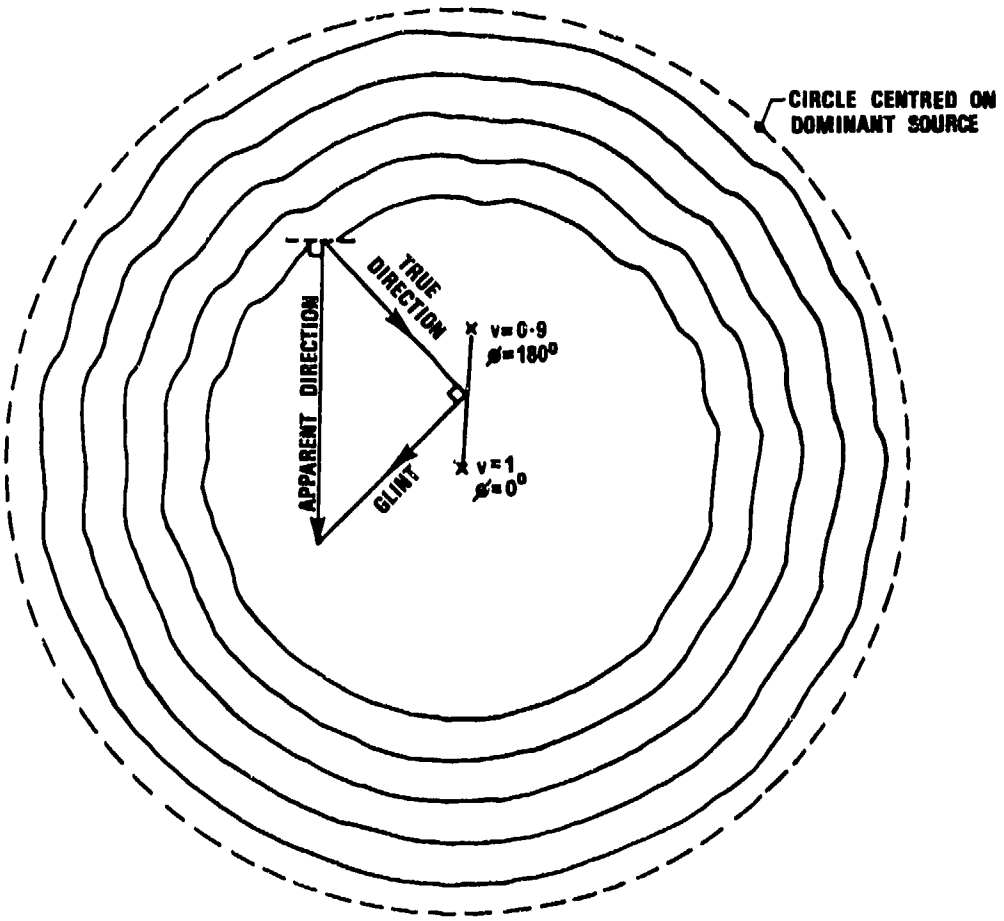

Fig 2.2a Phase front plots around a two-source reflector

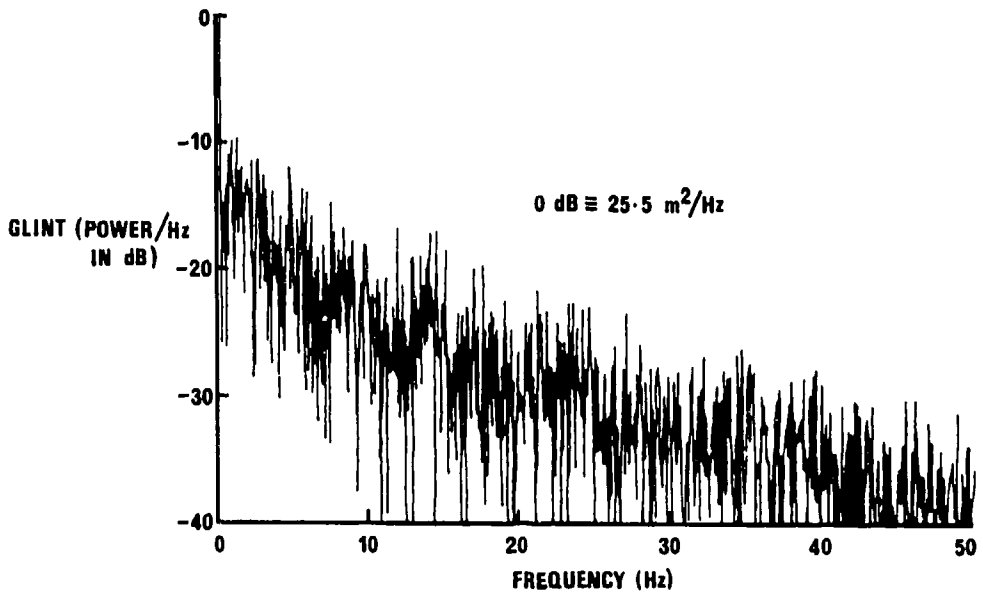

Fig 2.2b Glint spectrum for a twin-jet aircraft

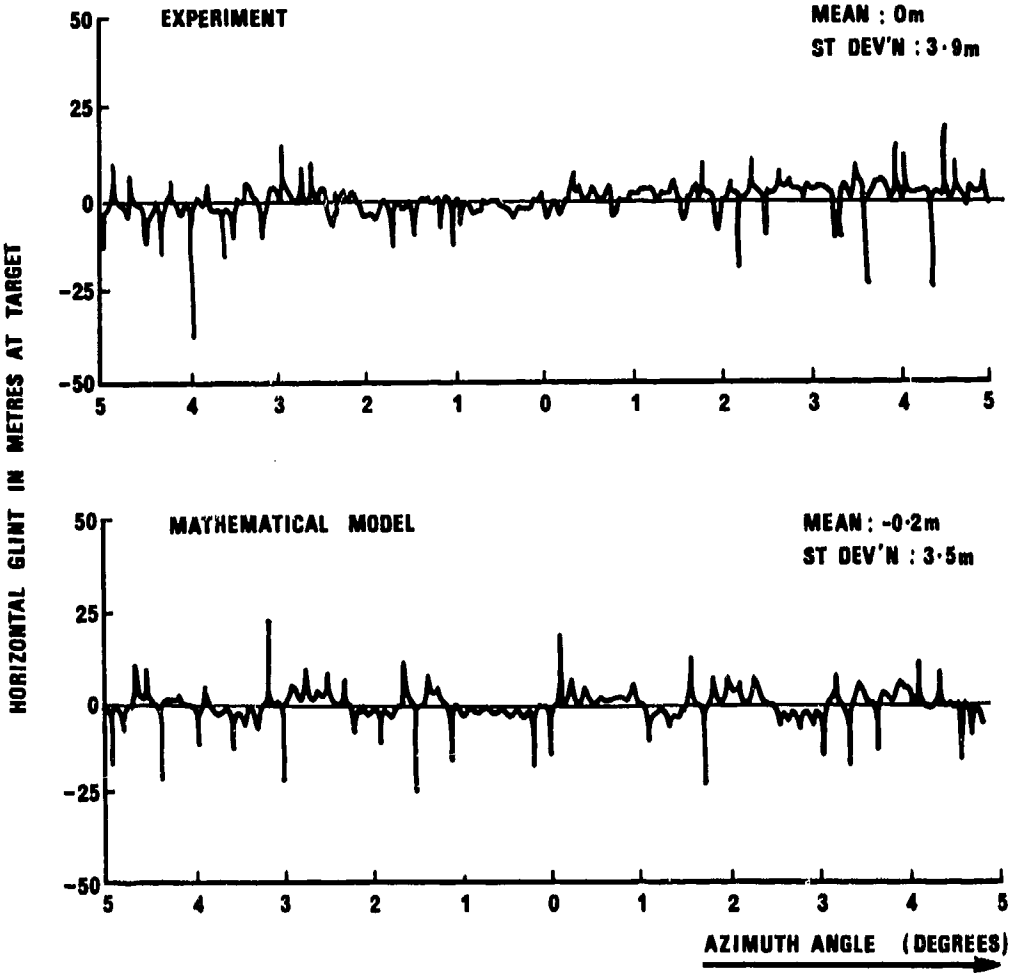

Fig 2.2c Comparison of measured glint with glint derived from a mathematical model of the same aircraft model

Variation of the radar centre is known as angular glint and while the significance on radar performance is not great at long ranges, it is most important at short ranges, say 10 km and less. Angular glint is most often quantified as a linear displacement normal to the incident illumination direction, of the radar centre from the defined physical target centre and expressed in, "metres at the target" (Fig 2.2c).

2.1.3 Polarisation

The polarisation of an electromagnetic wave can be characterised by the direction of its electric field vector E. Hence, for example, vertical polarisation means that the E vector is vertical.

Referred to the scattering body it is sometimes convenient to define parallel and perpendicular polarisation.

For a plane surface parallel polarisation implies that the E vector is parallel to the plane containing the incident sight line and the normal at the point of reflection. Perpendicular polarisation has the E vector perpendicular to that plane.

(a) Power Scattering Matrix

The scattering from a target is usually depolarised, i.e. the reflection in the direction of the receiver antenna has a different polarisation from that incident on the target.

Thus for example if the target is illuminated with vertical linear polarisation, vertical and horizontal components can be selected by the receiver antenna. These associated RCS values can be denoted VV, HV respectively.

The concept of a power scattering matrix has been used (Ref 27) to describe in compact form the four RCS values obtained by using, in turn, orthogonal polarisation illumination of the target.

Thus for vertical and horizontal illumination

$$\left[\sigma_A\right] = \begin{bmatrix} \sigma_{VV} & \sigma_{HV} \\ \sigma_{VH} & \sigma_{HH} \end{bmatrix} \tag{2.1}$$

and for circular polarisation

$$\left[\sigma_B\right] = \begin{bmatrix} \sigma_{RR} & \sigma_{LR} \\ \sigma_{RL} & \sigma_{LL} \end{bmatrix} \tag{2.2}$$

It can be shown for a monostatic radar (transmitter and receiver co-located) that $\sigma_{VH} = \sigma_{HV}$ and $\sigma_{RL} = \sigma_{LR}$ at all times.

(b) Voltage Scattering Matrix

A voltage scattering matrix is now generally used to describe the total receivable scattering from a target.

Then using the notation of (Ref 28)

$$E_1^s = a_{11}E_1^i + a_{12}E_2^i \tag{2.3}$$

$$E_2^s = a_{21}E_1^i + a_{22}E_2^i \tag{2.4}$$

Here E_1, E_2 are two orthogonal polarisation components representing the incident illumination field or the scattered field, eg E_1^i, $E_2^i = E_V^i$, E_H^i for vertical and horizontal linear polarisation illumination.

Using a matrix notation

$$\begin{bmatrix} E_1^s \\ E_2^s \end{bmatrix} = \begin{bmatrix} a_{11} & a_{12} \\ a_{21} & a_{22} \end{bmatrix} \begin{bmatrix} E_1^i \\ E_2^i \end{bmatrix} = S \begin{bmatrix} E_1^i \\ E_2^i \end{bmatrix} \tag{2.5}$$

The a_{ij} are, in general, complex quantities so that

$$\left[S\right] = \begin{matrix} |a_{11}|e^{i\phi_{11}} & |a_{12}|e^{i\phi_{12}} \\ |a_{21}|e^{i\phi_{21}} & |a_{22}|e^{i\phi_{22}} \end{matrix} \tag{2.6}$$

Then

$$\sigma = |a_{11}|^2, |a_{12}|^2, \text{ etc.}$$

The above scattering matrix values can be used to calculate the received scattering for any combination of transmitter and receiver polarisations.

(c) Relative Scattering Matrix

Study of the voltage scattering indicates that 8 components, (4 amplitude and 4 phase), need to be measured in its determination. However, by factoring out, for example, ϕ_{11} from the voltage matrix

$$\left[S\right] = \frac{e^{i\phi_{11}}}{\sqrt{4\pi R_R^2}} \begin{bmatrix} \sqrt{\sigma_{11}} & \sqrt{\sigma_{12}}\, e^{i(\phi_{12}-\phi_{11})} \\ \sqrt{\sigma_{21}}\, e^{i(\phi_{21}-\phi_{11})} & \sqrt{\sigma_{22}}\, e^{i(\phi_{22}-\phi_{11})} \end{bmatrix} \tag{2.7}$$

Thus 7 quantities are required to describe the magnitude and polarisation of the scattering for any illumination polarisation (Ref 28).

For a monostatic radar only 5 components need to be determined since the two cross polarisation terms are identical.

Considering linear polarisation in terms of vertical and horizontal components and defining a_{VH} to apply to vertically polarised incident energy and horizontally polarised scattered energy etc., we obtain:

$$\begin{bmatrix} E_V^s \\ E_H^s \end{bmatrix} = \begin{bmatrix} a_{VV} & a_{HV} \\ a_{VH} & a_{HH} \end{bmatrix} \begin{bmatrix} E_V^i \\ E_H^i \end{bmatrix} \times \frac{1}{4\pi R_r^2} \qquad (2.8)$$

and for circular polarisation

$$\begin{bmatrix} E_R^s \\ E_L^s \end{bmatrix} = \begin{bmatrix} a_{RR} & a_{LR} \\ a_{RL} & a_{LL} \end{bmatrix} \begin{bmatrix} E_R^i \\ E_L^i \end{bmatrix} \times \frac{1}{4\pi R_r^2} \qquad (2.9)$$

Again $a_{VH} = a_{HV}$ and $a_{RL} = a_{LR}$ for a monostatic radar.

2.1.4 Near Zone, Fresnel Zone and Fraunhofer Zone

The power emitted from a radar antenna travels a short distance before merging into a coherent beam. This distance is known as the Near zone (or Near field) and marks the beginning of the Fresnel zone.

In the Fresnel zone the energy in the beam travels forward with a spherical wavefront until at infinity, the radius of curvature would be infinite and the wavefront strictly planar. For obvious practical reasons an acceptable approximation must be used so that at some real range (and beyond) the wavefront may be taken to be sensibly planar. This range is usually chosen to be D^2/λ where D is the maximum dimension of the antenna and λ is the radar wavelength. The region beyond this range is known as the Fraunhofer zone. A radar-illuminated target can be considered as a radiating aperture, but because of the phase taper of the illuminating field, $2D^2/\lambda$ applies, when D is now the maximum lateral dimension of the target. This $2D^2/\lambda$ range is frequently referred to as the Rayleigh distance of the target and equates to 45° maximum differential phase variation across the target for two way propagation.

2.2 THE PARAMETRIC DEPENDENCE OF σ IN THE RADAR EQUATION

2.2.1 Derivation of the Radar Equation

Assume a transmitter of power P_t with an antenna of gain G_t. Then at a target range R_t the power density is

$$\frac{P_t G_t}{4\pi R_t^2}$$

Let this target have an RCS equal to σ, then a portion of the power intercepted is re-radiated in the direction of the radar and the power density at the receiver antenna is

$$\frac{P_t G_T}{4\pi R_t^2} \cdot \frac{\sigma}{4\pi R_r^2}$$

where R_r is the range to the receiver. Let the receiver antenna have an effective interception area equal A_r. Then the power received is

$$P_r = \frac{P_t G_t}{4\pi R_t^2} \cdot \frac{\sigma}{4\pi R_r^2} \cdot A_r$$

and

$$\sigma = 4\pi R_r^2 \frac{P_r/A_r}{G_t P_t / 4\pi R_t^2} = 4\pi R_r^2 \times \frac{\text{Power density at receiver}}{\text{Incident power density at the target}}$$

But antenna theory shows that

$$A_r = \frac{G_r \lambda^2}{4\pi}$$

where G_r is the gain of the receiver antenna. Substituting for A_r and rearranging the terms,

$$P_r = \frac{P_t G_t G_r \lambda^2 \sigma}{(4\pi)^3 R_t^2 R_r^2}$$

If the radar is monostatic,

$$R_t = R_r = R \text{ and } G_t = G_r = G$$

and

$$P_r = \frac{P_t G^2 \lambda^2 \sigma}{(4\pi)^3 R^4}$$

which is the basic Radar Equation. For maximum range R_{max}, P_r equals the minimum detectable signal, S_{min}. Hence

$$R_{max} = \left[\frac{P_t G^2 \lambda^2 \sigma}{(4\pi)^3 S_{min}}\right]^{1/4}$$

and $S_{min} = KT_o B_n F_n$ S/N

K = Boltzmann's constant

where B_n = Noise bandwidth

and F_n = Receiver noise figure.

There are a great many factors affecting the value of σ and the more important ones relating to the radar parameters are discussed in the following paragraphs. Factors relating to the physical target are discussed in Section 2.2.6.

Radar clutter comprises spurious signals at the radar receiver due to the presence of unwanted reflectors. In the case of outdoor measurements these may be the ground, mountains, buildings, vehicles etc, and indoors, the floor, walls, ceiling, other equipment, people etc. In both cases unwanted radar or radio transmissions can also be included in causes of radar clutter.

ECM (Electronic Counter Measures) include techniques for deliberately creating spurious or misleading signals at the radar receiver.

Both clutter and ECM are neglected in this Volume (Part 2) since the subject measurements are assumed to be made in free space. When special precautions have to be taken to ensure this state is achieved, for example in the elimination of multipath reflections from the ground, or the gating-out of background echoes, then these are described.

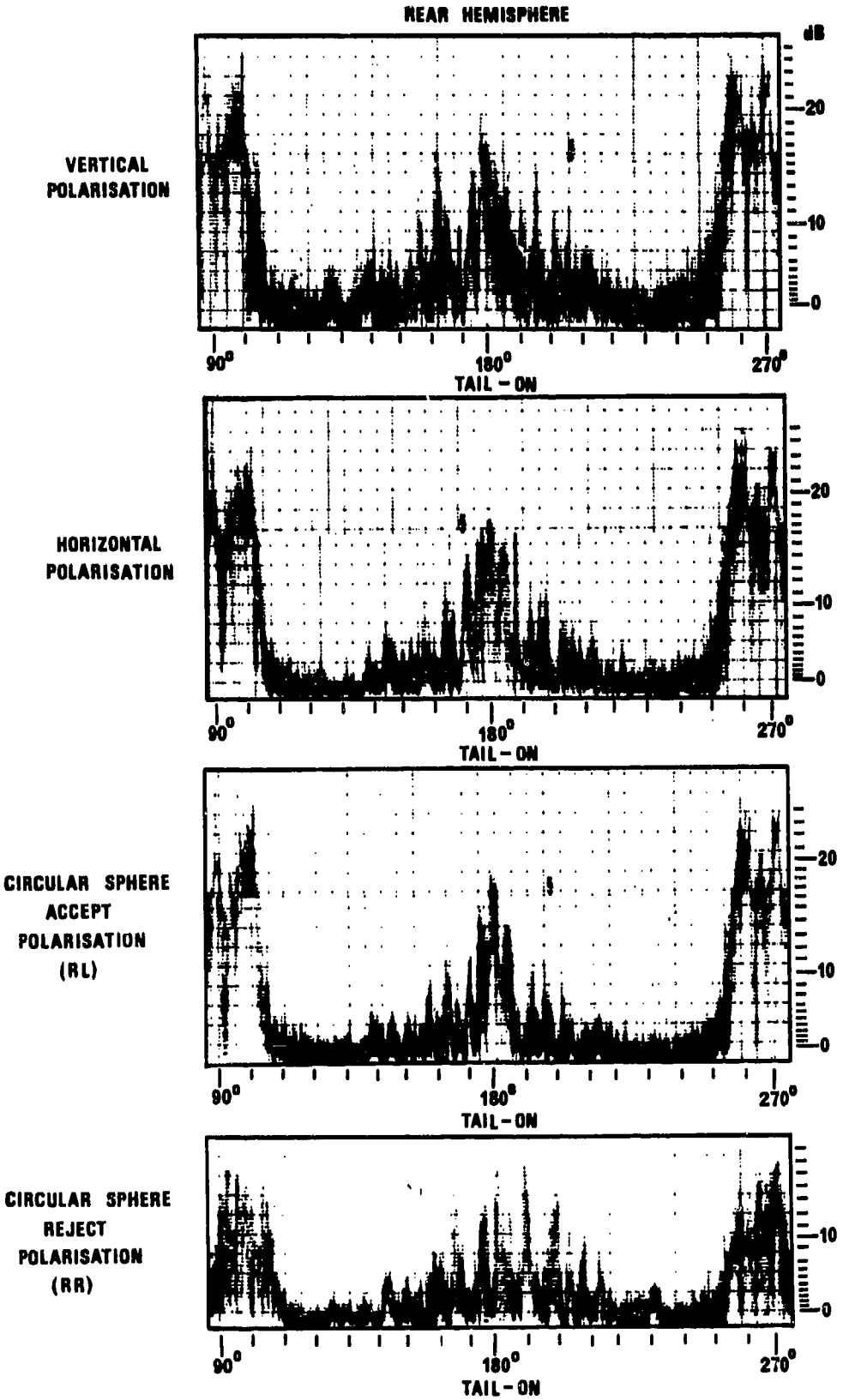

Fig 2.3 Wing plane RCS plots of twin-jet aircraft. Radar frequency 10 GHz

2.2.2 The Effect of Radar Frequency

Some of the physical features of an aircraft target contribute to the total radar return by producing specular echoes. These features are comparatively large, uniform surfaces such as the fuselage, wing leading edges, doubly curved nose regions etc. Other specular echoes originate from multiple reflections at corners - such as wing-to-fuselage and intake-to-wing junctions.

The magnitude and angular spread of some of these are frequency or frequency squared dependent. However, except for the special case of a 90° corner, these specular echoes, whilst of large magnitude, are angularly extremely narrow and contribute much less than might be expected to an average RCS over say 10° angular range.

Echo sources such as radars and radomes, intakes and engines, various other cavities etc are in general less frequency sensitive, and usually reflect over wide angles.

Some modern radars use, of course, frequency agility, or pulse compression or other forms of frequency modulation or switching and each will impress such characteristics on the radar returns to some degree.

2.2.3 The Effects of Radar Polarisation

Virtually all radars have specific polarisation characteristics. Current examples include:-

(a) Transmit E vertical, receive E vertical .
(b) Transmit E horizontal, receive E horizontal

These are known as co-planar polarisation systems.

(c) Transmit right hand circular, receive E vertical
(d) Transmit and receive right hand circular
(e) Transmit rotating linear, receive E vertical.

Each of these polarisation systems produces its characteristic returns from the target and hence the value of σ and its variation with aspect angle exhibit differences for each system (Fig 2.3).

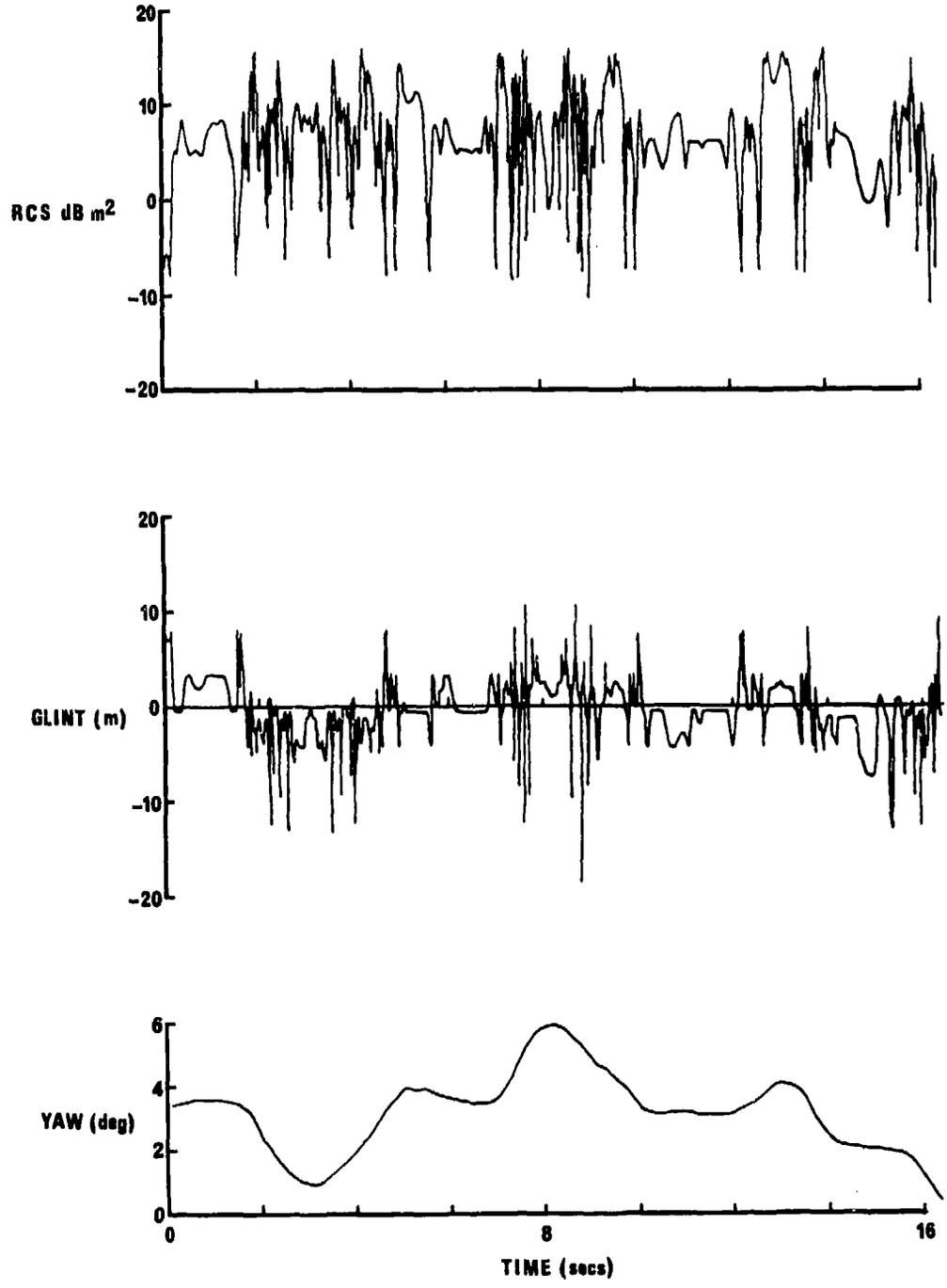

Fig 2.4 Time series plots for a twin-engined aircraft

2.2.4 The Effects of Target Aspect Angle

The target to radar transmitter aspect angle and that of the radar receiver to the target (identical in a monostatic radar) are of extreme importance to the value of σ. Typically, an aircraft target return may vary in magnitude over a range of 30 dB for a change of less than 1° (depending on radar frequency and target size).

Although it may reasonably be concluded that an average value of σ over, say, 10° aspect change is the "practical answer", it must not be forgotten that a real (dynamic) engagement can produce geometries which maintain the target-radar aspect to dwell on a peak or trough return for several seconds.

Real (dynamic) engagements relate not to averages of the static re-radiation pattern of 30 dB lobes at say 5 per degree, but to a time average as this pattern is sampled, ie from time series information (Fig 2.4).

2.2.5 Transmitter Waveform and Receiver Processing

The types of radar in current use fall into one of three general categories: CW (continuous wave), Pulsed or Pulse Doppler. There are sophisticated variants but it is sufficient for the purpose of this section to consider only the three basic types.

2.2.5.1 CW Radar. Without added facilities, such a radar measures target relative velocity only and may use a velocity gate to track a target. It is intrinsically a NARROW BAND system - typically 200 Hz.

2.2.5.2 Pulsed Radar. This system measures target range, using a range gate for tracking purposes. It has invariably a WIDE BAND receiver, the IF bandwidth being approximately inversely proportional to half the pulse width and a typical figure is 5 MHz.

2.2.5.3 Pulsed Doppler. This form of coherent radar combines pulse and CW features and has the ability to measure both relative velocity and range - albeit with controllable ambiguities. The bandwidth of such a system lies between that of CW and pulsed radars and is typically of the order 12 kHz. The receivable radar doppler returns from a jet aircraft, for example, have a significant spectral width to which a most important contribution derives from the rotating compressors and turbines of its engines.

Typical doppler spectral widths of radar returns from modern jet aircraft approximate 20-30 kHz and often most of the power is associated with the sidebands when the target is viewed within 30° or so of front or rear (Fig 2.5).

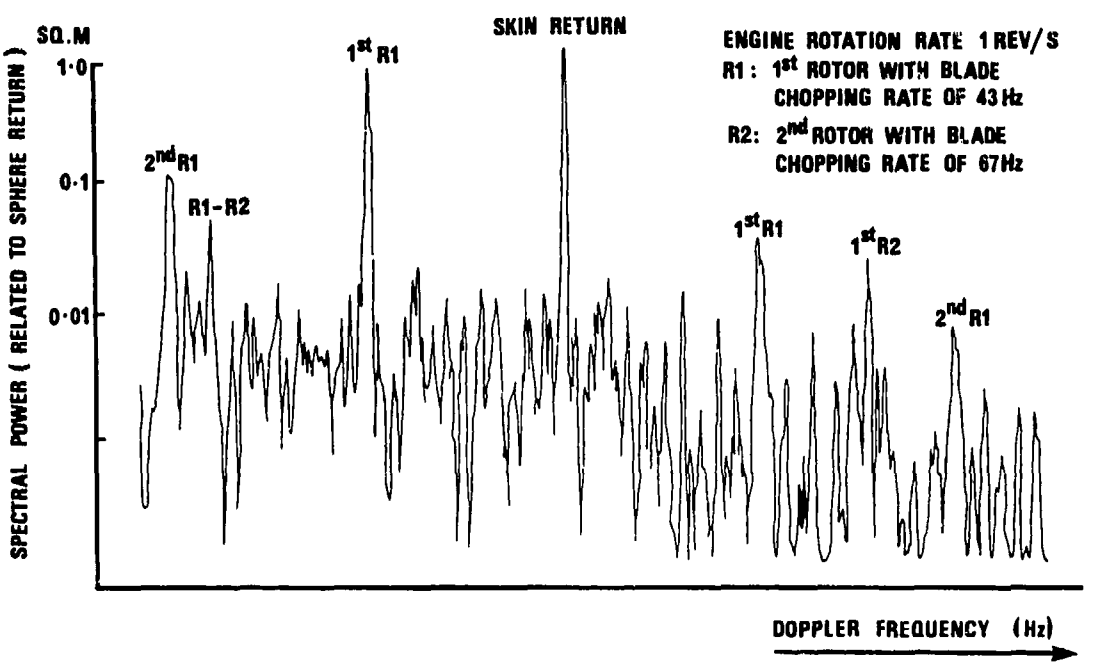

Fig 2.5 9.5 GHz doppler spectrum for engine viewed 20 deg from head-on aspect

It is hence clear that in terms of magnitude of σ different answers will be obtained for Pulsed Radars, which will receive all reflection components, and CW or Pulse-Doppler radars which will be doppler selective.

2.2.6 The Effect of Target Range

It is convenient to divide the sources of radar echoes on a target into two categories, specular and non-specular. Specular reflections occur when the radar beam is normal to some sensibly uniform surface whose dimensions are large compared with the radar wavelength. Typical regions on an aircraft are: the nose with its doubly curved surface, wing tip tanks, wing leading edges, wing and fuselage surfaces. In addition, there are specular returns caused by multiple reflections from corners, such as wing to fuselage junctions, and by images of sources in large areas, for example, the reflections of a wing pod in the wing surface.

Sources not included above are: engine air intakes, jet pipes, radar antennas and cavities. These sources, in general, give smaller peak returns than the above, but over much wider angles. These, and returns such as specular side lobe echoes and surface wave echoes, when combined, cause the return signal to be very complex with fine lobes. The specular side lobes result because, in radar as distinct from optics, the reflector size to wavelength ratio is not huge.

Schnetsler (Ref 29) shows that when considering reflections from large surfaces considerably within the Fresnel Zone, peak echoes can be range dependent. For doubly curved surfaces, such as nose ogives, the dependence on range is small. For cylinder-like reflectors such as wing leading edges, the normal incidence RCS is proportional to range. Lastly, for flat surfaces, such as under and top surfaces of wings, the specular reflection has a range squared dependence. However, these large surfaces and linear reflectors give highly directive flashes and the probability of being normal to such a reflector on a target is very small. Echoes from sources of smaller dimensions such as engine intakes and radar installations, are not very range sensitive because, considered singly, they are viewed usually in the far field. As will be shown later these sources are the most important contributors to RCS.

2.2.7 The Effect of Partial Illumination

Should the width of the radar beam be insufficient fully to illuminate the target in azimuth and elevation, the average value of σ determined will be less than that for full illumination.

2.2.8 The Effect of Pulse Length

It is possible that the pulse length used by a radar is shorter, in spatial terms, than the major dimension of the target along the direction of the radar sight line. If this occurs the pulse will scan the length of the target and the value of σ determined by the radar will depend on the receiver processing employed.

2.3 THE DETERMINATION OF RCS OF REAL AIRCRAFT IN FLIGHT

This section concerns the measurement of the radar reflectivity of an aircraft in its normal operating environment. It will be apparent that in such a dynamic experiment many problems are present (Ref 30).

Following sections discuss two other techniques for the determination of radar scattering and these are:

1 Measurement of real aircraft on the ground, and

2 Measurement of sub-scale model aircraft using radars with similarly scaled parameters. For each technique several examples of existing facilities are described.

It will be seen that each method has its own advantages and disadvantages, the importance of which will depend upon the requirements of the measurement programme.

2.3.1 Purpose: Advantages and Disadvantages

The major advantage, and the one most often used as a justification for such dynamic RCS measurements, is the obvious fact that "Real World" data are obtained. Clearly, all the target details as well as effects of target motion and environment are available to exert their influence on RCS. Another advantage in some cases is that dynamic data are quicker to obtain. Naturally this presumes the availability of a vehicle in an operational state. In practice, however, this requirement for availability is often a major disadvantage of dynamic measurements because the concern is frequently with the RCS during design stages or, alternatively, of vehicles of unco-operative ownership.

Among the major disadvantages of dynamic measurements are limitations on the range of viewing angles, on control and determination of aspect angles and on detail in the data. The limitations on viewing angles are obvious from the geometry of the experiment. Limitations in determining the aspect angles are due largely to the high speed motion of the target and the influence of winds and turbulence upon that motion. This limitation is very significant since it ultimately eliminates the possibility of comparing the detailed structure of dynamic data with that of the static data and the data must be averaged until an adequately defined relationship between measured data and target aspect can be established. This might mean averaging RCS values over 3 to 5 degrees when the data comprises (say) 2 to 10 lobes per degree, depending on the radar frequency and target size.

A significant drawback to dynamic measurements is cost. Flying an aircraft is obviously more expensive than simply having it stand still while its RCS is measured. Together with the fact that limitations in determining aspect etc, encourages repetitive measurements to improve accuracy, the requirement for vehicle operation can easily produce costs which exceed those of static measurements by orders of magnitude.

Thus, while dynamic data are without question very practical in the eyes of many users, care must be taken before concluding that they are the best data. Not surprisingly, the choice of static (2.4) or dynamic measurement is most often determined by the intended use of the data.

2.3.2 System Considerations

In dynamic RCS measurement one of the more important parameters is the range at which the measurements are to be made, and this in turn is a compromise between conflicting requirements. The usual need is for "Far zone" data and the problem is to reconcile the need for uniform illumination of the target in both phase and amplitude, with the necessity for echo signals at least 20 dB greater than total noise (S/N > 20 dB).

The accepted criterion for the "Far zone" is given by

$$R > \frac{2D^2}{\lambda}$$

when R = Range to target in metres
D = Maximum target dimension in metres (supposed effective aperture)
λ = Operating wavelength in metres.

This relationship assumes that the phase taper across the target is $\lambda/16$ (22.5°) or less, as a reasonable approximation of a plane wave. This range can be shown, (Fig 2.6) to be greater than 160 km for most aircraft at 10 GHz upwards.

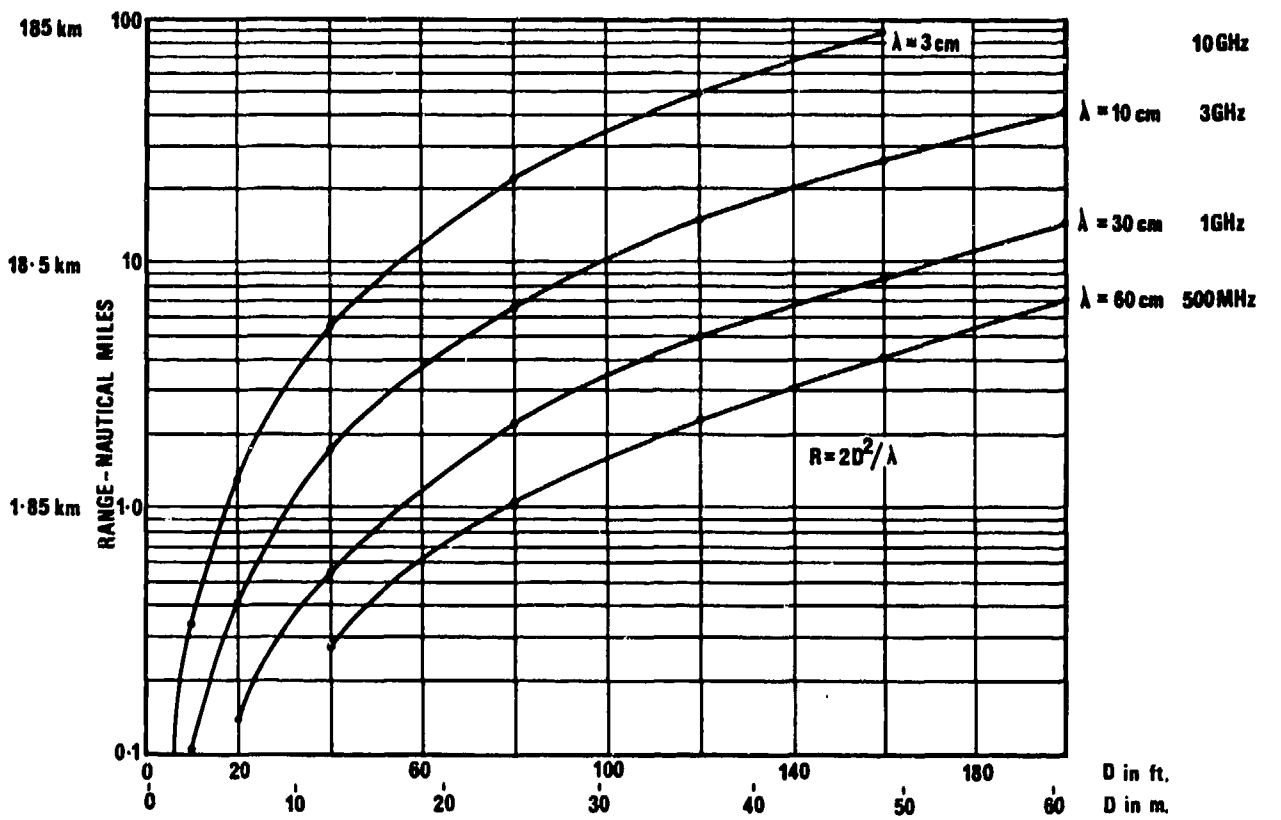

Fig 2.6 Far zone range vs target size

On the other hand, there is a range requirement determined by the need for data accuracy. The effect of coherently related clutter on observed signal strength is given by the following:

$$\sigma = \sigma_T + \sigma_B + 2\sqrt{\sigma_T \sigma_B}\cos\phi$$

where

σ_T = apparent RCS
σ_B = equivalent RCS of coherently related clutter
ϕ = relative phase between signals from target and coherent clutter.

The limits to the value of σ will occur when $\phi = 0, \pi, 2\pi$, etc. These are plotted in Fig 7 as a function of the ratio σ_T/σ_B. To obtain an accuracy of $\pm$ 1 dB instantaneous observed σ, σ_T must be at least 20 dB greater than σ_B.

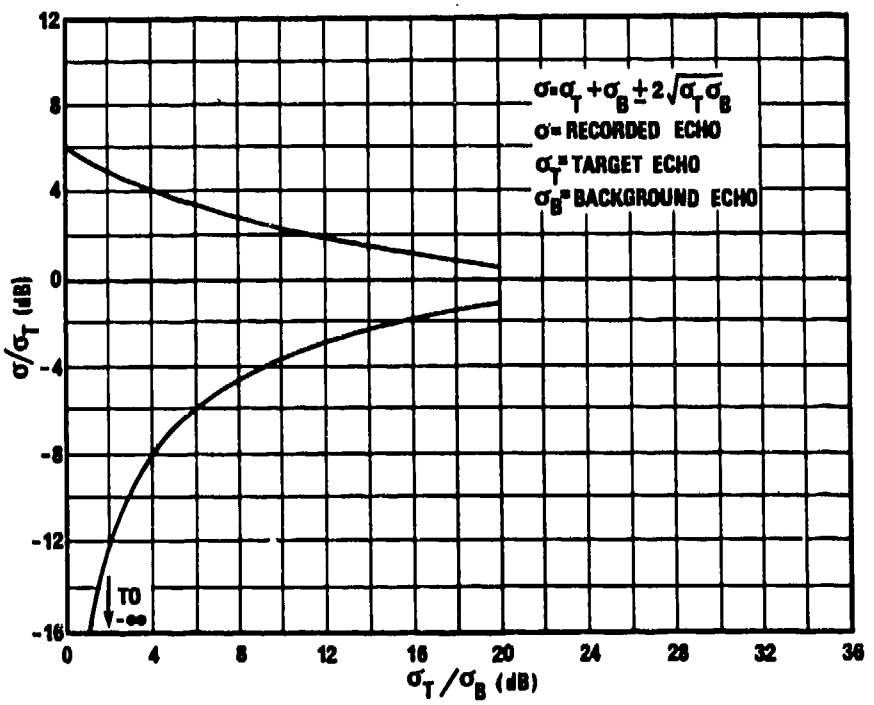

Fig 2.7 Limits to apparent RCS vs ratio of true RCS to background

At the same time, the power received from the target is given by the Radar Equation as shown earlier.

$$P_r = \frac{P_t G^2 \lambda^2 \sigma}{(4\pi)^3 R^4} \quad \text{ie} \quad P_r \sim \frac{1}{R^4}$$

The shorter the range, the stronger the echo signal, and the greater the accuracy in observed echo level.

Although many radars have the theoretical capability to detect a target of given RCS at some range, the echo level from the target will probably be 20 dB above system noise (without integration) at no more than one third the detection range. Thus, a radar capable of "seeing" a target at say 150 km could not provide satisfactory RCS data at measurement ranges in excess of 50 km.

This conflicts with the Far Zone requirement and represents one of the trade-offs in dynamic measurements. The dilemma is not unique to the dynamic experiment and, particularly in the field of sub-scale modelling dealt with in later chapters, much work has been done to validate techniques which apparently violate the Far Zone criteria used above.

The literature [2] shows, and experience confirms that the effect of measurement at ranges less than $2D^2/\lambda$ can result in reduced depth of troughs and eventually reduced amplitude of peaks. Even so, down to $0.5D^2/\lambda$ median values over small angular intervals remain within 2 dB of the far field value for simple reflectors such as large cylinders. An aircraft is not such a simple reflector and comprises a number of major echo sources, each of which is itself likely to be viewed in its own far zone. Other echo sources on aircraft are usually large flat areas, doubly curved surfaces and cylindrical structures

mostly yielding specular flashes of very small angular persistence. Hence the median values of RCS over some small angle (say 10°) are usually dominated by the responses of the physically smaller sources such as engine intakes, airborne radars and other cavities which would not be significantly range dependent.

In summary, the trade-off in choosing measurement range is that "Far Zone" range yields valid peak and null data but requires maximum capability from instrumentation, while shorter range distorts peak and null levels, but provides valid medians, and eases instrumentation requirements, especially sensitivity. One other factor which complicates the problem is that frequently when echo details are important (implying the need for long range to preserve the peaks and nulls) amplitude scintillation is of major concern. To record high scintillation rates accurately requires that the sampling rate (pulse repetition rate in this case) be twice as high to avoid aliassing or fold-over in the frequency domain. Since it is well known that scintillation rates of the total return from large targets extend to the kilohertz range, it follows that transmitted pulses must be at rates in excess of 10 kHz if best results are to be obtained. However, high repetition rates cause range ambiguities when

$$R > \frac{c}{2f_r}$$

R = range in metres

c = velocity of light

f_r = pulse repetition rate in Hz

If f_r is chosen as, say, 8 kHz, range must be less than 18.5 km to eliminate ambiguity.

It should be noted that Fig 2.8a and 2.8b show the body returns where most of power is in the very low frequency part of the spectrum. This would be a typical result of using a cw radar with a narrow band tracking loop. The wide bandwidth normally associated with a pulsed radar accepts also the side band power resulting from the rotating engines which significantly lifts the scintillation spectral power at higher frequencies out to the several kilohertz region (see Section 2.2.5).

A further consideration involving range is the method adopted to track the target. In order to avoid loss of lock due to target return fades it is customary to include a radar beacon, or repeater in the target aircraft. In either case the frequency it transmits back to the radar must be off-set or time coded to allow separation of target and beacon signals at the receiver. There remains, however, the probability of modulation of the target returns by the angular tracking system, and such modulations are often within the spectrum covered by target echo fluctuations which are to be measured.

The problem can be overcome by slaving the antenna of the RCS measuring radar to a separate tracking system, radar or optical, the latter, though cheaper and simpler, unfortunately impressing a range limitation in many atmospheric conditions.

Improvement in tracking performance can always be obtained through sophistication and cost. Ultimately it is the latter as related to the data needs which decides most questions of equipment design and operating techniques.

Turning now to available target aspect angles, as mentioned earlier, the geometry of a dynamic experiment inherently limits the aspect angles at which an aircraft target can be viewed by any one measuring site. Consequently, dynamic experiments cannot usually provide aircraft target cross section data for arbitrary use. Assuming the willingness to accept the limitation on viewing angle, there remains the important matter of determining the angle at which the target is viewed. It has been pointed out that the value of RCS can change by several orders with changes of aspect angle of fractions of one degree. Fig 2.1. Any single figure offered as the RCS of an aircraft over (say) 90° aspect change could probably be guessed as accurately as measured, with considerable saving of cost and time. Clearly data are needed as a function of aspect angle. The question is only to what level of detail.

Consideration of cost, need for accuracy, the statistical nature of echo signals etc, usually leads to acceptance of $\pm$ 5° angular accuracy in dynamic measurements. This is a compromise between too fine an increment, which is very expensive to obtain, and a very coarse increment which would cause over-smoothing of the data. It is a practical choice in that it can be achieved without resort to adding on-board attitude sensors, telemetry, antennas etc to the target aircraft. One significant shortcoming is that, without on-board attitude sensors, it is not possible to determine crab angle with accuracy; yet it could easily exceed the desired angular accuracy. The implication is that low wind conditions are necessary for good results using a target without on-board attitude sensors and recorders with time reference.

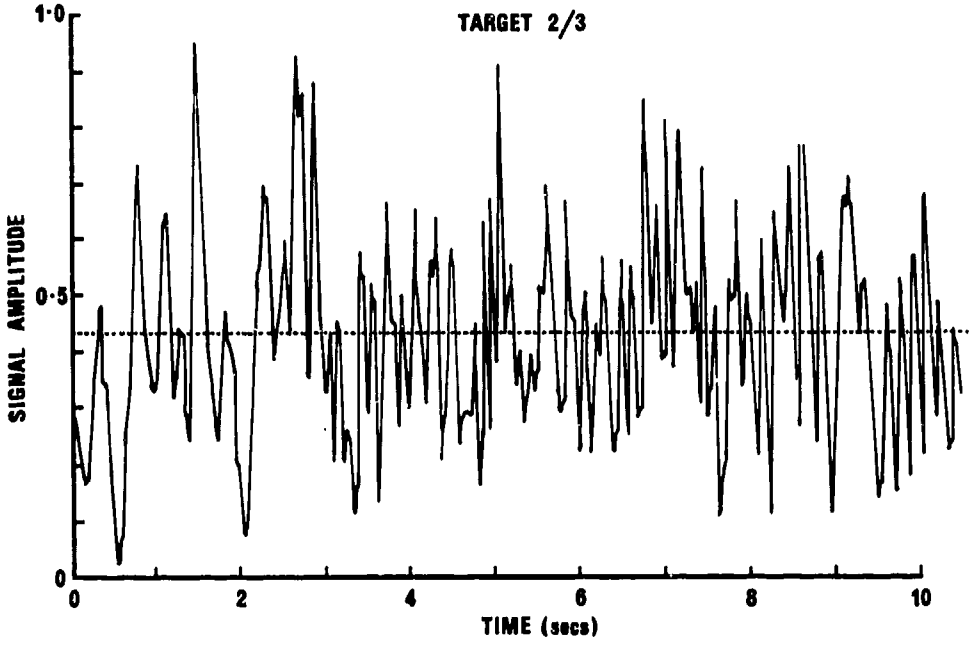

Fig 2.8a Signal amplitude scintillation

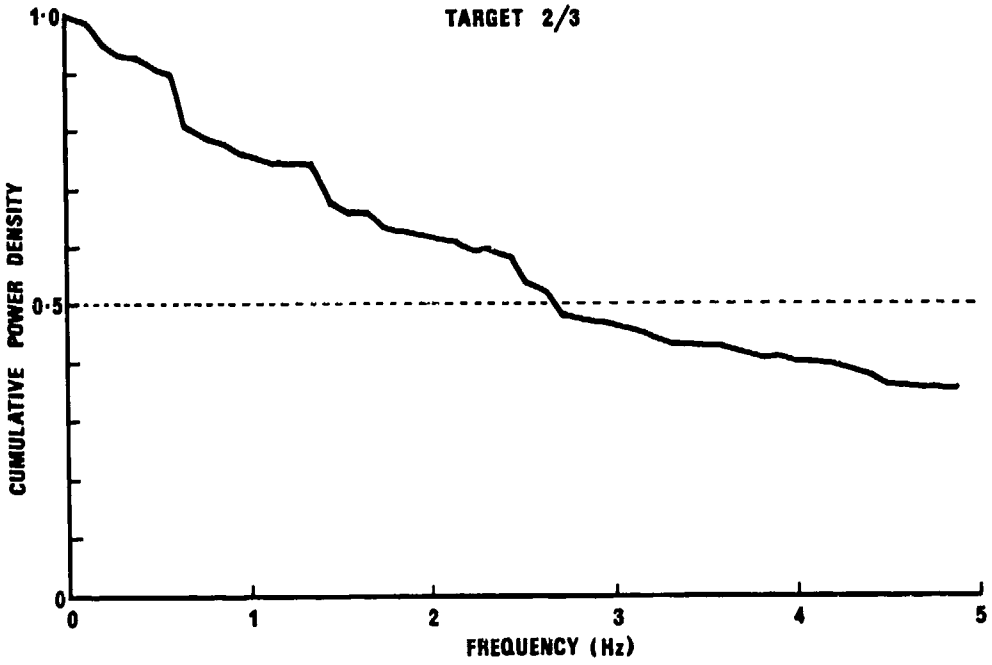

Fig 2.8b Signal scintillation power spectrum

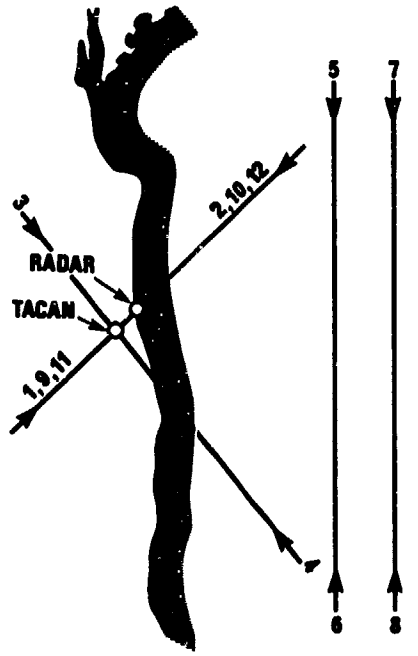

Fig 2.9 Typical NRL flight patterns

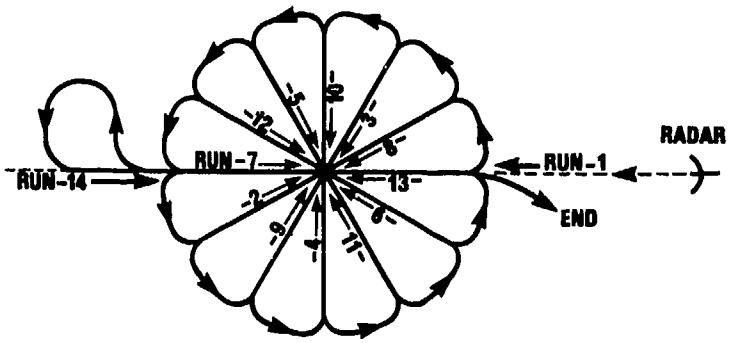

Fig 2.10 Typical rosette flight pattern

Two methods have been used successfully to provide a range of viewing angles during aircraft measurements. The first, Fig 2.9, involves long, straight and level passes toward and away from a ground radar at selected offset distances. Additional data for the important nose-on and tail-on views is obtained by shallow dives toward and climbs away from the radar. This method has the advantage of providing a wide range of azimuthal viewing angles on a continuous basis. However there are disadvantages in that variation of range is great which may introduce dynamic range problems, and the measurement period is very non-uniform over the aspect region observed.

An alternative method for varying aspect angle is to fly a rosette pattern.Fig 2.10, shows a reference point at a series of reducing altitudes. This has the disadvantage of requiring steps in azimuth as well as elevation, but if these are fine enough, say 10° intervals, a reasonably complete data set is obtained:

a. Advantages of offset flight patterns:
   (1) Continuous data.
   (2) With correctly selected offset points the lower hemisphere can be effectively mapped.

b. Disadvantages of offset flight patterns:
   (1) Difficult to measure data near nose or tail of the aircraft.
   (2) May require large amounts of flight time.

c. Advantages of rosette flight patterns:
   (1) Minimal range variation.

d. Disadvantages of rosette flight patterns:
   (1) Very large flight time required.
   (2) Very few discrete data points attained with no information on the trend of the RCS near the measured data points.

e. A skidding turn flight pattern could be added as an alternative to rosette pattern. This is an antenna pattern measurement flight technique used at AFFTC which has the aircraft complete a 360 degree wings level skidding turn.

   (1) Advantages - short flight time and continuous data.
   (2) Disadvantages - moderate changes in range.

To conclude this section the following summarises the desired performance of a typical dynamic measurements facility.

(1) Must track target in azimuth, elevation and range with no effects of tracking function upon the recorded echo data.
(2) Must record at a high pulse rate on a pulse-to-pulse basis to provide amplitude scintillation data.
(3) Must transmit and receive all frequencies and polarisations for which data are required.
(4) Must have capability to provide signal levels substantially above noise for smallest target RCS anticipated.
(5) Must be able to handle a large dynamic range of signal levels without saturation or non-linearity.
(6) Must provide real-time capability to monitor test conditions and data output to preclude continuing bad experiment.
(7) Must record data in a manner compatible with automatic processing.

Fig 2.11a NRL dynamic measurements facility

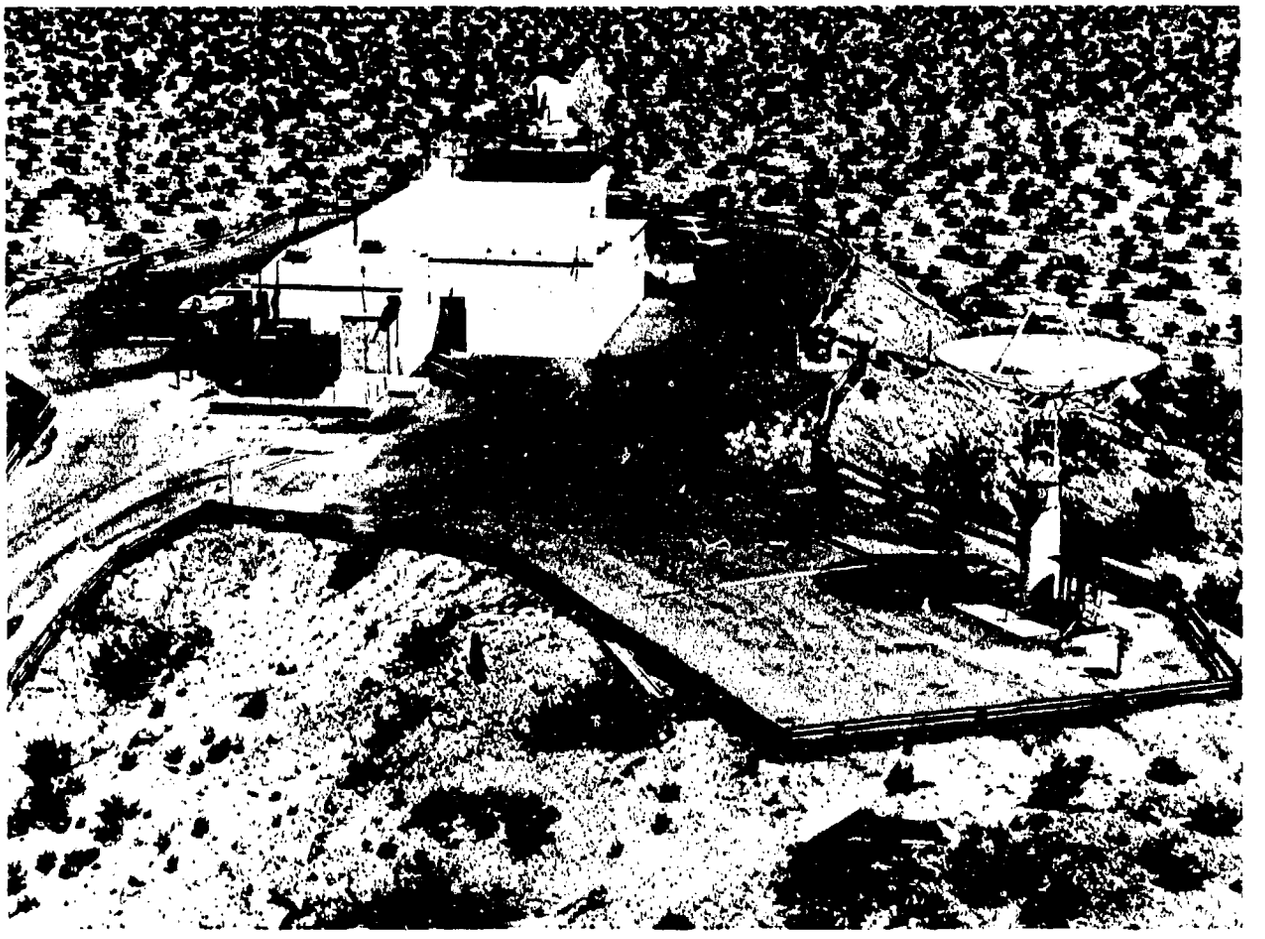

Fig 2.11b AN/FPS16 radar. NASA, Edwards AFB

2.3.3 Existing Measurement Facilities

2.3.3.1 The US Naval Research Laboratory (NRL) Dynamic Measurement Facility

NRL, at Chesapeak Bay, Maryland, has for many years set high standards in the field of RCS measurement of both air and seacraft. It is a well designed facility whose instrumentation and operating techniques have been improved through the years so that they are versatile and provide much data at several frequencies with commendable accuracy (Fig 11a).

The basic equipment of a few years ago, and undoubtedly extended and further improved more recently, comprised radars at nominally 1, 3, 5 and 9 GHz operating through antennas mounted on a common pedestal whose orientation was controlled by an optical tracker. At the two higher frequencies any of four polarisations, (righthand circular, lefthand circular, linear horizontal and linear vertical) could be transmitted with simultaneous reception of the same and orthogonal components. At the lower frequencies, linear horizontal or linear vertical could be transmitted with co-planar reception only.

The receiver system employed a range tracking gate to isolate the target echo and used no AGC whilst achieving a linear, instantaneous dynamic range of 40 dB. Servo controlled RF and IF attenuators exercised by comparison at video frequency of maximum and minimum signal levels, resulted in the dynamic range of the receiver extending to 105 dB. Attenuator settings were continuously recorded during measurements for subsequent use in data analysis.

Output of the receiver was recorded (1) in analogue form on a visual rectangular chart, (2) in digital form on magnetic tapes and (3) on 35 mm film. The visual chart recording required integration and filtering of the pulsed signals to satisfy bandwidth limitations of the analogue recorder. It was used mainly as an on-line indicator that valid test data were being obtained.

Before data were taken, a warm-up period was followed by an intensive check and adjustment of all functions including range attenuator servo operation, transmitter and local oscillator frequencies, calibration of the recording systems, receiver sensitivity and antenna mount servo. RF signals during these checks were provided by calibrated remote beacons, so that system sensitivities were brought to the same level for each aircraft test. Final calibration was accomplished before and after each flight by measuring

a balloon-borne metal sphere which served as the RCS standard. This was an extremely important part of the operating procedure for which no suitable substitute has yet been found. The use of such a standard target eliminates the need for precise data on radar parameters (except for calibration of receiver dynamic range) by making the measurements relative rather than absolute, but precise nevertheless.

In addition to the data on magnitude of RCS, the pulse-to-pulse echo recorded can also yield information on amplitude scintillation rates. Raw data are processed through the use of auto-correlation and Fourier transform routines to determine power spectral density. As mentioned earlier amplitude fluctuation rates result from two separate occurrences, the change of viewing angle and the relative motion of parts of the target - most significantly yaw motion. Larger targets and shorter wavelengths produce finer lobe structure which for a given target yaw rate and amplitude yield faster signal fluctuation rates at the radar receiver. However, modern aircraft, unless operating in a fast manoeuvring mode, tend to have very little natural motion (weathercocking) and a typical median value for amplitude fluctuation is 2 Hz (Figs 2.9a and 2.9b).

2.3.3.2 Edwards AFB, California, USA

The AMES Dryden Flight Research Facility, belonging to NASA has demonstrated its ability to make accurate RCS - versus aspect angle measurements of a suitably instrumented air vehicle in flight (Fig 2.11b).

Great attention is paid to pre-flight radar alignment and calibration, including recording the AGC calibration which serves as a basis for fast-flight conversion of AGC voltages to signal-to-noise (S/N) values for each even second of flight.

As an example, two accurate AN/FPS16 radars, spaced apart by approximately 380 m, are used. Both radars may be operated in a dual local oscillator mode, separately and simultaneously receiving and processing the signals from the on-board radar beacon, and the radar return from the air vehicle skin. Since the tracking function is locked on to the on-board beacon signal, the angular noise which would otherwise cause the apparent source of the radar return to wander back and forth about the physical centre, is virtually eliminated.

During flight, target range, azimuth and elevation data are recorded in digital form by the Aeronautical Test Range (ATR) real-time tracking data processing system. AGC values from the radar(s) are recorded together with IRIG B timing.

Immediately following a flight, a 0.25 m^2 target balloon is used to calibrate simultaneously the AGC values from both radars. Each 991.4 m (1 kiloyard) point on the plot is identified as the range increases. All tracking system configurations are the same as used during the air vehicle flight. Achieved results of such post-flight calibrations are:

AN/FPS-16 Average RCS of 5.84 dBm^2 with a standard deviation of 1.09 dBm^2
AN/MPS-19c Average RCS of 6.26 dBm^2 with a standard deviation of 0.38 dBm^2
(0.25 m^2 ≡ -6.02 dBm^2)

Thus it may be expected that an accuracy of $\pm$ 1 dB is achievable in measurement of air vehicle average RCS.

To establish RCS as a function of the impinging angle of the illuminating radar energy on the body axis triad, it is first necessary to time correlate data from three separate sources. Body axis data are obtained from on-board inertial recordings. Radar signal-to-noise (S/N) measurements are obtained from strip chart recordings of IF signal levels at each radar. Position data relative to each of the two radars are obtained from digital recordings of range, azimuth and elevation from the two radars. Separate IRIG B timing is provided for each of these recordings.

After each flight, the data set is combined and time correlated to provide the source material for a cross-sectional analysis based on the S/N measurements recorded at the two trackers. The source data set for each radar hence includes:

1 IRIG B time reference (even seconded).
2. Range, azimuth and elevation of the target at each even second.
3. Signal-to-noise (S/N) at each even second, correlating with item 1.
4. Body axis angles measured on board the vehicle and interpolated to even seconds.

To compute the impinging angle of the illuminating radar energy, the following sequence is used (Ref 31).

1. Air vehicle position is converted from spherical coordinates into radar centred, east-north-vertical (ENV) aligned right hand Cartesian coordinates.
2. The Cartesian ENV coordinates are rotated to provide air vehicle position referenced to a radar-centred Cartesian frame spatially offset from, but in angular alignment with the earth-centred, right handed Greenwich equatorial-polar coordinate frame.
3. The air vehicle position is then translated to earth-centred EFG triad.
4. From the EFG coordinates of the air vehicle, and the EFG coordinates of the tracking radar, the ΔE, ΔF and ΔG elements of the air vehicle-to-radar vector are determined.
5. From the EFG coordinates of the air vehicle, its geodetic position is determined.
6. Using the geodetic coordinates of the air vehicle and the elements of the air vehicle-to-radar vector in the vehicle-centred, EFG-aligned coordinate frame, it is possible to rotate the position vector of the radar into a vehicle-centred, ENV reference frame.
7. Knowing the body axis angles existing at the air vehicle at the same instant in time, it is possible to rotate the vehicle-to-radar position vector through the body axis Euler angles to obtain the position of the radar with respect to the vehicle-centred, right handed, body axis frame of reference.
8. The position of the radar with respect to the air vehicle body axes is then converted from Cartesian to Spherical coordinate form, thus providing the position of the radar in terms of azimuth, elevation and range.

This sequence of conversions, rotations and translations provide the impinging angle of the illuminating radar energy referenced to the air vehicle's body axis triad for each even second during flight. Using the Radar Equation in suitable form, the RCS is computed from known radar parameters, the recorded S/N value and target range existing at each one second interval.

By correlating the RCS computations for each even second in the analysis interval with the corresponding body axis angles of the impinging radar energy, RCS with target aspect angle plots may be produced. The comprehensive computer programme for these real-time calculations includes a routine necessary to correct the angular data acquired at long radar ranges for refraction effects.

Whilst this excellent facility achieves high standards in the detailed (in flight) measurement of air vehicle RCS, the complexity of the operation is obvious. Also, of course, such detailed data can be obtained only from specially instrumented air vehicles and not from targets of opportunity.

2.3.3.3 Griffiss AFB, New York State, USA

At Griffiss, Rome Air Development Center (RADC) has a sophisticated equipment, the Precision Antenna Measurement System (PAMS). This was developed for RADC by Actron Industries Inc. for the evaluation and calibration of RF radiating systems and RCS measurements under dynamic conditions. The PAMS is slaved to an AN/FPS-16 tracking radar and monitors and records the RF emitting characteristics of the electronic systems under test as a function of vehicle position and attitude. In addition, the PAMS can receive scattered and reflected energy from the vehicle when the FPS-16 is operating in the skin track mode.

The system operates over the frequency range of 0.1 GHz through 18 GHz in either CW, AM, FM or pulse mode with any polarisation. The system can monitor and record data on up to 12 frequencies and either both linear or both circular polarisations simultaneously throughout the operating range. The data are reduced and plotted as a radiation pattern relative to the vehicle's heading in Effective Radiated Power (ERP). When required, the RCS of the vehicle can be plotted in dB above a square metre (dBm^2).

In order to determine the attitude of co-operative vehicles, ancillary equipment was developed. The Airborne Monitoring System measures and records heading, roll and pitch throughout the flight test. Fig 2.13. These data are merged with data acquired on the ground to present the actual conditions of the vehicle during flight.

As can be seen from Fig 2.12, the PAMS has a bistatic geometry, i.e. the transmitter and receiver are separated by some distance; however, if the baseline distance is small with respect to the range from the transmitter to the target a pseudo monostatic condition will exist. The bistatic RCS will be different from the monstatic case since it has a different aspect angle and is the result of a different set of scatterers due to the complex geometry of the vehicle and various polarisation transformations. Consequently, it is necessary to ensure that the range is great enough to minimise the effect of the bistatic angle if the RCS results are to be taken to represent the monostatic case.

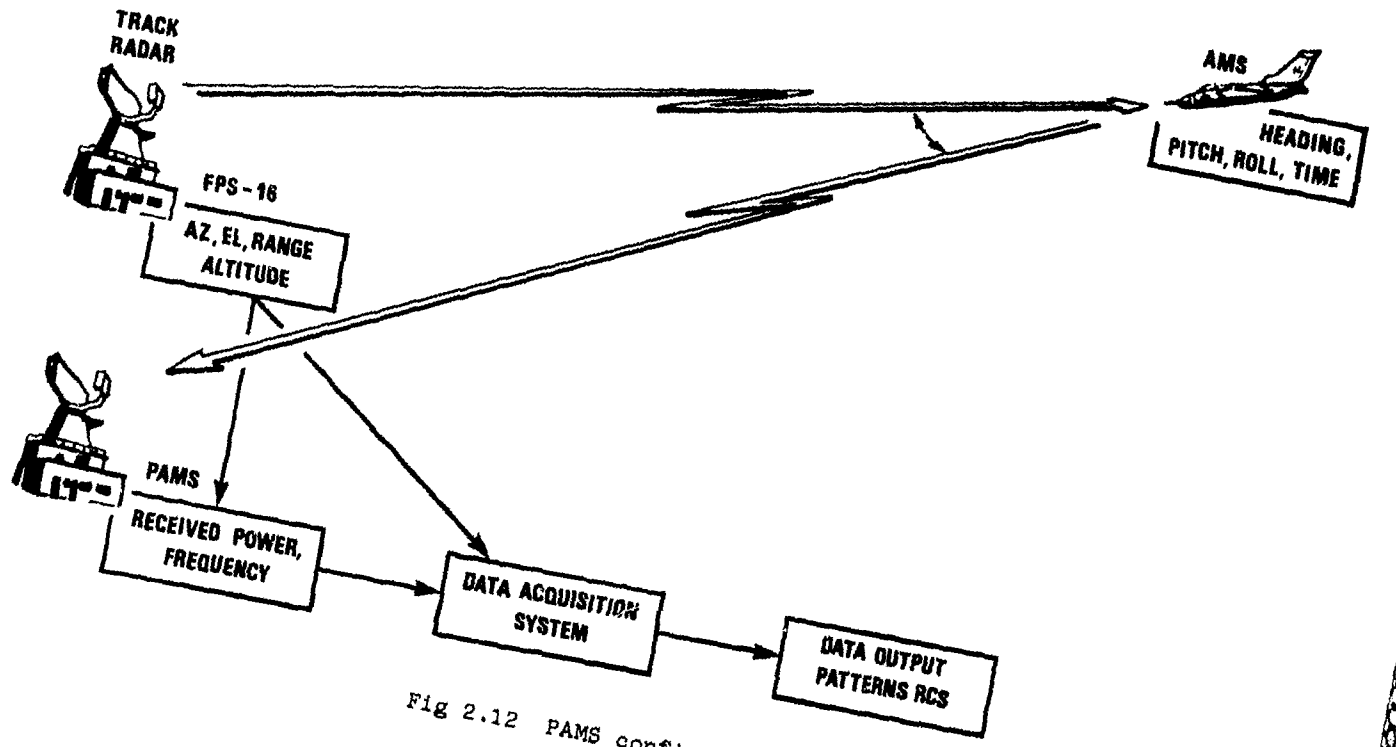

Fig 2.12 PAMS configuration

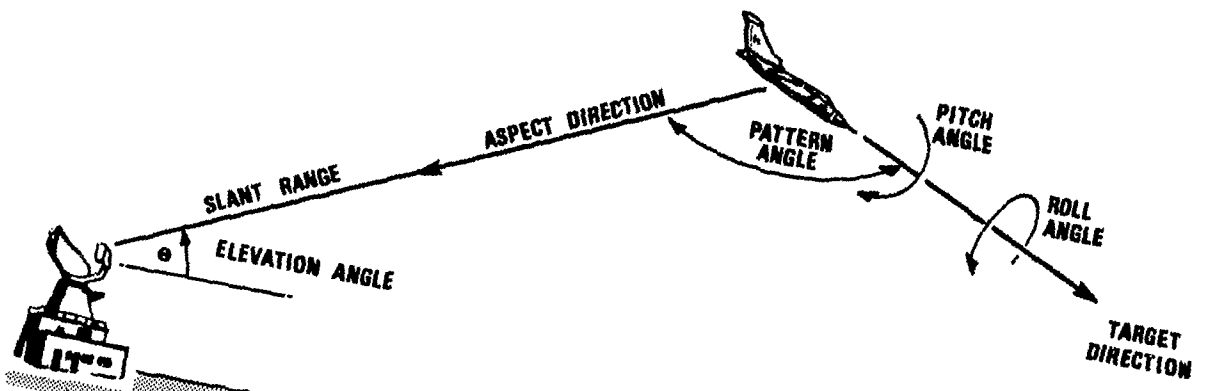

Fig 2.13 Target aspect direction

The PAMS has much to commend it and has great potential for improvement, for example to include the capability of resolution of the scattering matrix. In its present configuration, PAMS can be used in a wide variety of applications to measure RCS and RCS distributions of aircraft etc. The principal features are

(a) precision and good calibration
(b) automatic data processing
(c) extremely wide frequency range
(d) polarisation diversity.

2.3.3.4 CEV Bretigny, France

CEV (Centre d'Essais en Vol) is one of several French establishments involved with investigations relating to aircraft in flight. At Bretigny measurements of in-flight aircraft RCS are made and interesting methods of determining target to radar aspect angle performed. The radars involved are called Brahms 1 and 2. The former operates simultaneously within the two bands 8-12 GHz and 12-18 GHz, whilst Brahms 2 operates in bands D, E and G.

The Brahms 1 station uses a converted Bofors gun turret to mount the transmitter and receiver antennas, a television camera and a pair of collimated binoculars. The pointing direction of the antenna array is slaved to that of the binoculars which the operator uses to track the target aircraft. Fig 2.14a. Two types of information are recorded:

(1) information on the radar signals scattered back from the target, and
(2) information about the target to radar aspect angles.

Dealing first with (1), the two received signals are heterodyned down to a low frequency and simultaneously recorded on magnetic tape together with reference time signals. RCS values are extracted from this by the following means.

The signals, seen in the frequency domain, have variable widths of amplitude spectra. Filtering is simpler if these amplitude spectra are extracted (in a CW mode) rather than the signals themselves. From the spectra the coherent frequency bands can be isolated (except for the contributions from the rotating compressors and turbines). This band of frequencies is about 50 Hz/GHz for an aircraft and is dynamically centred on the mean doppler frequency of the target.

Information about the target to radar aspect angles (2) is obtained as the operator tracks the target, when the images from the slaved television camera are recorded on video tape together with reference time markers. To provide for the requirement to record and track the target trajectory, the azimuth and elevation angles of the tracking radar antennas are also continuously recorded on the video tape.

Extraction of target attitudes is achieved by evaluating the two angles $\theta + \phi$ which are polar coordinates referred to the vector $\vec{w}$ along the line joining the radar to the target - using aircraft x, y and z coordinates (Fig.2.14b).

The resulting RCS values and aspect angles are correctly associated in relation to target trajectory in a manner consistent with the accuracy claimed (1-2°) by quantifying angles in units of 1.125° (ie 320 steps in θ and 160 steps in ϕ). Three 320 x 160 matrices are used, the first filled with RCS values for each of the radar frequency bands, the second filled with derived aspect angles and the third filled with correction operators. These three matrices thus represent the global statistics of the target in the two frequency bands.

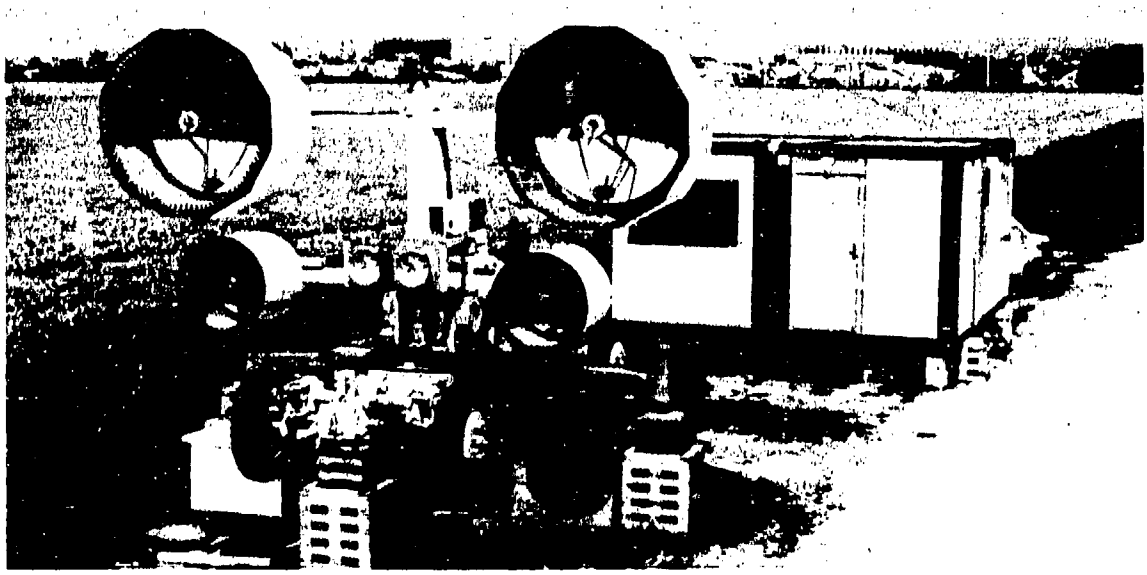

Fig 2.14(a) The Brahms radar at Bretigny

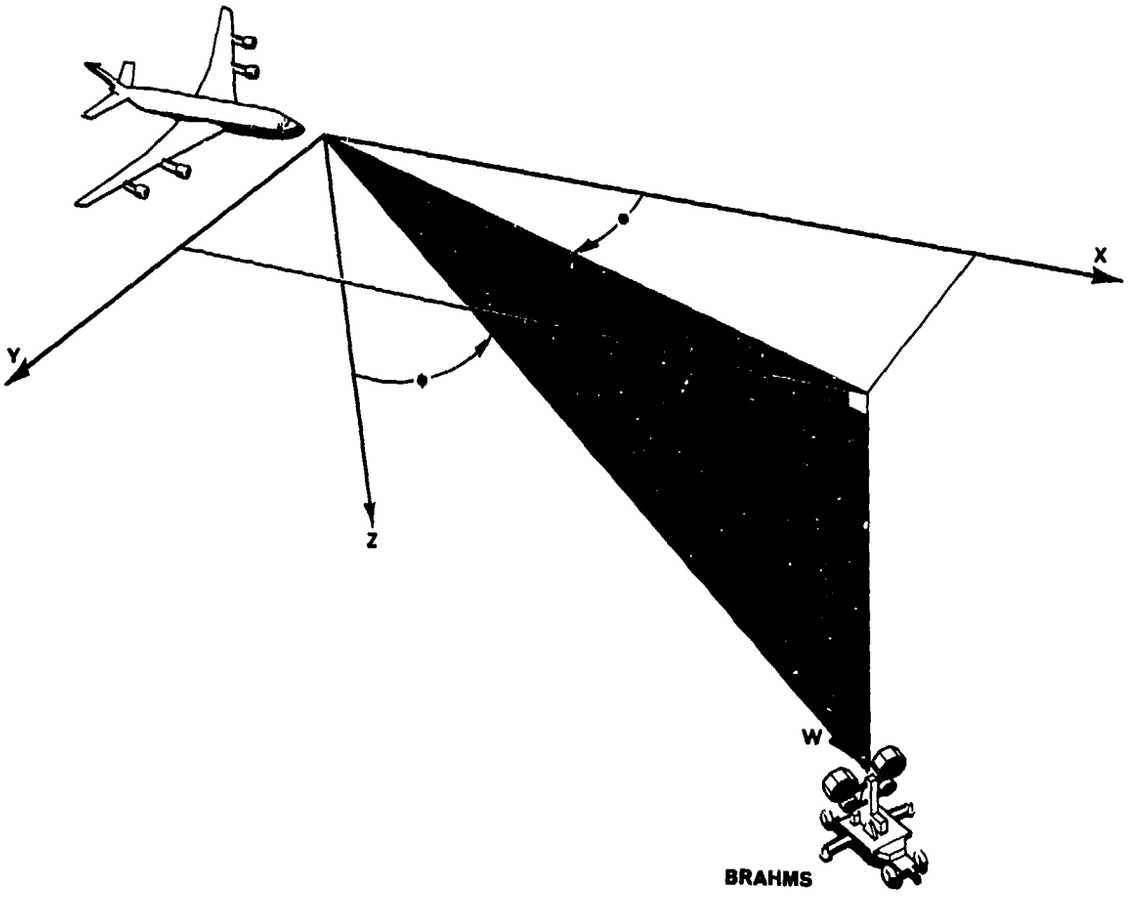

Fig 2.14(b) Axis convention

Additional computer processes facilitate investigation of RCS differences due to small errors in derived aspect angles.

2.4 THE DETERMINATION OF RCS OF REAL AIRCRAFT, STATISTICALLY, ON THE GROUND

2.4.1 Purpose: Advantages and Disadvantages

There are basically two types of outdoor, static measurement ranges; the ground plane range and the direct path range. In the latter the ground reflections must be eleminated either by inclining the antenna and suspending the target in a suitable manner, or by scattering the ground reflections using a diffracting ramp arrangement between the radar antenna(s) and the target, so that only the direct path incident and scattered energy is transmitted and received. The ground plane range is based upon the utilisation of the ground illumination by the antenna in simulating free space conditions. It should be noted that a basic assumption made is that the monostatic RCS of the target in the direction of the radar is equal to its monostatic RCS in the direction of its radar image, which are both equal to its bistatic RCS. This, of course, would not be true for a large corner reflector or flat plate target. However, the practical bistatic angle (θ) is very small so the approximation is tenable.

The ground plane technique is often preferred for the following reasons:

(i) Reduction of return from ground near the target.
(ii) Target near the ground - assuring relative ease of access.
(iii) Theoretical 12 dB increase in system sensitivity due to utilisation of ground-reflected energy.
(iv) Comparative simplicity of range geometry and equipment.

The ground plane range provides two principle paths by which energy may be propagated from the antenna to the target. Fig 2.15 illustrates the direct and reflected paths. The interference pattern obtained as a result of the two-element array of the antenna with its virtual image below the ground plane is due to a 180° phase reversal upon reflection of the incident wave from the ground. This 180° phase shift is assumed for low grazing angles at high frequencies, where the ground is a perfect reflector. Fig 2.16 indicates

the lobing pattern which results from the two antennas, with image antenna assumed to be fed with reversed phase from the actual antenna. The path length difference is essential in the calculation of the interference pattern. In Fig 2.15, ABC, the reflected path length, equals DBC since the angle of incidence equals the angle of reflection for assumed perfect conductor.

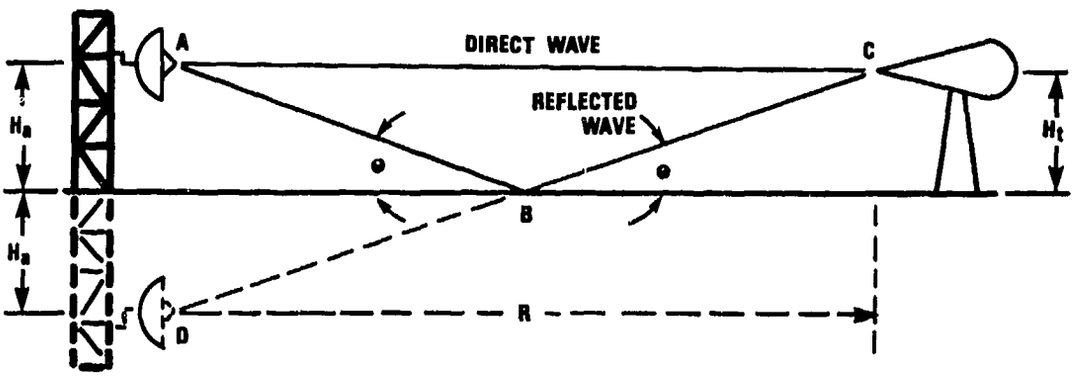

Fig 2.15 Ground plane geometry

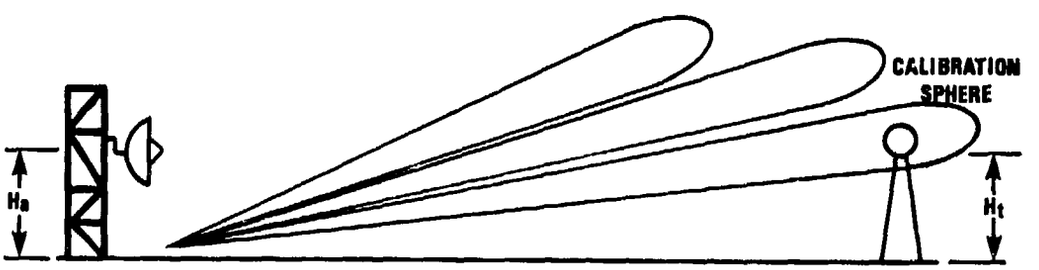

Fig 2.16 Vertical lobing pattern

For perfect reflection, the transmitted field intensity is doubled in the target area, and the power density increased by a factor of 4. The same process occurs for the reflected power, so that the power received from the target, due to its RCS, is increased by a factor of 16 over that which would have been received under free space conditions. Since the radar is calibrated using a precision sphere placed at the unknown target location, measurement errors are minimised. A power gain of 12 dB (max) is thus ideally obtained by taking advantage of the ground reflection. It could be said that there is no other practical method of making radar measurements of large targets such as real aircraft on or very near to the ground, at anything other than unrealistic, very short ranges. In sub-scale radio modelling of aircraft targets a typical full scale equivalent range used is 350 m for 1/15th scaling. To reproduce these conditions using full scale equipment and aircraft would require the aircraft target to be suspended at some 100 m height and there retain the capability for accurate aspect variation.

Appendix 2.A1, Section 3 deals at length with Radio Modelling data comparability with real life dynamic measurement output. Many of the arguments apply equally to the static measurements of real aircraft targets, since, "real", does not usually imply "the same real aircraft". Often, smaller targets, for example, missiles, light aircraft, RPV's etc. do provide the opportunity for static and in-flight measurements of the same vehicle.

2.4.2 System Considerations

Reverting to the ground plane range, the usual method of supporting the target aircraft is on specially shaped pillars of polystyrene foam. Care is taken to minimise backscatter from these pillars, which tend to be massive to carry the weight of a military aircraft. Unfortunately, the best attention paid to minimising the RCS of the pillars can easily be frustrated by the need for other appendages ensuring the stable support of the target, particularly in windy conditions. For example, between the tops of the pillars and the target it is necessary to use large saddles of polystyrene (or similar), and ropes are often used to tie down the target and reduce the chance of movement (Fig 2.17).

The difficulties of determining aircraft radar characteristics by radar measurements of the vehicle in flight were discussed in the previous chapter. Measurement of the same aircraft set up in an equivalent clutterfree situation on the ground with fully adjustable aspect angle potential is a simpler matter. If performed properly, results are repeatable and detailed scattering phenomena can be investigated. However, millitary

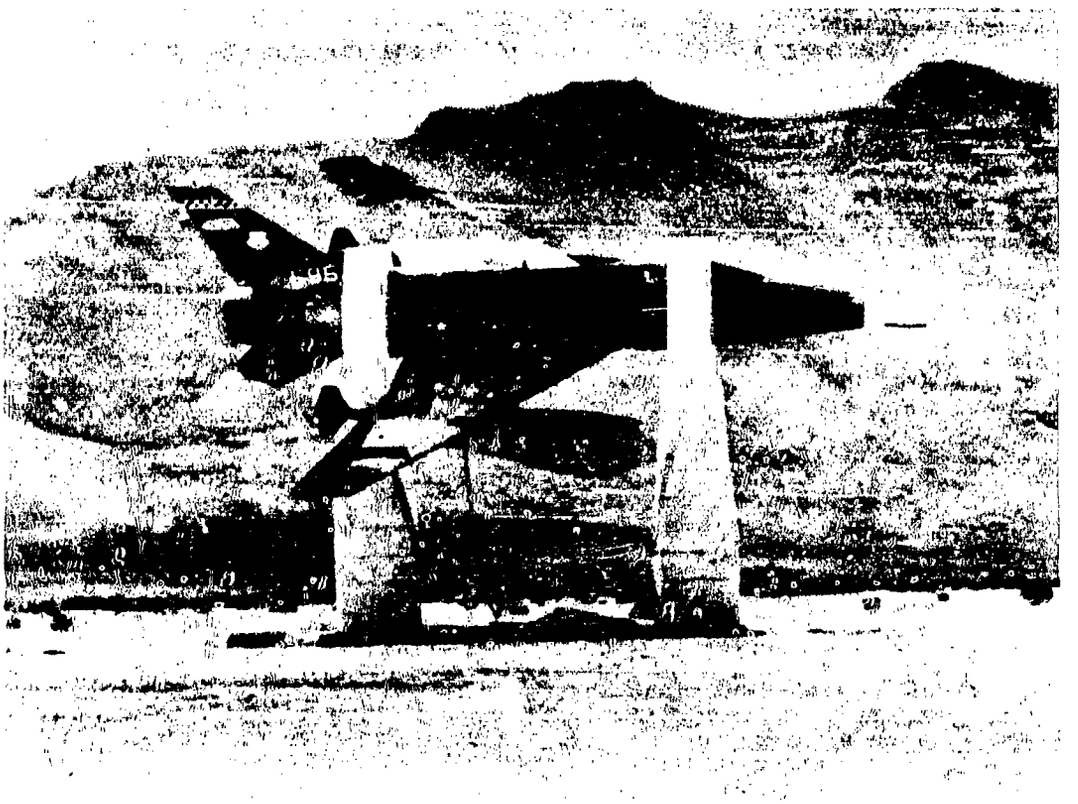

Fig 2.17 QF 100 target drone

aircraft or equivalent size civil vehicles are almost invariably too heavy to be supported on any existing measurement ra.. It is also unlikely that an operational aircraft could be made available to suffer t unusual handling implied, or for the necessary time period required for numerous measurements.

The normal procedure is to use an expendable version of the designated aircraft, and this is then stripped of many of its heavy components and certainly its more interesting avionics. Although care is clearly taken to avoid changes which might alter the radar characteristics of the aircraft, it is the author's experience that this requirement is not necessarily met. For example suppose the aircraft under investigation is fitted with a particular AI radar in its nose radome. It is often the case that this has been removed from the version available to be measured. Even if it is then replaced there is often bulkhead damage or modification which can radically alter the detailed, and sometimes gross, radar returns. It should be remembered that the nose radar complex and the engine/engine intakes are the most important sources of echo on the frontal hemisphere of a modern aircraft. Further, it is not an easy matter to rotate the engines smoothly and at a rate low enough to be compatible with the radar receiver bandwidth, and to preclude unrepresentative vibration. Engine rotation is necessary if the dynamic data are to be matched in achievable detail.

Reverting to the radar measurement system, care must be taken to ensure the assumed reflection coefficient of the ground plane is -1. It is unlikely that the surface will have this ideal property in a major, long range RCS measurement facility. There will be limits to the radar frequencies which can be used with confidence. For example, at lower and upper radar frequencies, depolarising mechanisms are likely to operate since the reflection coefficient will depart from -1 differently for different radar polarisations. Also, and probably depending on moisture content, there may be some penetration of the ground plane at lower frequencies and at high frequencies its surface may be unacceptably rough. Special care, perhaps using field probes in the target vicinitiy, must be taken to make the necessary small changes to antenna positioning in an attempt to compensate for such effects. Similar techniques are required to optimise the geometry of the situation to make best use of the theoretical 12 dB gain in system sensitivity in a situation where the target is large.

2.4.3 Examples of Established Measurement Facilities

2.4.3.1 Holloman AFB, New Mexico

The Radar Target Scatter Facility (RATSCAT) of the 6585th Test Group (Rx), was established in the early 60s and is, perhaps, the best known centre for the static measurement of RCS of full scale targets using the ground plane method. RATSCAT is located on the White Sands Missile Range of the US Army, but is operated by the Air Force Systems Command from Holloman AFB. The site was chosen for the uniform electrical properties of the gypsum soil and for the flatness of the terrain (Ref 32).

Radar targets are supported by low reflectivity dielectric pillars which stand on large turntables flush with the ground surface and concealing the rotation mechanisms which are remotely controlled from the radar site Fig 17. There are seven such turntables at ranges to the radars varying from approximately 150 m to 2,400 m. Radar to target depression angles achievable are, for example, 20° at 120 m and 2.1° at 1700 m using specific radars at the top of one of two available towers. However, most measurement work uses the radars and targets at very similar heights, a few metres from the ground.

Radars for many purposes are available, non-coherent for measurement of monostatic and bistatic RCS only, coherent for measurement of relative phase in addition to signal amplitude, very short pulse (< 1 nsec), short pulse (10-70 nsec) with incremental frequency steps at 0.1 GHz intervals etc. Concentrating on RCS measurement of aircraft target, radars are used at frequencies from 0.03 to 30 GHz; and with spot frequencies between 30 and 100 GHz.

The principles of operation and the inherent difficulties experienced with ground plane ranges using real aircraft targets were dealt with in the preceding section, and both are seen in practice at RATSCAT where the difficulties are understood and every effort is made to overcome them. Recently, operational aircraft have been flown in, measured and returned to service. This is an important advance but the extra weight of such a target creates even greater problems of target support and stability, which in turn raise the level of spurious radar returns. It must also be noted that the aircraft engines are not rotated during radar measurement so that the RCS data will be different in amplitude detail and doppler spectral content, from in-flight measurement data over most aspect angles. One widely used facility is the "Automated Radar Measurement System" (ARMS). Here four non-coherent radar systems with (linear) polarisation diversity, are operating at (nom) 3, 5, 10 and 15 GHz under computer control and with on-line data processing. Calibration accuracy is averagely $\pm$ 1 dB assuming constant monitoring of transmission path characteristics is employed. Many RCS measurements of various aircraft have been made using this equipment over a number of years and improvements are continually adding to its usefulness.

2.4.3.2 Teledyne-Micronetics, RCS Measurement Facilitiy, San Diego, USA

This facility may be considered a halfway house between the Ground Plane method for radar measurement of aircraft on the ground, and the free space measurement of sub-scale models. The facility comprises three parallel ranges, two of which are nominally 320 m and the other 200 m long. These three ranges are paved with inverted-vee shape blocks which serve to deflect skip-path reflections away from the target and the radars to allow the target rotating mechanism to be below line-of-sight and out of the radar field of view. The radars are pulse range gated and background levels of less than 10^{-7} m^2 can be achieved in the absence of any model support.

However, sub-scale models of aircraft targets are sometimes used rather than real aircraft. The similarity of the measurement techniques with those of Radio Modelling make it more appropriate for further description to appear in Section 2.5.2.4.

2.4.3.3 ONERA. Chalais Meudon, France

At Chalais-Meudon one of the establishments under the control of the "Office Nationale d'Études et de Récherchés Aérospatiales (ONERA)" a large wind tunnel has been converted to provide a useful RCS measurement range, Fig 2.18. This has been equipped at one end with a roof mounted gantry and gimbal system which controls dielectric strings capable of suspending and rotating real aircraft of fighter size.

The measurement radar sited 70 m away at the far end of the tunnel, operates at frequencies between 8 and 16 GHz, has selectable linear polarisations and provides direct full illumination of the target in free space by means of pulse range gating and highly directional antennas. Absolute values of RCS are obtained by reference to that of an accurately made calibration sphere. Measurement of phase enables angular glint also to be derived.

2.4.3.4 CELAR. Bruz (Rennes), France

CELAR (Centre d'Electronique de l'Armement) includes several established RCS measurement sites among its facilities and new ones are being added.

Two anechoic chambers comprise useful indoor facilities. The smaller of these is 7 x 4 x 4 m and allows for radar measurements between 1 and 18 GHz with targets of maximum dimensions of 1 m and weight 100 kg. The larger chamber is 25 x 12 x 12 m and is designed for radar frequencies from 3 to 100 GHz, with targets of maximum dimensions of

6 m and weight 1 tonne.

Concentrating on the larger chamber, Fig 2.19(b), the targets are suspended by dielectric strings but stabilised by a polystyrene column protruding from a 4 m pit on the centre line of the chamber. A high resolution, frequency stepped radar is often used at frequencies up to 40 GHz and following computerised correction as necessary for far field equivalence, it is possible to locate scattering centres from the radar images produced, in addition to establishing total RCS and angular glint. It is anticipated that the radar frequency coverage will be extended to 94 GHz in the near future.

A new outside facility nearing completion (mid '84) is known as the SOLANGE (Systems Orientable Lourd pour Aeronefs et Gros Engins), Fig 2.19(a). This will be used to measure the radar characteristics of real air vehicles and components of maximum dimensions 20 m and weight 15 tonnes. The targets will be suspended by dielectric strings from a reinforced concrete gantry of dimensions 35 x 35 m. The target will have a minimum of 15 m clearance in all directions and the radar will be at a range of 55 m and will be contained in a "lift" permitting a 30° change of radar sightline. Pulse range gated, frequency stepped radars will be used on the range which, it is hoped, will have the mechanical stability for measurements at 94 GHz. To this end the wall at the radar end forms part of a concrete cylinder of 55 m diameter and 35 m height and includes the target support gantry.

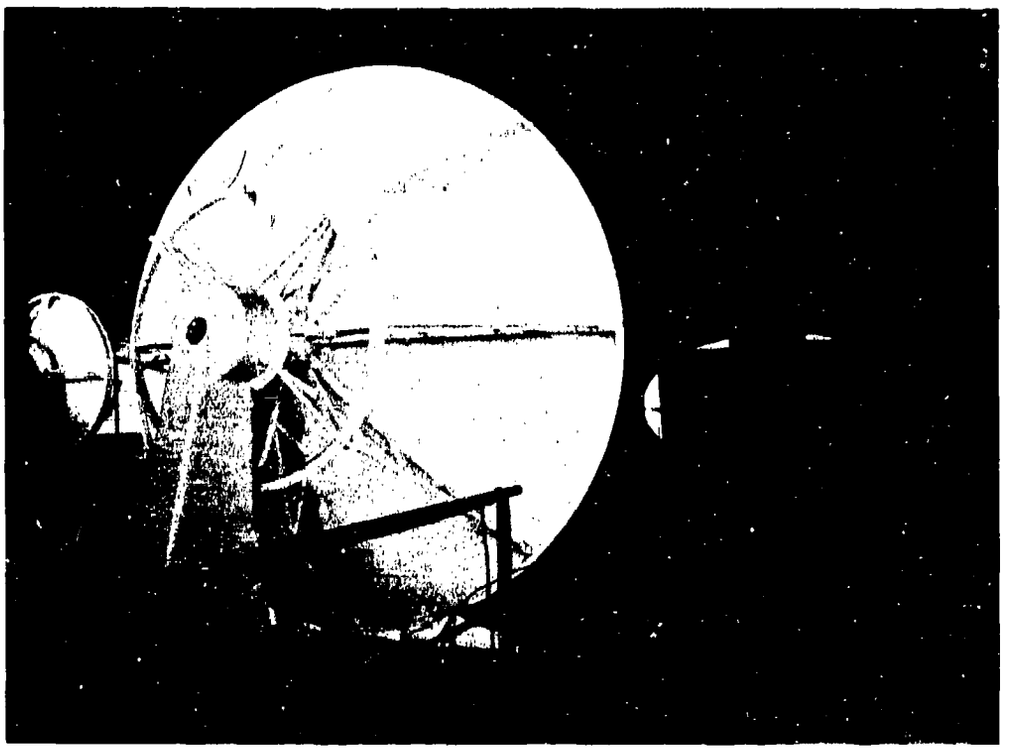

Fig 2.18 Converted wind tunnel RCS measurement range

2.4.3.5 DFVLR, Oberpfaffenhofen, Germany

A recent report published by DFVLR considers the case of an RCS Range where both transmitter and target are within a very few metres of the ground (Ref 33). Novel means of improving the homogenity of the em field at a zone enclosing the target are described. The design and application of special scattering fences are discussed and examples of results of subsequent RCS measurement of classical shapes are given.

Fig 2.19(a) The SOLANGE at CELAR

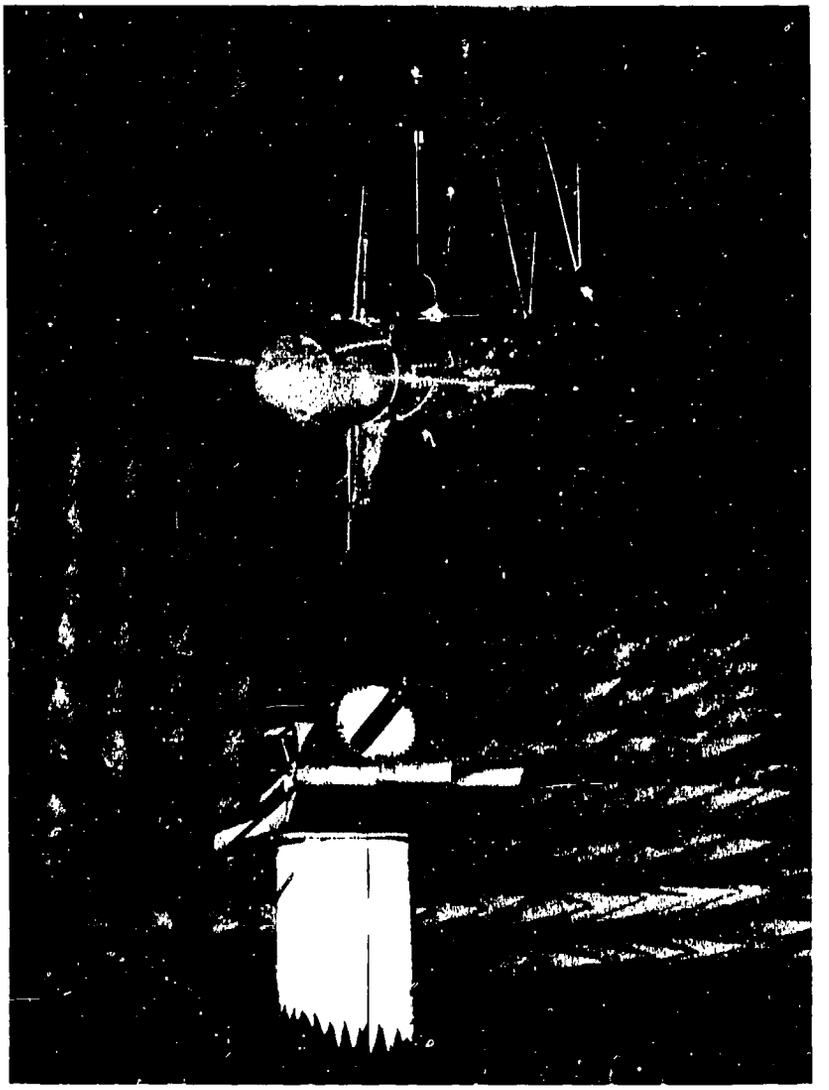

Fig 2.19(b) Large anechoic chamber at CELAR

2.5 THE DETERMINATION OF RCS AND GLINT BY SUB-SCALE METHODS

2.5.1 General

The value of scaled modelling of radar targets and events has long been recognised because the cost of carrying out full scale trials involving flying aircraft or missiles is high, even in small numbers, and it is never possible to repeat any given flight with precision. The principle of electromagnetic wave scaling has been invoked with varying degrees of licence and success as described below, but undoubtedly the most valid is the method of Radio Modelling.

2.5.2 The Principle of Scaled Modelling

The principles of electromagnetic scale modelling have been discussed by Sinclair (Ref 34) and Stratton (Ref 35). Briefly, provided that no materials are involved whose electromagnetic properties display either non-linearity or frequency dependence (for example no ferrites), the field patterns described by Maxwell's Equations can be scaled without alteration by changing all linear dimensions in the same ratio. Hence the technique is to construct an accurate model of a radar target at a reduced scale and to examine the reflections from this with a special radar whose wavelength has been scaled in the same ratio (say P). Since area has dimensions of (length)^2 the radar echoing area (RCS) of the model target will be accurately P^2 less than for the full scale target. Electrical resistivity incorporates length dimensions and should be scaled by making the model of increased conductivity. However, this is only important if the target incorporates lossy dielectric or resistive metals and, in practice the scaling of resistivity is very rarely necessary since most targets are constructed from high conductivity metal and low loss dielectrics. It is important that the polarisation and field illumination taper should be similar in the model and full scale case. This can be achieved by use of a scaled radar antenna and by scaling the range from the radar by the factor P. In practice a "Far Field" situation from the antenna can often be adequately represented at a lesser range than the correctly scaled distance.

When modelling pulsed radars, the pulse length should also be scaled for exact simulation and this becomes important when the physical length of the pulse is comparable with the target length. Similarly a frequency modulated radar must be thought of as a wavelength modulated radar and consequently the frequency deviation of the model radar must be P times that of the full scale radar.

2.5.3 Some Implementations of Scaled Modelling

Several practical methods of simulating or modelling radar events have been used. These include optical, ultrasonic and radio methods. Although only the latter meets the requirements implied above, the optical and ultrasonic methods may sometimes be adequate and are briefly described.

2.5.3.1 Optical Simulation

A light detector is used to examine and measure the reflections of a light source produced by a polished model of a target. Some useful information can be derived but only specular echoes are investigated and,

(1) No account is taken of the phases of reflections from different parts of the target and their mutual interference.
(2) Reflections from frequency sensitive components of the target are not properly represented.
(3) No account is taken of polarisation.
(4) No travelling wave contributions are measured.

The method is clearly of very limited value and is not used seriously since other techniques have become available.

2.5.3.2 Ultrasonic Simulation

The laws of reflection of ultrasonic waves are very similar to those for electromagnetic waves. Taking advantage of this,a sub-scale model target is constructed and immersed in a water tank. An ultrasonic source (which has the advantage of coherence) at suitable scaled frequency is also immersed in the water and irradiates the model target using a beam shaped by a lens antenna (transducer). This technique represents a marked improvement on optical methods and, because of the wavelength scaling, overcomes the first two disadvantages listed above. However, ultrasonic waves are longitudinal and the transmission medium is a fluid which, being incapable of supporting shear waves, means that no travelling wave or polarisation effects can be measured.

A well established Ultrasonic Radar Simulator exists at Thorn EMI Ltd., Feltham, UK and is worthy of description (Fig 2.20).

Fig 2.20 Ultrasonic simulator tank

Description of the Ultrasonic Fuze Simulator

The pool

The simulator tank is 9.75 metres long, 7 metres wide and 5.25 metres deep and contains approximately 280,000 litres of water. It is constructed of reinforced concrete and the base of the tank is some 3 metres below ground level. An underground passageway runs along one side and one end of the tank to provide access to viewing ports mounted in the walls of the tank. A closed circuit television camera, with motorised zoom lens, is fitted behind each window to enable the operator seated at the central console to see clearly what is happening underwater, particularly with engagements involving close misses.

Target complex

Approximately four metres from one end, the tank is spanned by the target supporting gantry, across which the target carriage travels on overhead rails. The target carriage in turn carries a slew ring, upon which rotates the target boom. The target is supported from a sting attached to the roll gearbox which itself is free to move vertically up and down the target boom. The target has freedom of movement in four axes, two linear and offset, and two rotational, slewing and roll.

The ultrasonic fuze probe complex

Mounted on the side walls of the tank and running its full length are two horizontal rails which are set accurately at right angles to the target gantry rails. Upon these runs the carriage supporting the ultrasonic probe which simulates the radar aerial system. This carriage consists of two wheeled assemblies connected by a rigid beam which spans the width of the tank. Mounted upon this beam is a hinged boom assembly which carries the probe manipulator. In the operating position the boom consists of a vertical tube mounted on the carriage beam, to the bottom of which is attached a horizontal tube held parallel to the running rails and pointing towards the target assembly. At the end of this horizontal boom is mounted the three axis probe manipulator.

The eight axes of the simulator are controlled by digital computer operated from a conveniently placed console.

Ultrasonic measurements

The velocity of ultrasonic waves in water is approximately 1500 m/s. When using, for example, a 1/20 scale model to obtain data pertinent to a 10 GHz radar wavelength, ie 30 mm, the ultrasonic radiation wavelength in water must be 1.5 mm. This implies a transmission frequency of 1 MHz.

High reflectivity, coupled with negligible transmission into a model, is achieved by the use of low density materials in the construction. Initially balsa wood was used and great care had to be taken to avoid ingress of water; the model had to be sealed by coating it with a thin layer of metal. Today improved model construction methods and materials are used. However, dielectrics cannot be modelled and hence some important features such as radomes and plastic panels on real aircraft cannot be represented in the model.

Summary

The advantages of ultrasonic radar simulation are: -

(1) it is fully automatic and fast in operation,
(2) because of its low frequency of operation, simulation of radar waveforms is simple and thus inexpensive,
(3) it has flexibility for changing antenna arrays, etc., and can model frequency agility over bandwidths comparable to most radars,
(4) its short operating-pulse capability permits (neglecting polarisation) echo source location techniques to be employed and thus isolate reflectors on targets and to determine their individual polar diagrams. This data can then be stored for use in an appropriate form for the immediate generation of mathematical models of the echoing area of the targets. Care must be taken if the target is one of very low RCS since surface wave echoes may predominate.
(5) The measurement environment is extremely stable and measurements are readily repeatable.

The disadvantages of the simulation are: -

(1) its inability to model polarisation effects, because sonic waves are longitudinal rather than transverse,
(2) the different behaviour of acoustic travelling waves on a target from that of the corresponding electromagnetic waves,
(3) the departure from correspondence when some individual reflectors have characteristic dimensions of the order of a wavelength or smaller
(4) simulation of very short wavelengths can be restricted by attenuation of the appropriate ultrasonic waves in water,
(5) no means is currently available to duplicate in the ultrasonic domain the effects of dielectric structures,
(6) the effects of radar returns from receiver hardware, as seen through antenna apertures, cannot be covered,
(7) target models have to present a large acoustic impedance mismatch at a true surface, attenuate rapidly any signal which does penetrate the target and have to withstand the underwater environment; this is a severe requirement.

2.5.3.3 Radio Modelling - Thorn-EMI, UK

The technique of radio modelling has been well developed over many years in the UK and it is convenient to exemplify the principles by direct reference. The UK Radio Modelling Facility has been developed, and is operated by Thorn-EMI Ltd on behalf of the UK Ministry of Defence, represented by The Royal Signals and Radar Establishment (RSRE) Malvern. It is contained in a building approximately 76 x 35 x 15 m, and comprises eight fixed site measuring radars and target suspension systems.

Most of the radars can operate at any of several frequencies, and coherent and non-coherent operation and polarisation diversity are common features. All sites can operate simultaneously without mutual interference or background clutter. To achieve this, several techniques are used, the most powerful being range gating, and this together with antenna beam shaping, is often completely satisfactory. Additional precautions include IF interlacing and a minimal use of radar absorbent material (RAM) (Fig 2.21a and b).

The pulsed radars used for measurements employ a pulse width chosen to be at least 2.5 times the target length, and the beam width is shaped to subtend approximately 1.5 target widths, and to produce realistic amplitude taper at the target. The receiver processing is arranged to gate out the first and last parts of the return signal and accept only the middle section which is the "steady state" echo. This can be considered to be equivalent to CW operation. If the full scale radar being modelled has a pulse length smaller than or comparable with the target dimensions, then these circumstances are reproduced at model scale. Modelling frequencies from 1 to 890 GHz are available and Fig 2.22 shows the layout of the sites within the Facility. Many accurately detailed sub-scale models of aircraft, missiles, RPV's, ships and ground vehicles exist and the inventory is continually increasing. A more comprehensive description of these facilities is given in Appendix 2.A1, together with examples of data acquired, and a discussion on validation.

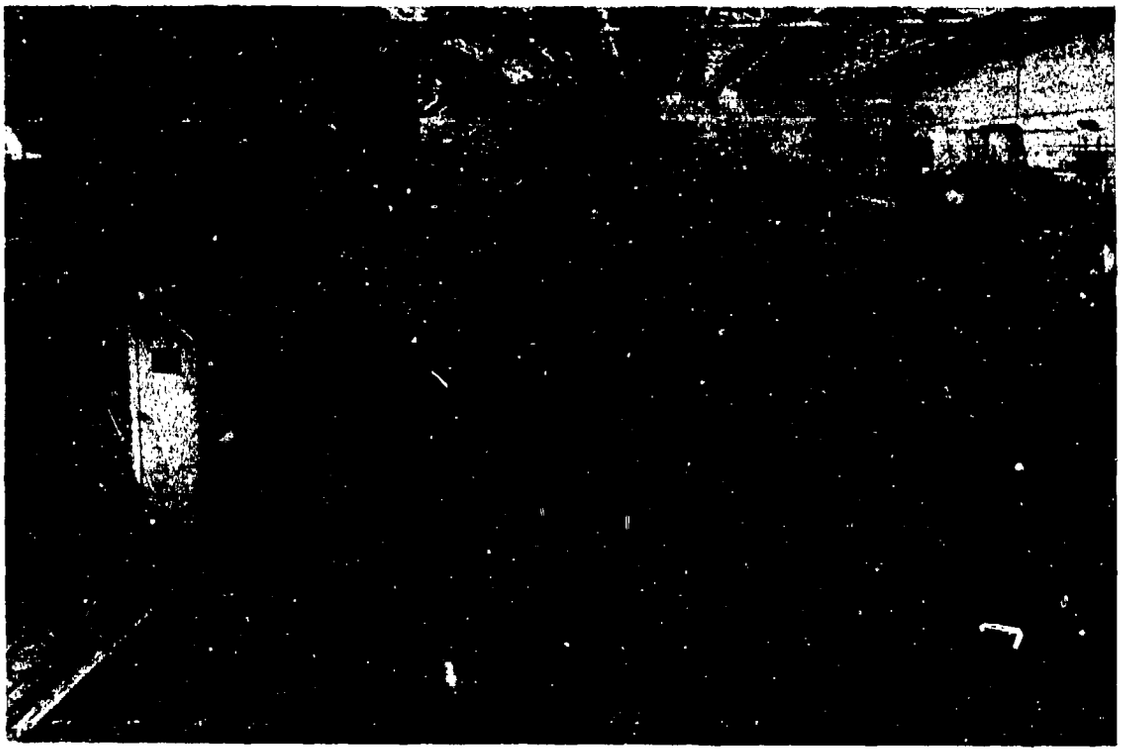

Fig 2.21a Panoramic view of Radio Modelling Facility from East

Fig 2.21b View from West

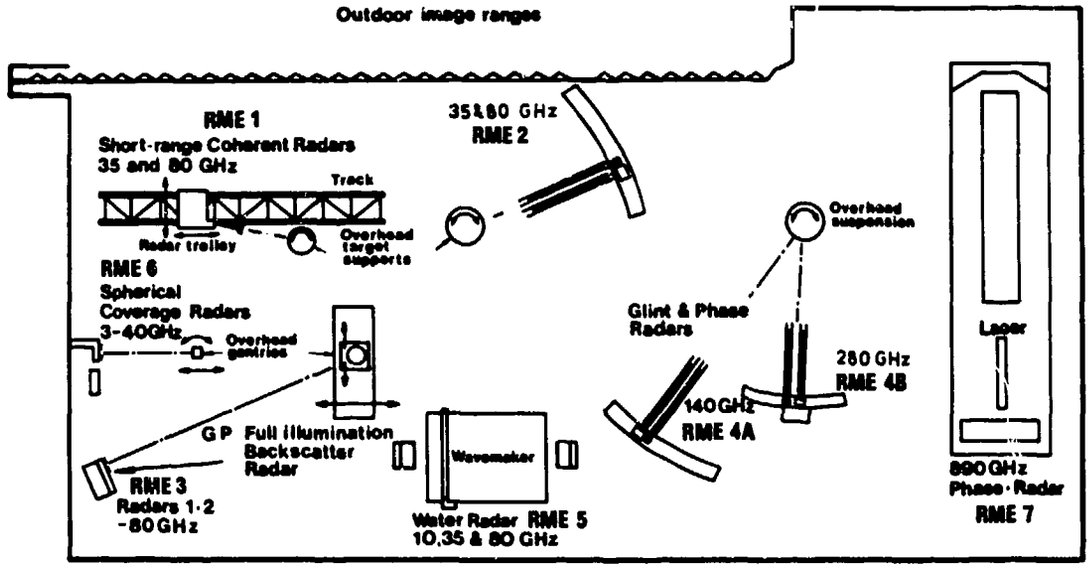

Fig 2.22 Plan of measurement ranges: UK Radio Modelling Facility

Fig 2.23 Measurement ranges of Teledyne Micronetics, San Diego

2.5.3.4 Radio Modelling - Teledyne Micronetics, USA

Reference was made in Section 2.4.3.2 to the Teledyne Micronetics facilities and Fig 2.23 shows the measuring site with the three parallel ranges to the right of a fourth which provides a water surface deepening to some 12 m at the target end.

In a similar manner to that adopted by radio modelling, pulse range gating is used, here with pulse lengths between 100 and 250 nsecs. These transmissions are adequate to simulate any situations where the target is immersed in a field that is essentially CW (ie where the pulse length is greater than 3 or 4 times the maximum linear dimensions of the target). At the same time these pulses are short enough to minimise background noise. This technique, together with the ground reflection minimisation due to the inverted Vee ground plane and final coherent background subtraction methods, ensure effective "freespace" measurement capabilty.

The targets, which must not be greater than 7 m in maximum dimension, are either full scale or at small ratio sub-scale (1/2 or 1/3). These are supported on plastic foam columns constructed as necessary by layering cone frustrums of decreasing diameter - without use of adhesives. The maximum weight supportable is 5 tonnes.

Measurement of RCS (monostatic and bistatic), angular glint, phase, effects of frequency and polarisation changes etc are successfully undertaken. A recently added measurement capability at 10 GHz is a frequency stepping pulse coherent radar with facility for alternate orthogonal polarisation transmissions and simultaneous orthogonal polarised receiver channels. This allows a full polarisation matrix determination of the radar scattering from a target to be measured.

A further similarity to the UK Radio Modelling is the presence of a strong theoretical team to back up the measurement methods and data interpretation.

Of course, the fact that the Teledyne Micronetics ranges are open to the natural environment imposes some restrictions. Particularly in desert climates, changes occur in the transmission medium due to significant temperature changes predominantly near the beginning and end of a day. Such effects must be taken into account and indeed compensation methods are used here as they are at RATSCAT.

The Teledyne Micronetics facilities are widely used by US agencies and appear to provide dependable data.

2.5.3.5 Radio Modelling - Pacific Missile Test Centre, Pt Mugu, USA

Within the department now known as the Microwave Branch of the PMTC, RCS measurements are, and have been made using sub-scale models of targets over a number of years. The standard of detail and accuracy of the sub-scale models used is not of the facsimile standard normal to radio modelling, but is adequate for average RCS measurements. These are supported in an anechoic chamber of dimensions 12 x 12 x 30 m Fig 2.24a and RCS measurements are made at many frequencies. A bibliography of Radar Reflectivity Reports from PMTC exists and is included in the references of this AGARDograph (Ref 36).

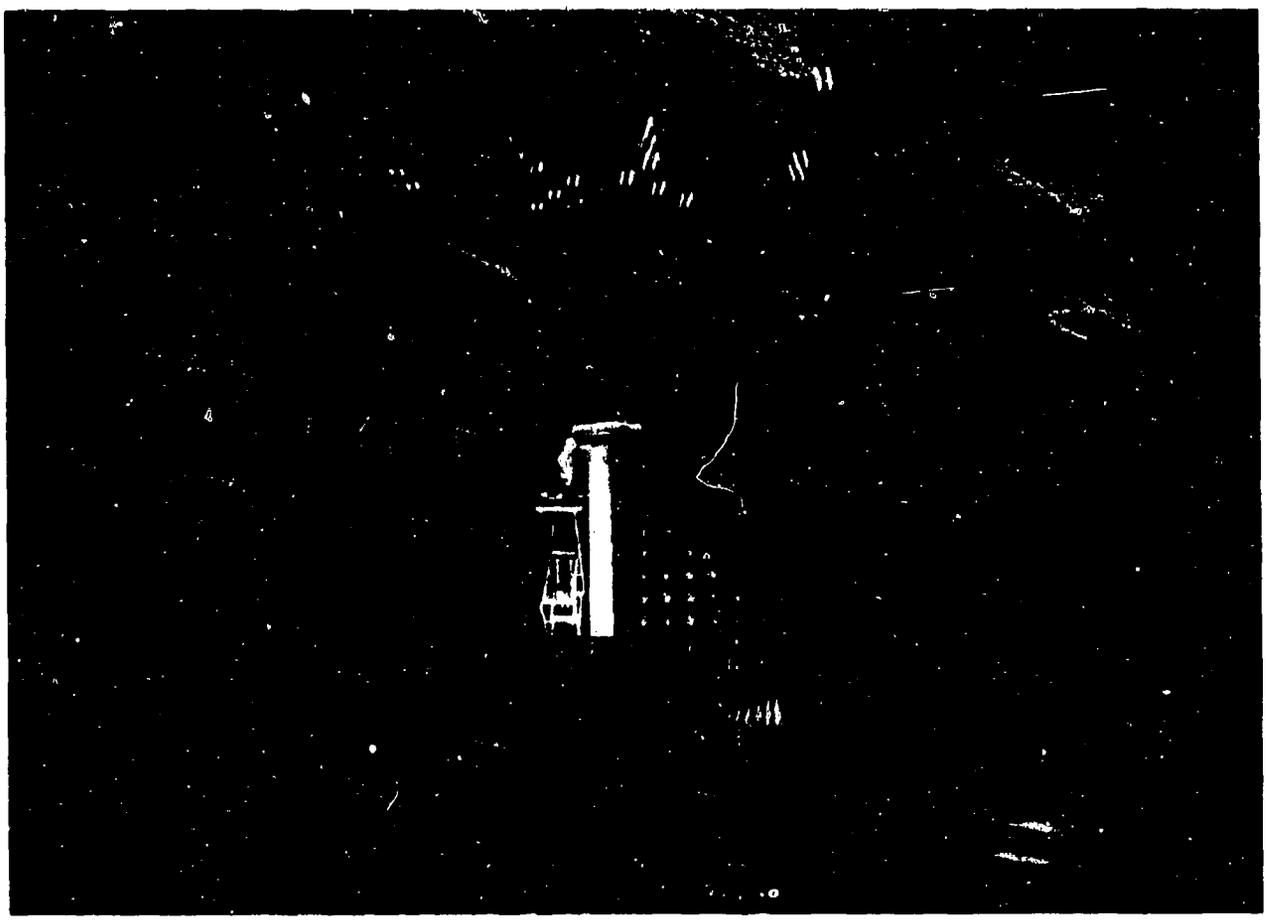

Fig 2.24(a) Large anechoic chamber at PMTC California

Currently a high resolution imaging (mapping) radar is in use in a smaller anechoic chamber. This is a coherent system which accurately measures signal amplitude and phase in the azimuth plane and achieves high range resolution by an FM-CW technique. Data is available in real time via an array processor and isometric, biplanar maps clearly indicate the individual scattering sources on a target (Fig 2.24b, Ref 36).

Two systems with centre frequencies of 10 and 15 GHz and maximum operating bandwidths of 4 GHz are currently operational. Range resolution of two equal simple targets separated by 5 cm has been experimentally demonstrated and approaches the theoretical limit of 3.75 cm established by the signal bandwidth and being independent of frequency and range.

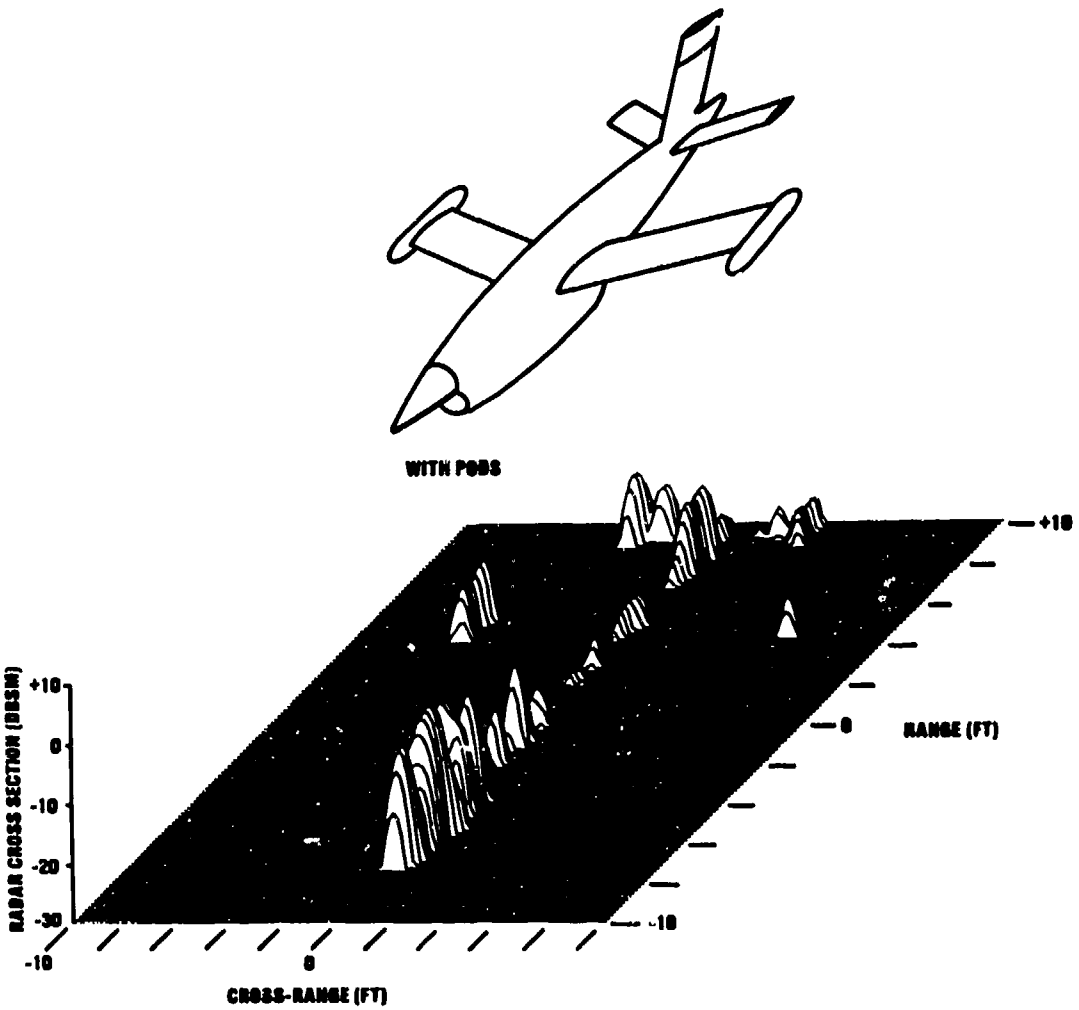

Fig 2.24(b) Two dimensional map of RCS

The measurement facilities at PMTC are well used by military and commercial agencies within the USA and, in common with other facilities mentioned in this paper, their employment by other NATO users is negotiable.

2.6 CONCLUDING COMMENTS

The prime subject of Part 2 of this Volume is the determination of aircraft RCS. The opportunity has been taken to give some idea of the complexities involved in defining and measuring the RCS of an aircraft in flight and the precision which can be achieved by sub-scale and full scale static measurements.

It has been shown that the RCS depends on the type of radar used - and its parameters, and it has been pointed out that the dynamic range over which the RCS of an aircraft varies with aspect angle, can readily be 60 dB. The importance of signal fading rate has been mentioned and the difference between the non-ergodic statistics of these data, and the ergodic nature of the classic distributions (Swerling, Rayleigh et al) has been highlighted.

Appendix 2.A1 deals, inter alia, with the subject of validity of sub-scale radio modelling, and to some extent of full scale static measurement. The intention of that section was to attempt to decouple the validity of measurements made, "on the ground", which is limited only by the equipment and expertise available, and the standard of comparison which should be employed to judge the degree of agreement of such data with those from dynamic real-life measurements. An appreciation of this section is important since, only by modelling methods can the radar characteristics of many targets be obtained.

The nature of this AGARDOgraph prohibits detail of many relevant scattering phenomena, clutter backgrounds, camouflage, classification, recognition methods etc. Similarly, the concentration on aircraft targets leads to omission of material relevant to the many other "targets", both artificial and natural, which are subjects of investigation by radio modelling.

Finally, although in the sub-scale and full-scale static measurement areas, techniques continually improve and understanding of the scattering phenomena grows greater, the introduction of new structural materials (eg composites) in the manufacture of air vehicles provides cause for continuing study and measurement. Similarly, the vast amount of data now becoming available through the use of polarisation scattering matrix radars, high resolution mapping radars etc are requiring highly sophisticated processing, much of it in real time. This processing is likely to grow in complexity as more and more intelligence is sought from the target radar returns in many different background environments.

Examples of measurement facilities have been described but many more exist. The ones chosen as examples are those best known to the author, and possibly there are others equally good. However, the UK Radio Modelling Facility, with which the author has been associated for many years is believed to be unique in its versatility and the experience of its engineers and theoreticians.

The employment of dynamic, static or sub-scale methods for the determination of RCS has different advantages and disadvantages. It is the prerogative of the potential user to decide which method is likely to provide the best, and most cost-effective data.

REFERENCES

1		IEEE Standard Test Procedures for Antennas IEEE Std. 149, 1979
2		Standard Coordinate System and Data Formats for Antenna Patterns. Electronic Trajectory Measurements Working Group, Inter-Range Instrumentation Group, Range Commanders Council, United States National Ranges. IRIG, Document AD 637 189, May 1966
3	Mattes, H. Clemens, E.	Modell-Antennenvermessung für das Forschungsvorhaben BMV L-6/76 "Montageplätze von Antennen an kleinen Flugzeugen". DFVLR-IB 551-79/4, Oberpfaffenhofen 1979
4	Klein, K.	Antennenvermessung im Fluge für das Forschungsvorhaben "Montageplätze von Antennen an kleinen Flugzeugen". DFVLR-IB 153-78/19, Braunschweig, 1978
5	Stein, V.	Lösung elektromagnetischer Randwertprobleme bei komplizierten Strukturen - Grundlagen der Integralgleichungsmethode. DFVLR-FB 78-01 (1978), 92 Seiten, 19 Bild., 30 Lit.
6	Stein, V.	Numerische Lösung der Integralgleichungen für das elektrische und magnetische Feld. DFVLR-FB 78-05 (1978), 101 Seiten, 37 Bild., 36 Lit.
7	Stein, V.	Berechnung der elektrodynamischen Eigenschaften komplizierter Strukturen mit Hilfe der Integralgleichungsmethode - Anwendungsbeispiele. DFVLR-FB 78-18 (1978), 56 Seiten, 30 Bild., 1 Tab., 20 Lit.
8	Schrott, A.	Berechnung der Strahlungscharakteristik von Antennen auf komplizierten Körpern im Hochfrequenzfall - Prinzip der geometrischen Beugungstheorie. DFVLR-FB 78-02 (1978), 110 Seiten, 42 Bilder, 2 Tab., 58 Lit.
9	Schrott, A.	Feldberechnungen mit Hilfe der geometrischen Beugungstheorie. DFVLR-FB-78-06 (1978), 96 Seiten, 38 Bilder, 3 Tab., 51 Lit.
10	Schrott, A.	Konstruktion der Strahlenwege und Anwendung der geometrischen Beugungstheorie zur Berechnung von Streufeldern komplizierter Körper. DFVLR-FB-78-19 (1978), 82 Seiten, 53 Bilder, 23 Lit.
11	Hufford, G.A. Longley, A.G.	Characterization of a VHF Air-Ground Channel. U.S. Department of Commerce, ITS Boulder Colorado, OT Report 74-47, 1947
12	Bothe, H.	In-Flight Measurement of Aircraft Antenna Radiation Patterns. AGARD CP 139 (1973)
13	Mahlum, R.W.	Flight Measurement of Aircraft Antenna Radiation Patterns. AFFTC-TD-75-3 Edwards Air Force Base, Cal., USA, 1975
14	Pietersen, O.B.M.	Determination of Antenna Radiation Patterns, Radar Cross Sections and Jam-to-Signal Ratios by Flight Tests. AGARD CP 223 (1977)
15	Bothe, H.	Real Time Data Transmission and Processing for the Determination of Aircraft Antenna Radiation Patterns. AGARD CP 223 (1977)
16	Bothe, H. Klein, K.	In-Flight Accuracy and Coverage Tests of ESM and ECM Systems. AGARD CP 373 (1984)

17	Bothe, H.	In-Flight Calibration of Aircraft Antenna Radiation Patterns. IEEE Transactions on Instrumentation and Measurement, Vo. IM29, No. 4, Dec. 1980
18	Reed, H. Russell, C.	Ultra High Frequency Propagation. John Wiley and Sons Inc., NY, 1953
19	Bothe, H.	Calibration of In-Flight Measured Aircraft Antenna Radiation Patterns by Means of Ground Reflection Calculations. DFVLR Internal Report IB 112-81/21 Braunschweig/Germany 1981
20	Ancona, M.C.	Etude des Conditions de mesure sur maquette des diagrammes de rayonnement d' aériens á bord d'avions. Rapport Nr. 154, S.T.A.R.E.C. Montrouge (Seine) 1957
21	Koob, K. Liesenkötter, B.H.C.	Antenna Testing Techniques. ESA-SP 127 Preprint, European Space Agency, Paris 1977
22	Delogu, A.	Compact Range Description. AERITALIA RCE 2516 Caselle, Italy, 1982
23	Delogu, A.	Spherical Near-Field Description. AERITALIA RCE 2517 Caselle, Italy, 1982
24	Tavormia, J. Hess, D.	Spherical Near-Field Antenna Measurements with the SCIENTIFIC-ATLANTA MODEL 2022. Application Note AN-22 Scientific-Atlanta, Inc., 1980
25	Schrott, A. Stein, V.	Determination of the Far-Field from Measured Near-Field Data: Theory and Measuring Technique of the Near-Field Far-Field Transformation. Techn. Transl. ESA-TT-616 (1980) of DFVLR Mitteilung 79-07, Köln, 1979
26	Gellert, W.	Kleine Enzyklopädie Mathematik, p 556. Pfalz Verlag, Basel 1969
27	Graves, C.D.	The Radar Polarisation Power Scattering Matrix. Proc. IRE, Feb '56, Vol 44, Pages 248-252
28	Ruck, G.T.	The Radar Cross Section Handbook. Plenum Press 1970, Vol 1, Pages 17-21
29	Schnetsler	The Reflection of e.m. waves by single surfaces towards a point source. EMI Research Lab. Report RL/107 Sept. 1953
30	Bahret, W.F.	"Dynamic Full Scale Measurements of RCS". AGARD Lecture 59, Oct. 1973. Lecture 1d
31	Cooper, Dale W. James, Robert	NASA Tech. Memo 72870 - Shuttle Orbiter RCS Analysis. Oct. 1979
32		RATSCAT, Facilities and Capabilities 1980. Issued by 6585th Test Group, Holloman, AFB
33	Bethke, K.-H.	Untersuchungen zur Störstreuung und Methoden zu deren Unterdrückung bei bodennahen Radarrückstrahlmessungen. DFVLR-FB 85-42(1985), 64 Seiten, 51 Bild., 1 Tab., 16 Lit.
34	Sinclair, J.A.	Theory of Models of e.m. Systems. Proc. IRE, Nov. 1948
35	Stratton, J.A.	Electromagnetic Theory.
36		Bibliography of Radar Reflectivity Reports, Microwave Branch, Code 1221 PMTC, Pt. Mugu, California 93042
37	Mensa, D.L.	High Resolution Radar Imaging. Artech House, Mass. USA - 1981

APPENDICES

APPENDIX 1.A

DERIVATION OF RADIO WAVE PROPAGATION PARAMETERS

Fig 1.A1 shows the geometry of a two-path radio wave propagation between the points A and B in more detail than in Fig 1.24.

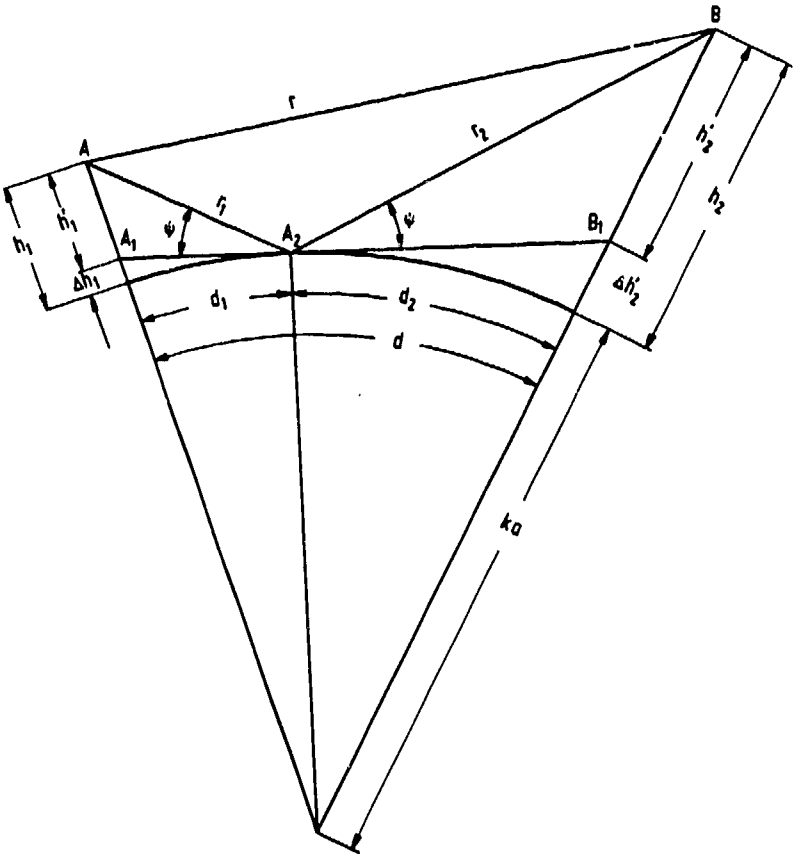

Fig 1.A1 Geometry of two-path propagation

The equation of the divergence factor D, defined in section 1.4.5.2, is developed in Ref 18 by comparing the cross-section area of a diverging beam from a plane surface with the cross-section area of a diverging beam reflected from the curved surface of the earth. With the notations of Fig 1.A1, D becomes

$$D = \left(1 + \frac{2r_1 r_2}{kad \tan\psi}\right)^{-\frac{1}{2}} \qquad (1.A1)$$

where a is the radius of the earth and k = 4/3 is the refraction correction coefficient. If d << ka then r_1 and r_2 are approximately equal to $h_1'/\sin\psi$ and $h_2'/\sin\psi$, respectively, and for small grazing angles $\sin\psi$ approximates $\tan\psi$. Thus Eq (1.A1) can be rewritten

$$D = \left(1 + \frac{2h_1' h_2'}{kad \tan^3\psi}\right)^{-\frac{1}{2}} \qquad (1.A2)$$

The following relationships are derived from Fig 1.A1

$$\tan\psi = \frac{h_1'}{d_1} = \frac{h_2'}{d_2} \qquad (\text{since } d_1 << ka,\ d_2 << ka) \qquad (1.A3)$$

$$h_2' = h_2 - \Delta h_2 \tag{1.A4}$$

$$(ka + \Delta h_2)^2 = (ka)^2 + d_2^2 \quad (\text{since } A_2 B_1 \approx d_2)$$

$$(ka)^2 + 2\Delta h_2 ka + \Delta h_2^2 = (ka)^2 + d_2^2$$

$$\Delta h_2 = \frac{d_2^2}{2ka} \qquad (\text{since } \Delta h_2^2 << 2\Delta h_2\, ka) \tag{1.A5}$$

$$d_2 = d - d_1 \tag{1.A6}$$

Considering Eqs (1.A3) through (1.A6), (1.A2) can be rewritten in order to obtain D as a function of d, d_1 and h_2.

$$D = \left(1 + \frac{2d_1}{d\left(\frac{ka\, h_2}{(d-d_1)^2} - \frac{1}{2}\right)}\right)^{-\frac{1}{2}} \tag{1.A7}$$

The angle of incidence ψ is given by Eq (1.A3), and if (1.A4) and (1.A5) are taken into account, (1.A3) yields

$$\psi = \tan^{-1}\left(\frac{h_2}{d_2} - \frac{d_2}{2ka}\right) \tag{1.A8}$$

and from symmetry

$$\psi = \tan^{-1}\left(\frac{h_1}{d_1} - \frac{d_1}{2ka}\right) \tag{1.A9}$$

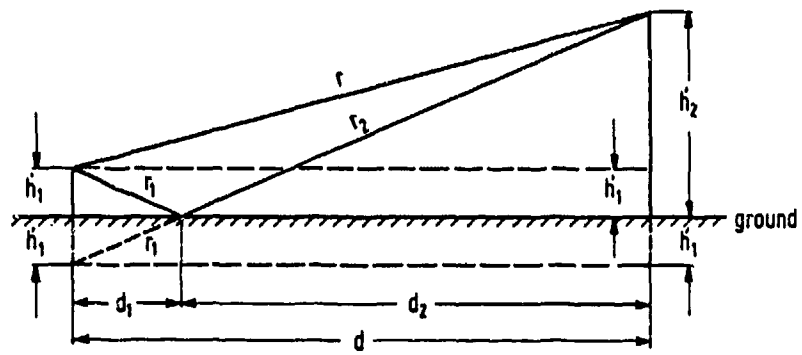

Fig 1.A2 Determination of physical path-length difference between direct and reflected ray

The angular physical path length difference θ between the direct and reflected rays is illustrated in Fig 1.A2.

$$\theta = \frac{360°}{\lambda} \cdot ((r_1 + r_2) - r) = \frac{360° \cdot f}{c}\ ((r_1 + r_2) - r) \tag{1.A10}$$

The following relations are also derived from Fig 1.A2

$$(r_1 + r_2) = \left((h_2' + h_1')^2 + d^2\right)^{\frac{1}{2}} \quad \text{and} \quad r = \left((h_2' - h_1')^2 + d^2\right)^{\frac{1}{2}}$$

and for $d \gg h_2' + h_1'$ and $d \gg h_2' - h_1'$

$$r_1 + r_2 = d + \frac{(h_2' + h_1')^2}{2d} \quad \text{and} \quad r = d + \frac{(h_2' - h_1')^2}{2d} \tag{1.A11}$$

Considering (1.A11), (1.A10) yields

$$\theta = 360° \cdot \frac{f}{c} \cdot \frac{2h_1'h_2'}{d} \tag{1.A12}$$

Similarly from (1.A4) and (1.A5)

$$h_1' = h_1 - \Delta h_1 \tag{1.A13}$$

$$\Delta h_1 = \frac{d_1^2}{2ka} \tag{1.A14}$$

Using the Eq (1.A3), (1.A6), (1.A13) and (1.A14), (1.A12) may be rewritten

$$\theta = 720° \cdot \frac{f}{c} \cdot \left(h_1 - \frac{d_1^2}{2ka}\right)^2 \cdot \frac{d-d_1}{d \cdot d_1} \tag{1.A15}$$

The equation for calculating the distance d_1 of the reflection point from the receiving antenna is developed as follows. First considering (1.A4) and (1.A5) yields

$$h_2 = h_2' + \frac{d_2^2}{2ka} \tag{1.A16}$$

Now introducing the relations of Eq (1.A3), (1.A13), (1.A14) and (1.A6), (1.A16) becomes

$$h_2 = \left(h_1 - \frac{d_1^2}{2ka}\right) \cdot \frac{d-d_1}{d_1} + \frac{(d-d_1)^2}{2ka} \tag{1.A17}$$

which is a cubic equation for d_1.

APPENDIX 1.B

DERIVATION OF THE TRANSFORMATION EQUATIONS FOR THE ASPECT ANGLE

For the computation of the horizontal and vertical aspect angle the following parameters have to be considered:

Azimuth and elevation angles of the ground tracking system (e.g. Telemetry, Radar)	ρ, ρ_E
Distance between the vehicle and the ground station	D
Vehicle heading relative to true North (right turn is positive)	Ψ
Vehicle pitch (nose up is positive)	θ
Vehicle roll (right wing down is positive)	ϕ

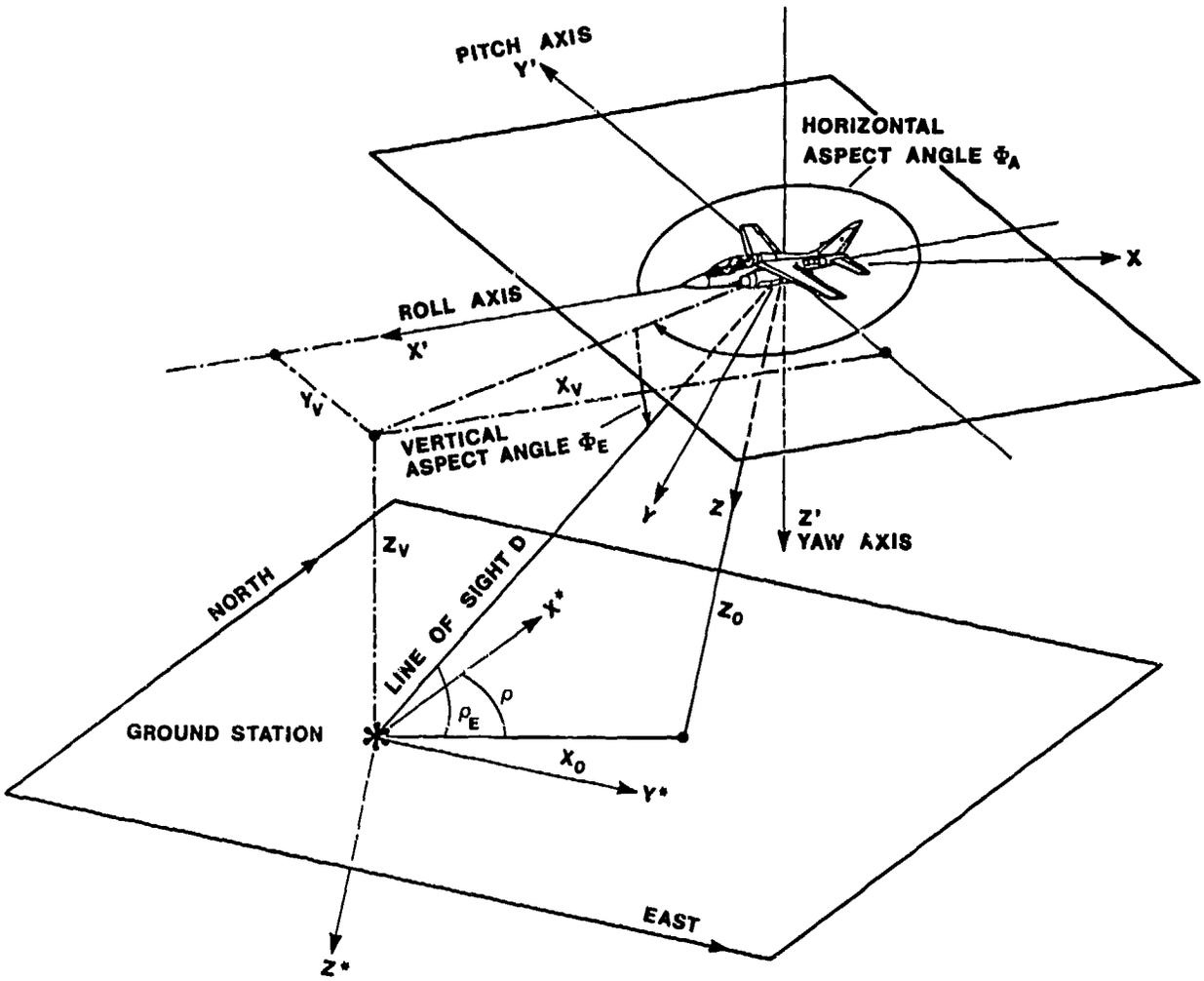

Fig 1.B1 Coordinate systems and parameters for aspect angle computation

Three cartesian coordinate systems are chosen as illustrated in Fig 1.B1:

X*, Y*, Z*	with its origin at the ground station, X* pointing North, Y* pointing East, Z* pointing down
X, Y, Z	with its origin at the vehicle, the X Y plane parallel to the X* Y* plane and X along the projection of the range vector on the X Y plane
X', Y', Z'	with its origin at the vehicle, X' the roll axis, Y' the pitch axis and Z' the yaw axis of the aircraft.

The ground station location in X, Y, Z coordinates is denoted by X_o, Y_o, Z_o and in X', Y', Z' coordinates by X_v, Y_v, Z_v.

The vector which points from the vehicle to the ground station is given in its components X_v, Y_v, Z_v of the X', Y', Z' coordinate system. It can be transformed to the coordinates X_o, Y_o, Z_o of the X, Y, Z system by rotation matrices M, as both systems have the same origin.

$$\begin{bmatrix} X \\ Y \\ Z \\ o \end{bmatrix} = M_1 M_2 M_3 M_4 \cdot \begin{bmatrix} X_v \\ Y_v \\ Z_v \end{bmatrix} = M(\theta_E) M(\Psi - \rho) M(\theta) M(\phi) \cdot \begin{bmatrix} X_v \\ Y_v \\ Z_v \end{bmatrix} \qquad (1.B1)$$

M_1 takes care of the rotation due to the earth curvature θ_E given by Eq 1.13. Next the nose of the vehicle must be rotated to the projection of the line of sight in the XY-plane. The angle on which this rotation takes place is equal to the difference between heading Ψ and the azimuthal tracking angle ρ and is taken into account by M_2. M_3 allows for the pitch angle θ of the vehicle and M_4 for its roll angle ϕ.

The basic matrix M_B for the rotational transformation of a cartesian coordinate system by the angles λ (around X), μ (around Y) and ν (around Z) is given in Ref 26 as:

$$M_B = \begin{bmatrix} \cos\mu\cos\nu & -\cos\mu\sin\nu & \sin\mu \\ \cos\lambda\sin\nu + \sin\lambda\sin\mu\cos\nu & \cos\lambda\cos\nu - \sin\lambda\sin\mu\sin\nu & -\sin\lambda\cos\mu \\ \sin\lambda\sin\nu - \cos\lambda\sin\mu\cos\nu & \sin\lambda\cos\nu + \cos\lambda\sin\mu\sin\nu & \cos\lambda\cos\mu \end{bmatrix} \qquad (1.B2)$$

For M_1, θ_E equals μ and $\lambda = \nu = 0$, so that

$$M_1 = M(\theta_E) = \begin{bmatrix} \cos\theta_E & 0 & \sin\theta_E \\ 0 & 1 & 0 \\ -\sin\theta_E & 0 & \cos\theta_E \end{bmatrix} \qquad (1.B3)$$

For M_2, $(\Psi - \rho)$ equals ν and $\lambda = \mu = 0$, so that

$$M_2 = M(\Psi - \rho) = \begin{bmatrix} \cos(\Psi-\rho) & -\sin(\Psi-\rho) & 0 \\ \sin(\Psi-\rho) & \cos(\Psi-\rho) & 0 \\ 0 & 0 & 1 \end{bmatrix} \qquad (1.B4)$$

For M_3 the pitch angle θ equals μ and $\lambda = \nu = 0$, therefore

$$M_3 = M(\theta) = \begin{bmatrix} \cos\theta & 0 & \sin\theta \\ 0 & 1 & 0 \\ -\sin\theta & 0 & \cos\theta \end{bmatrix} \qquad (1.B5)$$

For M_4 the roll angle ϕ equals λ and $\mu = \nu = 0$, so that

$$M_4 = M(\phi) = \begin{bmatrix} 1 & 0 & 0 \\ 0 & \cos\phi & -\sin\phi \\ 0 & \sin\phi & \cos\phi \end{bmatrix} \qquad (1.B6)$$

Solving for the ground station coordinates X_v, Y_v and Z_v we get

$$\begin{bmatrix} X_v \\ Y_v \\ Z_v \end{bmatrix} = \left(M(\theta_E)\right)^{-1} \cdot \left(M(\Psi-\rho)\right)^{-1} \cdot \left(M(\theta)\right)^{-1} \cdot \left(M(\phi)\right)^{-1} \cdot \begin{bmatrix} X_o \\ Y_o \\ Z_o \end{bmatrix} \qquad (1.B7)$$

or after multiplication of the 4 matrices

$$X_v = X_O\,(\cos\theta_E\cos(\Psi-\rho)\cos\theta - \sin\theta_E\sin\rho) + Y_O\,(\sin(\Psi-\rho)\cos\theta) + Z_O\,(-\sin\theta_E\cos(\Psi-\rho)\cos\theta - \cos\theta_E\sin\theta)$$

$$Y_v = X_O\,(\cos\theta_E\cos(\Psi-\rho)\sin\theta\sin\phi - \cos\theta_E\sin(\Psi-\rho)\cos\phi + \sin\theta_E\cos\theta\sin\phi) + Y_O\,(\sin(\Psi-\rho)\sin\theta\sin\phi + \cos(\Psi-\rho)\cos\phi) + Z_O\,(-\sin\theta_E\cos(\Psi-\rho)\sin\theta\sin\phi + \sin\theta_E\sin(\Psi-\rho)\cos\phi + \cos\theta_E\cos\theta\sin\phi)$$

$$Z_v = X_O\,(\cos\theta_E\cos(\Psi-\rho)\sin\theta\cos\phi + \cos\theta_E\sin(\Psi-\rho)\sin\phi + \sin\theta_E\cos\theta\cos\phi) + Y_O\,(\sin(\Psi-\rho)\sin\theta\cos\phi - \cos(\Psi-\rho)\sin\phi) + Z_O\,(-\sin\theta_E\cos(\Psi-\rho)\sin\theta\cos\phi - \sin\theta_E\sin(\Psi-\rho)\sin\phi + \cos\theta_E\cos\theta\cos\phi) \quad (1.B8)$$

As illustrated by Fig 1.B1

$$X_O = -D\cos\rho_E,\ Y_O = O \text{ and } Z_O = D\sin\rho_E \quad (1.B9)$$

Substituting (1.B9) into (1.B8) yields

$$X_v = D\,(\cos\rho_E(\sin\theta_E\sin\theta - \cos\theta_E\cos(\Psi-\rho)\cos\theta) - \sin\rho_E(\sin\theta_E\cos(\Psi-\rho)\cos\theta + \cos\theta_E\sin\theta)$$

$$Y_v = D\,(\cos\rho_E(\cos\theta_E\sin(\Psi-\rho)\cos\phi - \sin\theta_E\cos\theta\sin\phi - \cos\theta_E\cos(\Psi-\rho)\sin\theta\sin\phi) + \sin\rho_E(\sin\theta_E\sin(\Psi-\rho)\cos\phi + \cos\theta_E\cos\theta\sin\phi - \sin\theta_E\cos(\Psi-\rho)\sin\theta\sin\phi)$$

$$Z_v = D\,(-\cos\rho_E(\cos\theta_E\cos(\Psi-\rho)\sin\theta\cos\phi + \cos\theta_E\sin(\Psi-\rho)\sin\phi + \sin\theta_E\cos\theta\cos\phi) + \sin\rho_E(\cos\theta_E\cos\theta\cos\phi - \sin\theta_E\cos(\Psi-\rho)\sin\theta\cos\phi - \sin\theta_E\sin(\Psi-\rho)\sin\phi)) \quad (1.B10)$$

Now the horizontal aspect angle Φ_A can be calculated substituting the terms of Eq (1.B10)

$$\Phi_A = \tan^{-1}\left(\frac{X_v}{Y_v}\right) \quad (1.B11)$$

and the vertical aspect angle Φ_E correspondingly

$$\Phi_E = \tan^{-1}\left(\frac{-Z_v}{\sqrt{X_v^2 + Y_v^2}}\right) \quad (1.B12)$$

APPENDIX 2.A

RADIO MODELLING IN THE UK

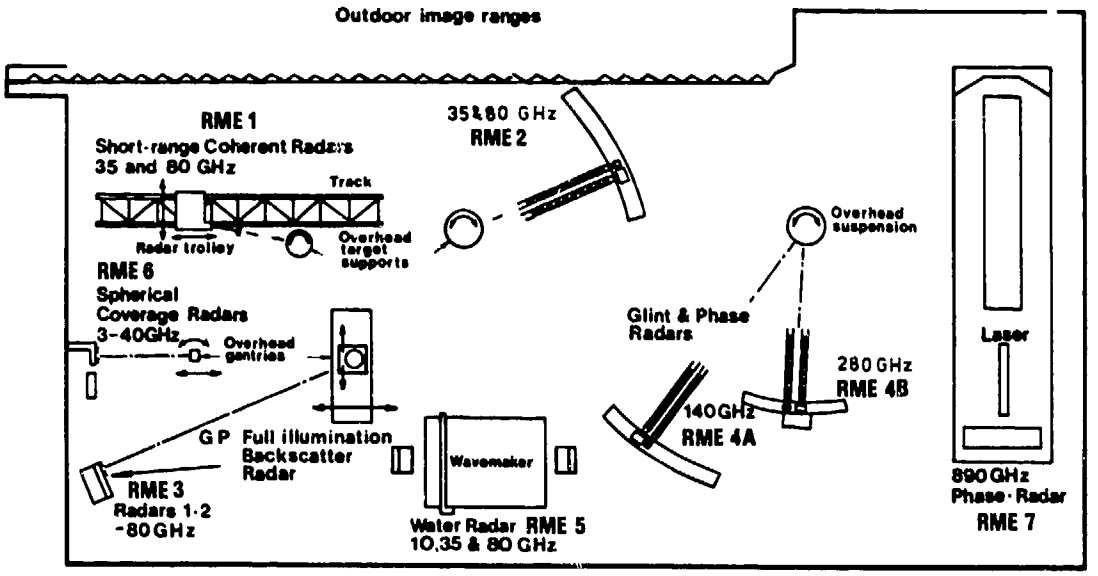

Fig 2.A1 Plan of measurement ranges: UK Radio Modelling Facility

A knowledge of the value of reflections from targets is an essential prerequisite for assessing the performance of existing radar systems and for designing and developing new ones. This applies to all types of radar, such as surveillance, tracking, guidance and fuzing. Frequently, a statistical representation of target scatter is not adequate because the time varying (non-ergodic) nature of the scatter is of interest and this would be dependent not only on the radar parameters, but also on the movement of the target and its position relative to the environment. In the UK a comprehensive Radio Modelling Facility has been evolved over the last 20 years in order to study the scattering processes involved in radar engagements, and to provide measurement facilities capable of investigating most radar problems. Fig 2.A1 shows a schematic layout of the facility.

This Appendix describes the target models and the measuring ranges and gives some examples of the types of radar applications which have been investigated.

2.A1 Description of Facility

2.A1.1 Target Models

Over 50 detailed models of targets are available with scale factors varying from 0.3 to 0.01. The scaling factor is usually chosen to maintain a reasonable size of model, and preferably is not greater than 5 m in maximum dimension. Since most of the measurement requirement is for data at 3 GHz and above, it is necessary for the models to be very complete in detail. Appreciable energy is often scattered from small components, such as internal engine detail, air scoops, landing lights, antennas, bulkheads and radar installations. For many applications it is necessary to rotate engines. Such rotation results in large fluctuations in the return signal and the generation of doppler side bands which can upset the performance of guidance, arming or fuzing radar systems. A small number of the models are shown in Figs 2.A2 and 2.A3.

The models are constructed of various materials. Larger items, such as a fuselage, are made from glass fibre mouldings and timber. Such items are finally coated with silver to a depth of some 5 electrical skin depths at the lowest modelling frequency. Aircraft wing edges, tail planes, control surfaces, radar dishes, engines and small details are made in metal. Dielectric components such as radomes, cockpit canopies, glass fibre panels etc are modelled in plastics of the same dielectric constant and similar loss tangent and have appropriately scaled thickness.

Suspension of a target model for radar measurement was the subject of much experiment. The results showed that in order best to simulate free space conditions it is necessary to suspend the target models by very thin strings. In practice these are terylene (or nylon) cords which are arranged in planes not normal to the incident radiation. In order to obtain independent movement in roll, pitch, yaw and spin, the system of strings (usually 4 or 8) is supported by a gimbal and pulley system in the roof. Thus, models may be set to any attitude and may be rotated about a vertical axis at closely controlled rates under computer control (Fig 2.A6).

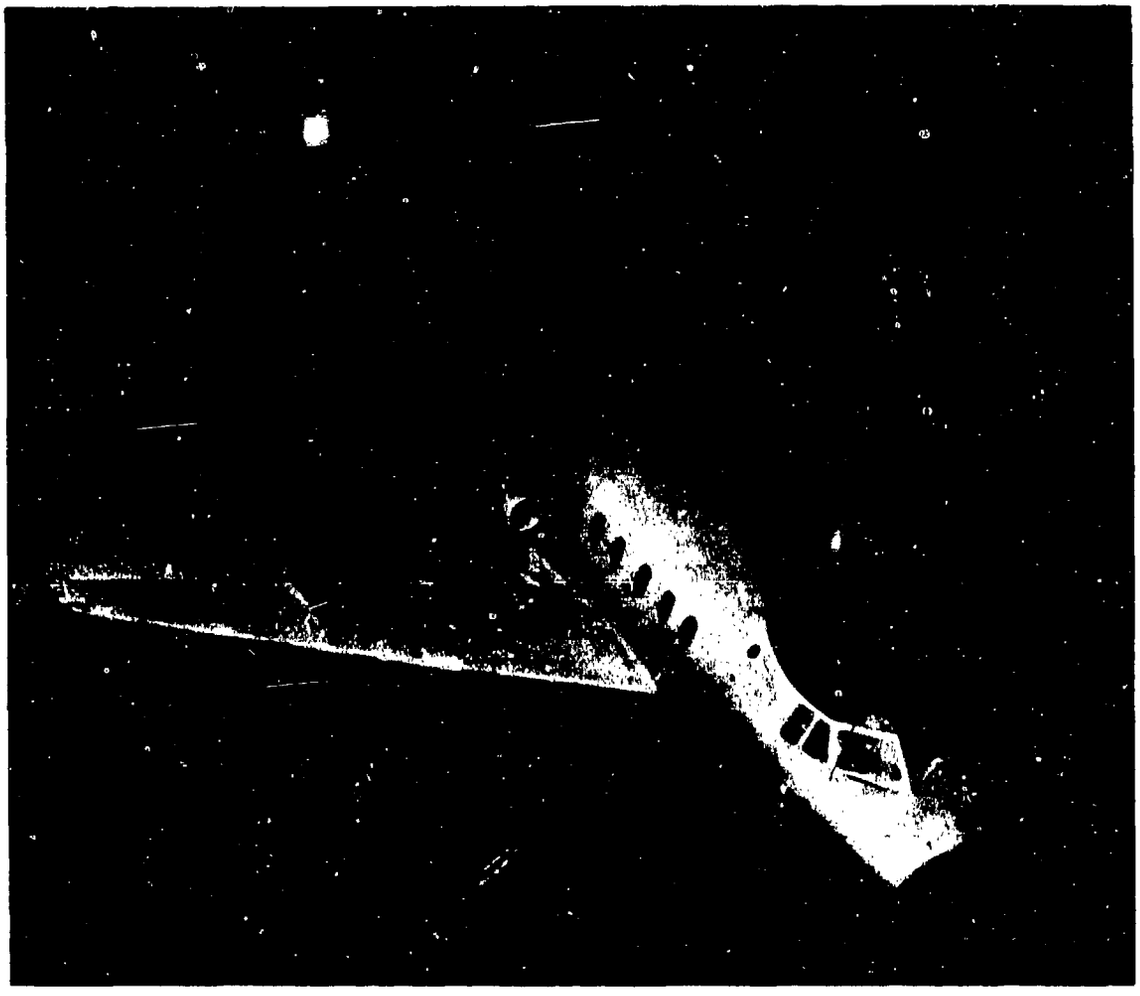

Fig 2.A2 Model aircraft

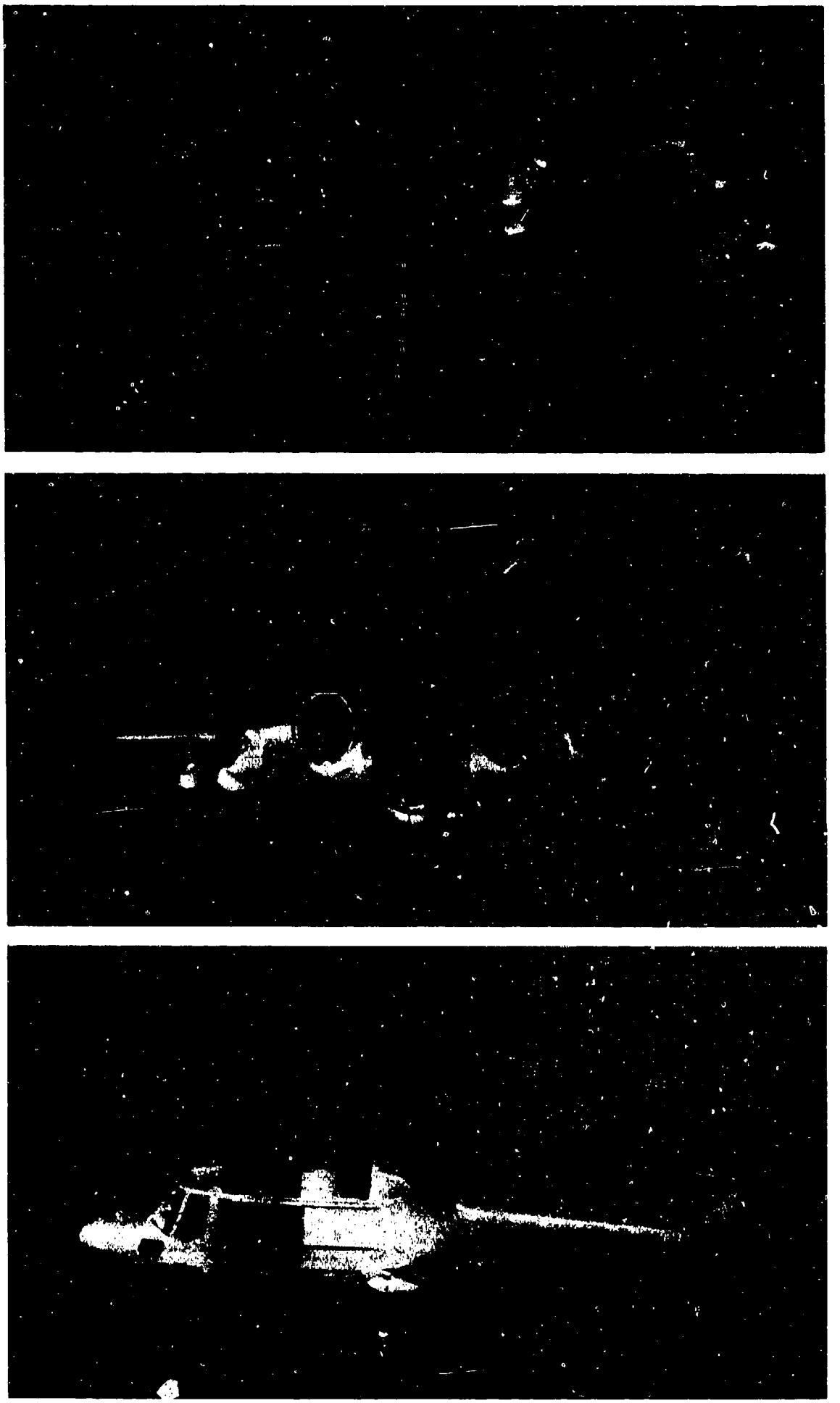

Fig 2.A3 Models of battle tank and small aircraft

Exceptions to this method of model suspension occur for two reasons. Firstly in the case of a pure doppler measurement of a rotating component of a target, the whole model is rigidly supported on a stalk. Since the stalk and the model are stationary the return from the rotating components is the only doppler signal recorded.

Secondly, the accuracies demanded of the 890 GHz Laser radar preclude the use of a string suspension. Ships are the usual targets of interest on this Range, and the RCS with aspect changes, typically, at 100 lobes per degree, leads to the requirement for a phase measuring accuracy of 2° for perfect data. In terms of displacement, this means maintaining relative path lengths to better than 1 micrometre. Hence a stalk is used to support models on this range; this is of very specialised design and is described further below.

2.A1.2 Fuze Range: RME 1

This Range is shown in Fig 2.A4 and has, alternatively, 80 GHz and 35 GHz radars. The radar, which is mounted on a trolley running smoothly on a track, is driven on an engagement path past a target suspended by strings from a gimbal at fixed height, offset and aspect. Each radar (which uses a narrow antenna beam only partially illuminating a target) has a choice of range gate, range law and antennas. These are modelled versions of fuze systems in research or development. Two sets of antennas can be switched sequentially, while quadrature doppler signals are obtained for each as the trolley moves along the track.

2.A1.3 Coherent Full Illumination and Mapping Range: RME 2

This facility, Fig 2.A5, comprises a pulsed 80 GHz full illumination, scattering matrix phase radar. This can either be moved around an accurate circular track, for

Fig 2.A4 RME 1

example to view a target with rotating engines, supported by strings from a gimbal system in the roof, or maintained stationary to record doppler returns, for example from a model tank moving along the floor. On-line computer facilities provide real time processing of the radar output as well as derivation of the scattering matrix elements.

In its alternative function, a frequency modulated CW radar which produces a sawtooth frequency sweep covering 21 GHz to 24 GHz is used. This radar has pencil shaped antenna beams for angular discrimination and has a range resolution of 80 mm. Thus, as the radar is stepped along the track, brightness modulation of an oscilloscope display by the radar output will produce a map of the target which is either on the floor or suspended by strings.

2.A1.4 Full Illumination Backscatter Range: RME 3

This multipurpose Range is shown in Fig 2.A6. Using one of the wide number of pulse radars available (frequencies from 1 GHz to 80 GHz), backscatter coherent and non-coherent measurements can be made on this Range. The pulse length is adjustable between 2 ns and 60 ns, the longer pulse length being used for CW equivalent data. The 4 GHz IF receiver is controlled by a narrow gate so that the front and back edges of the received pulses are eliminated when CW measurements are being made.

The target model is suspended by nylon strings from an overhead gantry, as shown in Fig 2.A6, and can be rotated or translated through the radar gate. Low side lobe, flat topped antenna beams are used to eliminate roof and floor echoes and to minimise amplitude taper across the target.

In addition to general measurements, echo source identification can be accomplished by camouflaging the target and then selectively exposing the echo sources. A circular track is available for making bistatic measurements, during which the receiver is moved and the target kept stationary.

Fig 2.A5 RME 2 80 GHz scattering matrix range

2.A1.5 Glint and Phase Range: RME 4A

On this Range, Fig 2.A7, a target is suspended by strings at a desired fixed aspect while, for example, a 140 GHz radar is moved around it on a precision circular track. At 1/200 degree intervals around the track, the received information, a $\exp(j\phi)$, is recorded. These data are processed in the on-line computer to produce RCS and Glint. Typical plots are shown in Fig 2.A8. The phase data are used in digital form for angular spectral analysis. This provides information for the formulation of multi-source mathematical models of target scatter. Other radar frequencies can be used on this range, typically 80 GHz, 40 GHz and 10 GHz.

Glint and Phase Range: RME 4B

This is a recent addition to the facilities and performs the same function as RME 4A but uses a 280 GHz radar on a new precision circular track. This addition facilitates modelling of higher frequency full scale radars whilst using existing sub-scale models.

Fig 2.A6 RME3 showing target suspension method

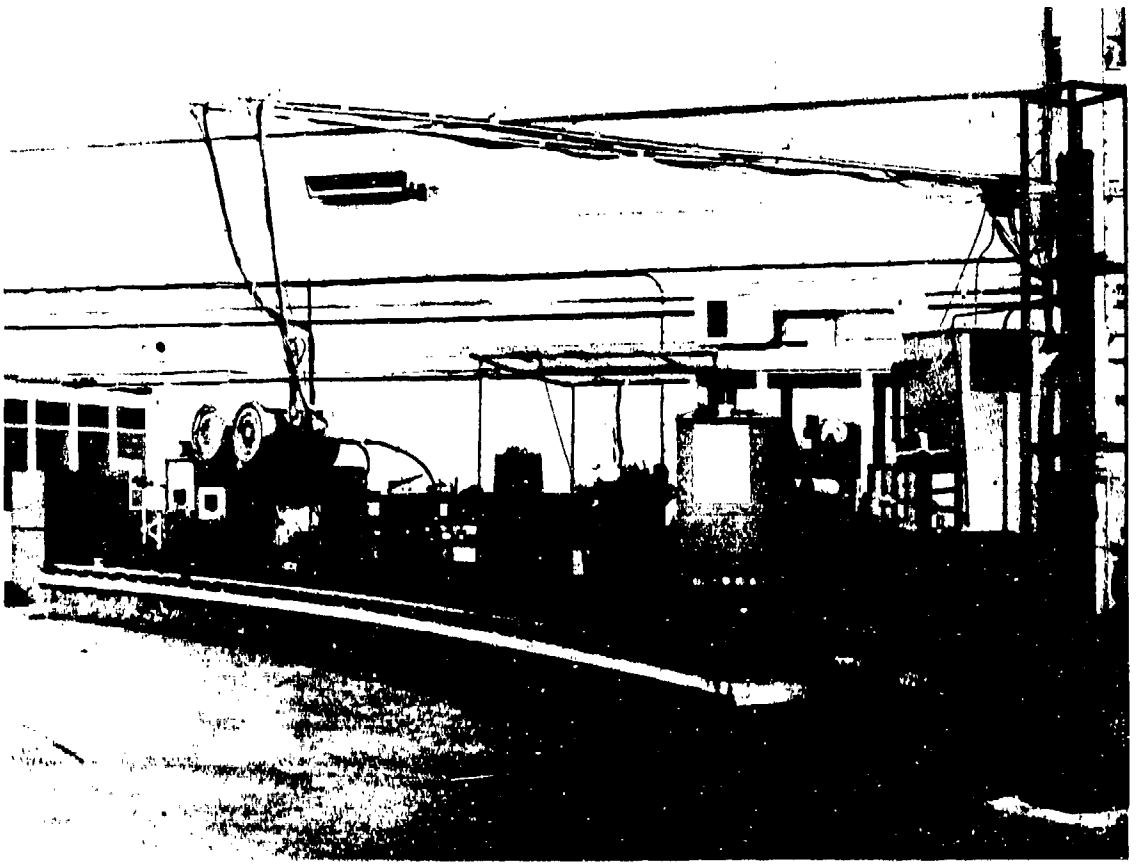

Fig 2.A7 RME 4 140 GHz phase measuring range

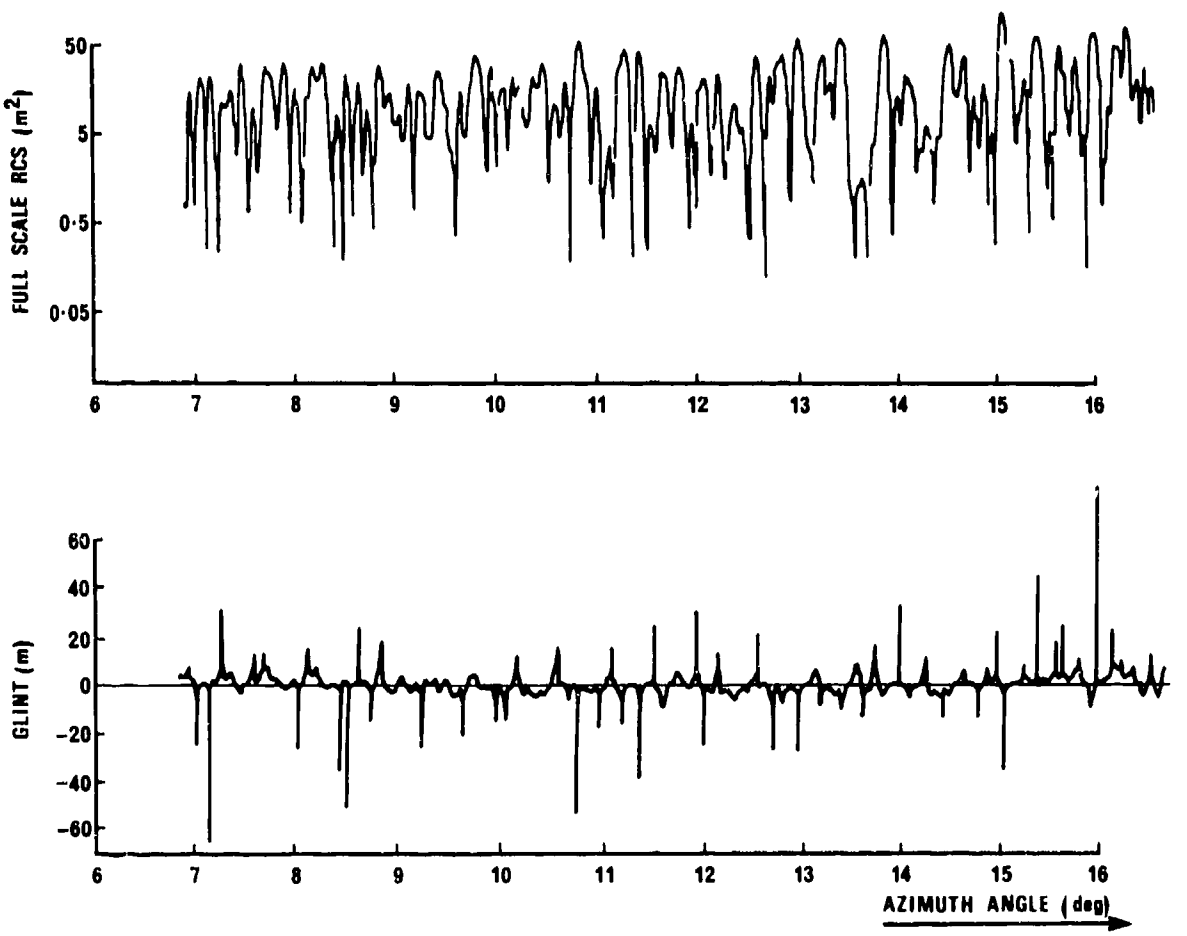

Fig 2.A8 Monostatic RCS and glint for an aircraft model

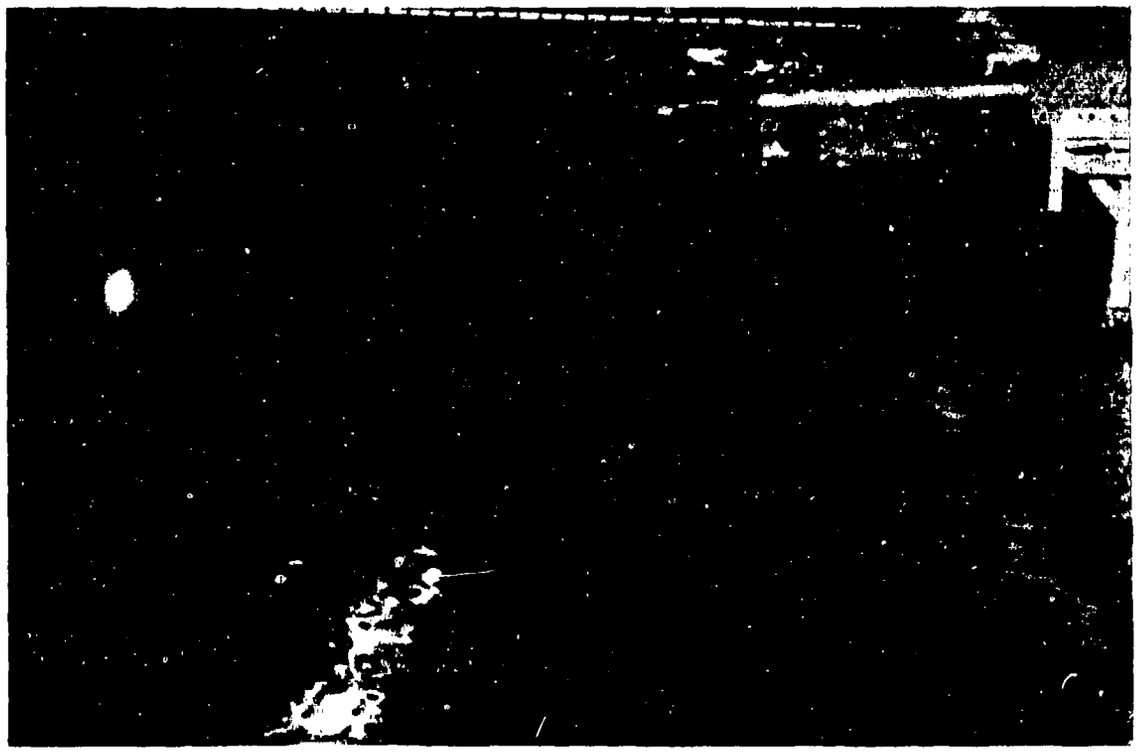

Fig 2.A9 RME 5 showing simulated beach

2.A1.6 Water Range: RME 5

Fig 2.A9 shows this Range on which coherent and non-coherent radar measurement facilities are available at 10 GHz, 35 GHz and 80 GHz. Water waves, trochoidal and broken, are generated by a reciprocating paddle, by fans and immersed water pumps. A horse-hair "beach" is used to absorb the 150 mm peak-to-peak waves produced.

Forward scatter measurements can be made with the radar transmitter and receiver on towers at either end of the water tank. Alternatively, backscatter measurements can be made using either a radar suspended from a gantry in the roof, or a model missile proximity fuze radar resting on the edge of the tank.

2.A1.7 Spherical Coverage Range: RME 6

On this Range, Fig 2.A10, a small target such as an artillery shell is suspended and rotated about a vertical axis at a distance of 5 m from the radar. The radar can be moved up and down a vertical track to view the target at any aspect, with any polarisation setting. Radars are available at spot frequencies between 3 GHz and 80 GHz.

2.A1.8 Laser Phase Radar Range: RME 7

A continuous wave HCN discharge laser or an optically pumped laser system is used as the transmitter power source. Typically, a 0.01 scale model of a ship, is supported at 1500 m full scale equivalent range on a stalk protruding from an optical quality turntable buried in the floor.

The layout of the range can be seen in Fig 2.A11 which shows an 890 GHz discharge laser radar and the optical precision turntable for supporting targets, mounted on a raft in the floor. This raft, constructed of reinforced concrete, is floating on cork so that vibration from the hangar floor is minimised.

Referring to Fig 2.A12, a model ship target can be seen mounted on a stalk. This is constructed in a material of very low Q and hence is not subject to mechanical ringing. Great care was taken in the construction of the model to achieve a good surface finish and detail of adequate accuracy. The stalk, provided it is never set near normal incidence to the radar, gives negligible reflection. The target can be rotated, pitched or rolled with precision, at as low a speed as 5 arc sec/sec (Fig 2.A13). Thus individual echo lobes of the scattered signal, which may be as narrow as 1/200°, can be completely resolved.

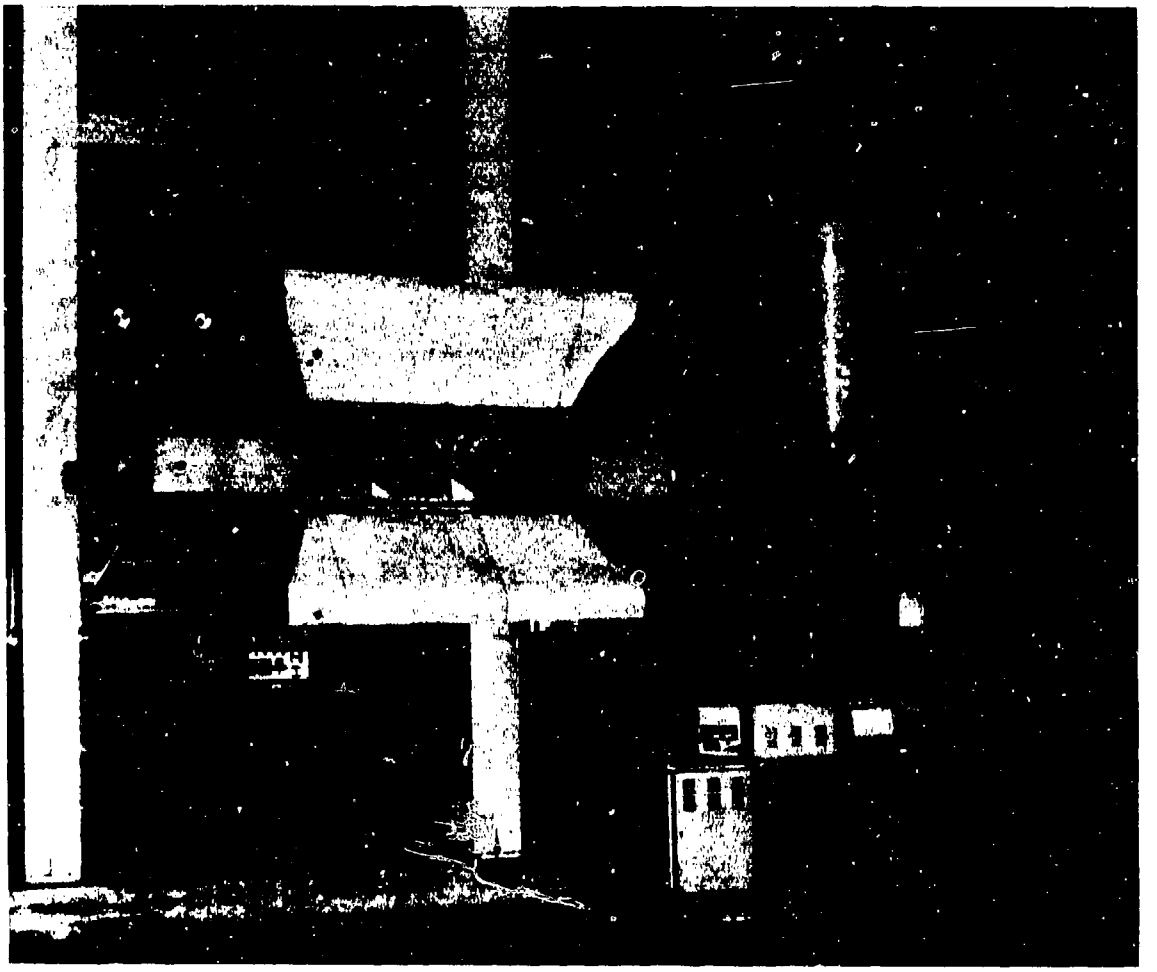

Fig 2.A10 RME 6 with artillery shell target

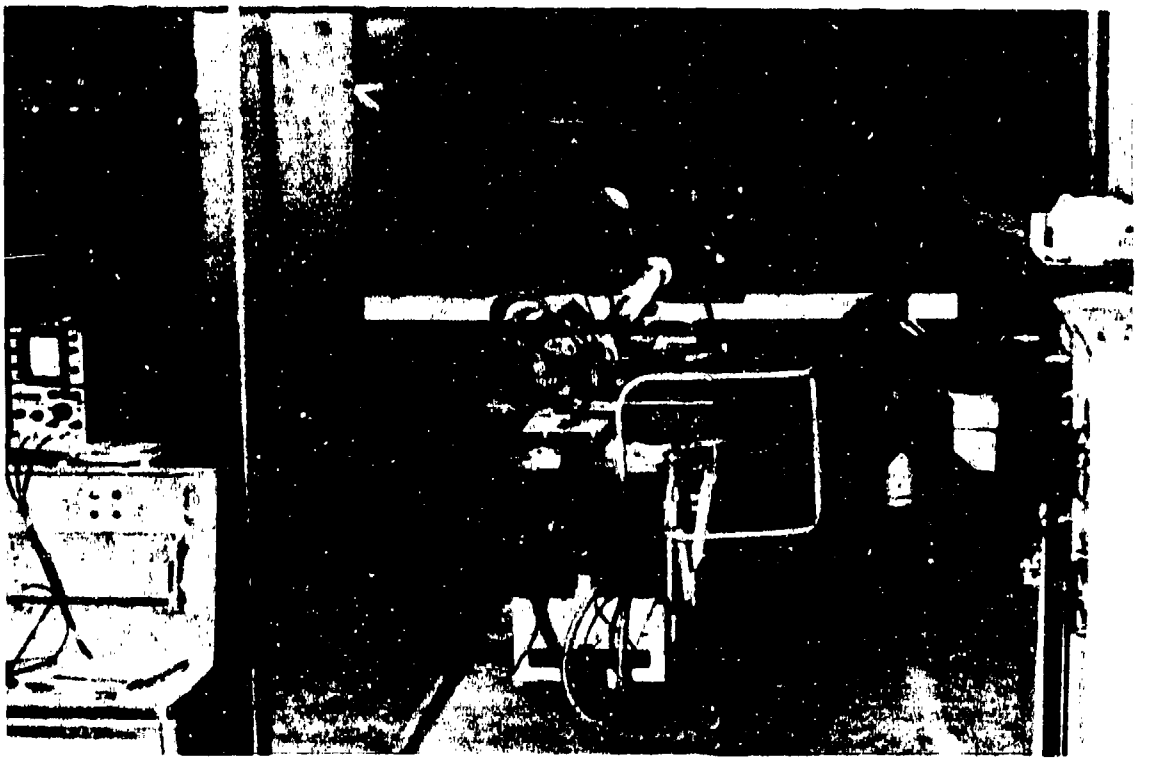

Fig 2.A11 RME 7 890 GHz radar

Fig 2.A12 1:100 scale model ship on measurement range

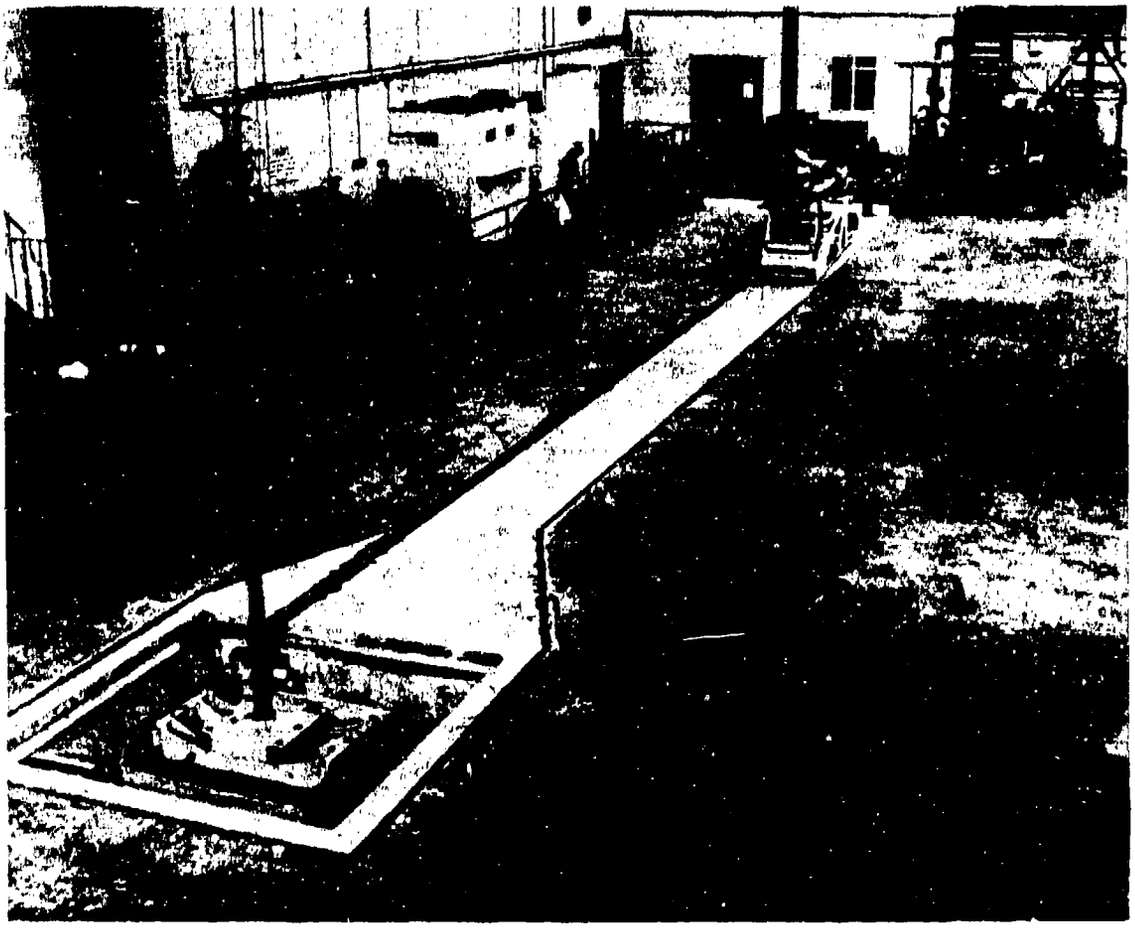

Fig 2.A13 RME 7 showing target orientation mechanism

2.A1.9 Outdoor Range

On the outdoor range, measurements have been made of full scale target components at radar ranges of up to 250 m, using coherent radars at 9 GHz and 35 GHz. In particular, the doppler spectra from aircraft engines with slowly rotating compressors and turbines have been measured. Instrumentation is as on the other ranges and one advantage resulting from use of this Range is the supply of model validation data. For example the doppler spectrum determined from a full scale engine can be compared with that obtained from a sub-scale model of the same engine.

2.A1.10 Chart of Measurement Facilities

Fig 2.A14 shows, in diagramatic form, the various facilities available. The diagram shows how the different target models, indicated on the left side, may be used with the different millimetric and sub-millimetric wave radars, indicated at the top, to obtain measurements at various full scale equivalent frequencies, indicated by the slanting lines.

2.A2 Typical Measurements and Studies

Table 1 indicates generically the range of work undertaken by the Radio Modelling Facility. Whilst priority is given to work for the UK MOD, the capacity of the Facility has proved to be adequate to provide a service for other users, both national and foreign.

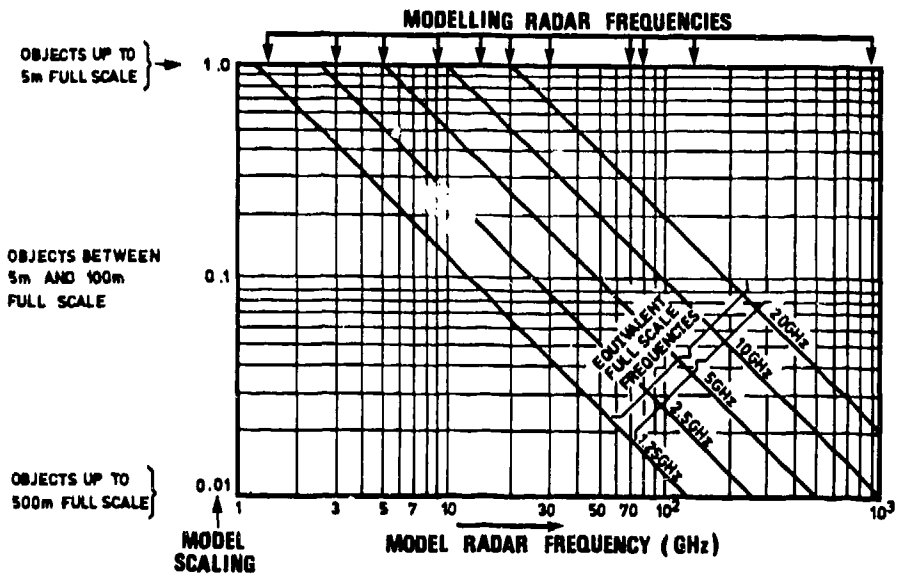

Fig 2.A14 Chart relating model size to radar frequencies

TABLE 1

Measurements:

(1) Radar Cross Section
(2) Scintillation spectra
(3) Angular noise (glint)
(4) Glint spectra
(5) Polarisation sensitivity
(6) Frequency response of radar return
(7) Spectral distribution due to moving parts eg turbine blades
(8) Target imaging
(9) Echo source identification
(10) Scattering properties of materials or components
(11) Target classification

Studies:

(1) Mathematical modelling of target radar characteristics
(2) System simulation
(3) Minimisation of Radar Cross Section
(4) Enhancement of Radar Cross Section
(5) Disguise of Radar Cross Section

The measurement of the RCS of various objects is a distinctly ordinary aspect of the work which is heavily weighted towards fundamental investigations into radar scattering. These investigations, involving targets of all types and materials are directed towards the design of new radar systems and new vehicles. It is clear, for example, that a requirement for a vehicle to have specific radar characteristics must be given adequate consideration at the earliest design stage, when radio modelling is a most powerful tool.

The input data to any radar are obviously contained in the signals received at its antenna(s). A quantitative assessment of the power and spectral content of these signals is essential to achievement of optimum design criteria. Similar information can also be used to evaluate the performance of existing radars and perhaps point the way to viable improvements.

The rapidly growing use of composite materials in vehicle structures, particularly air-vehicles, has created new problems and opened up the area of investigation into scattering, absorption and attenuation properties of various dielectrics and semiconductors at different radar frequencies. A significant part of these investigations must be carried out within the Facility, at full scale, and as a by-product, the means of scale modelling at least some of these non-linear structures is being determined.

2.A3 Validity of Data Produced in Relation to Full Scale Dynamic Measurements

Validation of radar target characteristics as determined by modelling methods is of prime importance but presents considerable practical difficulties. Firstly, what is meant and required by validation? It should be understood that the requirement is not to validate the radio modelling techniques per se. The technique is valid if carried through as described in section 2.5. The validation required is, in fact, an evaluation of the differences (if any) between the radar characteristics produced by radio modelling and those from the real life dynamic measurements being investigated. It will be shown that the difficulties in making this judgement lie almost entirely in the inadequacy of information relating to the full scale case, however well and expensively instrumented. This in no way challenges the integrity of the modelling data.

However, in the end, the objective must be to provide confidence to any potential user that the results obtained by modelling are truly representative of the real world. This statement is open to many interpretations, for example:

(1) Is a precise match of detailed data implied?
(2) Is there to be no more than a statistical equivalence, and if so, of what?
(3) Is a close similarity of patterns with near equality of magnitudes sufficient?

Considering real targets, and taking things by stages, consider a real life (full scale) clutter free radar measurement using a specific aircraft in flight. Let the supposition be made that a perfect sub-scale model of the target aircraft (not another like it) can be made. Let it also be supposed that the radar used in the real life measurements is reproduced with precisely scaled parameters for use in the modelling work. Thirdly, let it be assumed that the real life geometries applying in the measurements are known with precision (better than 0.1 degree in angular terms) and that these geometries can be reproduced with appropriate linear scaling at the modelling site. Then it can be stated with confidence that the resulting modelling data should precisely match the real life data on any basis of comparison - provided that the model engines are rotated at a rate compatible with the modelling requirements. Third order effects due to in-flight vibrations and jet efflux are not included.

Thus, in an ideal world, "interpretation (1)" is possible. However, the real world is not ideal and neither is this perfection of validation obtainable in practice. The reasons are not difficult to find. Firstly, whilst it is, in principle, possible to manufacture a sub-scale model aircraft of impeccable precision and fidelity, it is virtually impossible, in practice, to obtain the necessary manufacturing drawings to include every necessary detail of the build standard, modifications to fittings etc which apply to the actual aircraft flown. (An obvious omission would be slightly damaged, bent, displaced or omitted features incurred during in-service life).

This, alone, would preclude the possibility of achieving the precise matching of all the data. Secondly, it is most probable that the geometries occurring during the real life measurements will not be known to the required precision. Lastly, it is most unlikely that the ranges used in the full scale radar measurements can be accurately scaled at the modelling site. Whilst this is not serious for the real requirements of the model measurements, it would again prevent achievement of point by point matching of data. At this stage it must be stressed that the comparison of full scale radar measurement results from nominally identical flights of the same aircraft by a common radar could not be made with any greater precision. It should therefore surprise no-one that Interpretation (1) cannot be implied.

Interpretation (2), suggests only a similarity of statistics as a means of comparison. Chapter 2.3 made the point that expediency usually led to acceptance of angular measurement accuracies of $\pm$ 5° for in-flight experiments (of viable cost), which would certainly point in the direction of statistical comparison methods. A suitable approach may be the comparison of cumulative probability plots (eg probability of exceeding given values of σ per angular intervals of, say, 10°).

There are, however, other target characteristics which may be required from a dynamic experiment, for say the determination of detection or acquisition probability. Here the required data include fading rate in addition to absolute RCS. The fading rate is due largely to the rate of change, by very small angular increments, of yaw, pitch and roll of the target aircraft which result in small changes of target aspect to the radar. These fading data which can readily be extracted from the full scale radar receiver, which should have a channel with no AGC for this purpose, are of course not directly obtainable from static modelling data. However, these can be produced by storing the statically derived data in a computer and addressing these (σ with aspect angle) with the detailed target motion. This may originate from on-board recordings or may be simulated by stimulating the aerodynamic derivatives of the target with realistic wind gust analogues in a computer. Comparison of real-life with modelling data is again accomplished by statistical methods.

Fig 2.A15 shows samples of real yaw spectra derived from on-board measurements. Fig 2.A16 shows a comparison of a measurement derived yaw spectrum with a mathematical synthesised spectrum for the same aircraft in similar conditions.

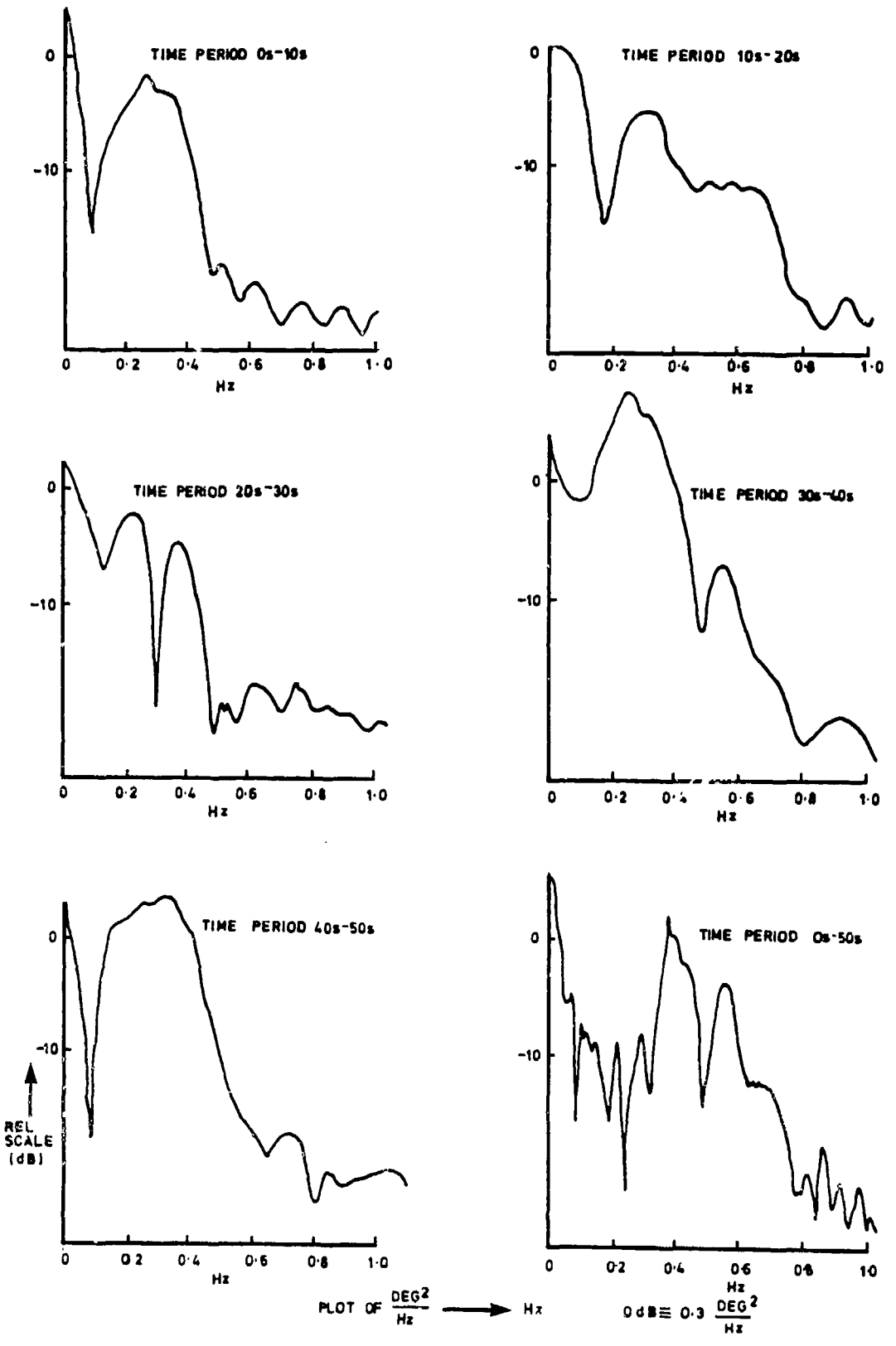

Fig 2.A15 Yaw spectra for an approaching aircraft

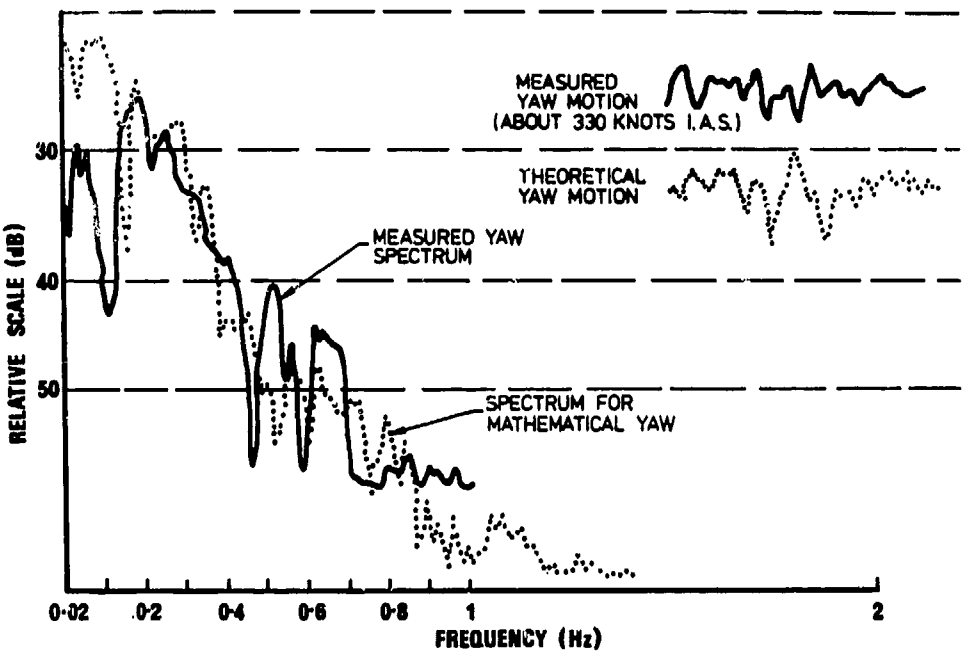

Fig 2.A16 Comparison of measured and computed yaw spectra

A particular feature of the radar return which lends itself well to comparison between real life and modelling methods - and in principle should inspire confidence in the validity of radio modelling is the doppler content of the echoes from the engine(s) of an aircraft. The scattering processes involved in the generation of these echoes are very complex and involve multiple reflections in and out of air intakes terminated by rotating machinery. Study of these spectral data can yield unmistakable target "thumb-prints". Since such echoes persist over some tens of degrees the lack of precise knowledge of aspect angles is not a serious disadvantage. It has been demonstrated many times that such echoes from properly constructed sub-scale models yield precisely the same "thumb-print" as echoes from real targets.

To summarise, validation methods applicable to the modelling of real life determination of the radar characteristics of an "in-service" aircraft target in flight are largely statistical, but can be reinforced by direct comparisons of certain spectral data. Much improved validation can be achieved if the aircraft is in development, or is for some other reason unique, and for which there are definitive manufacturing data. Further improvement results from the use of attitude recording equipment in the target and very accurate radar instrumentation in the real life measurements. This provides more quantitative data for comparision purposes and the best practical validation which can be achieved is therefore a combination of "Interpretations (2) and (3)".

2.A3.1 Examples of Validation Evidence

(1) During the development phase of radio modelling in the UK, in the early 60's, a co-operative exercise between the USA and the UK set out to evaluate certain fuze radars: real life and sub-scale modelling measurements were involved. It was realised that the planned task would afford an excellent opportunity to acquire modelling validation data and, incidentally, evaluation of the importance of target detail.

On a well instrumented Range in the USA, two types of fuze radars were set up on the ground with their sensitivity in an upward direction. At very low altitudes a fighter aircraft was flown, repetitively, across, and within the range gate of each fuze in turn. The Range instrumentation was able to place the aircraft (target), relative to the fuzes, to $\pm$ 300 mm, and its attitude to 0.5°. At these close ranges the antenna beams of the fuze radars only partially illuminated the aircraft so that as it passed over, it was scanned from nose to tail by each fuze in turn. The signals received by the fuzes, and known as "fuze-target signatures", were recorded on magnetic tape.

These fuze-target engagements were later modelled at sub-scale at the UK Radio Modelling Facility and the detailed signatures compared with those from the real life measurements. Details cannot be given here but the following conclusions were substantiated.

(i) Exploring the error volume defined by the tolerances on accuracy of full scale geometric measurements enabled target aspects to be set up at sub-scale which resulted in fuze-target signatures closely matching their full scale equivalents. The differences in detail over limited regions were shown to arise from (a) not rotating the model engine and (b) an inadequately modelled radome. Fig 2.A17.

(ii) In some of the engagements modelled, a significant difference persisted in the part of the signature originating near to the tail of the aircraft. The offending feature was identified on the model as the arrester hook. On investigation in the USA it was found that this hook was severely bent on the actual aircraft. Reproducing this bend on the model eliminated that difference in the comparison.

(iii) No significant effects due to aircraft flight vibration or jet efflux were detected.

(2) Fig 2.A18 shows an RCS with aspect angle plot over $\pm$ 1° of head-on, of a Canberra bomber in-flight. The aircraft was closely controlled, in ideal meteorological conditions to make straight, shallow dives directly at and away from a ground radar instrumented to measure RCS and Glint.

Flights which resulted in greater than 1° deviation from dead head-on or tail-on were rejected. Natural yaw motion of the aircraft caused the aspect angle to cycle about the axial reference so that significant fluctuations of RCS were present in the results.

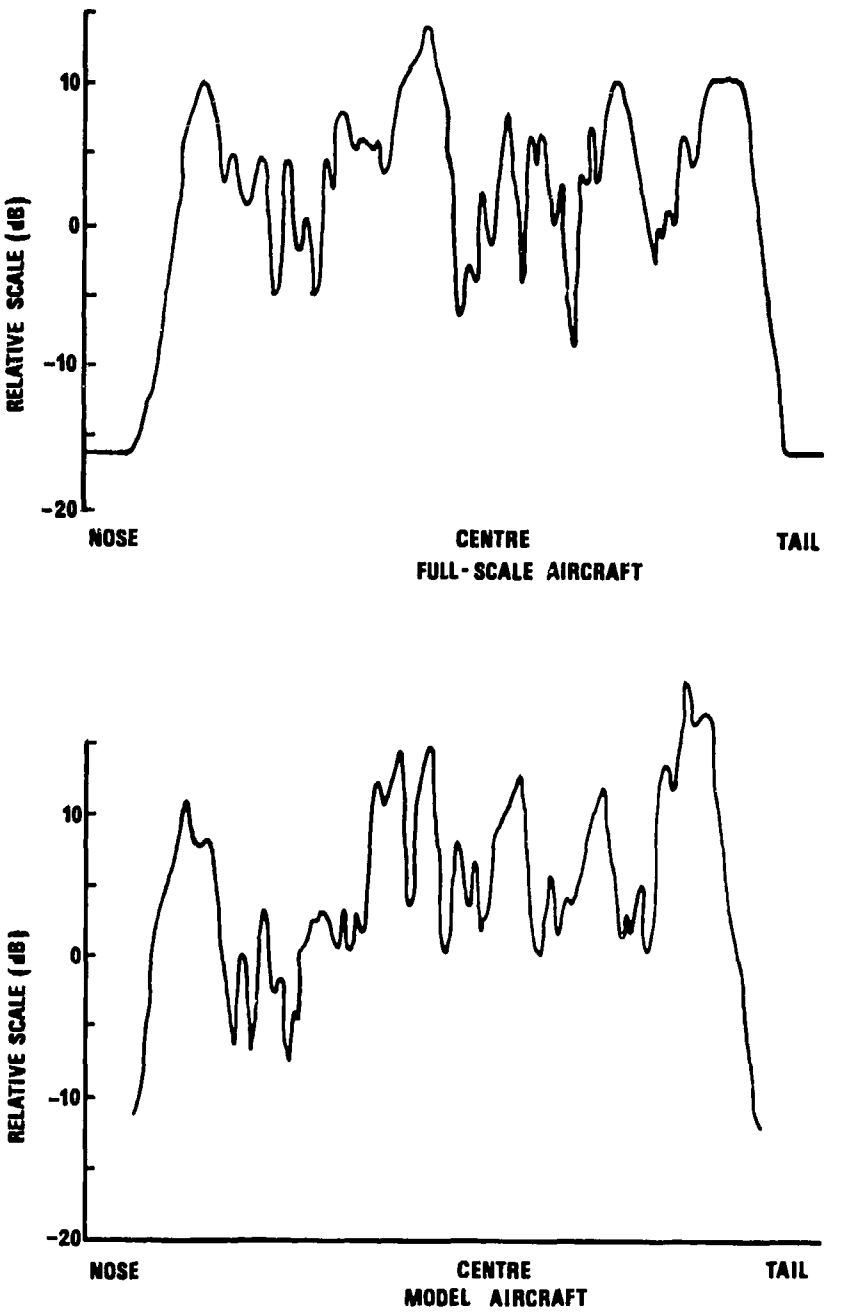

Fig 2.A17 Comparison of fuze-target signatures

Fig 2.A19 shows the relevant part of a static plot resulting from sub-scale modelling measurements using a model of an identical Canberra. The similar pattern cycled due to yaw motion in flight can be clearly seen by comparing the ringed sections of the two figures.

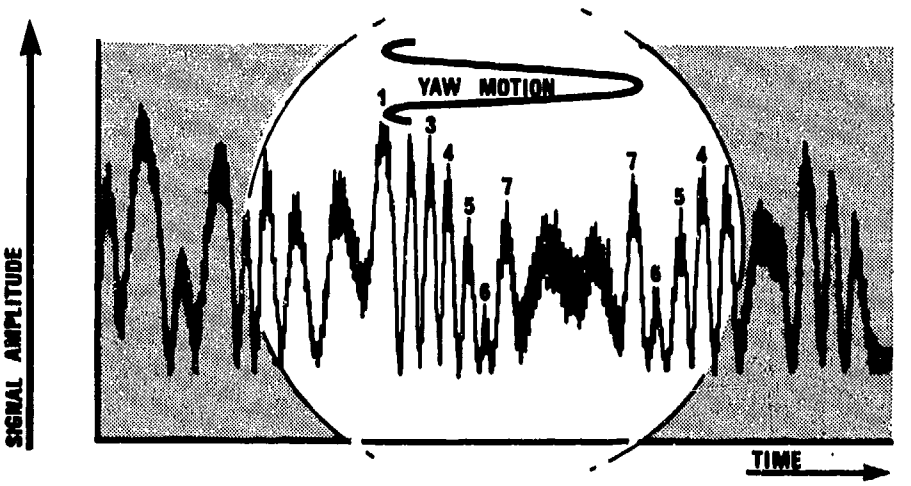

Fig 2.A18 RCS of nose region of aircraft in flight (Time series)

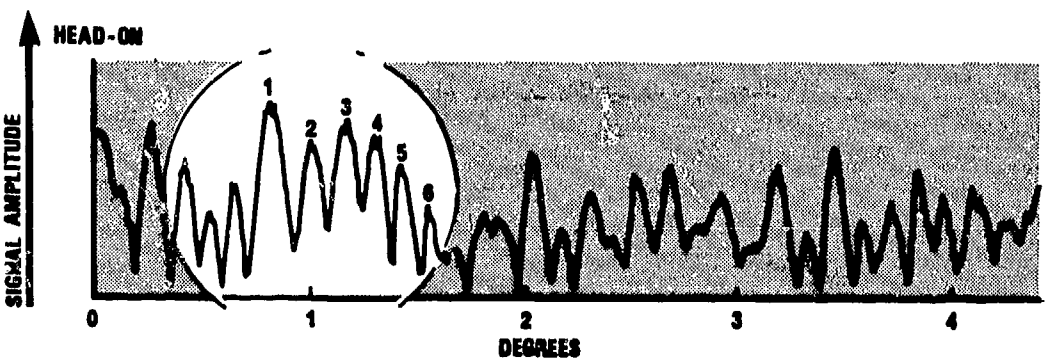

Fig 2.A19 Static plot of model of same aircraft in same region

(3) Fig 2.A20 shows comparison of the doppler spectra of radar returns from aircraft in flight and corresponding sub-scale radio modelling measurements. The frequency correlation of significant spectral lines is obvious. The probability of achieving a precise match of amplitudes is infinitesimal since these vary rapidly with time and aspect angles and with individual characteristics.

Comparisons of radio modelling data with corresponding full scale static measurement data are significantly easier than with dynamic flight measurement data. However, even these are fraught with practical difficulties in achieving the necessary identities and equivalences:

(i) Real and sub-scale model identity.
(ii) Measurement radar equivalence.
(iii) Data processing method equivalence.
(iv) Clutter levels zero or identical.

At the end of the 70's, another co-operative exercise between USA (RATSCAT) and the UK (Radio Modelling) included a comparison of a 'real aircraft' and a sub-scale model made in the UK from drawings provided by the USA. Fig A21 shows the comparison of RCS with aspect angle plots produced by each Facility over the aspect range where identity of targets was achievable, ie where the real aircraft was still represented accurately by the drawings provided for model manufacture.

2.A3.2 To summarise, there is good reason for confidence in measurements made by the radio modelling method provided that it is carried out properly, using high quality models and with full understanding of the physics involved. Complete validation of this claim is extremely difficult, but such evidence as is available is very convincing.

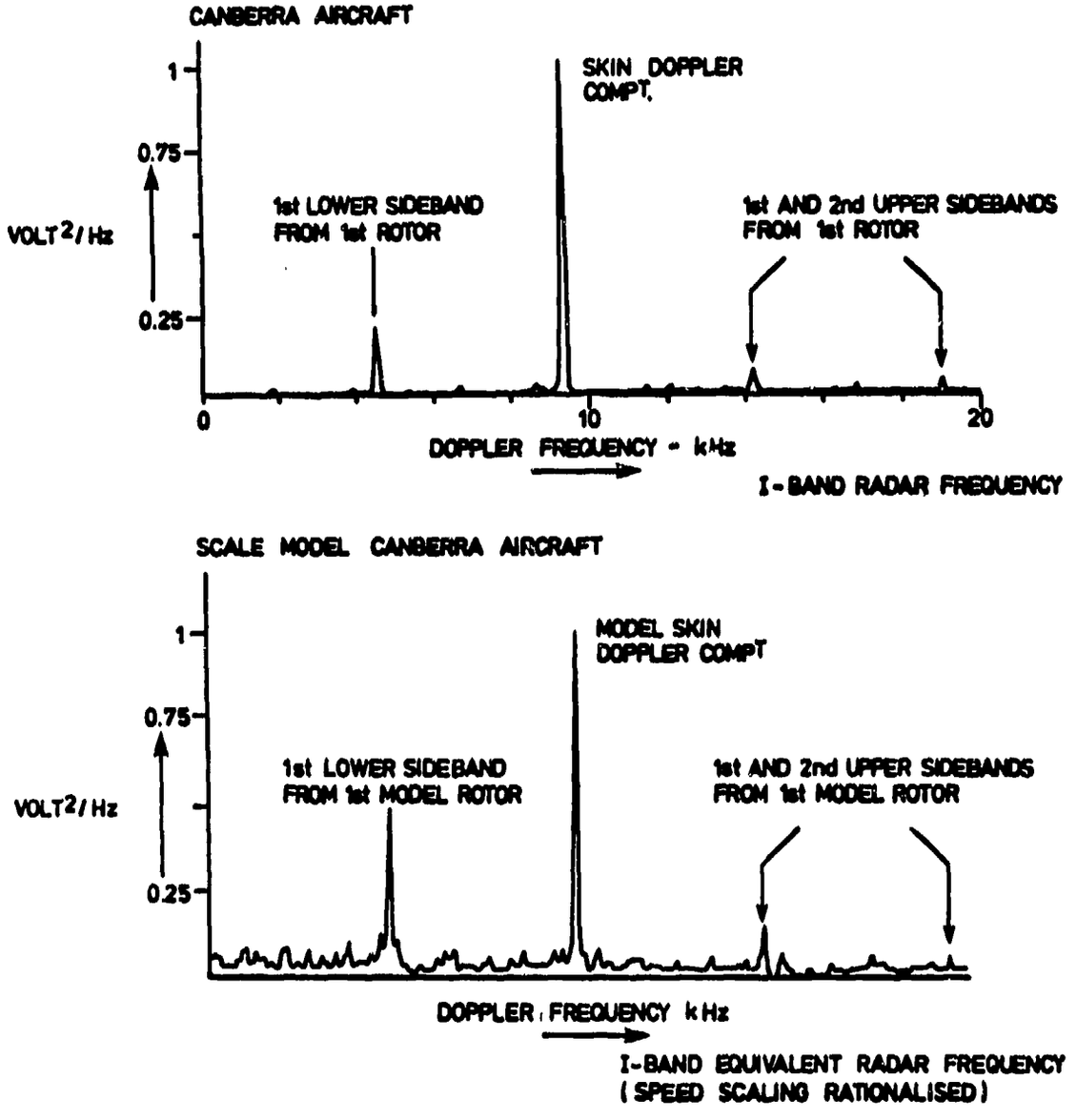

Fig 2.A20 Comparison of doppler spectra from engines of aircraft in flight with spectra from sub-scale model

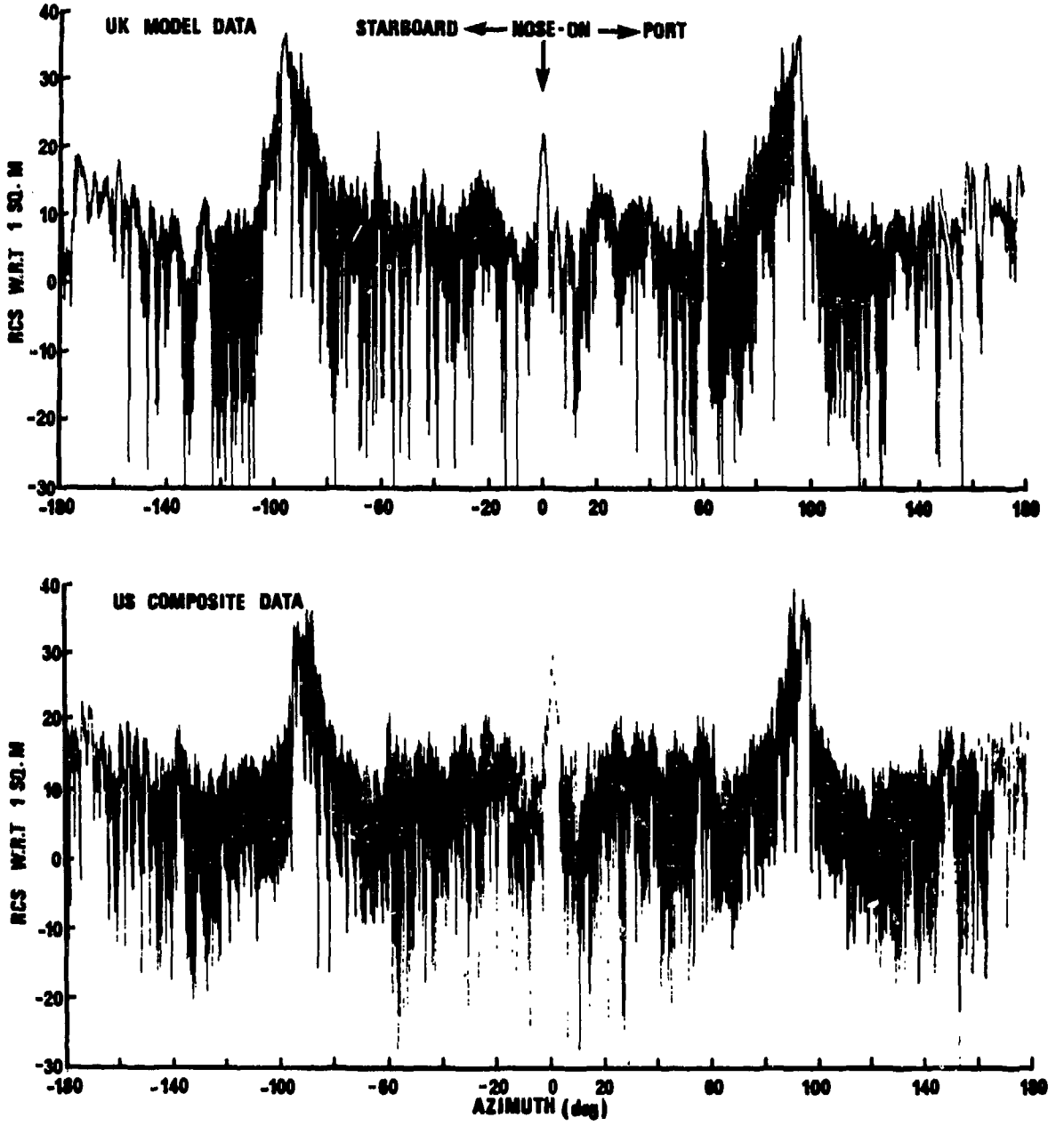

Fig 2.A21 Comparison of RCS measurements of real aircraft on the ground in the USA with same from sub-scale model in the UK

2.A4 Data Reduction

The wide range of measurement activities in radio modelling calls for several different approaches to data acquisition and processing. Concentrating on the measurement of RCS and Angular Glint, it will be remembered that the signals recorded are a sin ϕ and a cos ϕ (ie the quadrature pair equivalent to an exp $j\phi$). These signals are recorded on magnetic tape for subsequent detailed analysis off-line. In addition the data are processed on-line to obtain immediate specific information, such as RCS and angular glint for real time visual checking both by VDU and hard copy. Sphere derived calibration signals are, of course, included but the 'quick-look' data remain in scaled units.

The off-line data processing employed depends entirely upon the requirement of the user. These may be purely scientific so that the data describe the signals received at the radar with no characteristics due to the measurement process impressed on the data. For example, no antenna integration, no bandwidth limitation, no sampling ambiguities: the original phase and amplitude distributions and spectral content are preserved. Such data are most useful in understanding the scattering processes taking place at the target, and are usually stored on disc and addressed as required by the research engineer.

More often, measurements are made to understand the interaction of a target and a radar of given parameters: antenna size and polarisation, receiver processing and bandwidth etc. These system parameters can be applied to the original data to produce specific results - assuming the target illumination polarisation was included in the original measurements. Alternatively, the system parameters can be physically represented in the measurement radar, with appropriate linear scaling. Data are usually required in several forms including tables and plots of cumulative probability of RCS over angular increments of, say, 10°; tables of angular glint values with aspect angle, tables of running means - and so on.

Often the final data reduction is the formulation of a mathematical model of the scattering by the target when interrogated by a specific radar. This is a well established practice in the radio modelling department and examples of using such models are compared with radar measurements in Figs 2.A22 and 2.A23.

The technique used for echo sources identification and subsequent mathematical description includes a process known as angular spectral analysis (of a exp $j\phi$) which in execution resembles the processing used in aperture synthesis. Sources are found and described in terms of their x, y and z coordinates and their individual polar diagrams (Fig 2.A24). These data may be fed to a computer where a special program performs the necessary vectorial arithmetic to yield the total return from the target with aspect.

With the new generation of radio modelling measurement radars, which implement the measurement of the total, or alternatively the relative scattering matrix, all radar polarisation cases are covered in one set of measurements. Combining this facility with the measurement of the spectral data due to rotating engines, scanning radars, etc, an enormous amount of data are yielded and many forms of analysis and data reduction can be employed.

2.A5 Continuing Developments

Full scale radars in development or study phases, seek to make increasing use of the intelligence available in the target radar returns, and some are moving into the millimetric wavebands. In order to keep ahead of such developments the evolution of the Radio Modelling Facility is continuous in terms of both improvements and new capabilities. Improvements relate largely to engineering methods, up-dating technologies and more sophisticated data processing, and are subjects of detail not strictly appropriate to this paper. However, mention of imminently available new capabilities is of interest since they represent the current, 'state of the art'.

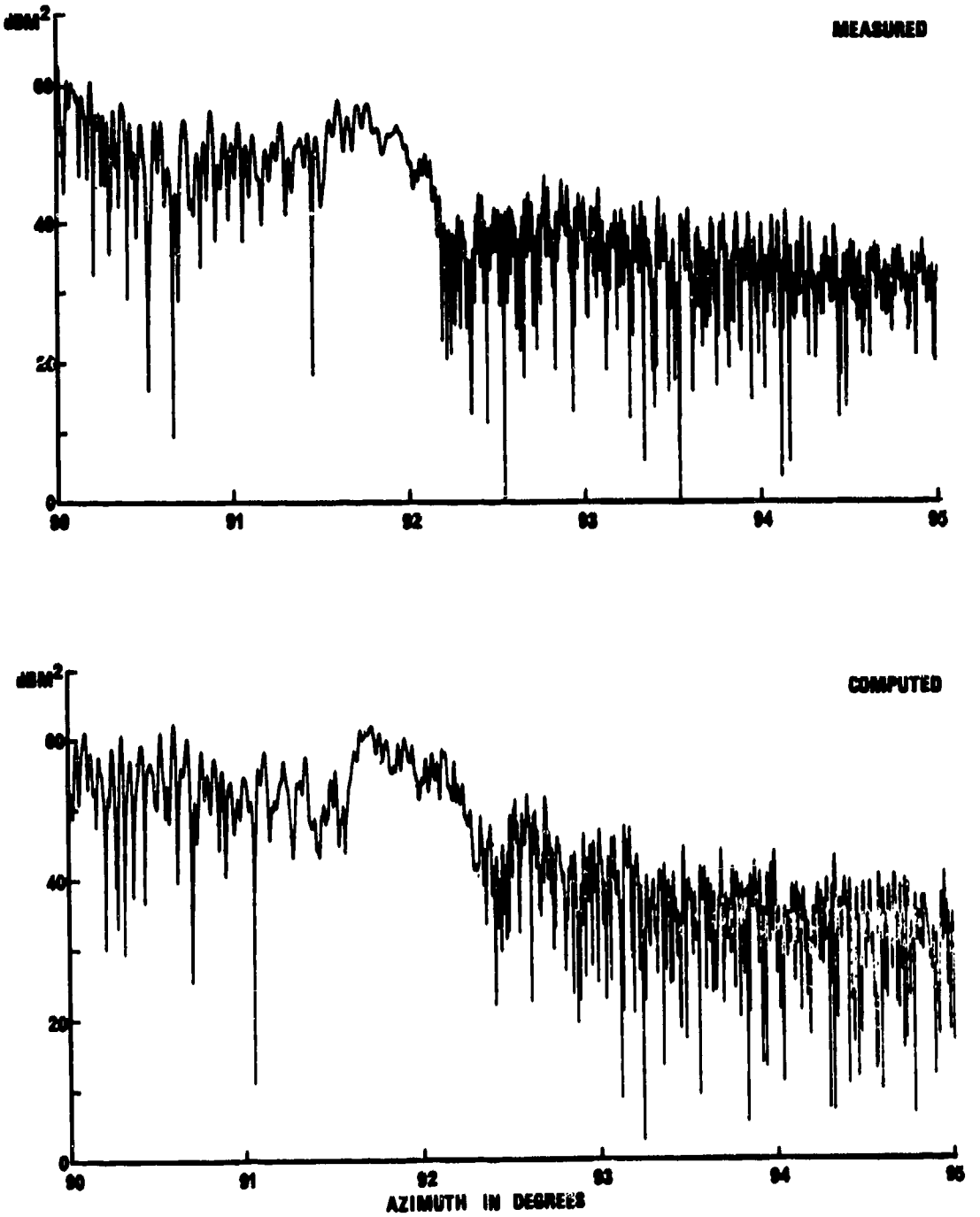

Fig 2.A22 Comparison of measured and computed RCS of aircraft near broadside-on

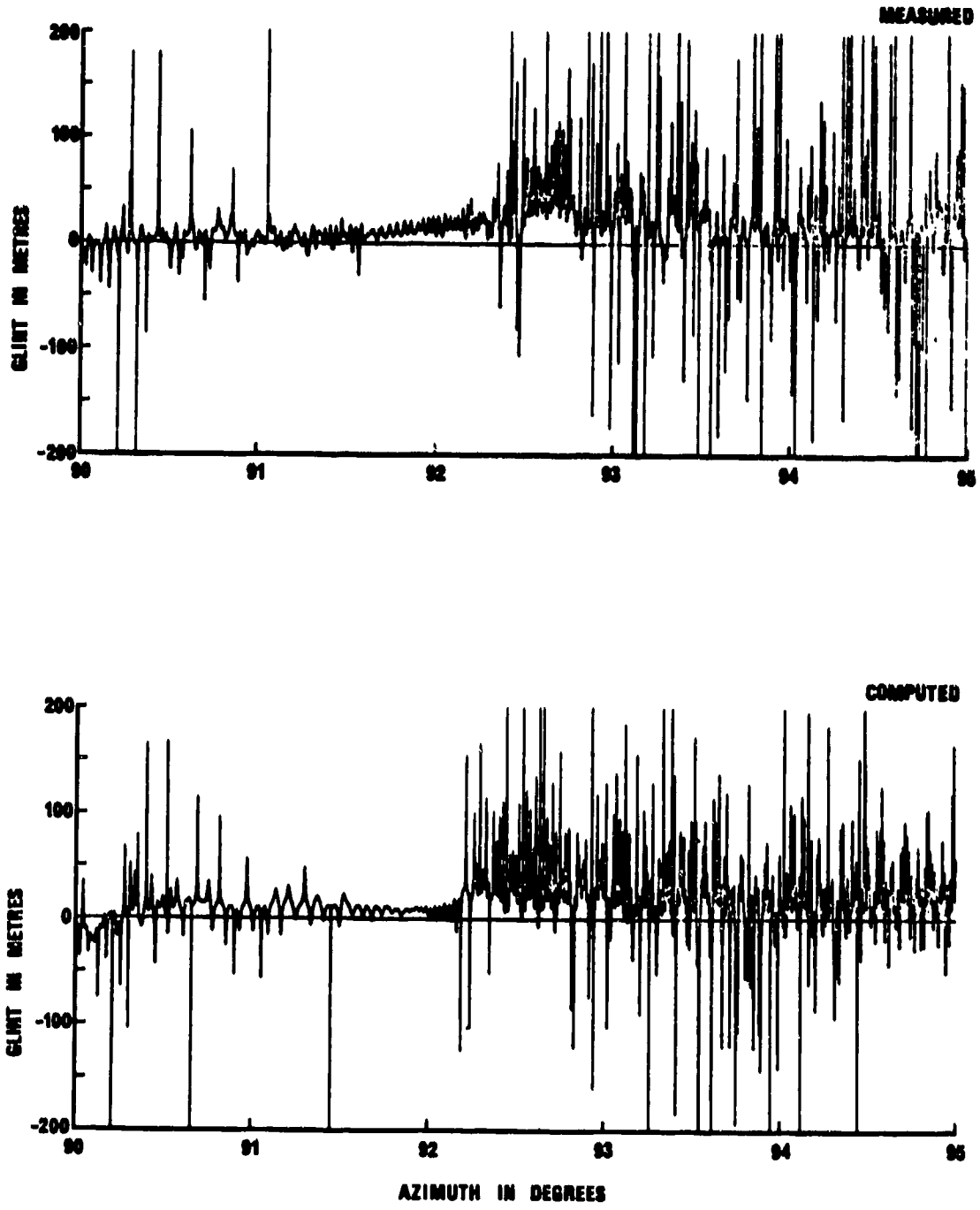

Fig 2.A23 Comparison of measured and computed glint of aircraft near broadside-on

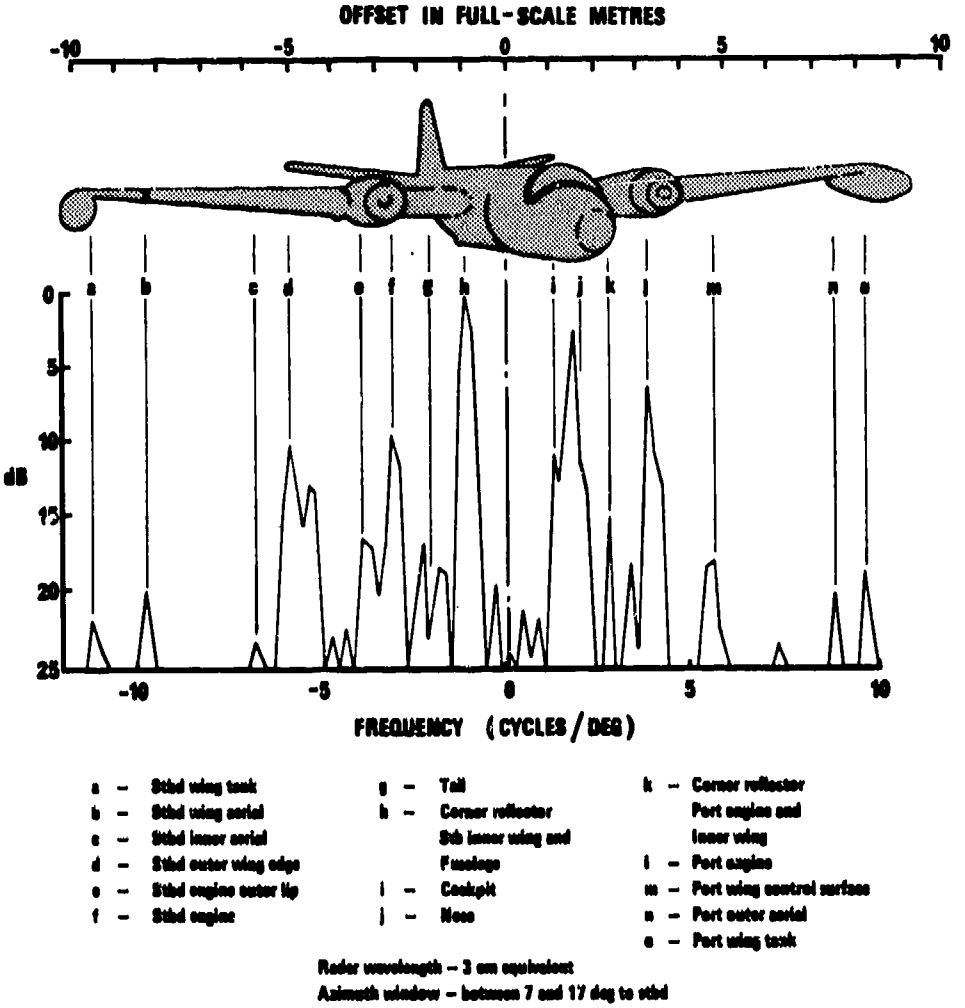

Fig 2.A24 Sources of reflection on a detailed model of a trials aircraft: identified by angular spectral analysis

(i) Scattering Matrix Measurement Radars

Reference back to Section 2.1.3 shows that the total steady state scattering from a target can be characterised in terms of a scattering matrix. A modelling radar at 80 GHz was recently developed and demonstrated which can, in one measurement run, acquire the total scattering and on-line processing of the matrix elements can yield results apertaining to any combination of illuminating and receiving radar polarisation. This is a considerable step forward and similar radars at 10 GHz, 15 GHz and 140 GHz are now available.

(ii) Modelling of Millimetric Radars

The advent of real life radars operating between 30 and 100 GHz requires the sub-scale modeller either to make new target models with scale factors to fit existing measurement radars or, to develop new radars with frequencies high enough to utilise the existing range of excellent target models. The latter option is chosen for several reasons, the most practical of which being that the small scaling factors implied in the former option would result in target models too large to handle.

Hence, new measuring radars at frequencies in the range 280 GHz to 2.5 THz are required. Radars at 280 GHz using carcinotrons, and at 890 GHz using a discharge laser (more correctly, a maser) have been described. Currently the method of 'optically pumping gas cells' is the technique being used to provide power sources at many optional points in the desired frequency range. Basically, a CO_2 laser is used to excite molecular vibrational levels in an organic gas (or isotope thereof). Different gases can be made to yield adequate power at discrete spectral points in the desired range. Such power sources are inherently 'quiet' and the technique has been demonstrated in prototype radars at the Modelling Facility. It is intended to replace the sources of both the 280 GHz and 890 GHz radars by the optically pumped devices, and to be able to change gas cells and certain narrow-band components with reasonable ease to provide adequate spot frequency coverage up to 2.5 THz.

To date such radars are being evaluated at nominally 400 GHz and 600 GHz while work on radars at 1,600 and 2,500 GHz is in progress. It is not possible to make use of the power available at some frequencies since absorption by CO_2 and H_2O is such as to prohibit adequate radar range in average atmospheres. Where necessary it is planned that the propagation path will be enclosed and filled with an inert medium.

Fig 2.A25 show two of the optically pumped radars to one side of the 890 GHz discharge laser radar.

The availability of measurement radars at these high frequencies also facilitates radio modelling measurments of large ships which, for practical reasons, may have to made at 1/300th scaling and for which scattering data equivalent to full scale H to J bands may be required.

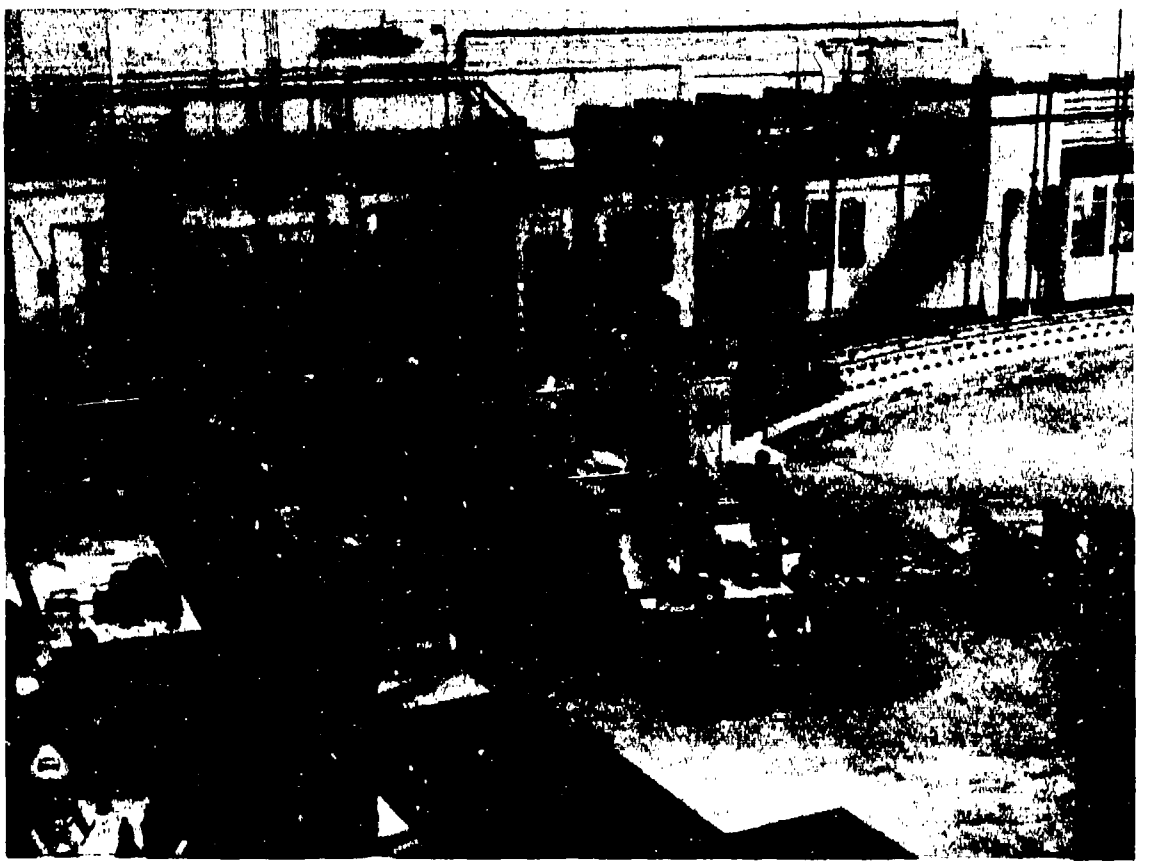

Fig 2.A25 Two optically pumped laser radars - shown to the right of a discharge laser radar

Annex 1

AGARD FLIGHT TEST INSTRUMENTATION AND FLIGHT TEST TECHNIQUES SERIES

1. Volumes in the AGARD Flight Test Instrumentation Series, AGARDograph 160

Volume Number	*Title*	*Publication Date*
1.	Basic Principles of Flight Test Instrumentation Engineering by A.Pool and D.Bosman	1974
2.	In-Flight Temperature Measurements by F.Trenkle and M.Reinhardt	1973
3.	The Measurement of Fuel Flow by J.T.France	1972
4.	The Measurement of Engine Rotation Speed by M.Vedrunes	1973
5.	Magnetic Recording of Flight Test Data by G.E.Bennett	1974
6.	Open and Closed Loop Accelerometers by I.Mclaren	1974
7.	Strain Gauge Measurements on Aircraft by E.Kottkamp, H.Wilhelm and D.Kohl	1976
8.	Linear and Angular Position Measurement of Aircraft Components by J.C.van der Linden and H.A.Mensink	1977
9.	Aeroelastic Flight Test Techniques and Instrumentation by J.W.G.van Nunen and G.Piazzoli	1979
10.	Helicopter Flight Test Instrumentation by K.R.Ferrell	1980
11.	Pressure and Flow Measurement by W.Wuest	1980
12.	Aircraft Flight Test Data Processing — A Review of the State of the Art by L.J.Smith and N.O.Matthews	1980
13.	Practical Aspects of Instrumentation System Installation by R.W.Borek	1981
14.	The Analysis of Random Data by D.A.Williams	1981
15.	Gyroscopic Instruments and their Application to Flight Testing by B.Stieler and H.Winter	1982
16.	Trajectory Measurements for Take-off and Landing Test and Other Short-Range Applications by P.de Benque d'Agut, H.Riebeek and A.Pool	1985
17.	Analogue Signal Conditioning for Flight Test Instrumentation by D.W.Veatch and R.K.Bogue	1986

At the time of publication of the present volume the following volume was in preparation:

Microprocessor Applications in Airborne Flight Test Instrumentation
by M.Prickett

2. Volumes in the AGARD Flight Test Techniques Series

Number	*Title*	*Publication Date*
AG 237	Guide to In-Flight Thrust Measurement of Turbojets and Fan Engines by the MIDAP Study Group (UK)	1979

The remaining volumes will be published as a sequence of Volume Numbers of AGARDograph 300.

Volume Number	*Title*	*Publication Date*
1.	Calibration of Air-Data Systems and Flow Direction Sensors by J.A.Lawford and K.R.Nippress	1983
2.	Identification of Dynamic Systems by R.E.Maine and K.W.Iliff	1986
3.	Identification of Dynamic Systems Applications to Aircraft Part 1: The Output Error Approach by R.E.Maine and K.W.Iliff	1985
4.	Determination of Antenna Patterns and Radar Reflection Characteristics of Aircraft by H.Bothe and D.Macdonald	1986
5.	Store Separation Flight Testing by R.J.Arnold and C.S.Epstein	1986

At the time of publication of the present volume the following volumes were in preparation:

Identification of Dynamic Systems. Applications to Aircraft
Part 2: Nonlinear Model Analysis and Manoeuvre Design
by J.A.Mulder and J.H.Breeman

Flight Testing of Digital Navigation and Flight Control Systems
by F.J.Abbink and H.A.Timmers

Technqiues and Devices Applied in Developmental Airdrop Testing
by H.J.Hunter

Aircraft Noise Measurement and Analysis Techniques
by H.H.Heller

Air-to-Air Radar Flight Testing
by R.E.Scott

The Use of On-Board Computers in Flight Testing
by R.Langlade

Flight Testing under Extreme Environmental Conditions
by C.L.Hendrickson

Flight Testing of Terrain Following Systems
by C.Dallimore and M.K.Foster

Annex 2

AVAILABLE FLIGHT TEST HANDBOOKS

This annex is presented to make readers aware of handbooks that are available on a variety of flight test subjects not necessarily related to the contents of this volume.

Requests for A & AEE documents should be addressed to the Defence Research Information Centre, Glasgow (see back cover). Requests for US documents should be addressed to the Defense Technical Information Center, Cameron Station, Alexandria, VA 22314 (or in one case, the Library of Congress).

Number	*Author*	*Title*	*Date*
NATC-TM76-ISA	Simpson, W.R.	Development of a Time-Variant Figure-of-Merit for Use in Analysis of Air Combat Maneuvering Engagements	1976
NATC-TM76-3SA	Simpson, W.R.	The Development of Primary Equations for the Use of On-Board Accelerometers in Determining Aircraft Performance	1977
NATC-TM-77-IRW	Woomer, C. Carico, D.	A Program for Increased Flight Fidelity in Helicopter Simulation	1977
NATC-TM-77-2SA	Simpson, W.R. Oberle, R.A.	The Numerical Analysis of Air Combat Engagements Dominated by Maneuvering Performance	1977
NATC-TM-77-1SY	Gregoire, H.G.	Analysis of Flight Clothing Effects on Aircrew Station Geometry	1977
NATC-TM-78-2RW	Woomer, G.W. Williams, R.L.	Environmental Requirements for Simulated Helicopter/ VTOL Operations from Small Ships and Carriers	1978
NATC-TM-78-1RW	Yeend, R. Carico, D.	A Program for Determining Flight Simulator Field-of-View Requirements	1978
NATC-TM-79-33SA	Chapin, P.W.	A Comprehensive Approach to In-Flight Thrust Determination	1980
NATC-TM-79-3SY	Schiflett, S.G. Loikith, G.J.	Voice Stress Analysis as a Measure of Operator Workload	1980
NWC-TM-3485	Rogers, R.M.	Six-Degree-of-Freedom Store Program	1978
WSAMC-AMCP 706-204	—	Engineering Design Handbook, Helicopter Performance Testing	1974
NASA-CR-3406	Bennett, R.L. and Pearsons, K.S.	Handbook on Aircraft Noise Metrics	1981
—	—	Pilot's Handbook for Critical and Exploratory Flight Testing. (Sponsored by AIAA & SETP — Library of Congress Card No. 76-189165)	1972
—	—	A & AEE Performance Division Handbook of Test Methods for Assessing the Flying Qualities and Performance of Military Aircraft. Vol.1 Airplanes	1979
A & AEE Note 2111	Appleford, J.K.	Performance Division: Clearance Philosophies for Fixed Wing Aircraft	1978

Number	*Author*	*Title*	*Date*
A & AEE Note 2113 (Issue 2)	Norris, E.J.	Test Methods and Flight Safety Procedures for Aircraft Trials Which May Lead to Departures from Controlled Flight	1980
AFFTC-TD-75-3	Mahlum, R.	Flight Measurements of Aircraft Antenna Patterns	1973
AFFTC-TIH-76-1	Reeser, K. Brinkley, C. and Plews, L.	Inertial Navigation Systems Testing Handbook	1976
AFFTC-TIH-79-1	—	USAF Test Pilot School (USAFTPS) Flight Test Handbook. Performance: Theory and Flight Techniques	1979
AFFTC-TIH-79-2	—	USAFTPS Flight Test Handbook. Flying Qualities: Theory (Vol.1) and Flight Test Techniques (Vol.2)	1979
AFFTC-TIM-81-1	Rawlings, K., III	A Method of Estimating Upwash Angle at Noseboom-Mounted Vanes	1981
AFFTC-TIH-81-1	Plews, L. and Mandt, G.	Aircraft Brake Systems Testing Handbook	1981
AFFTC-TIH-81-5	DeAnda, A.G.	AFFTC Standard Airspeed Calibration Procedures	1981
AFFTC-TIH-81-6	Lush, K.	Fuel Subsystems Flight Test Handbook	1981
AFEWC-DR 1-81	—	Radar Cross Section Handbook	1981
NATC-TM-71-ISA226	Hewett, M.D. Galloway, R.T.	On Improving the Flight Fidelity of Operational Flight/ Weapon System Trainers	1975
NATC-TM-TPS76-1	Bowes, W.C. Miller, R.V.	Inertially Derived Flying Qualities and Performance Parameters	1976
NASA Ref. Publ. 1008	Fisher, F.A. Plumer, J.A.	Lightning Protection of Aircraft	1977
NASA Ref. Publ. 1046	Gracey. W.	Measurement of Aircraft Speed and Altitude	1980
NASA Ref. Publ. 1075	Kalil, F.	Magnetic Tape Recording for the Eighties (Sponsored by: Tape Head Interface Committee)	1982

The following handbooks are written in French and are edited by the French Test Pilot School (EPNER Ecole du Personnel Navigant d'Essais et de Réception ISTRES — FRANCE), to which requests should be addressed.

Number EPNER Reference	*Author*	*Title*	*Price (1983) French Francs*	*Notes*
2	G.Leblanc	L'analyse dimensionnelle	20	Réédition 1977
7	EPNER	Manuel d'exploitation des enregistrements d'Essais en vol	60	6ème Edition 1970
8	M.Durand	La mécanique du vol de l'hélicoptère	155	1ère Edition 1981
12	C.Laburthe	Mécanique du vol de l'avion appliquée aux essais en vol	160	Réédition en cours
15	A.Hisler	La prise en main d'un avion nouveau	50	1ère Edition 1964
16	Candau	Programme d'essais pour l'évaluation d'un hélicoptère et d'un pilote automatique d'hélicoptère	20	2ème Edition 1970
22	Cattaneo	Cours de métrologie	45	Réédition 1982

Number EPNER Reference	*Author*	*Title*	*Price (1983) French Francs*	*Notes*
24	G.Fraysse F.Cousson	Pratique des essais en vol (en 3 Tomes)	T 1 = 160 T 2 = 160 T 3 = 120	1ère Edition 1973
25	EPNER	Pratique des essais en vol hélicoptère (en 2 Tomes)	T 1 = 150 T 2 = 150	Edition 1981
26	J.C.Wanner	Bang sonique	60	
31	Tarnowski	Inertie-verticale-sécurité	50	1ère Edition 1981
32	B.Pennacchioni	Aéroélasticité — le flottement des avions	40	1ère Edition 1980
33	C.Lelaie	Les vrilles et leurs essais	110	Edition 1981
37	S.Allenic	Electricité à bord des aéronefs	100	Edition 1978
53	J.C.Wanner	Le moteur d'avion (en 2 Tomes) T 1 Le réacteur ..... T 2 Le turbopropulseur	 85 85	Réédition 1982
55	De Cennival	Installation des turbomoteurs sur hélicoptères	60	2ème Edition 1980
63	Gremont	Aperçu sur les pneumatiques et leurs propriétés	25	3ème Edition 1972
77	Gremont	L'atterrissage et le problème du freinage	40	2ème Edition 1978
82	Auffret	Manuel de médicine aéronautique	55	Edition 1979
85	Monnier	Conditions de calcul des structures d'avions	25	1ère Edition 1964
88	Richard	Technologie hélicoptère	95	Réédition 1971

REPORT DOCUMENTATION PAGE

1. Recipient's Reference	2. Originator's Reference	3. Further Reference	4. Security Classification of Document
	AGARD-AG-300 Volume 4	ISBN 92-835-1530-7	UNCLASSIFIED

5. Originator Advisory Group for Aerospace Research and Development
North Atlantic Treaty Organization
7 rue Ancelle, 92200 Neuilly sur Seine, France

6. Title
DETERMINATION OF ANTENNAE PATTERNS AND RADAR REFLECTION CHARACTERISTICS OF AIRCRAFT

7. Presented at

8. Author(s)/Editor(s)	9. Date
H.Bothe and D.Macdonald edited by A.Pool	May 1986
10. Author's/Editor's Address	**11. Pages**
Various	138

12. Distribution Statement This document is distributed in accordance with AGARD policies and regulations, which are outlined on the Outside Back Covers of all AGARD publications.

13. Keywords/Descriptors

Radar antennas
Radar scanning
Radar signals
Radar cross sections
Radar images
Aircraft equipment

14. Abstract

This AGARDograph is divided into two parts: Determination of Antenna Patterns of Aircraft, by H.Bothe, and Determination of Radar Reflection Characteristics of Aircraft, by D.Macdonald.

Part 1 describes the different types of aircraft antennas, their radiation characteristics and their preferred siting on the airframe. Great emphasis is placed on the various methods for determining aircraft antenna radiation patterns (ARP) and advantages, disadvantages and limitations of each method are indicated. Mathematical modelling, model measurements and in-flight measurements in conjunction with the applied flight test technique are included. Examples of practical results are given.

Part 2 describes methods of determining aircraft radar characteristics, indicating advantages, disadvantages and limitations of each method. Relevant fundamentals of radar theory are included only as necessary to appreciation of the real meaning of radar cross section (RCS) and angular glint. The measuring methods included are dynamic full-scale, static full-scale, sub-scale optical, ultrasonic and radio modelling. References are made to RCS measuring facilities in the USA and Europe and the UK Radio Modelling Facility is used extensively to exemplify the sub-scale technique.

This AGARDograph has been sponsored by the Flight Mechanics Panel of AGARD.

AGARDograph No.300 Volume 4
Advisory Group for Aerospace Research and Development, NATO
DETERMINATION OF ANTENNAE PATTERNS AND RADAR REFLECTION CHARACTERISTICS OF AIRCRAFT
Published May 1986
by H.Bothe and D.Macdonald and edited by A.Pool
138 pages

This AGARDograph is divided into two parts: Determination of Antenna Patterns of Aircraft, by H.Bothe, and Determination of Radar Reflection Characteristics of Aircraft, by D.Macdonald.

Part 1 describes the different types of aircraft antennas,

P.T.O

AGARD-AG-300
Volume 4

Radar antennas
Radar scanning
Radar signals
Radar cross sections
Radar images
Aircraft equipment

AGARDograph No.300 Volume 4
Advisory Group for Aerospace Research and Development, NATO
DETERMINATION OF ANTENNAE PATTERNS AND RADAR REFLECTION CHARACTERISTICS OF AIRCRAFT
Published May 1986
by H.Bothe and D.Macdonald and edited by A.Pool
138 pages

This AGARDograph is divided into two parts: Determination of Antenna Patterns of Aircraft, by H.Bothe, and Determination of Radar Reflection Characteristics of Aircraft, by D.Macdonald.

Part 1 describes the different types of aircraft antennas,

P.T.O

AGARD-AG-300
Volume 4

Radar antennas
Radar scanning
Radar signals
Radar cross sections
Radar images
Aircraft equipment

AGARDograph No.300 Volume 4
Advisory Group for Aerospace Research and Development, NATO
DETERMINATION OF ANTENNAE PATTERNS AND RADAR REFLECTION CHARACTERISTICS OF AIRCRAFT
Published May 1986
by H.Bothe and D.Macdonald and edited by A.Pool
138 pages

This AGARDograph is divided into two parts: Determination of Antenna Patterns of Aircraft, by H.Bothe, and Determination of Radar Reflection Characteristics of Aircraft, by D.Macdonald.

Part 1 describes the different types of aircraft antennas,

P.T.O

AGARD-AG-300
Volume 4

Radar antennas
Radar scanning
Radar signals
Radar cross sections
Radar images
Aircraft equipment

AGARDograph No.300 Volume 4
Advisory Group for Aerospace Research and Development, NATO
DETERMINATION OF ANTENNAE PATTERNS AND RADAR REFLECTION CHARACTERISTICS OF AIRCRAFT
Published May 1986
by H.Bothe and D.Macdonald and edited by A.Pool
138 pages

This AGARDograph is divided into two parts: Determination of Antenna Patterns of Aircraft, by H.Bothe, and Determination of Radar Reflection Characteristics of Aircraft, by D.Macdonald.

Part 1 describes the different types of aircraft antennas,

P.T.O

AGARD-AG-300
Volume 4

Radar antennas
Radar scanning
Radar signals
Radar cross sections
Radar images
Aircraft equipment

their radiation characteristics and their preferred siting on the airframe. Great emphasis is placed on the various methods for determining aircraft antenna radiation patterns (ARP) and advantages, disadvantages and limitations of each method are indicated. Mathematical modelling, model measurements and in-flight measurements in conjunction with the applied flight test technique are included. Examples of practical results are given.

Part 2 describes methods of determining aircraft radar characteristics, indicating advantages, disadvantages and limitations of each method. Relevant fundamentals of radar theory are included only as necessary to appreciation of the real meaning of radar cross section (RCS) and angular glint. The measuring methods included are dynamic full-scale, static full-scale, sub-scale optical, ultrasonic and radio modelling. References are made to RCS measuring facilities in the USA and Europe and the UK Radio Modelling Facility is used extensively to exemplify the sub-scale technique.

This AGARDograph has been sponsored by the Flight Mechanics Panel of AGARD.

ISBN 92-835-1530-7

their radiation characteristics and their preferred siting on the airframe. Great emphasis is placed on the various methods for determining aircraft antenna radiation patterns (ARP) and advantages, disadvantages and limitations of each method are indicated. Mathematical modelling, model measurements and in-flight measurements in conjunction with the applied flight test technique are included. Examples of practical results are given.

Part 2 describes methods of determining aircraft radar characteristics, indicating advantages, disadvantages and limitations of each method. Relevant fundamentals of radar theory are included only as necessary to appreciation of the real meaning of radar cross section (RCS) and angular glint. The measuring methods included are dynamic full-scale, static full-scale, sub-scale optical, ultrasonic and radio modelling. References are made to RCS measuring facilities in the USA and Europe and the UK Radio Modelling Facility is used extensively to exemplify the sub-scale technique.

This AGARDograph has been sponsored by the Flight Mechanics Panel of AGARD.

ISBN 92-835-1530-7

their radiation characteristics and their preferred siting on the airframe. Great emphasis is placed on the various methods for determining aircraft antenna radiation patterns (ARP) and advantages, disadvantages and limitations of each method are indicated. Mathematical modelling, model measurements and in-flight measurements in conjunction with the applied flight test technique are included. Examples of practical results are given.

Part 2 describes methods of determining aircraft radar characteristics, indicating advantages, disadvantages and limitations of each method. Relevant fundamentals of radar theory are included only as necessary to appreciation of the real meaning of radar cross section (RCS) and angular glint. The measuring methods included are dynamic full-scale, static full-scale, sub-scale optical, ultrasonic and radio modelling. References are made to RCS measuring facilities in the USA and Europe and the UK Radio Modelling Facility is used extensively to exemplify the sub-scale technique.

This AGARDograph has been sponsored by the Flight Mechanics Panel of AGARD.

ISBN 92-835-1530-7

their radiation characteristics and their preferred siting on the airframe. Great emphasis is placed on the various methods for determining aircraft antenna radiation patterns (ARP) and advantages, disadvantages and limitations of each method are indicated. Mathematical modelling, model measurements and in-flight measurements in conjunction with the applied flight test technique are included. Examples of practical results are given.

Part 2 describes methods of determining aircraft radar characteristics, indicating advantages, disadvantages and limitations of each method. Relevant fundamentals of radar theory are included only as necessary to appreciation of the real meaning of radar cross section (RCS) and angular glint. The measuring methods included are dynamic full-scale, static full-scale, sub-scale optical, ultrasonic and radio modelling. References are made to RCS measuring facilities in the USA and Europe and the UK Radio Modelling Facility is used extensively to exemplify the sub-scale technique.

This AGARDograph has been sponsored by the Flight Mechanics Panel of AGARD.

ISBN 92-835-1530-7